



Università degli Studi di Cagliari

DOTTORATO DI RICERCA
SCIENZE E TECNOLOGIE CHIMICHE

Ciclo XXVI

TITOLO TESI

**Design, synthesis and characterization of new iron and
aluminium chelating agents**

Settore/i scientifico disciplinari di afferenza

CHIM/01

Presentata da	Leonardo Toso
Coordinatore Dottorato	Prof. Mariano Casu
Tutor/Relatore	Prof. Guido Crisponi

Esame finale anno accademico 2012 – 2013

Dedication

This dissertation is dedicated to

Raquel

Acknowledgments

I am most grateful to my research supervisor Professor Guido Crisponi, Professor Valeria Nurchi, and Professor Maurizio Remelli for their guidance and advice during the last years.

I would specially like to thank to the co-authors of the original publications of this thesis.

I am thankful to all members of our research Group. I am especially grateful to Miriam, Delara, Joanna and Lupe for all the good moments we shared in the lab. I wish you all a lot of success for the continuation of your scientific careers.

I am very grateful to Professor Amelia Santos of Centro de Química Estrutural of Lisbon for giving me the opportunity to work in her research group and for helping me whenever I needed. Also I want to appreciate the friendship of all my friends of the IST. I acknowledge, Sérgio, Andreia, Patrik, André, Quaresma, Pedro, Raquel, Sofia, Isabel, Marta, Emilio and Guimarães for all the good moments in Lisbon.

I am also grateful to Professor Juan Niclos-Gutierrez and Josefa M. Gonzalez-Perez from the University of Granada for the kind access to their facilities and instrumentation. I wish to thank Alicia and Hanan for introducing me crystallographic technique and for answering to all my questions when running the experiments.

Also I want to appreciate the friendship over the last years to all my friends of Cagliari Chemistry Department. I acknowledge Danilo, Flavia, Elisa, Davide, Sergio, Claudia, Francesca, Luca, Francesco, Americo, and Salah for all the good moments.

The financial support from University of Cagliari through the PhD grant is greatly acknowledged.

Finally, I would like to thank my family. This work would have not been possible without the love and constant support of my parents, Graziella and Francesco, and my brother Davide. I cannot thank them enough. I wish to express my love to Raquel and thank her for his endless patience and support, and for always being at my side whenever I need it.

All contributed to make my PhD work a great experience and an enjoyable time.

Abstract

Chelation therapy is widely used for metal-unbalance related diseases, namely those due to disorders on metal metabolism, such as beta-thalassemia, hemochromatosis (Fe), and neurodegenerative diseases (Cu, Fe, Zn and Al). The study of metal chelators for clinical applications, either as chelating therapeutics able to target specific metal ions in the body, or as metal-carriers for therapeutic or imaging purposes, is a topical research area which faces up to urgent medical problems. Metal-chelating drugs are used in many ways for the prevention, diagnosis and treatment of cancer, since cancer cells, like normal cells, require essential metal ions such as iron, copper and zinc for growth and proliferation. Chelators can target the metabolic pathways of cancer cells through the control of proteins involved in the regulation of these metals and also of other molecules involved in cell cycle control, angiogenesis and metastatic suppression. The thermodynamic aspects regarding the complexation of metal ions of medical interest are of primary importance for a correct understanding of the role of metals in human diseases in order to rationalize the design of new molecules for diagnostic and therapeutic purposes. A typical case is the treatment of metal overload diseases where the highest thermodynamic stability and largest selectivity of the complexes are crucial factors in the ligand design.

This thesis is focused on the development and study of new compounds which, as a result of their strong interaction with specific metal ions, can be potentially used as pharmaceutical drugs for diagnosis or therapy. The work was performed with a multidisciplinary approach regarding mostly chemistry, but including also biochemistry and biology.

The work presented in this thesis is devoted to reach the following aims:

- Design and synthesis of new multivalent ligands in order to enhance the efficiency and selectivity of both metal-interaction and biomolecular recognition of available ligands (or metal complexes), as well as the targeting for drug delivery;
- Assessment of the most important physical and chemical properties of metal related compounds, namely metal-chelating efficacy and selectivity (thermodynamic and kinetic) with respect to other biometals or biological molecules, mostly in solution but also *in silico*;
- Bioevolution, *in vitro* and *in vivo*, for the most promising compounds.

This thesis is divided in two chapters. **Chapter I** is dedicated to a description of Chelation Therapy for treating metal intoxication in humans. The importance of chelating agents in neurodegenerative diseases like Alzheimer disease, is introduced. The main aspects of Fe, Al, and Cu metabolism in humans are presented. The **papers I, II, III and IV** relative to this chapter has been appended.

Chapter II describes the synthesis of the new studied ligands, and the experimental methods and techniques that were used for the investigation of the ligands and of their complexes with a number of metal ions. Important features of the used techniques are briefly described including basic principles, advantages and limitations. The **papers V, VI, and VII** explain in detail the developed work.

The main conclusions of this work are:

- A new family of hydroxypyrrone ligands (**L4**, **L5**, **L6**, **L7**, **L8**, and **L9**) has been synthesized and fully characterized. These ligands are easy and cheap to produce;
- Complex formation equilibria showed good efficiency and selectivity for iron and aluminium. With Fe^{3+} various protonated 2:3 Fe:L species have been detected (with exception for **L7**). Experimental data give evidence of a strong chelating ability for **L8** and, in order of decreasing ability, for ligands **L5** > **L4** > **L9** = **L6** > **L7**. Al^{3+} also forms 2:3 Al:L complexes with the ligands **L4**, **L5**, **L6**, and **L9**. The ligand with a shorter linker, **L8**, forms the most stable complexes of stoichiometry 2:2 (Al:L). Also Al^{3+} forms with **L8** the strongest complexes, and in order of decreasing stabilities with the ligands **L6** > **L5** > **L4** > **L9** > **L7**.
- Studies in mice confirmed the high *in vivo* metal scavenging ability of the tetradentate ligands (**L4**, **L5**, **L6**, **L8**, and **L9**) in comparison with the corresponding bidentate (**L7**). The excellent chelating properties recommend further toxicological and pharmacological research on these new promising ligands.

Keywords

Chelation therapy, speciation, metal complexes, ligands, iron, aluminium, copper, hydroxypyrrones, kojic acid

Contents

<i>Dedication</i>	<i>i</i>
<i>Acknowledgments</i>	<i>iii</i>
<i>Abstract</i>	<i>v</i>
<i>Keywords</i>	<i>vii</i>
<i>List of Abbreviations</i>	<i>xiii</i>
<i>List of Figures</i>	<i>xvii</i>
<i>List of Tables</i>	<i>xxi</i>
<i>List of Publications</i>	<i>xiii</i>

Chapter 1

CHELATION THERAPY	25
1.1. Introduction	27
1.2. Metals as Essential Elements	29
1.3. Chelating Agents	31
1.4. Principle of Hard-Soft Acid and Bases	34
1.5. Ideal Chelator	36
1.6. Metal Ions in Neurodegenerative Diseases	38
1.6.1. Alzheimer's Disease	39
1.6.2. Parkinson's Disease	43
1.6.3. Prion's Disease	44
1.7. Diseases Caused by Metal Overload	48
1.7.2. Wilson's Disease	50
1.8. Chelators for Metals	51

1.8.1. Iron Chelators.....	51
1.8.1.1. Catechols	52
1.8.1.2. Hydroxamates.....	53
1.8.1.3. Aminocarboxylates	54
1.8.1.4. Hydroxycarboxylates	54
1.8.1.5. Hydroxypyridinones.....	55
1.8.1.6. Hydroxypyrones.....	56
1.8.2. Aluminium chelators	57
1.8.3. Copper Chelators.....	60
1.9. Bibliography.....	65

Chapter 2

EXPERIMENTAL	75
2.1. Reagents	77
2.2. Synthesis.....	78
2.3. Tetradentate Ligands	80
2.4. Analytical Methods in Solution	82
2.4.1. Balance of Complex Formation in Solution: Definitions	82
2.4.1.1. Solutions of a System with Multiple Equilibria	84
2.4.2. Potentiometry	86
2.4.2.1. Glass Electrode Calibration	88
2.4.3. Spectrophotometric Method	90
2.4.3.1. Decomposition of Spectral Gaussian	90
2.4.4. Simultaneous Potentiometric and Spectrophotometric Titrations.....	92
2.4.5. Nuclear Magnetic Resonance	94
2.4.6. Electrospray Ionization Mass Spectroscopy	98
2.5. Bibliography.....	101

Appendix 1

INTERMEDIATES AND OTHER LIGANDS SYNTHESIZED 103

Appendix 2

UNSUCCESSFUL SYNTHESIS 117

List of Abbreviations

1,2-HP	1-Hydroxypyridin-2-one
3,2-HP	3-Hydroxypyridin-2-one
3,4-HP	3-Hydroxypyridin-4-one
A β	β -Amyloid
AD	Alzheimer's disease
API	Atmospheric pressure ionization
ATP	Adenosine-5'-triphosphate
BAL	2,3-Dimercaptopropanol, Dimercaprol
BBB	Blood-brain-barrier
B_{eff}	Effective magnetic field
BF	Bifunctional chelators
Bisphosphonate (¹ L)	Hydroxy(phenyl)methylenediphosphonic acid
BSE	Bovine spongiform encephalopathy
CD	Circular dichroism
CP	Ceruloplasmin
CQ	Clioquinol, PBT1
Cyc	1,4,7,10-Tetraazacyclododecane, Cyclen
DFO	Desferrioxamine
DMPS	D,L-2,3-Dimercapto-1-propanesulfonic acid
DMSA	<i>Meso</i> -2,3-Dimercaptosuccinic acid
DNA	Deoxyribonucleic acid
	D-pen (2 <i>S</i>)-2-amino-3-methyl-3-sulfanyl-butanoic acid, dimethylcysteine
DPF	3-Hydroxy-1,2-dimethylpyridin-4(1 <i>H</i>)-one, Deferiprone
DPTA	Diethylenetriaminepentaacetic acid

EDTA	Ethylenediaminetetraacetic acid
en	Ethylenediamine
ESI-MS	Electrospray ionisation-mass spectrometry
GLEE	Glass Electrode Evaluation
H	Hydrogen
HPOs	Hydroxypyridinones
HSAB	Hard and soft acids and bases, Pearson acid base concept
HySS	Hyperquad simulation and speciation
IDA(3,4-HP) ₂	2,2'-Azanediylbis(N-(3-(3-hydroxy-2-methyl-4-oxopyridin-1(4H)-yl)propyl)acetamide)
IMPY	6-Iodo-2-(4-dimethylamino)phenylimidazo[1,2- <i>a</i>]pyridine
KO	2-(4-(Dimethylamino)phenyl)imidazo[1,2- <i>a</i>]pyridin-8-ol
KA	Kojic acid
KEMPBu(3,4-HP) ₃	1,3,5-Tris-[4-(3-hydroxy-2-methyl-4-oxo-4 <i>H</i> -pyridin-1-yl)-butylcarbamoyl]-1,3,5-trimethylcyclohexane
KEMPPr(3,4-HP) ₃	1,3,5-Tris-[3-(3-hydroxy-2-methyl-4-oxo-4 <i>H</i> -pyridin-1-yl)-propylcarbamoyl]-1,3,5-trimethylcyclohexane
KLVFF	(2 <i>S</i> ,5 <i>S</i> ,8 <i>S</i> ,11 <i>S</i> ,14 <i>S</i>)-14,18-Diamino-2,5-dibenzyl-11-isobutyl-8-isopropyl-4,7,10,13-tetraoxo-3,6,9,12-tetraazaoctadecan-1-oic acid
L	Ligand
Log P	Octanol-water partition coefficient
M	Metal ion
m.p.	Melting point
MECAM	1,3,5- <i>N,N',N''</i> -tris-(2,3- dihydroxybenzoyl)
MS	Mass spectrometry
NFTs	Neurofibrillary tangles
NMR	Nuclear magnetic resonance

NTA	Nitrilotriacetic acid
NTP	Nitrilotripropionic acid
O-trensox	7,7',7''-(2,2',2''-Nitrilotris(ethane-2,1-diyl)tris(azanediyl)) tris(oxomethylene)tris(8-hydroxyquinoline-5-sulfonate)
PD	Parkinson's disease
PrP	Prion protein
RNA	Ribonucleic acid
ROS	Reactive oxygen species
SN	Substantia nigra
SPs	Senile plaques
Trien	Triethylenetetramine, Trentine, TETA
Tht	Thioflavin T
TLC	Thin layer chromatography
TRENCAMS	5,5',5''-(2,2',2''-Nitrilotris(ethane-2,1-diyl)tris(azanediyl)) tris(oxomethylene)tris(3,4-dihydroxybenzenesulfonate)
TSE	Transmissible spongiform encephalopathy
TTM	Ammonium tetrathiomolibdate
UV	Ultra-violet
Ve	Equivalent volume
WD	Wilson's disease
XH1	2,2'-(2,2'-(Carboxymethylazanediyl)bis(ethane-2,1-diyl)bis((2-(4-(benzo[d]thiazol-2-yl)phenylamino)-2-oxoethyl)azanediyl))

List of Figures

Chapter 1

Figure 1.1. Structures of the various chelating agents used to treat cases of heavy metal poisoning	29
Figure 1.2. Essential and toxic metal ions	30
Figure 1.3. Formation of metal ligand complex using mono, bi, and polydentate ligands	32
Figure 1.4. Structures of two different metal complexes with a chelating agent (in red). A) Basket complex enhances interaction of the metal with biomolecules (in purple); B) The stable complex prevents interaction of the metal with biomolecules	37
Figure 1.5. A) Hypothetical interaction between Al^{3+} and phosphate groups of the hyper-phosphorylated tau proteins in AD [18]. B), C), D) and E) aluminium, iron, copper and zinc differentially alter $\text{A}\beta$ aggregation, respectively. Al^{3+} promotes the formation of highly hydrophobic $\text{A}\beta$ oligomers; Fe^{3+} promotes $\text{A}\beta$ deposition into amorphous structures; Cu^{2+} leads to the formation of disordered/amorphous structures; and Zn^{2+} triggers the formation of amorphous aggregates [19]	41
Figure 1.6. Dopamine oxidation to aminochrome catalyzed by manganese	43
Figure 1.7. Cu^{2+} and Fe^{3+} abilities to form complexes with dopamine, based on ionic binding between the positive charges of metal ions and negative charges of dissociated hydroxyl groups	44
Figure 1.8. Molecular models of the conversion of $\text{PrP}^{\text{C}} \rightarrow \text{PrP}^{\text{Sc}}$. Adapted from [27]	46
Figure 1.9. Hypothesis of the relationship between PrP^{C} , PrP^{Sc} with metal ions	47

Figure 1.10. Inheritance of β -thalassemia. Unaffected carrier parents have 25% of probably to have a sick child (illustrated in red)	49
Figure 1.11. Bilateral Kayser–Fleischer rings (panel A, within arrows). Five years after the initiation of copper-chelating treatment, the Kayser–Fleischer ring has almost disappeared (panel B) [37]	50
Figure 1.12. Hexadentate catechols	52
Figure 1.13. Hexadentate (DFO) and bidentate (L-lysinehydroxamic acid) hydroxamates	53
Figure 1.14. Aminocarboxylates	54
Figure 1.15. Hydroxycarboxylates	55
Figure 1.16. Bidentate and hexadentate HPOs	56
Figure 1.17. Kojic acid derivatives	57
Figure 1.18. Aluminium chelators	59
Figure 1.19. Main copper chelators for the treatment of WD	61
Figure 1.20. Copper chelators	62
Figure 1.21. Molecules capable to interact with A β	63
Figure 1.22. Example of incorporation (K0), linkage (XH1) and peptide (Cyc-KLVFF) approach	64

Chapter 2

Figure 2.1. Synthesized ligands L4, L5, L6, L7, L8, and L9	78
Figure 2.2. A) Fe_2L_3 model for the ligands L4, L5, L6, L8 and L9; B) Crystal of the complex $\text{Fe}_2(\text{L6})_3$; C) Fe_2L_3 model proposed for the complex $\text{Fe}_2(\text{IDAPr}((3,4\text{-HP})_2)_3$; D) Structural diagram for the complex $\text{Fe}_2(\text{IDAPr}((3,4\text{-HP})_2)_3$	81
Figure 2.3. Gran plot obtained with GLEE program	89
Figure 2.4. A) Potentiometric curve of ligand L9; B) Spectra collected during the potentiometric titration of the ligand L9, the red spectra was collected at pH acid, and basic pH; C) Speciation plot of the ligand L9	93
Figure 2.5. $^1\text{H-NMR}$ spectra of L4 in D_2O at pH 3.5 (in black), and Kojic acid in D_2O at pH = 7 (in red)	96
Figure 2.6. $^1\text{H-}^{13}\text{C}$ HSQC of L4 in MeOD	97
Figure 2.7. Schematic representation of a mass spectrometer	100

List of Tables

Chapter 1

Table 1.1. Thermodynamic data of a purely entropy-based chelate effect	33
Table 1.2. Acid and basic classification according to the HSAB principle of Pearson	35
Table 1.3. Metal levels in patients with Alzheimer's disease compared to healthy individuals	40

Chapter 2

Table 2.1. Reactional conditions of the synthesized ligands ^a	79
--	----

List of Publications

This thesis is based on the following published and to be submitted publications:

- I. G. Crisponi, V.M. Nurchi, M. Crespo-Alonso, L. Toso, *Chelating agents for metal intoxication*, *Curr. Med. Chem.* 19 (2012) pp. 2794-2815.
- II. V.M. Nurchi, M.C. Alonso, L. Toso, J.I. Lachowicz, G. Crisponi, *Chelation therapy for metal intoxication: comments from a thermodynamic viewpoint*, *Mini Rev. Med. Chem.* 13 (2013) pp. 1541-1549.
- III. G. Crisponi, V.M. Nurchi, D. Fanni, C. Gerosa, S. Nemolato, M.C. Alonso, L. Toso, J.I. Lachowicz, G. Faa, *Metal Ions in the Pathogenesis of Alzheimer's Disease: An Open Field*, *Frontiers in Clinical Drug Research – Alzheimer Disorders.* 1 (2013) pp. 411-431.
- IV. M. Tegoni, D. Valensin, L. Toso, M. Remelli, *Copper chelators: chemical properties and bio-medical applications*, *Curr. Med. Chem.* (2014, submitted).
- V. L. Toso, G. Crisponi, V.M. Nurchi, M. Crespo-Alonso, J.I. Lachowicz, M.A. Santos, S.M. Marques, J. Niclós-Gutiérrez, J.M. González-Pérez, A. Domínguez-Martín, D. Choquesillo-Lazarte, Z. Szewczuk, *A family of hydroxypyrrone ligands designed and synthesized as iron chelators*, *J. Inorg. Biochem.* 127 (2013) pp. 220-231.
- VI. L. Toso, G. Crisponi, V.M. Nurchi, M. Crespo-Alonso, J.I. Lachowicz, D. Mansoori, M. Arca, M.A. Santos, S.M. Marques, L. Gano, J. Niclós-Gutiérrez, J.M. González-Pérez, A. Domínguez-Martín, D. Choquesillo-Lazarte, Z. Szewczuk, *Searching for new aluminium chelating agents: A family of hydroxypyrrone ligands*, *J. Inorg. Biochem.* 130 (2014) pp. 112-121.
- VII. G. Crisponi, V.M. Nurchi, M. Arca, M. Crespo-Alonso, J.I. Lachowicz, D. Mansoori, L. Toso, G. Pichiri, M.A. Santos, S.M. Marques, J. Niclós-Gutiérrez, J.M. González-Pérez, A. Domínguez-Martín, D. Choquesillo-Lazarte, Z. Szewczuk, M.A. Zoroddu, M. Peana, *A bis-3-hydroxy-4-pyrone as a potential therapeutic iron chelating agent. Effect of connecting and side chains on the complex structures and metal ion selectivity*, *Inorg. Chem.* (2014, Submitted).

Other publications and Acta:

- VIII.** V.M. Nurchi, M. Crespo-Alonso, L. Toso, J.I. Lachowicz, G. Crisponi, G. Alberti, R. Biesuz, A. Domínguez-Martín, J. Niclós-Gutiérrez, J.M. González-Pérez, M.A. Zoroddu, *Iron(III) and aluminium(III) complexes with substituted salicyl-aldehydes and salicylic acids*, *J. Inorg. Biochem.* 128 (2013) pp. 174-182.
- IX.** M. Remelli, D. Valensin, L. Toso, E. Gralka, R. Guerrini, E. Marzola, H. Kozlowski, *Thermodynamic and spectroscopic investigation on the role of Met residues in Cu(II) binding to the non-octarepeat site of the human prion protein*, *Metallomics.* 4 (2012) pp. 794-806.
- X.** G. Crisponi, V.M. Nurchi, J.I. Lachowicz, M.C. Alonso, L. Toso, M.A. Zoroddu, M. Peana, *State of art in chelating agents for the clinical treatment of metal poisoning*, Medimond-Monduzzi editore international proceeding division, 11th European Biological Inorganic Chemistry Conference, EUROBIC 11, ISBN 978-88-7587-658-6, (2012) pp. 37-42.
- XI.** L. Toso, G. Crisponi, V.M. Nurchi, M. Crespo-Alonso, J.I. Lachowicz, M.A. Santos, S.M. Marques, J. Niclós-Gutiérrez, J.M. González-Pérez, A. Domínguez-Martín, M.A. Zoroddu, M. Peana, *Hydroxypyrones, an intriguing family of chelating agents for Fe(III) and Al(III)*, Medimond-Monduzzi editore international proceeding division, 11th European Biological Inorganic Chemistry Conference, EUROBIC 11, ISBN 978-88-7587-658-6, (2012) pp. 53-56.

Chapter 1

Chelation Therapy

Chapter 1

Chelation Therapy

1.1. Introduction

Chelation therapy is the process of removing from the body undesirable metal ions by administration of a drug, by injection or orally, that has suitable chelating properties. The concept of chelation derives from the Greek word “*chele*” that means claw of a lobster.

The chelation therapy transforms the toxic metal ion in less dangerous species that can be excreted from the organism. Three different categories of metal toxicity can be distinguished, according to their sources and effects:

- Acute ingestion of toxic metal ions, that can be accidental, as frequently happens to children, or caused by a voluntary homicidal or suicidal attempt;
- Chronic intoxication, which may depend on environmental, occupational or iatrogenic causes;
- Metal overload due to genetic diseases.

The new chelating agents proposed in this thesis (see Chapter 2) are suitable for the third point.

The use of chelation therapy to treat metal intoxication was developed during the 20th century, initially to moderate the toxicity of arsenic compounds used to treat syphilis. British Anti Lewisite, BAL (2,3 dimercaptopropan-1-ol, see Fig. 1.1), was first synthesized at Oxford by Sir Rudolph Peters as an antidote for war chemical agents [1]. For security reasons it was declared to the scientific community only after the end of the war in 1945 [2]. It was the first antidote for metal intoxication. The use of citrate for the treatment of lead poisoning was also investigated, but with limited success. The polyamine carboxylic acids (EDTA) and, more effectively, diethylenetriaminepentaacetic acid (DPTA) were used to treat lead intoxication (see Fig. 1.1). These two compounds are administered by slow intravenous infusion and are poorly absorbed by the gastrointestinal tract. They distribute into extracellular regions and are rapidly excreted in urine. Toxic effects can arise from their ability to sequester essential metal ions such as Ca^{2+} and Zn^{2+} , but these can be moderated by the use of $\text{CaNa}_2(\text{EDTA})$, $\text{Ca}_2(\text{EDTA})$, $\text{Zn}_2(\text{EDTA})$ or $\text{ZnNa}_3(\text{DPTA})$ instead of simple sodium salts. In the 1950s meso-2,3-dimercaptosuccinic acid (DMSA) and D,L-2,3-dimercaptopropane-1-sulfonic acid (DMPS) were used as metal sequestering agents (see Fig. 1.1). These chelators surpassed the unstable biologically and more toxic BAL. Also they have a stronger ability to access the intracellular metals [3].

Sequestering agents specific to iron and copper were also developed to treat chronic diseases, that originate toxic effects due to metal imbalance. Such ligands are discussed in more detail in the Section 1.8.

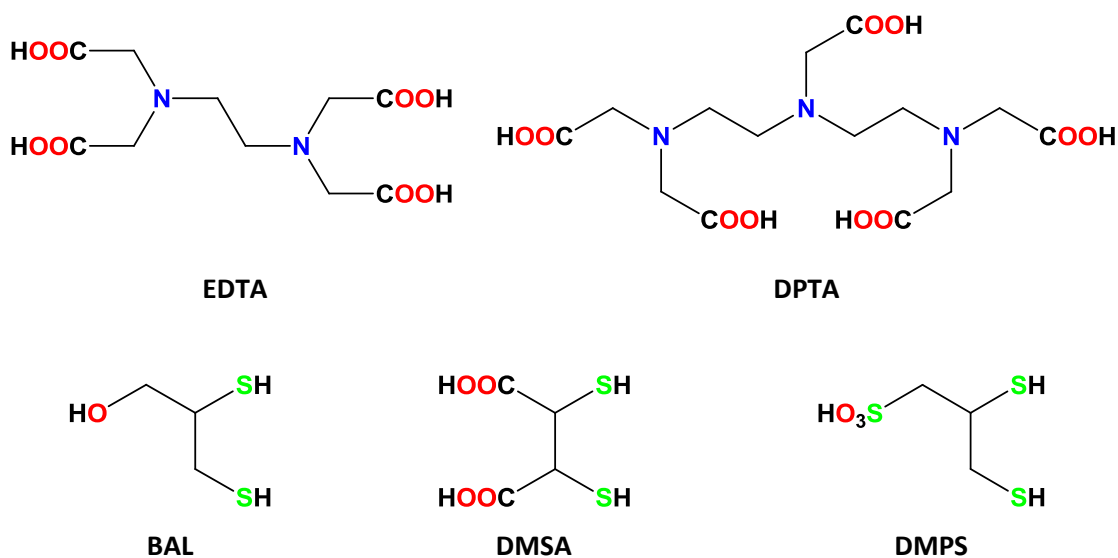


Figure 1.1. Structures of the various chelating agents used to treat cases of heavy metal poisoning.

1.2. Metals as Essential Elements

Essential elements are commonly classified as essential, inert, and toxic. The essential needs for the functioning of prokaryotic and eukaryotic cells require 17 metals of the 30 essential elements. Many metal ions play a dual role in organisms physiology in function of the concentration range considered. Toxic compounds can be tolerated in low doses, and essential elements can become toxic at high concentrations (Fig. 1.2, see also the Bertrand diagram in paper I).

Essential metals include copper, that is an essential cofactor for many oxidative enzymes, such as catalase and peroxidase, iron that is implied in hundred enzymatic reactions and is an essential component of hemoglobin (the oxygen carrier in red blood cells), and zinc that takes a role on enzymatic functions of more than three hundred proteins. Zinc deficiency that has been frequently identified in developing countries may lead to dwarfism, an adolescent nutritional deficiency. Cobalt is an

essential cofactor for vitamin B12 vital in protein formation and DNA regulation; manganese is a cofactor in many enzymatic reactions involving phosphorylation, cholesterol and fatty acid synthesis; selenium is essential for a variety of enzymes, including several anti-oxidants. Contrary to animals, plants do not require selenium for their survival, but they absorb it and for this reason selenium poisoning can occur from eating plants grown in selenium rich soils. Molybdenum, an essential cofactor for xanthine oxidase and aldehyde oxidase, is also an essential element to plants functioning, required to fix nitrogen through bacteria [4].

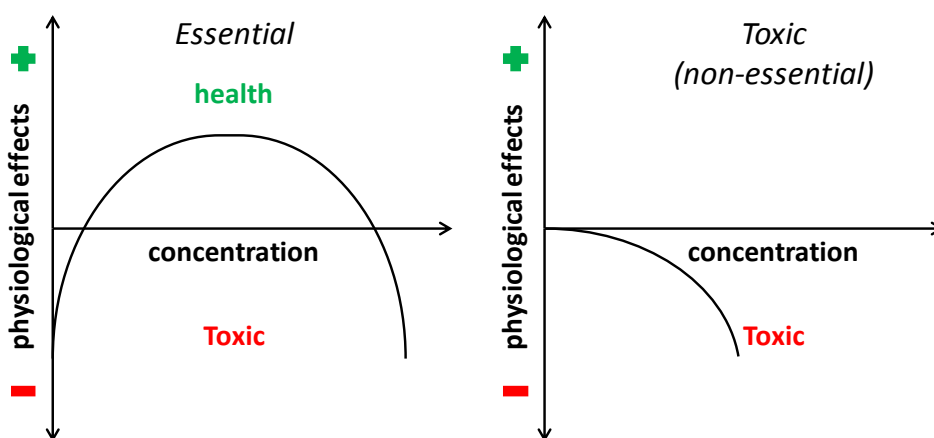


Figure 1.2. Essential and toxic metal ions.

Metals and metal compounds (mercury and organometallic compounds) can be absorbed by ingestion, inhalation and absorption through the skin. Metals and metal compounds taken orally are mainly absorbed in the intestinal tract and absorption occurs through diffusion processes due to gradient concentrations. In particular, for essential metal elements such as iron there are special transport mechanisms. When inhaled, the water-soluble gases and vapors are dissolved in the mucous membranes of the tracheobronchial and nasopharyngeal regions, while those less soluble reach the end zones of the airways and the alveoli of the lungs, and then take the bloodstream

and lymphatic system. Once absorbed into the bloodstream, the metal ions and their compounds are linked to blood plasma proteins. Metals are distributed in the organism through the blood circle [5]. The behavior of a metal in physiological conditions depends essentially from its "chemical speciation", that means the different forms in which it is located in a given environment. From thermodynamic equilibria studies in solution and the values of the formation constants obtained for complexes, various species present in solution and their concentrations can be determined. Therefore, the thermodynamic approach can be applied for the study of ligands that interact with metal ions, essential for living organisms or toxic due to accumulation. These ligands are interesting for the biomedical point of view as they can be used as a therapy to remove toxic metals from the human body in diseases due to accumulation of heavy metals (chelation therapy).

Chelation therapy occupies a central place in modern medicine and pharmacology, as continuous studies in laboratory and extensive clinical trials demonstrate that acute or chronic intoxication with a variety of metals (essential or non-essential) may be considerably improved by administration of a suitable chelating agent [6].

1.3. Chelating Agents

Chelating agents are organic or inorganic compounds capable of binding metal ions and form a complex ring-like structure called "chelates". A chelating agent has ligand binding atoms that form either two covalent linkages, or one covalent and one coordinate, or two coordinate linkages in the case of bidentate chelates. Mainly atoms like S, N and O act as ligand atoms in the form of chemical groups like $-SH$, $-S-S$, $-NH_2$, $=NH$, $-OH$, $-OPO_3H$, or $>C=O$. Bidentate or multidentate ligands form ring structures that include the metal ion and two-ligand atoms attached to the metal (Fig. 1.3).

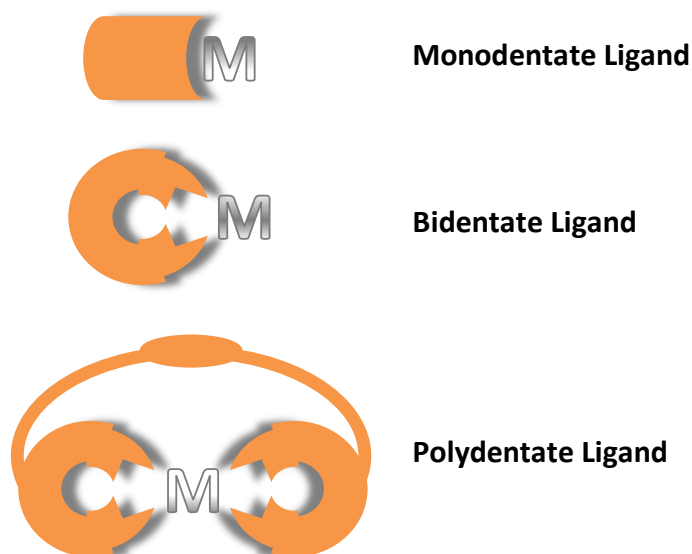
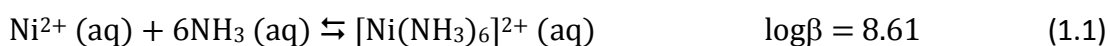


Figure 1.3. Formation of metal ligand complex using mono, bi, and polydentate ligands.

Many donors act as bidentate ligands. Five-membered chelate rings are specially stable. There are also examples of inorganic chelate ligands which form five-membered rings with metal ions. The stability of the complex respects the trend: monodentate < bidentate < tridentate...< hexadentate [3], due to chelate effect, that depends on entropic parameters. In order to explain this effect, consider the following equilibrium constants:



The system $[\text{Ni en}_3]^{2+}$ (en = ethylenediamine, $\text{NH}_2\text{CH}_2\text{NH}_2$) in which three chelate rings are formed is nearly 10^{10} times more stable than that without the formation of a ring.

Although the effect is not always so pronounced, this example can be considered as a general trend of the chelate effect. Taking into consideration the thermodynamic relationships:

$$\Delta G^\circ = -RT \ln \beta \quad (1.3)$$

$$\Delta G^\circ = \Delta H^\circ - T\Delta S^\circ \quad (1.4)$$

where ΔG° is the Gibbs free energy, R is the gas constant ($1.987 \text{ cal mol}^{-1} \text{ K}^{-1}$), and T is the temperature. Thus, β increases as ΔG° becomes more negative (due to more negative ΔH° or more positive ΔS°). As a very simple case, consider the following reactions (1.5 and 1.6) and the pertinent thermodynamic data for them, given in Table 1.1.

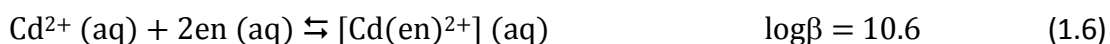
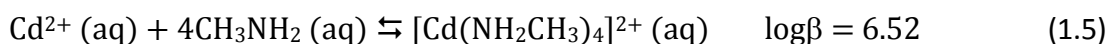


Table 1.1. Thermodynamic data of a purely entropy-based chelate effect

Ligands	ΔH° (kJ mol ⁻¹)	ΔS° (J mol ⁻¹ deg ⁻¹)	$-T\Delta S^\circ$ (kJ mol ⁻¹)	ΔG° (kJ mol ⁻¹)
4CH ₃ NH ₂	-57.3	-67.3	20.1	-37.2
2 en	-56.5	+14.1	-4.2	-60.7

In this case enthalpies are similar for the two reactions, and therefore the chelate effect can be attributed entirely to the entropy difference. Probably, the main cause for the large entropy increase in the two cases is the net increase in the number of

unbound water molecules. Thus, although 6NH_3 displace $6\text{H}_2\text{O}$, with no net change in the number of independent molecules, it takes only $3en$ molecules to displace $6\text{H}_2\text{O}$ [7].

1.4. Principle of Hard-Soft Acid and Bases

In recent years there has been a considerable progress in the design and synthesis of molecular systems able to selectively recognize metal ions. Several useful concepts have been developed for the design of these new ligands. The starting point to produce potential ligands is the study of the electronic and steric characteristics (inorganic chemistry research) of the various metal atoms from the periodic table. Secondly, the appropriate properties of the ligands, that have to match those of the metal, are searched.

For this purpose the classification of acids and bases in hard and soft, that is the principle of HSAB (hard-soft acid and bases), defined by Pearson (Table 1.2) is useful for determining the type of donor atoms to coordinate the relative cation [8].

According to HSAB classification the small metal atoms with high charge density, which are not easily polarizable, are called hard. These metals have the tendency to form ionic bonds with hard bases, while bigger and more polarizable atoms, belonging to the soft category, form mostly covalent bonds with the bases complementary to them (soft bases). Considering these principles it has been possible to make useful general predictions on the stability of metal complexes with various ligands. However, some uncertainties remain for the prediction of borderline cases such as Zn^{2+} , Pb^{2+} and Fe^{2+} , which can form stable complexes both with hard and soft bases.

In this thesis the ligands we propose (see Chapter 2) are formed by two hydroxypyrrone units (hard bases), and they are selective to Fe^{3+} and Al^{3+} (hard acids) as described by Pearson's. Furthermore, the strength of coordination of negatively charged groups (like OH^-) is related to their basicity. For example, the selectivity of a ligand towards a more acid metal, like Fe^{3+} and Al^{3+} in comparison to a less acid metal, such as Cu^{2+} and Zn^{2+} , increases with the number and basicity of the negatively charged groups [8-9].

Table 1.2. Acid and basic classification according to the HSAB principle of Pearson

Acids	
<u>Hard</u>	<u>Soft</u>
H^+ , Li^+ , Na^+ , K^+ , Be^{2+} , Mg^{2+} , Ca^{2+} , Sr^{2+} , Ba^{2+} , Al^{3+} , Sc^{3+} , Ga^{3+} , In^{3+} , La^{3+} , Gd^{3+} , Lu^{3+} , Cr^{3+} , Co^{3+} , Fe^{3+} , As^{3+} , Si^{4+} , Ti^{4+} , Zr^{4+} , Hf^{4+} , Th^{4+} , U^{4+} , Pu^{4+} , Ce^{4+} , WO^{4+} , Sn^{4+} , UO^{2+} , VO^{2+} , MoO^{3+}	Cu^+ , Ag^+ , Au^+ , Ti^+ , Hg^+ , Pd^{2+} , Cd^{2+} , Pt^{2+} , Hg^{2+} , CH_3Hg^+ , $\text{Co}(\text{CN})_5^{2-}$, Pt^{4+} , Te^{4+} , Br^+ , I^+
<u>Borderline</u>	
Fe^{2+} , Co^{2+} , Ni^{2+} , Cu^{2+} , Zn^{2+} , Pb^{2+} , Sn^{2+} , Sb^{3+} , Bi^{3+} , Rh^{3+} , Ir^{3+} , $\text{B}(\text{CH}_3)_3$	
Bases	
<u>Hard</u>	<u>Soft</u>
H_2O , OH^- , F^- , CH_3CO_2^- , PO_4^{3-} , SO_4^{2-} , Cl^- , CO_3^{2-} , ClO^- , NO_3^- , ROH , RO^- , R_2O , NH_3 , RNH_2 , NH_2NH_2	R_2S , RSH , RS^- , I^- , SCN^- , $\text{S}_2\text{O}_3^{2-}$, R_3P , R_3As , CO , $(\text{RO})_3\text{P}$, CN^- , RNC , C_2H_4 , H^- , R^-
<u>Borderline</u>	
$\text{C}_5\text{H}_5\text{NH}_2$, $\text{C}_5\text{H}_5\text{N}$, N_3^- , Br^- , NO_2^- , N_2 , SO_3^{2-}	

1.5. Ideal Chelator

To synthesize an ideal chelating agent it is necessary to consider the chemical and biomedical properties of the molecule (see paper I):

- Low toxicity of the chelating agent and formed complexes;
- Rapid elimination of the toxic complex-metal ion;
- High stability of the formed complexes, in competition with the stability of endogenous natural ligands in the body;
- High selectivity towards the target metal ion (good value of pM [10]);
- Biochemical metabolism of the chelating agent once entered into the body;
- Kinetic and mechanism of exchange with endogenous ligands;
- Factors affecting absorption and bioavailability.

Regarding the last point, the chelators have to be sufficiently absorbed through the cell membranes, but it is important that the metal ion complex do not cross the blood-brain-barrier (BBB) to prevent unexpected neurological damages. Three key parameters should be taken into account when considering diffusion through the biological membranes, namely molecular size, lipophilicity, and net charge.

Lipinski suggest very useful parameters to predict the membrane permeability. For a molecule to be absorbed it has to respect the following characteristics:

- Molecular weight < 500 g/mol;
- $\log P < 5$ (with P being the octanol-water partition coefficient);
- Less than 10 hydrogen bond donors in the molecule (expressed as a sum of OH and NH groups);

- Less than 10 hydrogen bond acceptors present in the molecule (expressed as the sum of O and N atoms).

The stability of the complex depends on the denticity of the ligand. Bidentate and tridentate ligands form complexes with lower stoichiometry than hexadentate ones. This can be potentially dangerous, because these complexes can be more toxic than the parent metal ion. However, not all hexadentate chelators can protect adequately the metal ion from deleterious reactions, as for example, ethylenediamine-tetraacetic acid (EDTA) that is not able to shield the surface of the Fe^{3+} ion, but it forms an open complex (Fig. 1.4 A, basket complex). The exposition of the molecule to the biological environment facilitates the interactions with the metal, and consequently originates Fenton reactions with reactive oxygen species (ROS). On the contrary, the iron chelator desferrioxamine (DFO) showed in Fig. 1.13, completely covers the surface of iron during complex formation, preventing iron-catalyzed free radical reactions (Fig. 1.4 B, stable complex) [3].

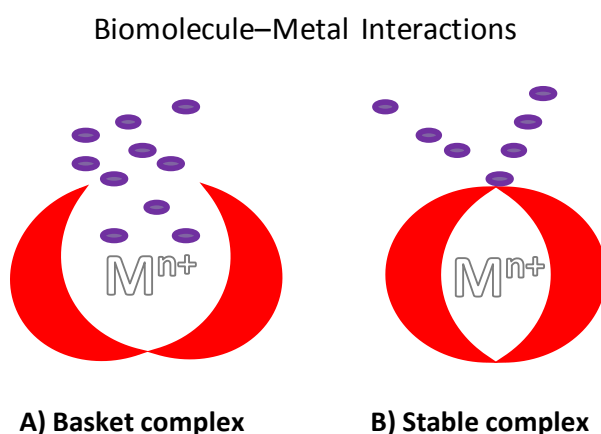


Figure 1.4. Structures of two different metal complexes with a chelating agent (in red); **A)** Basket complex enhances interaction of the metal with biomolecules (in purple); **B)** The stable complex prevents interaction of the metal with biomolecules.

1.6. Metal Ions in Neurodegenerative Diseases

As the population gets older, there is an increased prevalence of neurodegenerative diseases. These diseases can be hereditary or, in very special cases, can result from sporadic infection, and very often develop in individuals with more than 65 years old. This is the case of Parkinson (PD), Alzheimer (AD) and transmissible spongiform encephalopathy (TSE) diseases. These clinically different diseases have similar progressive and chronic nature. They are developed by the accumulation of a specific protein in the cells of tissues, called "amyloid", and recent evidences show that metal ion homeostasis may be involved in the progression of the disease. The hypothesis of the involvement of metal ions in neurodegenerative diseases has attracted a renewed attention to chelation therapy in the attempt to fight the neurological disorders.

Metals may have an effect on neurodegenerative diseases including, oxidative stress and signaling involvement, and protein aggregation. Evidences show that the binding of metal ions to proteins promotes folding and stabilizes folded or partially folded states, thus accelerating protein aggregation.

Amyloid is a general term that describes different types of protein aggregates, having some physico-chemical characteristics in common: a fibrillar morphology, a predominance of β -sheet secondary structure, resistance to proteolysis, insolubility in common solvents and detergents, and possibility of degradation after the reaction with the dye Congo red [11].

The formation of the so-called fibrills has been intensively studied. It was shown that fibrillization phenomenon has similarities with the classical increase of the size of crystals, being associated to the presence of small aggregates, called "seeds" or "nuclei", that increase in size for the incorporation of other molecules (nucleation) [11].

The involvement of particular proteins in the amyloid diseases was believed to be caused by specific conformational features. Recent observations have shown that in non-physiological conditions, many proteins form a fibrous gel very similar to amyloids. The ability to form amyloids appears to be a generic property of polypeptide chains, common to all proteins, and resulting from intermolecular interactions that stabilize the aggregate [12].

Amyloids are very stable under physiological conditions due to the number of hydrogen bonds present. Biological systems have developed various protective mechanisms to prevent aggregation. For example, the globular shape makes the main chain inaccessible to the formation of hydrogen bonds, except when the protein is exposed to denaturing conditions. Proteins with a high disorder can have a change in conformation, a variation of the secondary and tertiary structure, without alteration of the primary structure, which occurs for example in the case of AD [12]. This variation can be caused by a direct toxic activity and the absence of normal biological functions in the formation of proteins.

Normally, the protein associated with the neurodegenerative disease is found in the human body in equilibrium between normal and toxic forms; with the formation of the "misfolded" protein equilibrium is lost, and onset the disease: the protein aggregates in various organs and becomes amyloid. Antibodies, present in the body, do not intervene probably because they fail to distinguish between the two forms.

1.6.1. Alzheimer's Disease

AD is characterized by memory loss, confusion, irritability, language breakdown, and social withdrawal. It constitutes a dramatic health, social and economic problem, for all countries, as patients stop being self-sufficient. The problem is the worldwide rapid

increase of affected people. There are currently about 36 million people affected with this disease, and forecasts say that in the next 20 years will be 66 million, and 115 million in 2050 [13]. AD can be defined as a disarrangement of the cellular control system responsible for the correct protein folding (misfolding), in particular neurofibrillary tangles (NFTs) inside the neuron and neuritic senile plaques (SPs) in the extracellular space between neurons are produced, are these are two distinctive traits that define the disease. The main constituent of SPs is β -amyloid ($A\beta$), a proteolytic cleavage by-product of the precursor protein (β -APP) [14]. NFTs are mainly composed of hyperphosphorylated tau protein. Studies on plaques show that they contain many copies of the $A\beta$ peptide in a soluble oligomeric β -sheet aggregate with high amounts of Cu^{2+} , Fe^{3+} , and Zn^{2+} (see Table 1.3).

Table 1.3. Metal levels in patients with Alzheimer's disease compared to healthy individuals [15-16]

Location	Copper ($\mu g g^{-1}$)	Iron ($\mu g g^{-1}$)	Zinc ($\mu g g^{-1}$)
Plaque rim	23 ^a	52 ^a	67 ^a
Plaque core	30 ^b	53 ^a	87 ^a
Total senile plaque	25 ^a	52 ^a	69 ^a
Alzheimer's neuropil	19 ^b	39 ^b	51 ^c
Control neuropil	4	19	23

^a $P < 0.05$ (plaque values versus with Alzheimer's neuropils).

^b $P \leq 0.08$ (Alzheimer's neuropils versus with control neuropil).

^c $P < 0.05$ (Alzheimer's neuropils versus control neuropil).

Al^{3+} was found at elevated levels in NFTs, indicating that it may promote protein aggregation [17]. After that, it was proposed a hypothetical interaction between Al^{3+} and phosphate groups of the hyper-phosphorylated tau proteins [18] (see Fig. 1.5).

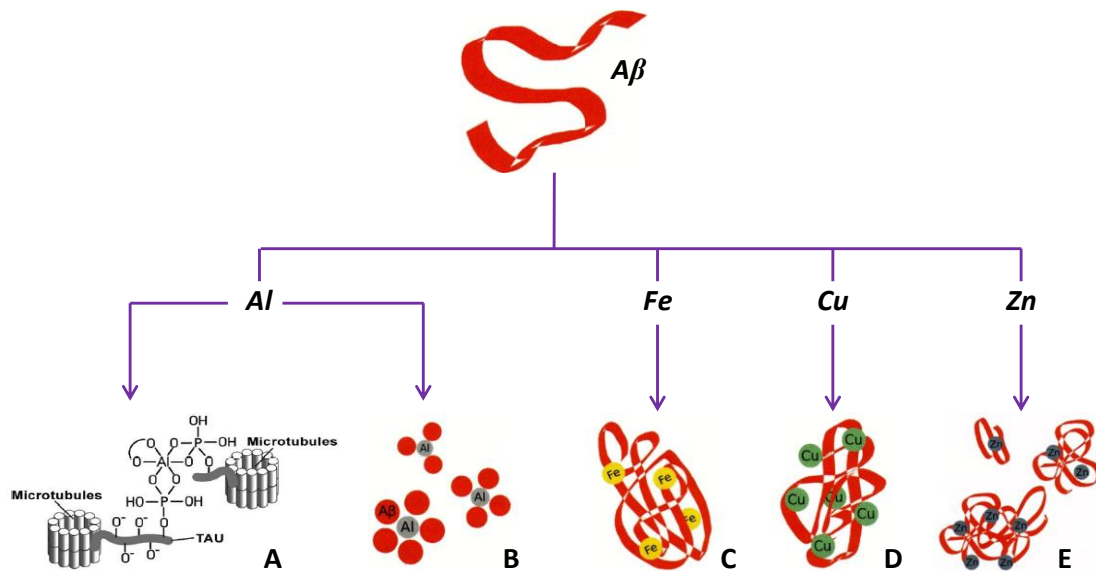


Figure 1.5. **A)** Hypothetical interaction between Al^{3+} and phosphate groups of the hyper-phosphorylated tau proteins in AD [18]. **B), C), D)** and **E)** aluminium, iron, copper and zinc differentially alter $\text{A}\beta$ aggregation, respectively. Al^{3+} promotes the formation of highly hydrophobic $\text{A}\beta$ oligomers; Fe^{3+} promotes $\text{A}\beta$ deposition into amorphous structures; Cu^{2+} leads to the formation of disordered/amorphous structures; and Zn^{2+} triggers the formation of amorphous aggregates [19].

The brain is an highly oxidative organ, and the presence of transition metals may lead to the generation of highly toxic free radicals. It was found *in vitro* that $\text{A}\beta$ can efficiently generate ROS in presence of copper and iron transition metals [20]. ROS in biological systems is the hydroxyl free radical, OH^{\cdot} , which can be formed by homolytic fission of the H_2O_2 molecule. This OH^{\cdot} radical can be also produced according to the

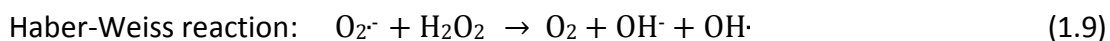
Fenton reaction (1.7) in the presence of metals (for instance Fe^{2+}):



while the Fe^{3+} ion can be reduced by superoxide to give Fe^{2+} and molecular oxygen:



The sum of the last two reactions is known as Haber-Weiss reaction (1.8). The presence of iron catalyzes the formation of the hydroxyl radical, and the reaction becomes thermodynamically favorable in biologic systems.



ROS generated by metals may in turn lead to toxic cellular events, such as DNA damage, protein and lipid oxidation. For this reason in our body there are complex pathways which ensure metal intake, distribution, utilization and excretion that contrast its toxicity (see paper IV).

Although there several studies in the literature concerning the role of $\text{A}\beta$ and its interaction with metals, the mechanism is not completely clarified. It has been proposed that the metal can encourage the formation of protein aggregates, or can affect the protection from the redox-active metal ions (ROS): “Amyloid paradox” [21]. In paper III we introduced the concept of “metal paradox”, meaning that traces of endogenous metal ions, putatively being neurotoxic can, under many circumstances be neuroprotective [22]. One thing is for sure, the introduction of metals in our lives must be reduced, because it is changing the regular metal homeostasis of our body.

1.6.2. Parkinson's Disease

The second neurodegenerative disease for number of incidence is PD. From 1-2% of people over sixties are affected. The disease was described by James Parkinson in 1817 and from then it is still not clear the causes and cure.

PD is a slowly progressive disorder that affects movement, muscle control, and balance. There are two the main hallmarks of the disease: firstly, the accumulation of a protein (alpha-synuclein) into inclusions called Lewy bodies in neurons, and secondly the selective degeneration of neuromelanin-containing dopaminergic neurons in the substantia nigra (SN) and locus coeruleus occurs.

Metals, such as manganese, iron, copper and zinc are thought to be involved in PD. Metals can induce both an increase in oxidative stress and facilitate protein aggregation. Recent studies have shown that alpha-synuclein is able to interact with zinc, copper, and iron and these interactions lead to protein aggregation and crosslinking [23]. In patients affected with PD, a change in the homeostasis of metal ions occurs. Zinc and iron increase, while copper decreases in the SN [24]. Interesting work developed by I. Paris *et al.*, has shown that these metals are able to induce neurotoxicity by reacting with the neurotransmitter dopamine. Mn^{3+} is able to oxidize dopamine to aminochrome (see Fig. 1.6), and Cu^{2+} and Fe^{3+} form complexes with dopamine (see Fig. 1.7) [25].

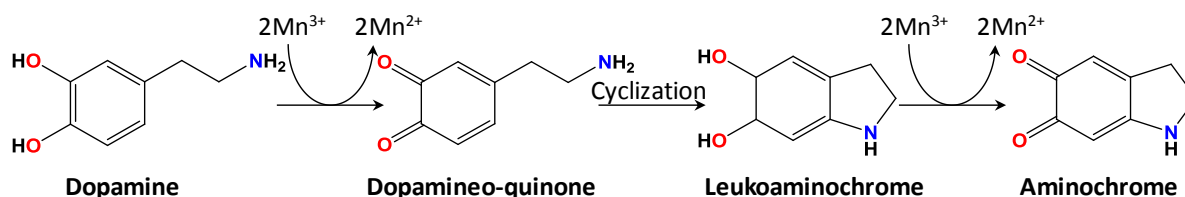


Figure 1.6. Dopamine oxidation to aminochrome catalyzed by manganese.

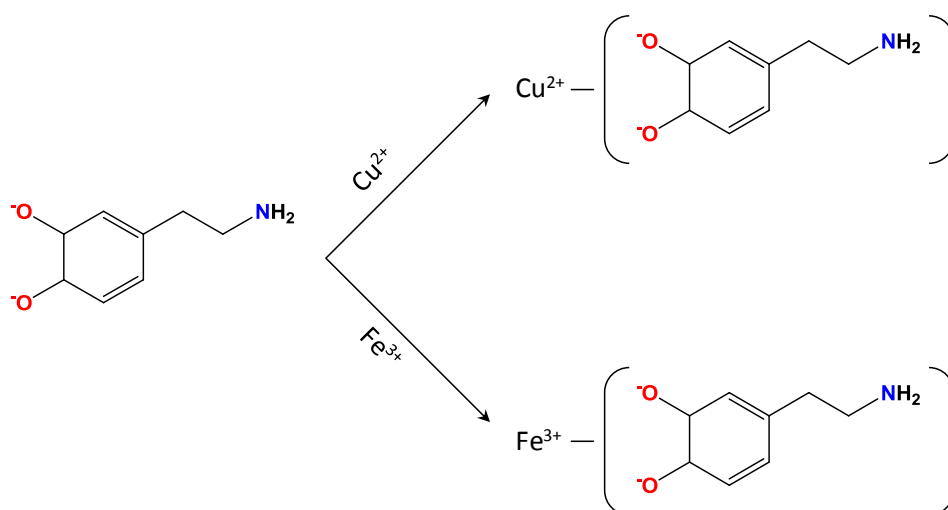


Figure 1.7. Cu^{2+} and Fe^{3+} abilities to form complexes with dopamine, based on ionic binding between the positive charges of metal ions and negative charges of dissociated hydroxyl groups.

1.6.3. Prion's Disease

Prion's disease also known as TSE's are a group of progressive neurodegenerative diseases. The term "prion" was introduced in 1982 by Stanley B. Prusiner that received a Nobel Prize in Physiology and Medicine in 1997 for this discovery. The term prion comes from the fusion of **proteinaceous** and **infectious**. Prion is in fact an infectious pathogen agent that causes a number of fatal neurodegenerative diseases through a new mechanism of action, not yet fully understood.

Prion is defined as proteinaceous because it appears to be without nucleic acid and exclusively constituted by a structural modification of the prion protein (PrP), which is a normal constituent of the living cells [26]. Prusiner, showed for the first time that the infectious agent was resistant to the treatments that destroy nucleic acids (which are based on virus), and was instead sensitive to agents that denature proteins. The normal PrP protein, called PrP^{C} is then converted to PrP^{Sc} through a process in which

there is a variation of the secondary and tertiary structures of the protein: a portion of α -helix is converted to a β -sheet (see Fig. 1.8), and this structural transition is accompanied by profound changes in the chemical-physical characteristics, such as insolubility and resistance to proteolysis. Prion diseases are transmissible genetic and sporadic, and can affect both men and animals. The forms that affect men include: Creutzfeldt-Jakob disease (CJD), Gertsman-Straussler-Schenker (GSS), Kuru and fatal insomnia. The disease can also affect different types of animals, including sheep (scrapie) and cattle (bovine spongiform encephalopathy, BSE). "Scrapie" that affect sheep's, is characterized not only by brain degeneration, but also by itching, causing injury to the woolly fleece.

The infectiousness of the disease was demonstrated, by inoculation of extracted contaminated brain to healthy animals. The first experiments were made on rodents that showed the disease after the injection of material from infected sheep. These and other studies showed that PrP^C is easily converted into the toxic form PrP^{Sc}, in the presence of another protein PrP^{Sc} [26]. In the 60s it was demonstrated the relationship between the scrapie disease and a disease found in populations that practiced cannibalism in New Guinea, called Kuru. Since that time, several diseases were found to have the same symptoms of the neurodegenerative diseases due to PrP [26]. Prion diseases have attracted a general interest when occurred the epidemic BSE ("mad cow disease") in England in 1986 and with the discovery of the possibility of the transmission to humans via food.

PrP is a glycoprotein, the primary structure is constituted by a polypeptide of 253 residues with a mass of about 34 kDa [27]. In the structure is present a characteristic domain 51-91 amino acid, in which is located a nonapeptide PQGGGGWGQ, followed by an octapeptide repeated for four times PHGGGWGQ. This region and the areas containing the histidine at position 96 and 111 are very important for the formation of bonds with metals, particularly with copper [27-28].

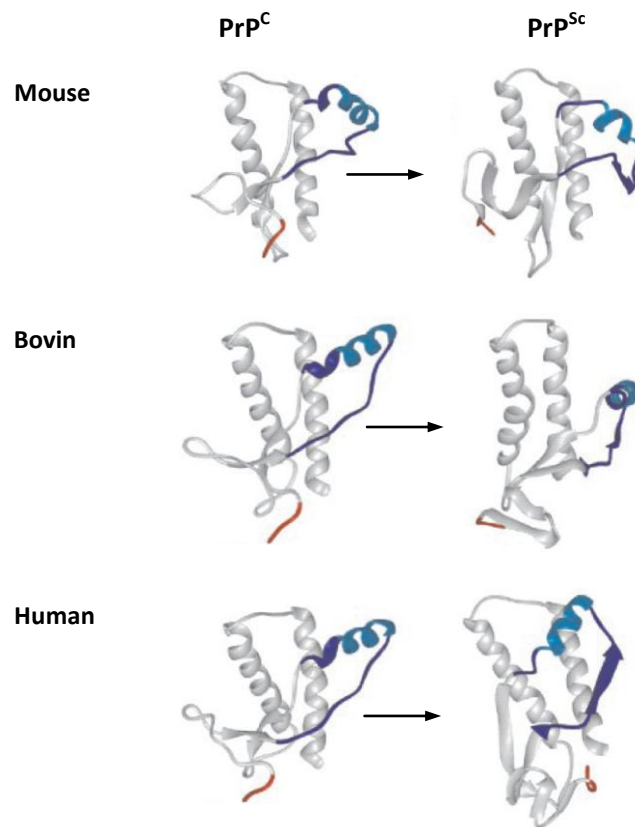


Figure 1.8. Molecular models of the conversion of PrP^C→PrP^{Sc}. Adapted from [29].

Affinity chromatography and circular dichroism (CD) measurements have demonstrated that the prion protein has higher affinity for metal ions, special copper and others (iron and manganese). A substantial difference between the two forms of PrP (normal and scrapie) is the affinity for copper; PrP^{Sc} prefers to bind manganese and zinc. It has been hypothesized a possible role of metal ions in the change of conformation of the PrP and thus in the onset of neurodegenerative diseases. The binding to copper has a direct consequence on the conformation of the terminal amino group of the molecule. Instead of a transition from α -helix to β -sheet, rotation and structuring occurs. It was hypothesized a relationship between PrP^C and PrP^{Sc} with metal ions in the onset of the disease (see Fig. 1.9) [27].

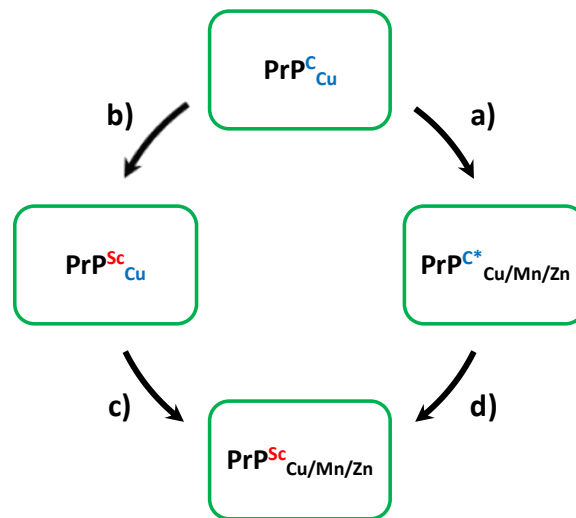


Figure 1.9. Hypothesis of the relationship between PrP^C, PrP^{Sc} with metal ions.

From the contact of PrP^C with copper (PrP^C_{Cu}) an abnormal form of PrP can be generated, called PrP^{C*}_{Cu/Mn/Zn} that it is not toxic, but has different properties compared to the normal PrP^C, as high insolubility and partial resistance to proteases. By the other hand, the toxic form PrP^{Sc}_{Cu} can derive directly from the native form by a mechanism not yet clearly understood. Changes in the protein conformation may change the affinity for metal ions, leading to the formation of new molecular species containing different metal ions, called PrP^{Sc}_{Cu/Mn/Zn}. Metal ions may also act directly on the intermediate form PrP^{C*}_{Cu/Mn/Zn} which becomes the toxic PrP^{Sc}_{Cu/Mn/Zn}. In conclusion, it is still necessary to verify the presence or absence of an intermediate in the conversion of PrP, and thus the possible involvement of metal ions in the conversion of the normal protein to the toxic form.

1.7. Diseases Caused by Metal Overload

1.7.1. Thalassemia

Thalassemia is a group of inherited disorders of globin synthesis due to defective or absent production of one of the globin chains (alpha, beta, gamma, delta) which constitute the molecules of human hemoglobin. The defective production of the globin chain determines a relative excess of the other, originating an imbalance which is the basis of the disease. Depending on the type of globin involved, two varieties of thalassemia can be distinguished, the beta- and alpha-thalassemia (β - and α -thalassemia, respectively). Due to its high frequency and gravity, β -thalassemia represents a significant health problem in many areas of the world, special in the Middle East, the Indian subcontinent, the Far East and in the Mediterranean area. In particular, in Italy the most affected regions are Sicily, Sardinia and near the river Po [30]. There is a strong correlation between these areas and the presence of *Falciparum malaria* in the past, because the natural selection has favoured the survival of people with the mutated gene that causes the disease. WHO has estimated that about 1-5% of the world's population might be healthy carriers of β -thalassemia and that about 60000 severely affected infants are born every year [31]. β -thalassemia occurs when the mutated genes are involved in the composition of the β -chains (on chromosome 11). There are two genes that can be affected. The mutation of a single gene, causes thalassemia minor, in which the patient has no relevant symptoms (see Fig. 1.10). The involvement of both genes constituting the β -chains of hemoglobin causes β -thalassemia major (Cooley's anemia), a severe symptomatology [32].

The conventional treatment of thalassemia includes transfusion therapy and iron chelation therapy. Transfusion therapy is used to correct anemia preventing the onset of cardiomyopathy and assuring the patient a regular growth, a good quality of life and normal resistance to infection.

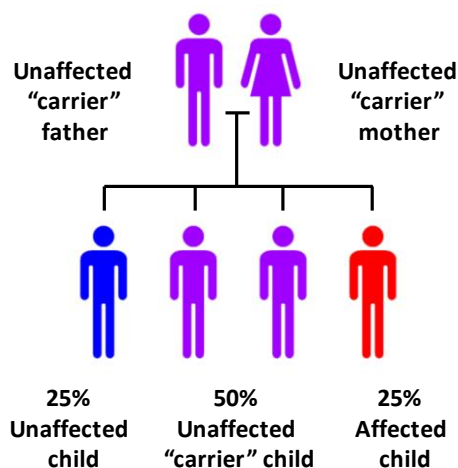


Figure 1.10. Inheritance of β -thalassemia. Unaffected carrier parents have 25% of probably to have a sick child (illustrated in red).

The transfusion regimen commonly adopted provides a blood transfusion every 2-4 weeks, maintaining the hemoglobin levels at about 110 g/L. To achieve this level, 1-3 units containing 200-250 mL of packed red cells (totaling about 200-250 mg of iron), are transfused. However, frequent transfusions cause iron deposition in the body (about 15-20 mg/day). Chelation therapy is therefore used to remove the excess of iron in order to maintain the right balance in the organism [33]. The most widely used chelating agent is DFO (see Fig. 1.13), which was introduced in the late 70's. From that date, mortality and complications related to the accumulation of iron have been drastically decreased. Nevertheless, DFO has various drawbacks; it is expensive, is poorly absorbed from the gut and it has short plasma half-life. For this reason, it has to be administered by slow subcutaneous infusions, leading to a very poor patient compliance. This explains why in the last 25 years, the chelation therapy research has been directed to the development of iron chelators orally administrable [30].

1.7.2. Wilson's Disease

Wilson's disease (WD), also known as hepatolenticular degeneration, was described for the first time in 1912 by Kinnear Wilson as a “progressive lenticular degeneration”. It is an hereditary lethal neurological disease, that is connected to a chronic liver disturb which leads to cirrhosis [34]. Only a few decades after its initial description, the role of copper in the pathogenesis of WD was determined, and the cause of hereditary was showed to be autosomal recessive [35]. In 1993, the abnormal gene in WD has been identified. This gene encodes the P-type adenosine triphosphatase (ATP7B), it is present in the hepatocytes and works in the transmembrane transport of copper to hepatocytes. The absence, or reduction of the functionality, of the ATP7B protein leads to a hepatocellular reduction, excretion of copper into bile, resulting in hepatic accumulation of copper. Finally, copper is released into the bloodstream and deposited in other organs, particularly in the brain, kidneys and cornea (called “Kayser-Fleischer rings”, showed in Fig. 1.11) [36-37].



Figure 1.11. Bilateral Kayser–Fleischer rings (panel **A**, within arrows). Five years after the initiation of copper-chelating treatment, the Kayser–Fleischer ring has almost disappeared (panel **B**) [37].

The failure to incorporate copper into ceruloplasmin (CP) is a further consequence of the loss of the function of ATP7B protein [38]. In WD the loss of ATP7B functionality leads to the synthesis of apoceruloplasmin, which is rapidly degraded in plasma.

Consequently, the concentration of serum CP is a very useful diagnostic parameter for WD [39]. About half of the patients with WD have signs and symptoms of neuropsychiatric disorders [40]. Often the neurological symptoms are initially undetectable. Patients not treated with chelation therapy have additional PD symptoms, due to the accumulation of copper in the basal ganglia [41]. The worldwide frequency of WD is estimated to be one for 35000-100000 people. However, in Sardinia, the disease has a higher frequency, with an incidence of one to 7000 people [42].

1.8. Chelators for Metals

1.8.1. Iron Chelators

Iron is one of the most important metals in our organism, and is critically fundamental for a variety of cellular events. In fact, no life form is possible without the presence of this element. Human metabolism is highly conservative with the majority of iron being recycled within the body. In a normal case, iron levels are under extremely tight control and practically iron-catalysed reactions that generate free radicals do not occur. However, this delicate equilibrium between iron uptake and iron loss can be broken, and this is the case of patients that suffer from iron overload. One of the most serious disease where iron overload plays an important role is β -thalassemia major. In order to protect patients from iron toxicity, iron chelating agents have been introduced in clinical practices. Unfortunately, an ideal chelator for treating iron overload in humans has not been identified yet.

Iron(III) is a spherically symmetrical tripositive cation of radius 0.65 Å, and is classified as a hard Lewis acid by virtue of its high charge density. It forms stable bonds with hard ligands which contain oxyanions as functional groups, such as catechols,

hydroxamates, aminocarboxylates, hydroxycarboxylates, hydroxypyridinones (HPOs) and hydroxypyrones.

1.8.1.1. Catechols

Catechol, as a functional group, is found in Enterobactin (see Fig. 1.12), a siderophore that acquires iron for microbial systems. It is primarily found in Gram-negative bacteria, such as *Escherichia coli* and *Salmonella typhimurium* [43]. In order to mimic the natural siderophore molecule, MECAM (1,3,5-N,N',N''-tris-(2,3-dihydroxybenzoyl)triaminomethylbenzene, see Fig. 1.12), was synthesized.

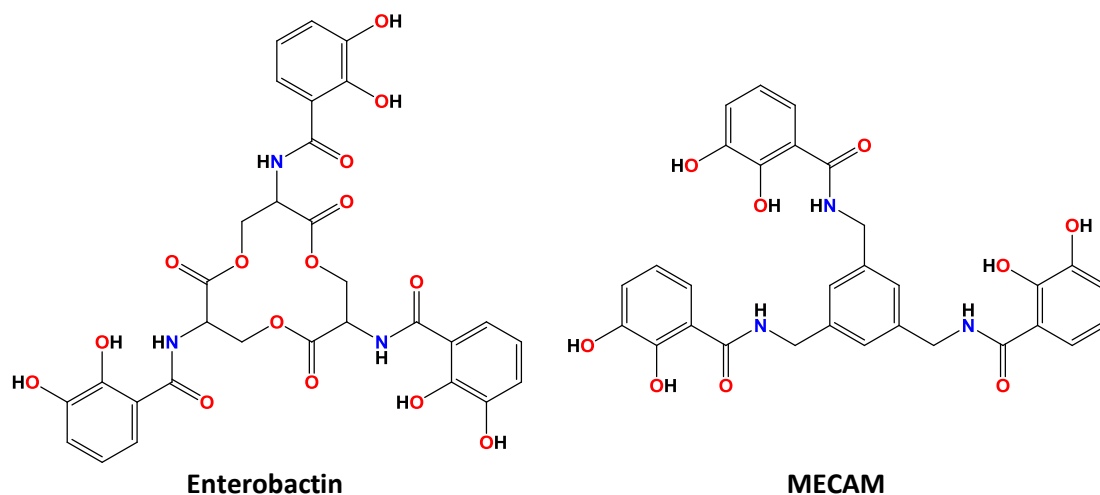


Figure 1.12. Hexadentate catechols.

MECAM binds strongly to iron with a pFe value of about 28 [44]. Considering only the catechol moiety, it has high electron density on both oxygen atoms. However, this high charge density is also associated with the high affinity for protons (pKa values of 12.1 and 8.4) [45]. Thus, the binding of cations by catechol has marked pH sensitivity. On

the other hand, the ligand, at physiological (pH 7.4), is in the totally protonated form and consequently having a net charge equal to zero it is able to penetrate the cell membranes more efficiently than a charged molecule.

1.8.1.2. Hydroxamates

Another important natural hexadentate ligand is DFO (see Fig. 1.13). DFO is the only iron chelating agent discovered for more than 40 years, and still continues to be extensively used. It is a siderophore produced by *Streptomyces pilosus* [46], and consists in three hydroxamate moieties. Compounds containing only a hydroxamate moiety are bidentate, (see Fig. 1.13) and can form 1:3 metal:ligand complexes at pH 7.4 and sufficient ligand concentration. The protonation constant ($pK_a \sim 9$), lower than that of the catechol moiety, allows the formation of stronger iron-ligand complexes. However, the affinity of the simple bidentate hydroxamate ligand for iron is insufficient to solubilize iron(III) at pH 7.4 at clinical concentrations. For this reason, only tetradentate and hexadentate ligands are considered as possible iron(III) scavengers under such conditions [44].

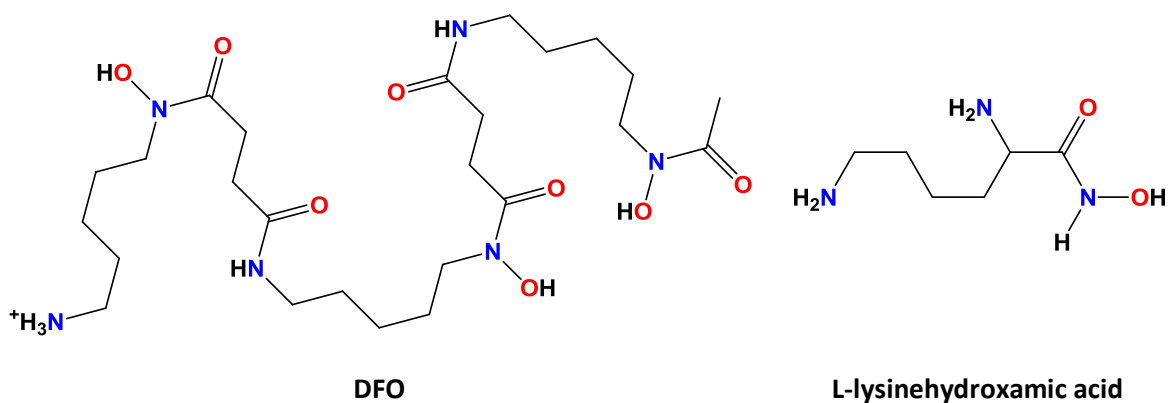


Figure 1.13. Hexadentate (DFO) and bidentate (L-lysinehydroxamic acid) hydroxamates.

1.8.1.3. Aminocarboxylates

This category includes EDTA and DPTA (see above Fig. 1.1) that are both able to chelate strongly to iron. However, they are not selective for iron and remove also other essential metals from the body like zinc. This ability is useful in certain plants like wheat, barley, rye, and oat: plants secrete phytosiderophores such as mugineic acid, shown in Fig. 1.14, from their roots which are capable of complexing iron(III) and zinc [47]. Moreover, the complexes formed with iron can catalyze redox reactions producing free radicals. Indeed, the redox potential of $\text{Fe}^{3+}/\text{EDTA}$ complex (+0.12 V/NHE) allows its reduction by physiological reductants [48].

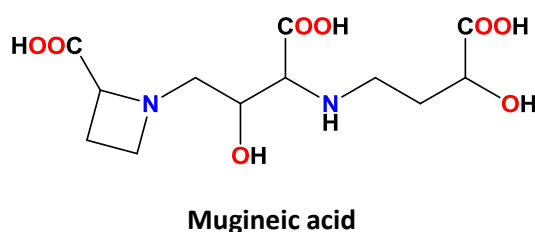


Figure 1.14. Aminocarboxylates.

1.8.1.4. Hydroxycarboxylates

Hydroxycarboxylates only have oxygen coordinating atoms, and they are more selective for iron than aminocarboxylates. This category includes rhizoferrin and its precursor citrate (see Fig. 1.15). Rhizoferrin was firstly isolated from *Rhizopus microsporus var. rhizopodiformis*, and it is able to form 1:1 iron-ligand complexes, similarly to DFO [49].

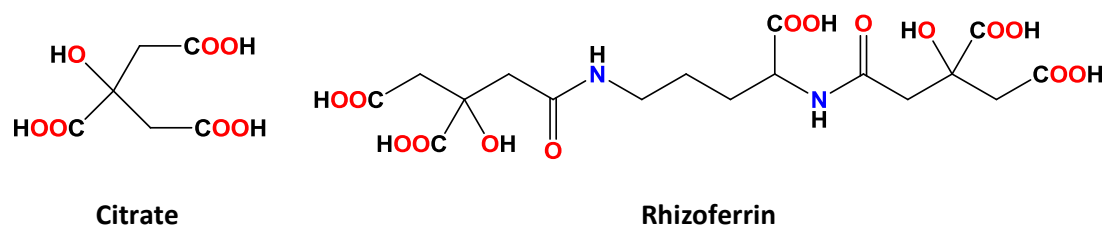


Figure 1.15. Hydroxycarboxylates.

1.8.1.5. Hydroxypyridinones

Hydroxypyridinones (HPOs) are a family of *N*-heterocyclic core chelators which combine the characteristics of the functional groups hydroxamates and catechols. They are the most studied class of compounds, due to the higher chelating capacity and selectivity for iron. The carbonyl and the phenolic oxygen coordinate iron, forming a stable 5-membered ring.

There are three main families of HPOs, namely, 1-hydroxypyridin-2-one (1,2-HP), 3-hydroxypyridin-2-one (3,2-HP), and 3-hydroxypyridin-4-one (3,4-HP), see Fig.1.16. At the last family takes part the 1,2-dimethyl-3-hydroxypyridin-4-one, called deferiprone (DFP or L1), which has the highest value of pFe 20.67 [48]. It is the most important oral chelator currently in use. Many derivatives have been synthesized by combining two or three units of HPOs [50-53] (see Fig. 1.16), due to the particular structure of the 6-membered ring scaffold that offers many possibilities of functionalization at different ring-positions, enabling the modulation of bioavailability and possibility of the interaction with several biological targets.

Tren(3,4-HP)₃ has an extremely high pFe value of 30.5 [52]. Unfortunately, tris-compounds have molecular weights too high to be absorbed in the gastrointestinal tract, and consequently they cannot be orally administered.

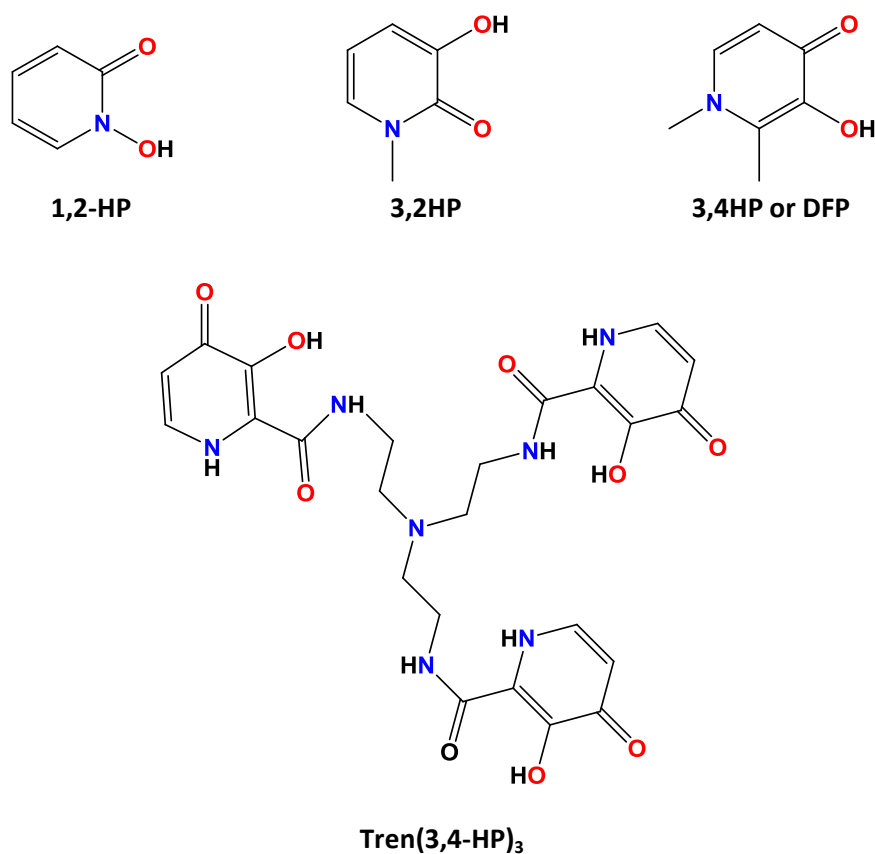


Figure 1.16. Bidentate and hexadentate HPOs.

1.8.1.6. Hydroxypyrones

In resemblance to HPOs, hydroxypyrones chelate iron forming stable five-membered rings. Hydroxypyrones differ for the oxygen in the ring which gives less affinity to the proton and consequently the pKa values are lower than that of HPOs, for more than two orders of magnitudes. For instance DFP has pKa 9.8 [48] and kojic acid pKa 7.7 [54].

Kojic acid (see Fig.1.17) is one of the most studied hydroxypyrones in the literature. It contains a polyfunctional heterocyclic ring, with several important centers enabling the occurrence of additional reactions like oxidation and reduction, alkylation and

acylation, nucleophilic and electrophilic substitution reactions. Kojic acid is a promising molecule for the development of more potent derivatives. Indeed, considering the ligands recently studied in our research group, namely L1, L2, and L3 (see Fig. 1.17), that are formed by two units of kojic acid joined by different linkers, the pFe values found were 23.1, 18.9 and 22.2, respectively [54-55], that are several orders of magnitude higher than that of the precursor. One of the most important advantages of these molecules is that they are easy and inexpensive to produce.

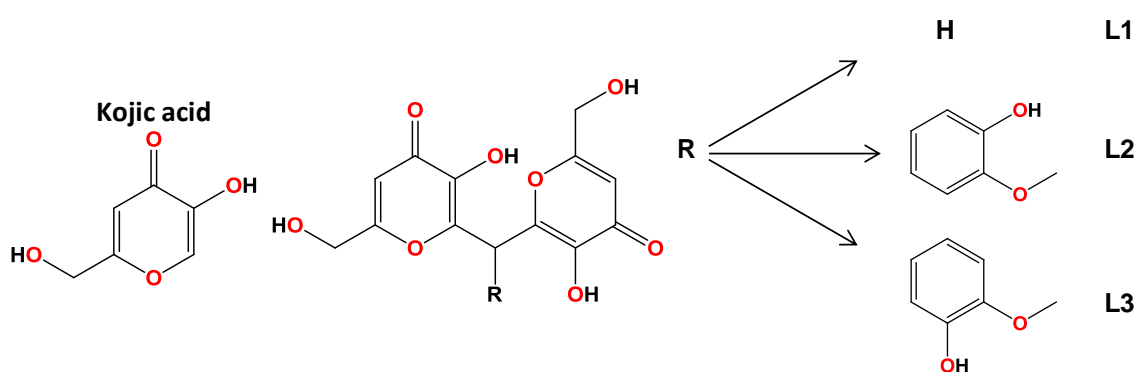


Figure 1.17. Kojic acid derivatives.

1.8.2. Aluminium chelators

Aluminium is the third most abundant element in earth's crust, after oxygen and silicon, and it is the most abundant metal. Due to its versatility, in the last century has been widely used in industry, for instance in automotive, and space aeronautics industries [56]. Also, it is used in the production of paper and textiles, in many cosmetics [57], in pharmaceutical drugs for human and veterinary medicine [58], in antiperspirants and in a variety of products that are in close contact with our skin. Aluminium salts are utilized in alimentary industry [59]. Additionally, aluminium salts are used in water purification, as well as in brewing and sugar refining [60].

Aluminium is not an essential metal for the human body [56], and its abuse can produce dangerous effects on our health. Since 1970, aluminium was recognized to cause serious diseases, such as osteodystrophy and dialysis dementia in patients with renal failure under dialysis treatment. The awareness of aluminium toxicity has led several research groups to study new possibilities for chelating agents, some of them being already used for iron chelation. Both iron and aluminium, due to their short ionic radius and their high charge, are hard metals. As seen for iron, also aluminium prefers to coordinate with hard bases containing oxygen atoms, as hydroxamates, catecholates, bisphosphonates, salicylates, HPOs and hydroxypyrones [61].

The first aluminium chelator, introduced in clinical practice, for osteomalacia was DFO (Fig. 1.13) [62]. In recent years, various chelating agents were synthesized. In particular, HPOs derivatives have been extensively studied (see Fig. 1.18).

Different polydentate 3,4-HP chelators have been proposed by the group of M. A. Santos: the tetradentate iminodiacetic acid bis-(3,4-HP) and derivatives called IDAPr(3,4-HP)₂ [63]; a ternary system composed by an arylpiperazine-containing bis-hydroxypyridone [51]; two hexadentate ligands, the tris-hydroxypyridinone-based compounds KEMPPr(3,4-HP)₃ and KEMPBu(3,4-HP)₃, derived from KEMP acid scaffold to which three 3,4-HP chelating moieties are attached via different size spacers [52]; two new tripodal tris(3,4-HP) hexadentate chelators NTA(BuHP)₃ and NTP(PrHP)₃ (NTA = nitrilotriacetic acid, NTP = nitrilotripropionic acid) [64-65]. The last hexadentate ligands present extremely high pAl values, 22.0 for NTA(BuHP)₃ and 22.4 for NTP(PrHP)₃. Other ligands with good pAl values are tripodal O-TRENSEX and the similar triscatechol derivative TRENCAMS, with values of pAl 20.0 and 26.2, respectively [66]. Bisphosphonate ligands were found to be very efficient chelating agents for Al³⁺. The stabilities of the complexes formed are higher than that found for DFP (pAl 16.05) and very close to DFO (pAl 19.43) [67-69]. Hydroxypyrene ligands

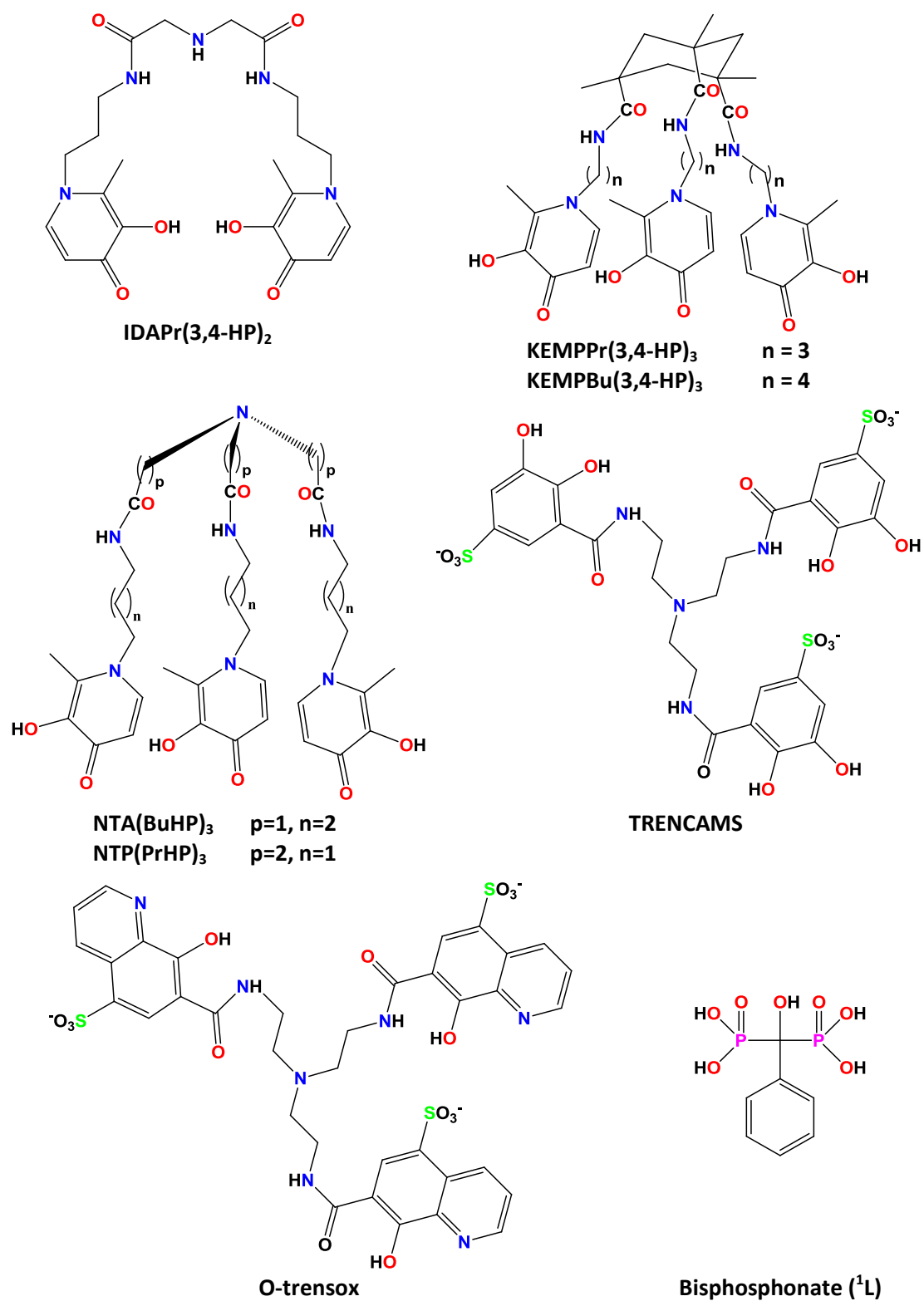


Figure 1.18. Aluminium chelators.

studied in our group of research (see Fig. 1.17), formed by two units of kojic acid linked by a methyl group (L1), orto-vanillin (L2), and vanillin (L3), are capable to chelate aluminium. From these, L3 has the highest value of $pAl= 13.9$ [55].

1.8.3. Copper Chelators

Copper was the first metal discovered by man and is still today extensively used. Copper production has lifted over the last decades and continues to increase, meaning that more copper ends up in the environment. World refined copper consumption amounts to 20.5 million tons in 2011 (16.7 million tons were achieved in 2005) [70]. Copper is a transition metal ion essential for human health. It acts as catalytic or structural cofactor of many enzymes. It is required for the development and function of nervous and cardiovascular systems and it is fundamental for skin, bone, reproductive and immune systems. Many body functions such as collagen production, formation of red blood cells, regulation of cholesterol level, iron adsorption, oxidation of fatty acids, melanin production and intracellular energy level control are all dependent on copper. The treatment for copper overloading or intoxication is chelation therapy. Different molecules are already in clinical use as chelators or under study in clinical trials. The three most important chelators used for the treatment of WD are D-penicillamine (D-pen), triethylenetetramine (trentine, Trien) and ammonium tetrathiomolibdate (TTM), whose structures are reported in Fig. 1.19.

The very first chelator used for WD was BAL (Fig. 1.1), originally developed during the World War II as an antidote for lewisite, a chemical warfare agent, which was later employed to treat metal intoxications [71]. After, it was replaced by the less toxic and orally available D-pen that it is still used today, although Trien revealed to be better tolerated [72]. TTM showed a remarkable efficacy in the treatment of patients with neurological symptoms [73], but unfortunately is not yet allowed for chemical

treatment. Other potentially efficient ligands, with higher specificity for certain tissues, are the sulfurated polydentate chelators as P^c (see Fig. 1.20) [74]. P^c has a very high selectivity for Cu^+ versus Zn^{2+} (ca. 10 orders of magnitude) [75].

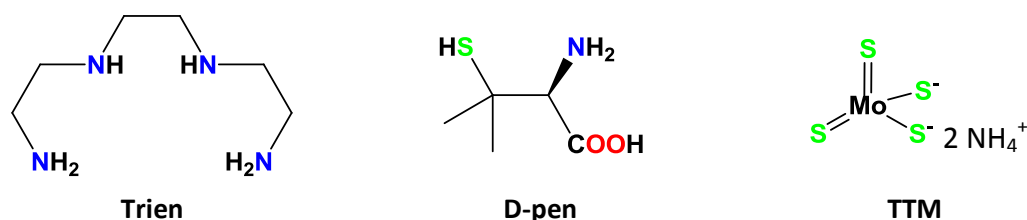


Figure 1.19. Main copper chelators for the treatment of WD.

Interesting examples of tripodal Cys-rich chelators have been reported (HnL^x , see Fig. 1.20) [76-77], which has been suggested to act as potential Cu^+ chelators *in vivo*. L^1 and L^2 forms very stable mononuclear and polynuclear Cu^+ complexes and they are selective for Cu^+ versus Zn^{2+} ; whereas the ligand L^3 gives polynuclear Cu^+ complexes of lower stability. An additional chelating agent for copper is Clioquinol (5-chloro-7-iodo-8-hydroxyquinoline, CQ, see Fig. 1.20) is an aromatic chelator which coordinates metal ions through its (*N,O*-) donor set [78]. CQ has been used in the past as an antibiotic [79], and more recently, as antiproliferative agents against tumor cell lines, in the form of copper complexes [78]. CQ was also found to reduce the formation of amyloid plaques [80], being able to partially disaggregate Cu-triggered $A\beta$ aggregates by virtue of its high affinity for Cu^{2+} [81]. Two CQ analogs have been reported in the literature, consisting of two 8-hydroxyquinoline moieties linked through a spacer (C1, C2, showed in Fig. 1.20) [82-84]. These tetradentate ligands, C1 and C2, showed higher copper binding affinities and remarkable capacity to reduce the production of ROS.

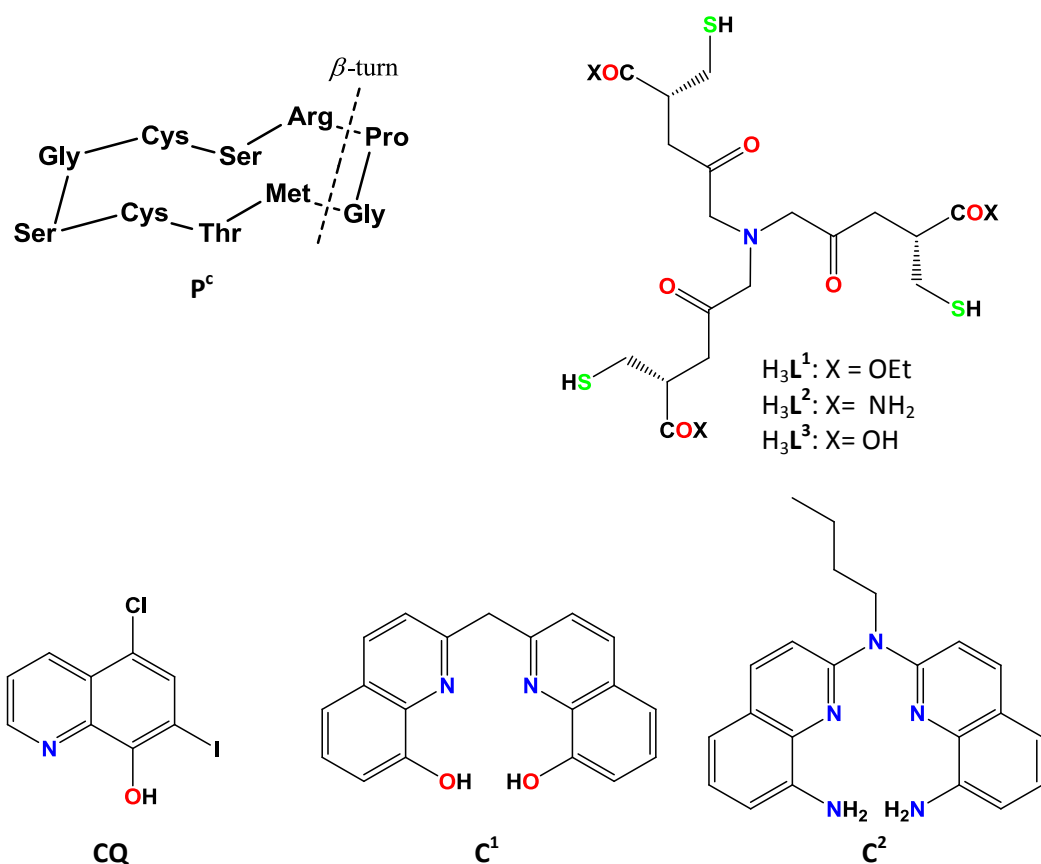


Figure 1.20. Copper chelators.

In recent years several bifunctional (BF) chelators for AD have been synthesized. BF are ligands that, beside the presence of a metal ion binding site, are designed to have a second function. This additional function can originate, for instance, the presence of a reducing moiety capable to inhibit the formation of ROS, or a group that may favor mechanisms of active transport of the chelator across membranes. Additional functions have also been introduced to prepare prodrugs, in which an activatable/cleavable protecting group allows the chelator to be inactive until it reaches specific tissues. Here, the protecting group is removed by enzymes or by ROS species making the chelator available for metal complexation. The general idea is that the introduction of a second function allows the chelator to work only under specific

conditions, in specific tissues, or in the presence of specific biomolecules [85]. There are three types of approaches used to synthesize BF_s for AD:

- the *incorporation* of a chelating moiety into a scaffold known to interact with A β , for instance KO ligand (Fig. 1.22), has been designed by merging the structural feature of CQ and the scaffold IMPY (see Fig. 1.21) [86-87];
- the *linkage* of a chelating group to a molecule that interacts with A β , as XH1 (see Fig.1.22) formed by two units of Tht (see Fig. 1.21) linked to DTPA [88];
- the *peptide* approach, as example Cyc-KLVFF (see Fig. 1.22) a cyclen moiety attached to a N-terminus of the KLVFF fragment (see Fig.1.21) [89], this oligopeptide is a β -sheet breaker which inhibits A β aggregation [90-93].

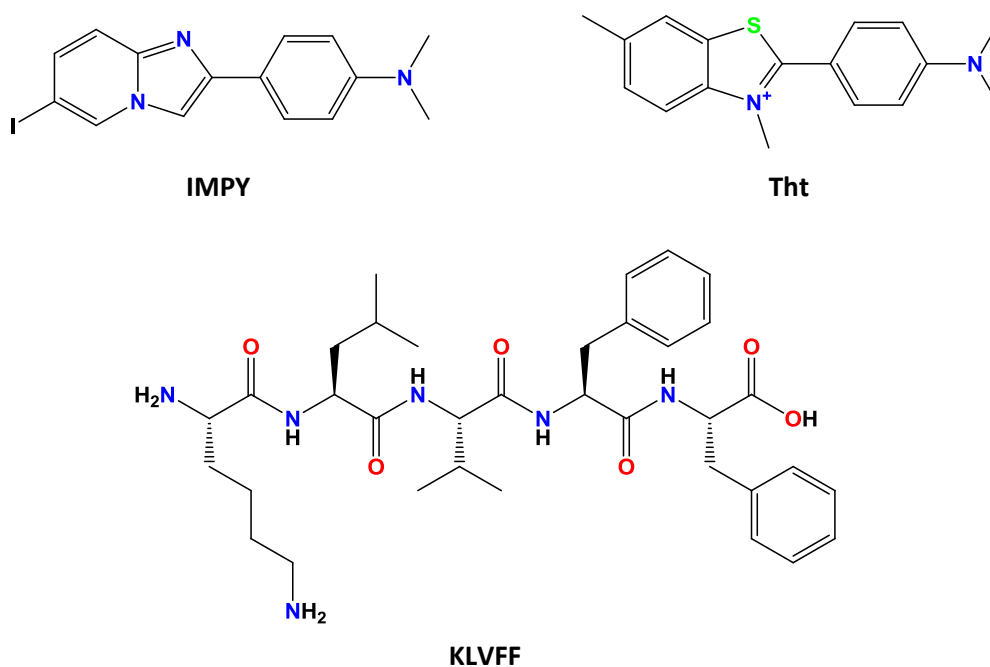


Figure 1.21. Molecules capable to interact with A β .

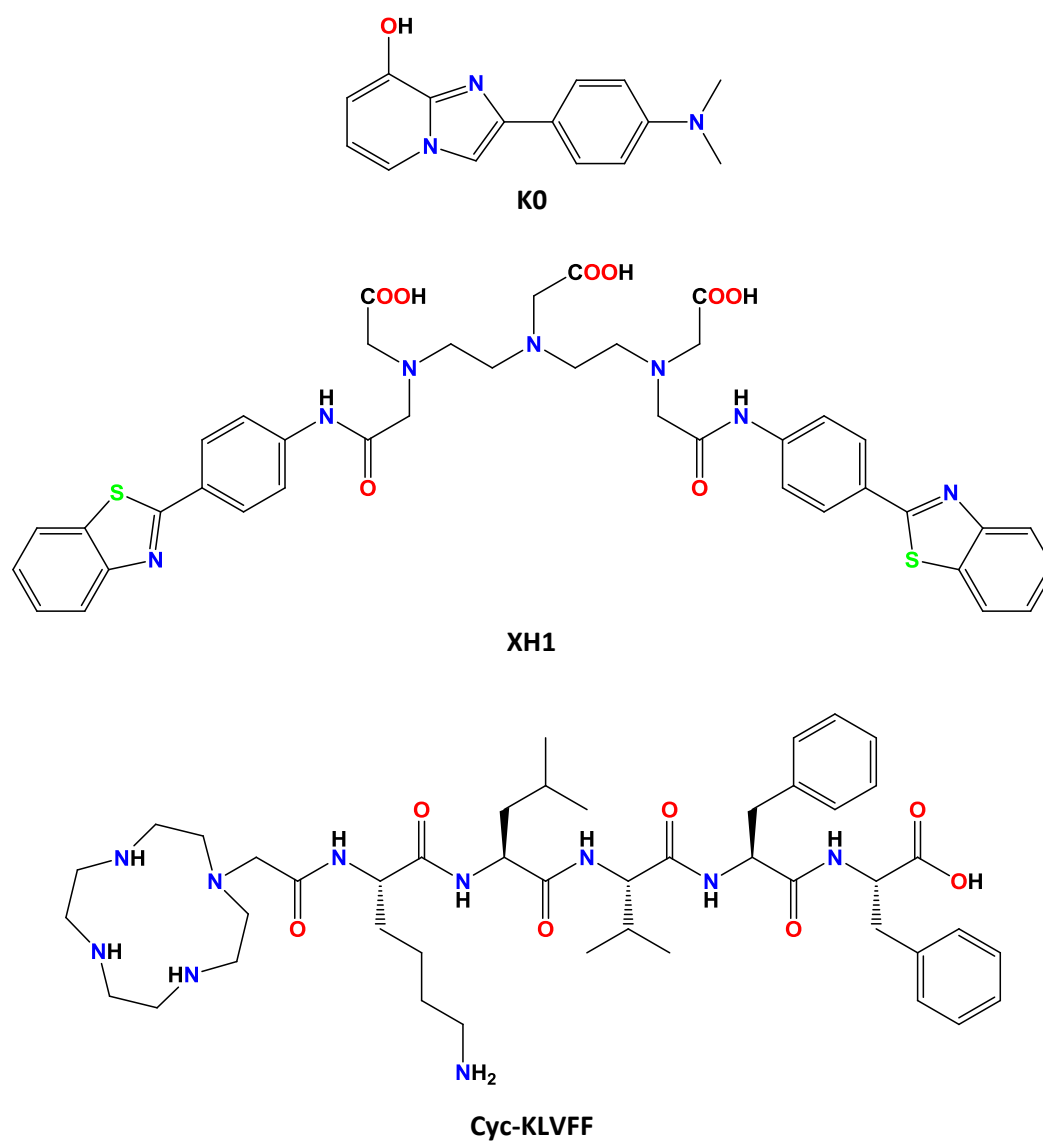


Figure 1.22. Example of incorporation (K0), linkage (XH1) and peptide (Cyc-KLVFF) approach.

1.9. Bibliography

- [1] M.G. Ord, L.A. Stocken, *A contribution to chemical defence in World War II*, Trends in Biochemical Sciences. 25 (2000) pp. 253-256.
- [2] R.A. Peters, L.A. Stocken, R.H.S. Thompson, *British Anti-Lewisite (BAL)*, Nat Biotechnol. (24 November 1945) pp. 616-619.
- [3] S.J.S. Flora, V. Pachauri, *Chelation in metal intoxication*, International Journal of Environmental Research and Public Health. 7 (2010) pp. 2745-2788.
- [4] G. Crisponi, V.M. Nurchi, M. Crespo-Alonso, L. Toso, *Chelating agents for metal intoxication*, Curr Med Chem. 19 (2012) pp. 2794-2815.
- [5] A.S. H.G. Seiler, H. Sigel, Handbook on Metals in Clinical and Analytical Chemistry. pp. 13.
- [6] E.J. Baran, *Chelation therapies: A chemical and biochemical perspective*, Curr Med Chem. 17 (2010) pp. 3658-3672.
- [7] F. Albert Cotton, G. Wilkinson, C.A. Murillo, M. Bochmann, *Advanced Inorganic Chemistry sixth Edition*, (1999) pp. 27-28.
- [8] R.G. Pearson, *Hard and Soft Acids and Bases*, Journal of the American Chemical Society. 85 (1963) pp. 3533-3539.
- [9] P. Faller, *Summer School of Bioinorganic Chemistry*, (2013) pp. 1-5.
- [10] V.M. Nurchi, M.C. Alonso, L. Toso, J.I. Lachowicz, G. Crisponi, *Chelation therapy for metal intoxication: comments from a thermodynamic viewpoint*, Mini Rev Med Chem. 13 (2013) pp. 1541-1549.
- [11] R.M. Murphy, *Peptide aggregation in neurodegenerative disease*, Annu Rev Biomed Eng. 4 (2002) pp. 155-174.
- [12] E. Rizzarelli, *Protein misfolding diseases and metal ions*, Ph.D Seminar, (2001 Parma) pp. 1-20.

- [13] M. Prince, R. Bryce, C. Ferri, *World Alzheimer Report 2011 : the benefits of early diagnosis and intervention*, Alzheimer's Disease International (ADI). (2011) pp. 1.
- [14] L.F. Querfurth HW, *Alzheimer's Disease*, New England Journal of Medicine. 362 (2010) pp. 1844-1845.
- [15] M.A. Lovell, J.D. Robertson, W.J. Teesdale, J.L. Campbell, W.R. Markesbery, *Copper, iron and zinc in Alzheimer's disease senile plaques*, Journal of the Neurological Sciences. 158 (1998) pp. 47-52.
- [16] C.J. Frederickson, J.Y. Koh, A.I. Bush, *The neurobiology of zinc in health and disease*, Nat Rev Neurosci. 6 (2005) pp. 449-462.
- [17] J.R. Walton, *Brain lesions comprised of aluminum-rich cells that lack microtubules may be associated with the cognitive deficit of Alzheimer's disease*, NeuroToxicology. 30 (2009) pp. 1059-1069.
- [18] Henryk Kozłowski, David R Brown, G. Valensin, *Metallochemistry of Neurodegeneration: Biological, Chemical and Genetic Aspects*, RSC Publishing, Cambridge. (2006) pp. 1-277.
- [19] A. Granzotto, P. Zatta, in: W. Linert, H. Kozłowski (Eds.), *Metal Ions in Neurological Systems*, Springer Vienna, 2012, pp. 77-83.
- [20] D.G. Smith, R. Cappai, K.J. Barnham, *The redox chemistry of the Alzheimer's disease amyloid beta peptide*, Biochim Biophys Acta. 1768 (2007) pp. 1976-1990.
- [21] G.M. Bishop, S.R. Robinson, *The amyloid paradox: amyloid-beta-metal complexes can be neurotoxic and neuroprotective*, Brain Pathol. 14 (2004) pp. 448-452.
- [22] G. Crisponi, V.M. Nurchi, D. Fanni, C. Gerosa, S. Nemolato, M.C. Alonso, L. Toso, J.I. Lachowicz, G. Faa, *Metal Ions in the Pathogenesis of Alzheimer's Disease: An Open Field* Frontiers in Clinical Drug Research – Alzheimer Disorders. 1 (2013) pp. 411-431.
- [23] N.B. Cole, D.D. Murphy, J. Lebowitz, L. Di Noto, R.L. Levine, R.L. Nussbaum, *Metal-catalyzed oxidation of alpha-synuclein: helping to define the relationship between oligomers, protofibrils, and filaments*, J Biol Chem. 280 (2005) pp. 9678-9690.

- [24] K.J. Barnham, A.I. Bush, *Metals in Alzheimer's and Parkinson's diseases*, *Curr Opin Chem Biol.* 12 (2008) pp. 222-228.
- [25] I. Paris, J. Segura-Aguilar, *The role of metal ions in dopaminergic neuron degeneration in Parkinsonism and Parkinson's disease*, *The role of metal ions in dopaminergic neuron degeneration in Parkinsonism and Parkinson's disease. Metal Ions in Neurological Systems.* (2012) pp. 31-39.
- [26] S.B. Prusiner, *Prions*, *Proc. Natl. Acad. Sci. USA.* 95 (1998 November) pp. 13363–13383.
- [27] S. Lehmann, *Metal ions and prion diseases*, *Current Opinion in Chemical Biology.* 6 (2002) pp. 187-192.
- [28] M. Remelli, D. Valensin, L. Toso, E. Gralka, R. Guerrini, E. Marzola, H. Kozlowski, *Thermodynamic and spectroscopic investigation on the role of Met residues in Cu(II) binding to the non-octarepeat site of the human prion protein*, *Metallomics.* 4 (2012) pp. 794-806.
- [29] B.J. Bennion, V. Daggett, *Protein conformation and diagnostic tests: The prion protein*, *Clinical Chemistry.* 48 (2002) pp. 2105-2114.
- [30] G. Crisponi, V.M. Nurchi, R. Silvagni, G. Faa, *Oral iron chelators for clinical use*, *Polyhedron.* 18 (1999) pp. 3219-3226.
- [31] B. Modell, M. Darlison, *Global epidemiology of haemoglobin disorders and derived service indicators*, *Bulletin of the World Health Organization.* 86 (2008) pp. 480-487.
- [32] D.R. Higgs, J.D. Engel, G. Stamatoyannopoulos, *Thalassaemia*, *The Lancet.* 379 (2012) pp. 373-383.
- [33] G.J. Kontoghiorghes, E. Eracleous, C. Economides, A. Kolnagou, *Advances in iron overload therapies. Prospects for effective use of deferiprone (L1), deferoxamine, the new experimental chelators ICL670, GT56-252, L1NAll and their combinations*, *Curr Med Chem.* 12 (2005) pp. 2663-2681.
- [34] S.A.K. Wilson, M.R.C.P. Lond, *Progressive lenticular degeneration: a familiar nervous disease associated with cirrhosis of the liver* *Brain.* 34 (1912) pp. 296-509.

- [35] M. Südmeyer, A. Saleh, L. Wojtecki, M. Cohnen, J. Gross, M. Ploner, H. Hefter, L. Timmerman, A. Schnitzler, *Wilson's disease tremor is associated with magnetic resonance imaging lesions in basal ganglia structures*, *Movement Disorders*. 21 (2006) pp. 2134-2139.
- [36] R.E. Tanzi, K. Petrukhin, I. Chernov, J.L. Pellequer, W. Wasco, B. Ross, D.M. Romano, E. Parano, L. Pavone, L.M. Brzustowicz, M. Devoto, J. Peppercorn, A.I. Bush, I. Sternlieb, M. Pirastu, J.F. Gusella, O. Evgrafov, G.K. Penchaszadeh, T.C. Gilliam, *The Wilson disease gene is a copper transporting ATPase with homology to the Menkes disease gene*, *Nature Genetics*. 5 (1993) pp. 344-350.
- [37] A. Schrag, J.M. Schott, *Kayser-Fleischer rings in Wilson's disease*, *New England Journal of Medicine*. 366 (2012) pp. e18.
- [38] N.A. Holtzman, B.M. Gaumnitz, *Studies on the Rate of Release and Turnover of Ceruloplasmin and Apoceruloplasmin in Rat Plasma*, *J Biol Chem*. 245 (1970) pp. 2354-2358.
- [39] N.E. Hellman, J.D. Gitlin, *Ceruloplasmin metabolism and function*, *Annu Rev Nutr*. 22 (2002) pp. 439-458.
- [40] J.L. Gollan, *Wilson disease in 1998: Genetic, diagnostic and therapeutic aspects*, *Journal of Hepatology*, Supplement. 28 (1998) pp. 28-36.
- [41] W. Oder, G. Grimm, H. Kollegger, P. Ferenci, B. Schneider, L. Deecke, *Neurological and neuropsychiatric spectrum of Wilson's disease: A prospective study of 45 cases*, *J Neurol*. 238 (1991) pp. 281-287.
- [42] G. Loudianos, V. Dessi, M. Lovicu, A. Angius, A. Figus, F. Lilliu, S. De Virgiliis, A.M. Nurchi, A. Deplano, P. Moi, M. Pirastu, A. Cao, *Molecular characterization of Wilson disease in the Sardinian population - Evidence of a founder effect*, *Human Mutation*. 14 (1999) pp. 294-303.
- [43] E.A. Dertz, J. Xu, A. Stintzi, K.N. Raymond, *Bacillibactin-Mediated Iron Transport in Bacillus subtilis1*, *Journal of the American Chemical Society*. 128 (2005) pp. 22-23.
- [44] Z.D. Liu, R.C. Hider, *Design of iron chelators with therapeutic application*, *Coordination Chemistry Reviews*. 232 (2002) pp. 151-171.

- [45] R.C. Hider, A.R. Mohd-Nor, J. Silver, I.E.G. Morrison, L.V.C. Rees, *Chem. Soc. Dalton Trans.* 2 (1981) pp. 609.
- [46] G. Faa, G. Crisponi, *Iron chelating agents in clinical practice*, *Coordination Chemistry Reviews*. 184 (1999) pp. 291-310.
- [47] N. von Wiren, H. Khodr, R.C. Hider, *Hydroxylated phytosiderophore species possess an enhanced chelate stability and affinity for iron(III)*, *Plant Physiol.* 124 (2000) pp. 1149-1158.
- [48] G. Crisponi, M. Remelli, *Iron chelating agents for the treatment of iron overload*, *Coordination Chemistry Reviews*. 252 (2008) pp. 1225-1240.
- [49] R.J. Bergeron, M. Xin, R.E. Smith, M. Wollenweber, J.S. McManis, C. Ludin, K.A. Abboud, *Total synthesis of rhizoferrin, an iron chelator*, *Tetrahedron*. 53 (1997) pp. 427-434.
- [50] M.A. Santos, S.M. Marques, S. Chaves, *Hydroxypyridinones as "privileged" chelating structures for the design of medicinal drugs*, *Coordination Chemistry Reviews*. 256 (2012) pp. 240-259.
- [51] S. Gama, M. Gil, L. Gano, E. Farkas, M. Amélia Santos, *Combined chelation of bi-functional bis-hydroxypyridinone and mono-hydroxypyridinone: Synthesis, solution and in vivo evaluation*, *Journal of Inorganic Biochemistry*. 103 (2009) pp. 288-298.
- [52] R. Grazina, L. Gano, J. Šebestík, M. Amelia Santos, *New tripodal hydroxypyridinone based chelating agents for Fe(III), Al(III) and Ga(III): Synthesis, physico-chemical properties and bioevaluation*, *Journal of Inorganic Biochemistry*. 103 (2009) pp. 262-273.
- [53] S. Piyamongkol, T. Zhou, Z.D. Liu, H.H. Khodr, R.C. Hider, *Design and characterisation of novel hexadentate 3-hydroxypyridin-4-one ligands*, *Tetrahedron Lett.* 46 (2005) pp. 1333-1336.
- [54] V.M. Nurchi, G. Crisponi, J.I. Lachowicz, S. Murgia, T. Pivetta, M. Remelli, A. Rescigno, J. Nicolás-Gutiérrez, J.M. González-Pérez, A. Domínguez-Martín, A. Castiñeiras, Z. Szewczuk, *Iron(III) and aluminum(III) complexes with hydroxypyridone ligands aimed to design kojic acid derivatives with new perspectives*, *Journal of Inorganic Biochemistry*. 104 (2010) pp. 560-569.

- [55] V.M. Nurchi, J.I. Lachowicz, G. Crisponi, S. Murgia, M. Arca, A. Pintus, P. Gans, J. Niclos-Gutierrez, A. Dominguez-Martin, A. Castineiras, M. Remelli, Z. Szewczuk, T. Lis, *Kojic acid derivatives as powerful chelators for iron(III) and aluminium(III)*, Dalton Trans. 40 (2011) pp. 5984-5998.
- [56] C. Exley, *A biogeochemical cycle for aluminium?*, Journal of Inorganic Biochemistry. 97 (2003) pp. 1-7.
- [57] S.L. Hem, *Elimination of aluminum adjuvants*, Vaccine. 20, Supplement 3 (2002) pp. S40-S43.
- [58] J.L. Greger, J.E. Sutherland, *Aluminum exposure and metabolism*, Critical Reviews in Clinical Laboratory Sciences. 34 (1997) pp. 439-474.
- [59] R.A. Yokel, C.L. Hicks, R.L. Florence, *Aluminum bioavailability from basic sodium aluminum phosphate, an approved food additive emulsifying agent, incorporated in cheese*, Food and Chemical Toxicology. 46 (2008) pp. 2261-2266.
- [60] R.B. Martin, *The chemistry of aluminum as related to biology and medicine*, Clinical Chemistry. 32 (1986) pp. 1797-1806.
- [61] G. Crisponi, V.M. Nurchi, V. Bertolasi, M. Remelli, G. Faa, *Chelating agents for human diseases related to aluminium overload*, Coordination Chemistry Reviews. 256 (2012) pp. 89-104.
- [62] D.J. Brown, J.K. Dawborn, K.N. Ham, J.M. Xipell, *Treatment of dialysis osteomalacia with desferrioxamine*, Lancet. 2 (1982) pp. 343-345.
- [63] S. Chaves, P.I. Dron, F.A. Danalache, D. Sacoto, L. Gano, M.A. Santos, *Combined chelation based on glycosyl-mono- and bis-hydroxypyridinones for aluminium mobilization: Solution and biodistribution studies*, Journal of Inorganic Biochemistry. 103 (2009) pp. 1521-1529.
- [64] S. Chaves, S.M. Marques, A.M.F. Matos, A. Nunes, L. Gano, T. Tuccinardi, A. Martinelli, M. Amélia Santos, *New tris(hydroxypyridinones) as iron and aluminium sequestering agents: Synthesis, complexation and in vivo studies*, Chemistry - A European Journal. 16 (2010) pp. 10535-10545.

- [65] S. Chaves, A. Capelo, L. Areias, S.M. Marques, L. Gano, M.A. Esteves, M.A. Santos, *A novel tripodal tris-hydroxypyrimidinone sequestering agent for trivalent hard metal ions: Synthesis, complexation and in vivo studies*, Dalton Transactions. 42 (2013) pp. 6033-6045.
- [66] F. Biaso, P. Baret, J.L. Pierre, G. Serratrice, *Comparative studies on the iron chelators O-TRENSEX and TRENCAMS: Selectivity of the complexation towards other biologically relevant metal ions and Al³⁺*, Journal of Inorganic Biochemistry. 89 (2002) pp. 123-130.
- [67] M. Gaspar, R. Grazina, A. Bodor, E. Farkas, M. Amelia Santos, *Siderophore analogues: a new macrocyclic tetraamine tris(hydroxamate) ligand; synthesis and solution chemistry of the iron(III), aluminium(III) and copper(II) complexes [dagger]*, Journal of the Chemical Society, Dalton Transactions. (1999) pp. 799-806.
- [68] E. Gumienna-Kontecka, R. Silvagni, R. Lipinski, M. Lecouvey, F. Cesare Marincola, G. Crisponi, V.M. Nurchi, Y. Leroux, H. Kozlowski, *Bisphosphonate chelating agents: Complexation of Fe(III) and Al(III) by 1-phenyl-1-hydroxymethylene bisphosphonate and its analogues*, Inorganica Chimica Acta. 339 (2002) pp. 111-118.
- [69] R. Ma, J.J. Reibenspies, A.E. Martell, *Stabilities of 1,2-diethyl-3-hydroxy-4-pyridinone chelates of divalent and trivalent metal ions*, Inorganica Chimica Acta. 223 (1994) pp. 21-29.
- [70] J.L. Jolly, *The U.S. copper-base scrap industry and its by-products. An overview*, 12 Edition (2012) pp. 1-100.
- [71] D. Denny-Brown, H. Porter, *The effect of BAL (2,3-dimercaptopropanol) on hepatolenticular*, The New England journal of medicine. 245 (1951) pp. 917-925.
- [72] J.M. Walshe, *Treatment of Wilson's disease with trientine (triethylene tetramine) dihydrochloride*, Lancet. 1 (1982) pp. 643-647.
- [73] G.J. Brewer, P. Hedera, K.J. Kluin, M. Carlson, F. Askari, R.B. Dick, J. Sitterly, J.K. Fink, *Treatment of Wilson disease with ammonium tetrathiomolybdate: III. Initial therapy in a total of 55 neurologically affected patients and follow-up with zinc therapy*, Archives of Neurology. 60 (2003) pp. 379-385.

- [74] P. Delangle, E. Mintz, *Chelation therapy in Wilson's disease: From d-penicillamine to the design of selective bioinspired intracellular Cu(i) chelators*, Dalton Transactions. 41 (2012) pp. 6359-6370.
- [75] P. Rousselot-Pailley, O. Sénèque, C. Lebrun, S. Crouzy, D. Boturyn, P. Dumy, M. Ferrand, P. Delangle, *Model peptides based on the binding loop of the copper metallochaperone Atx1: Selectivity of the consensus sequence MxCxxC for metal ions Hg(II), Cu(I), Cd(II), Pb(II), and Zn(II)*, Inorganic Chemistry. 45 (2006) pp. 5510-5520.
- [76] A.M. Pujol, C. Gateau, C. Lebrun, P. Delangle, *A cysteine-based tripodal chelator with a high affinity and selectivity for copper(I)*, Journal of the American Chemical Society. 131 (2009) pp. 6928-6929.
- [77] A.M. Pujol, C. Gateau, C. Lebrun, P. Delangle, *A series of tripodal cysteine derivatives as water-soluble chelators that are highly selective for copper(I)*, Chemistry - A European Journal. 17 (2011) pp. 4418-4428.
- [78] S. Tardito, A. Barilli, I. Bassanetti, M. Tegoni, O. Bussolati, R. Franchi-Gazzola, C. Mucchino, L. Marchiò, *Copper-dependent cytotoxicity of 8-hydroxyquinoline derivatives correlates with their hydrophobicity and does not require caspase activation*, Journal of Medicinal Chemistry. 55 (2012) pp. 10448-10459.
- [79] A.E. Khalifa, *Antiinfective Agents Affecting Cognition: A Review*, Journal of Chemotherapy. 19 (2007) pp. 620-631.
- [80] R.A. Cherny, C.S. Atwood, M.E. Xilinas, D.N. Gray, W.D. Jones, C.A. McLean, K.J. Barnham, I. Volitakis, F.W. Fraser, Y.S. Kim, X. Huang, L.E. Goldstein, R.D. Moir, J.T. Lim, K. Beyreuther, H. Zheng, R.E. Tanzi, C.L. Masters, A.I. Bush, *Treatment with a copper-zinc chelator markedly and rapidly inhibits β -amyloid accumulation in Alzheimer's disease transgenic mice*, Neuron. 30 (2001) pp. 665-676.
- [81] A.M. Mancino, S.S. Hindo, A. Kochi, M.H. Lim, *Effects of Clioquinol on Metal-Triggered Amyloid- β Aggregation Revisited*, Inorganic Chemistry. 48 (2009) pp. 9596-9598.

- [82] C. Deraeve, M. Pitié, H. Mazarguil, B. Meunier, *Bis-8-hydroxyquinoline ligands as potential anti-Alzheimer agents*, *New Journal of Chemistry*. 31 (2007) pp. 193-195.
- [83] C. Deraeve, A. Maraval, L. Vendier, V. Faugeroux, M. Pitié, B. Meunier, *Preparation of new bis(8-aminoquinoline) ligands and comparison with bis(8-hydroxyquinoline) ligands on their ability to chelate CuII and ZnII*, *European Journal of Inorganic Chemistry*. (2008) pp. 5622-5631.
- [84] C. Deraeve, C. Boldron, A. Maraval, H. Mazarguil, H. Gornitzka, L. Vendier, M. Pitié, B. Meunier, *Preparation and study of new poly-8-hydroxyquinoline chelators for an anti-alzheimer strategy*, *Chemistry - A European Journal*. 14 (2008) pp. 682-696.
- [85] C. Rodríguez-Rodríguez, M. Telpoukhovskaia, C. Orvig, *The art of building multifunctional metal-binding agents from basic molecular scaffolds for the potential application in neurodegenerative diseases*, *Coordination Chemistry Reviews*. 256 (2012) pp. 2308-2332.
- [86] S.S. Hindo, A.M. Mancino, J.J. Braymer, Y. Liu, S. Vivekanandan, A. Ramamoorthy, M.H. Lim, *Small molecule modulators of copper-induced A β aggregation*, *Journal of the American Chemical Society*. 131 (2009) pp. 16663-16665.
- [87] J.S. Choi, J.J. Braymer, S.K. Park, S. Mustafa, J. Chae, M.H. Lim, *Synthesis and characterization of IMPY derivatives that regulate metal-induced amyloid- β aggregation*, *Metallomics*. 3 (2011) pp. 284-291.
- [88] A. Dedeoglu, K. Cormier, S. Payton, K.A. Tseitlin, J.N. Kremsky, L. Lai, X. Li, R.D. Moir, R.E. Tanzi, A.I. Bush, N.W. Kowall, J.T. Rogers, X. Huang, *Preliminary studies of a novel bifunctional metal chelator targeting Alzheimer's amyloidogenesis*, *Experimental Gerontology*. 39 (2004) pp. 1641-1649.
- [89] W.H. Wu, P. Lei, Q. Liu, J. Hu, A.P. Gunn, M.S. Chen, Y.F. Rui, X.Y. Su, Z.P. Xie, Y.F. Zhao, A.I. Bush, Y.M. Li, *Sequestration of copper from β -amyloid promotes selective lysis by cyclen-hybrid cleavage agents*, *J Biol Chem*. 283 (2008) pp. 31657-31664.
- [90] C. Hilbich, B. Kisters-Woike, J. Reed, C.L. Masters, K. Beyreuther, *Substitutions of hydrophobic amino acids reduce the amyloidogenicity of Alzheimer's disease A β 4 peptides*, *Journal of Molecular Biology*. 228 (1992) pp. 460-473.

[91] W.P. Esler, E.R. Stimson, J.R. Ghilardi, Y.A. Lu, A.M. Felix, H.V. Vinters, P.W. Mantyh, J.P. Lee, J.E. Maggio, *Point substitution in the central hydrophobic cluster of a human β - amyloid congener disrupts peptide folding and abolishes plaque competence*, *Biochemistry*. 35 (1996) pp. 13914-13921.

[92] L.O. Tjernberg, J. Näslundt, F. Lindqvist, J. Johansson, A.R. Karlström, J. Thyberg, L. Tereniust, C. Nordstedt, *Arrest of β -amyloid fibril formation by a pentapeptide ligand*, *J Biol Chem*. 271 (1996) pp. 8545-8548.

[93] J. Bieschke, S.J. Siegel, Y. Fu, J.W. Kelly, *Alzheimer's A β peptides containing an isostructural backbone mutation afford distinct aggregate morphologies but analogous cytotoxicity. Evidence for a common low-abundance toxic structure(s)?*, *Biochemistry*. 47 (2008) pp. 50-59.

Chapter 2

Experimental

Chapter 2

Experimental

2.1. Reagents

Kojic acid, iron chloride FeCl_3 , aluminium chloride AlCl_3 , copper chloride CuCl_2 , and ethanol were purchased from Sigma-Aldrich. N,N-diethyl-ethylenediamine benzylamine hydrochloride, piperazine, methylamine hydrochloride were purchased from TCI Europe. N-benzylmethylamine was purchased from Alfa Aesar. Formaldehyde was purchased from Merck, HCl from Fluka, KCl and ZnCl_2 from Carlo Erba (Milan, Italy). Desferal (DFO) was obtained from Biofutura Pharma products. All the products were used without any further purification.

Fe^{3+} , Al^{3+} , Cu^{2+} and Zn^{2+} solutions were prepared by dissolving the respective amount of FeCl_3 , AlCl_3 , CuCl_2 and ZnCl_2 in pure bidistilled water. A stoichiometric amount of HCl was added to prevent hydrolysis. The Fe^{3+} solution was standardized by spectrophotometric titration with DFO; Al^{3+} solution was standardized with EDTA titration; Cu^{2+} and Zn^{2+} was standardized with KOH titration. In NMR experiments H_2O – D_2O were used.

2.2. Synthesis

In the framework of the collaboration between our research group and the group of professor Amelia Santos of the Technical Institute of Lisbon, 5 new ligands were synthesized (Fig. 2.1). The ligand L8 was previously synthesized in our group. The chelating properties of these ligands are described in papers V, VI and VII. In particular, paper V describes the equilibria in solution of the ligands L4, L5, L6, L7, and L8 with iron. These ligands are studied in paper VI with aluminium. Furthermore, in paper VII not only were investigated the chelating properties of L9 with aluminium and iron, but the selectivity properties were also evaluated for the ligand. The values of pM for other two fundamental metals of the human organism, copper and zinc, were determined.

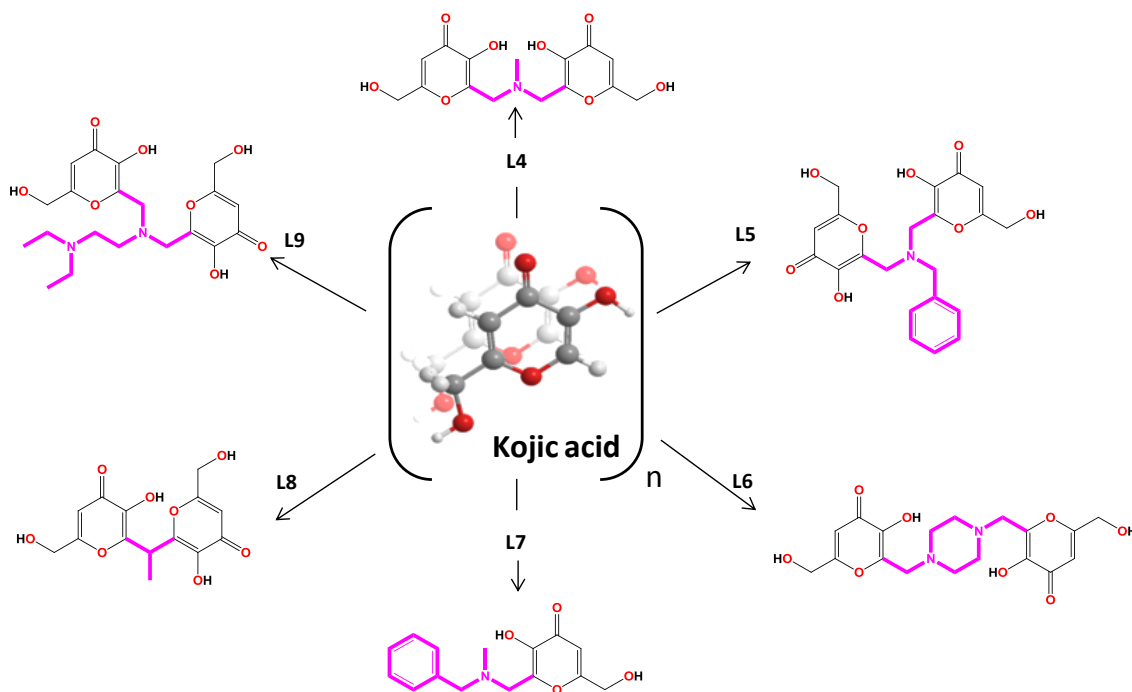


Figure 2.1. Synthesized ligands L4, L5, L6, L7, L8, and L9.

The ligands showed in Fig. 2.1 were obtained by a Mannich reaction in position six of kojic acid. These ligands are tetradentate and are formed by two units of kojic acid joined by different linkers that confer different properties, with the exception of L7 that is bidentate and formed by a single unit of kojic acid. In the Table 2.1 are described the reaction conditions for the synthesized ligands.

Table 2.1. Reaction conditions of the synthesized ligands^a

Ligand	Starting materials	Proportions (eq.)	T (°C)	Time (h)	Yield (%)
L4	Kojic acid	2	40/50	1.5	92
	Formaldehyde	2			
	Methylamine hydrochloride + NaOH	1			
L5	Kojic acid	2	40/50	3.5	52
	Formaldehyde	2			
	Benzylamine hydrochloride + NaOH	1			
L6	Kojic acid	2	RT	5	97
	Formaldehyde	2			
	Piperazine	1			
L7	Kojic acid	2	RT	5	87
	Formaldehyde	2			
	N-Benzylmethylamine	1			
L8	Kojic acid	2	60	3	68
	Acetaldehyde	1			
	Ammonium hydroxide	excess			
L9	Kojic acid	2	RT	5	67
	Formaldehyde	2			
	N,N-diethyl-ethylenediamine	1			

^a In all reactions ethanol was used as a solvent

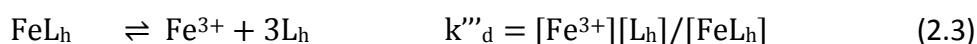
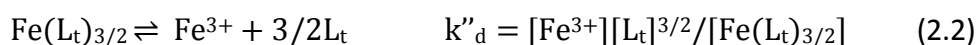
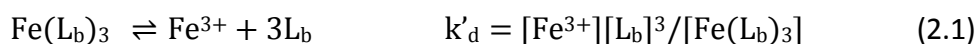
RT means room temperature

The synthesized intermediates and other bidentate ligands obtained are described in appendix 1. The reactions that were tested before obtaining the desired products are described in appendix 2.

2.3. Tetradentate Ligands

In comparison with bidentate and hexadentate ligands, tetradentate ligands have intermediate characteristics, namely:

- The complex formation is favored entropically in the following order hexadentate > tetradentate > bidentate (Chapter 1, section 1.3);
- Generally, the molecular weight of tetradentate ligands is lower than 500 g/mol, that is one important parameter for potential oral chelators, as defined by Lipinski rules;
- They can efficiently scavenge iron(III) at low metal concentrations. Considering the dissociation of bidentate (L_b), tetradentate (L_t) and hexadentate (L_h) ligands, we have the equilibrium equations:



Where K'_d , K''_d , and K'''_d are the equilibrium constants of dissociation. The degree of dissociation for bidentate ligand-metal complexes depends on $[\text{Ligand}]^3$, for tetradentate on $[\text{ligand}]^{3/2}$ and for hexadentate only on $[\text{ligand}]$, hence the dilution dependance of complex dissociation follow the order hexadentate < tetradentate <

bidentate [1-2]. The tetradentate ligands L4, L5, L6, L8 and L9 are able to form stable metal complexes (M_2L_3Hx) metal to ligand $M:L=2:3$ ratios at pH 7.4 [3-4], see Fig. 2.2 A and B and speciation plot reported in papers V, VI and VII. In these complexes each iron atom is fully coordinated in an octahedral configuration.

A similar behavior has been proposed for the complex $Fe_2(IDAPr(3,4-HP)_2)_3$, where each iron atom coordinates a tetradentate ligand ($IDAPr(3,4-HP)_2$) and the third forms a bridge to complete the octahedral coordination sphere of iron [5].

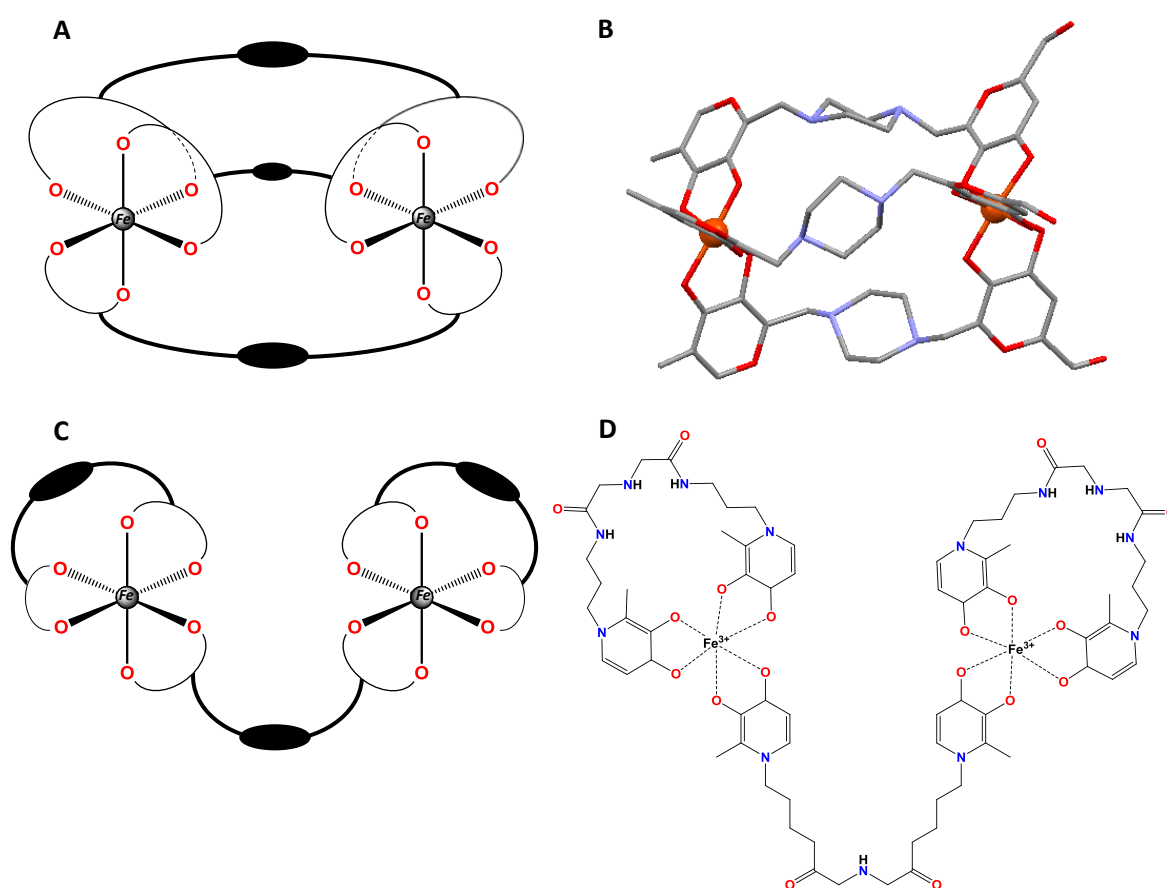


Figure 2.2. **A)** Fe_2L_3 model for the ligands L4, L5, L6, L8 and L9; **B)** Crystal of the complex $Fe_2(L6)_3$; **C)** Fe_2L_3 model proposed for the complex $Fe_2(IDAPr((3,4-HP)_2)_3$; **D)** Structural diagram for the complex $Fe_2(IDAPr((3,4-HP)_2)_3$.

2.4. Analytical Methods in Solution

2.4.1. Balance of Complex Formation in Solution: Definitions

The parameters necessary for the characterization of a system with simultaneous equilibria of complex-formation in solution are contained in the “model of speciation”. This model provides the stoichiometry of the formed species and the relative complex formation constants under known and controlled conditions of temperature and ionic strength. This allows to calculate the composition of the system in different conditions of pH, absolute concentrations of the components, and M:L ratios. Also, it is possible to describe a system in terms of the distribution diagram of species changing a given parameter, such as pH, concentration of metal, of ligand, and others.

The stoichiometric composition and the stability constant for a generic system consisting of a metal ion M, a ligand L and a proton H, are described by the following equations:



$$\beta_{pqr} = [M_pL_qH_r] / [M]^p[L]^q[H]^r \quad (2.5)$$

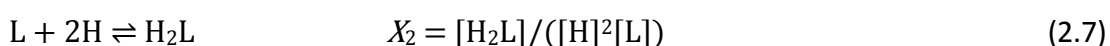
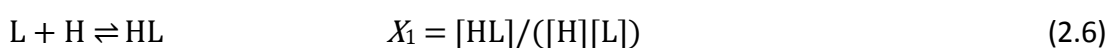
The terms in the square brackets of equation (2.5) represent the concentrations of the different species present at equilibrium (2.4). The charges and the solvent molecules are omitted for simplicity.

β_{pqr} is the global (or cumulative) constant of formation and provides quantitative information on the interaction between metal ion M and ligand L. The stoichiometry coefficient r , relative to proton, is negative when the number of protons lost by the ligand are greater than the maximum number of protons lost in the absence of the metal ion, i.e. when hydroxylated species are formed.

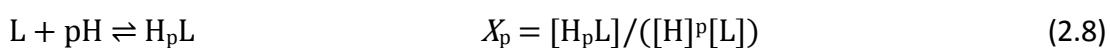
The species $M_pL_qH_r$ is often indicated simply by the relative stoichiometric index; for example, if pqr is equal to 111 the specie is MLH.

The protonation constants X , and the step complex formation constants k , are used to describe the equilibria in solution:

1) Ligand protonation:

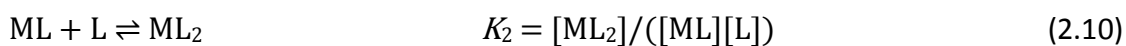
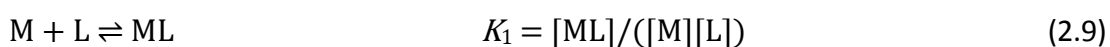


In subsequence:

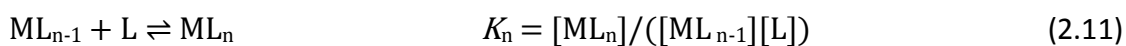


Where X_p is the global or cumulative protonation constant.

2) Complex formation between metal and ligand:



For n ligands (L) we obtain:



The partial K and cumulative β constants satisfy the following relations:

$$\beta_{110} = K_1 = [ML]/([M][L]) \quad (2.12)$$

$$\beta_{120} = K_1K_2 = [ML_2]/([M][L]^2) \quad (2.13)$$

And for n K we obtain:

$$\beta_{1n0} = K_1 K_2 \dots K_n = [ML_n] / ([M][L]^n) \quad (2.14)$$

2.4.1.1. Solutions of a System with Multiple Equilibria

The components of the system (metal, ligand and proton) can be described by the following equations:

- n mass balances of the n components;
- charge balance;
- N β constants of formation of the present species.

The three mass balances for a binary system are the following:

$$c_M = [M] + [ML] + [ML_2] + \dots + [ML_n] = [M] + \sum_{n=1}^n \beta_n [M] [L]^n \quad (2.15)$$

$$c_L = [L] + [HL] + [H_2L] + \dots + [H_pL] + [ML] + 2[ML_2] + n[ML_n] = [L] + \sum_{p=1}^p X_p [H]^p [L] + \sum_{n=1}^n n\beta_n [M] [L]^n \quad (2.16)$$

$$c_H = [H] - [OH] + [HL] + 2[H_2L] + \dots + p[H_pL] = [H] - K_w [H]^{-1} + \sum_{p=1}^p P X_p [H]^p [L] \quad (2.17)$$

where c_M , c_L and c_H are the analytical concentrations of M, L, H, and $[M]$, $[L]$, $[H]$ are the corresponding free concentrations.

The system consists of these three equations containing 3+N unknown factors, namely the free concentration of the components and global constants of formation. Experimental methods for the study of these systems are based on the determination

of the free concentration of at least one component, measured on systems at variable concentration of components (temperature and ionic strength must be constant).

In the case of labile complexes, those in which the ligands are not linked irreversibly to the metal and may be replaced by other metals with fast kinetics, there is a competition between the metal and proton for donor sites of the ligand. In this case, the investigation can be conducted through an acid-base titration, followed potentiometrically. Each point of the titration can thus measure the value of the concentration of the free proton. For each N_p point of the titration it is possible to write a system with three mass balances. This system has a total of $3 \cdot N_p$ equations with $(3-1) \cdot N_p + N$ unknown, there are $(3-1)$ free concentrations unknown while the N formation constants are the same for all points. The system can be solved if the number of unknown terms is the same of the number of equations, namely the number of experimental points.

Normally, the exact analytical solution of these systems can only be achieved in very simple cases. For high order equations, non-linear least squares methods are used. In this case, the number of points needed is at least double than that of the parameters to be determined [6].

Currently, there are several programs available that allows to process hundreds of experimental points for multi-metal and multi-ligand systems which have a large number of simultaneous equilibria. The goodness of the fit allows to evaluate the reliability of the model and results. Although potentiometry is the technique most widely used for this purpose, for its simplicity and accuracy, the method may be coupled to any analytical technique that is capable of measuring the free concentration of at least one component of the system in variable experimental conditions.

In general, the methods for determining the concentration of a component are based on the measurement of a physical quantity x , which is related to the unknown concentration. Depending on the relationship between the physical quantity x and concentration, the methods of analysis can be divided into:

- a) methods in which the quantity x is related with the concentration of single species present in the system. For example, in potentiometry the potential of glass electrode or electrodes sensitive to the metal ion, is given by the equation:

$$x \propto [M] \Rightarrow E = E^0 + \left(\frac{RT}{nF}\right) \ln[M] \quad (2.18)$$

- b) methods in which the relation between concentration x is complex. For example, the absorbance in spectrophotometry depends on all present species, and with calorimetry the measured heat comes from the contribution of all species and from non-chemical factors.
- c) methods based on colligative properties of the solution.

2.4.2. Potentiometry

The methods referred in group *a*) can be very simple to apply. The most widely used technique for the determination of free component concentration of a system is the potentiometric titration, which uses a glass electrode. This method is applicable both for the determination of the protonation and complex formation constants.

The technique can be used whenever the ligand involved in the equilibrium of complex formation is also involved in an acid/base type balance. In this system there is a competition between the proton and metal ion for the ligand.

The potential E of the system measured with a glass electrode is correlated with the activity of hydrogen ions, through an equation analogous to that of Nernst:

$$E = E^0 + \beta \left(\frac{RT}{F} \right) \ln a_{H^+} = E^0 + \beta \left(\frac{RT}{F} \right) \ln \gamma_{H^+} + \beta \left(\frac{RT}{F} \right) \ln [H^+] \quad (2.19)$$

E^0 is the standard or asymmetry potential, β is an experimental parameter that takes into account the deviation from the theoretical Nernst slope (is typically slightly less than 1), γ_{H^+} is the activity coefficient of the ion H^+ and a_{H^+} is the activity of proton and $[H^+]$ its concentration.

In solutions at constant temperature and ionic strength, the coefficient γ_{H^+} remains constant and can be incorporated in the standard potential E^0 :

$$E = E^{0^I} + \beta \left(\frac{RT}{F} \right) \ln [H^+] \quad (2.20)$$

where:

$$E^{0^I} = E^0 + \beta \left(\frac{RT}{F} \right) \ln a_{H^+} \quad (2.21)$$

E^{0^I} and β can be obtained through an appropriate calibration procedure, which is generally a titration of a strong acid with a strong base. The values of the measured potential can then be correlated with the concentration $[H^+]$, and the equilibrium constants obtained can be expressed in terms of concentration.

2.4.2.1. Glass Electrode Calibration

Calibration of the glass electrode must be performed daily before starting the measurements. The calibration of glass electrodes, in terms of hydrogen ion concentration, may be processed by:

1. Following IUPAC recommendations [7], which are based on the use of either one or two designated buffer solutions, or by using a regression procedure performed with data from more than two buffer solutions [8-9].
2. Titration of a strong acid with a strong base, with known acidic concentration [10].

The second procedure satisfies the normal conditions used in the determination of the stability constants (high ionic strength). GLEE (Glass Electrode Evaluation) [11] is the program used for the calculation of the slope and standard electrode potential of the glass electrode. The program was developed as part of Hyperquad, that is a program for determining the stability constants [12]. It uses a (non-linear) least-squares refinement to fit a modified Nerst equation:

$$E = E^0 + s \log[H^+] \quad (2.22)$$

where E is the measured electrode potential, E^0 and s are parameters of the refinement and represent the standard electrode potential and slope, and $[H^+]$ represents the hydrogen ion concentration. E^0 and s are used in Hyperquad data input. Equation (2.22) is an excellent approximation with the exception of the regions with high acidity or basicity, where junction potentials may be not negligible. GLEE allows to linearize the titration curve (Fig. 2.3).

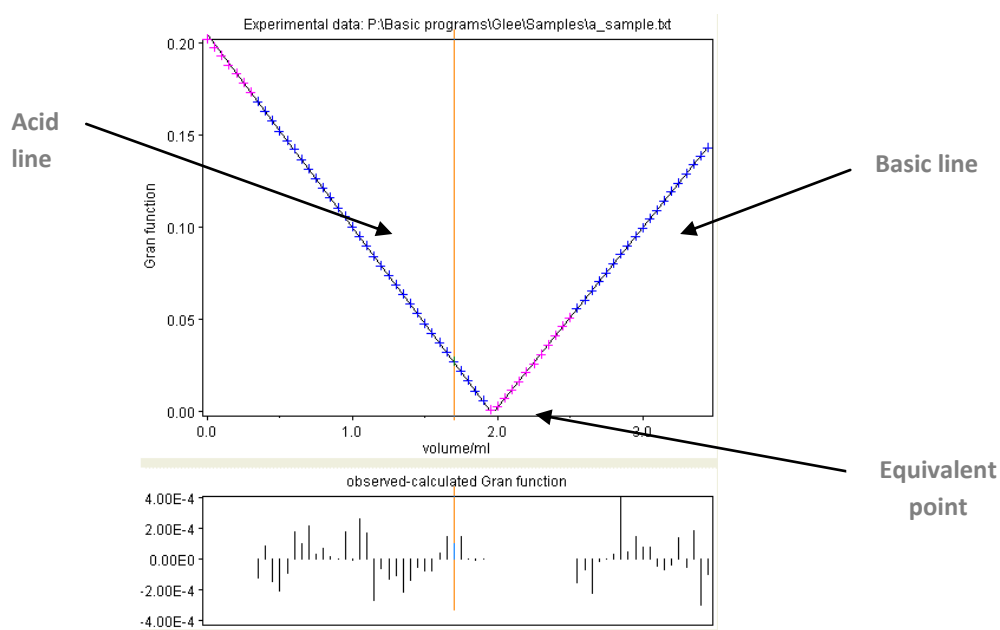


Figure 2.3. Gran plot obtained with GLEE program.

The points are plotted using the method of Gran that is useful to check the presence of impurities in the titrant (carbonate in the base). The graph is formed by two lines (acid and basic). The intersection of the two lines gives an estimate of the equivalent volume (V_e) *acid* and *basic*, (in this point the Gran function is equal to zero). Ideally, without experimental errors the two V_e must be equal. In reality, the alkaline solution is impure and $V_e(\text{basic})$ is higher. The alkalinity level can be used to evaluate this error:

$$\text{Alkalinity level in \%} = \left(\frac{V_e(\text{basic}) - V_e(\text{acid})}{V_e(\text{basic})} \right) 100 \quad (2.23)$$

In our laboratory the strong basic solution (KOH) is substituted when the alkalinity level is greater than 2%.

2.4.3. Spectrophotometric Method

Spectrophotometry is an important technique for the determination of stability of complexes in solution. This technique is very powerful, because measures quantitatively the absorption without perturbing the equilibrium.

Spectrophotometry is based on the Beer-Lambert law:

$$A = \varepsilon cl \quad (2.24)$$

where A is the absorbance, ε is the absorptivity (characteristic of each substance at each wavelength), c is the molar concentration of the absorbing species and l is the optical path length in cm. When considering systems with more than one component, each point of the spectrum is a sum of the contributions of each individual species:

$$A = (\varepsilon_1 c_1 + \varepsilon_2 c_2 + \dots + \varepsilon_{11} c_{11}) l \quad (2.25)$$

2.4.3.1. Decomposition of Spectral Gaussian

To describe an experimental signal of Gaussian shape the easily handled form is used:

$$G = H e^{\left[-\frac{k(\lambda - \lambda^0)^2}{W^2} \right]} \quad (2.26)$$

where H is the height of the peak, λ^0 the abscissa of the maximum, W the width of the band at half height (half-bandwidth) and the proportionality factor $k = 2.7725$. The UV-VIS spectrum of a single species is composed by several analytical signals, and can be expressed as the sum of N_{pks} Gaussian peaks:

$$A(X) = \sum_{j=1}^{N_{pks}} G_j (H_j, \lambda_j^0, W_j, X) \quad (2.27)$$

In many situations (as in equilibrium and kinetic studies or in analytical procedures) spectra from N_{sl} different solutions are recorded. The spectra are the sum of the contributions of two or more species, whose concentration varies among the solutions. These N_{sl} spectra can be expressed by a set of N_{sl} equations similar to equation 2.27, all of which have the same λ_j^0 and W_j values, while the N_{pks} intensive factors $H_{j,i}$ assume a definite value in each spectrum. The experimental absorbance values from N_{sl} solutions at N_w wavelengths are stored in a matrix $Y [N_w, N_{sl}]$ with indexes l and i respectively, where each column represents a single spectrum:

$$Y = \begin{bmatrix} Y_{1,1} & \cdots & Y_{1,N_{sl}} \\ \vdots & \ddots & \vdots \\ Y_{N_w,1} & \cdots & Y_{N_w,N_{sl}} \end{bmatrix} \quad (2.28)$$

Summing equation 2.26 with 2.27 is possible to describe each element:

$$A_{l,i} = \sum_{j=1}^{N_{pks}} H_{j,i} e^{\left[\frac{k(\lambda_l - \lambda_j^0)^2}{W_j^2} \right]} \quad (2.29)$$

Taking this equation into account, the matrix of calculated absorbances can be expressed as a product of a matrix $E [N_w, N_{pks}]$ of the exponential terms by a matrix of heights $H [N_{pks}, N_{sl}]$:

$$A = E \times H \quad (2.30)$$

The intent of any least-squares procedure is to find in the above equation the values of the parameters which minimize $\sum_{m=1}^{N_w} r_m^2$, namely the sum of the squares of residuals $r_m = A_{l,i} - Y_{l,i}$ extended to N_w wavelengths and N_{sl} solutions. In equation 2.30 the matrix A is linearly dependent on H , while it is a non-linear function of λ^0 and W . The least square procedure can be studied by two different types of calculation: *i*) a linear one for

the determination of the peaks height, and *ii*) non-linear for the determination of the position and width of the band. The decomposition of the bands is performed with the program SPECPEAK [13].

2.4.4. Simultaneous Potentiometric and Spectrophotometric Titrations

Potentiometric titrations were performed with an automatic titrator Dosimats Metrohm 665, connected to a Metrohm 691 pH-meter. All titrations were carried out at a temperature of 25.00 ± 0.02 °C. The solutions have been maintained under inert atmosphere by flushing with ultrapure argon in the cell. To keep the system in constant agitation magnetic stirring was used. A daily electrode calibration was performed.

The UV-Visible spectra were measured with a Varian Cary50 spectrophotometer with a fiber optical system using two different optical paths (0.2 cm for the pure ligands and 1 cm to analyze the ligands with metals). The immersion of the fiber on the titration cell allows the simultaneous determination of potentiometric and spectrophotometric data. The ability to record directly the spectrum in the cell eliminates some drawbacks associated with the use of cuvettes, in particular:

- Changes in temperature due to the transfer of the solution;
- Loss of substance by transfer into the cuvette;
- Formation of air bubbles in the cuvette.

The great advantage is that is possible to automate the entire process by synchronizing the titrator, the pH-meter and the spectrometer. This allows to perform titrations with a high number of experimental points.

The collected spectral data were analyzed with the programs SPECFIT and SPEAKPEAK [13], and the potentiometric data with the program HYPERQUAD [12]. Simultaneous spectrophotometric and potentiometric titrations were used for all the new ligands reported in this thesis (see papers V, VI and VII), firstly, to study and determine the dissociation constants pK of ligands (see Fig. 2.4), and secondly to determine the complex formation constants of the ligands with the metal ions.

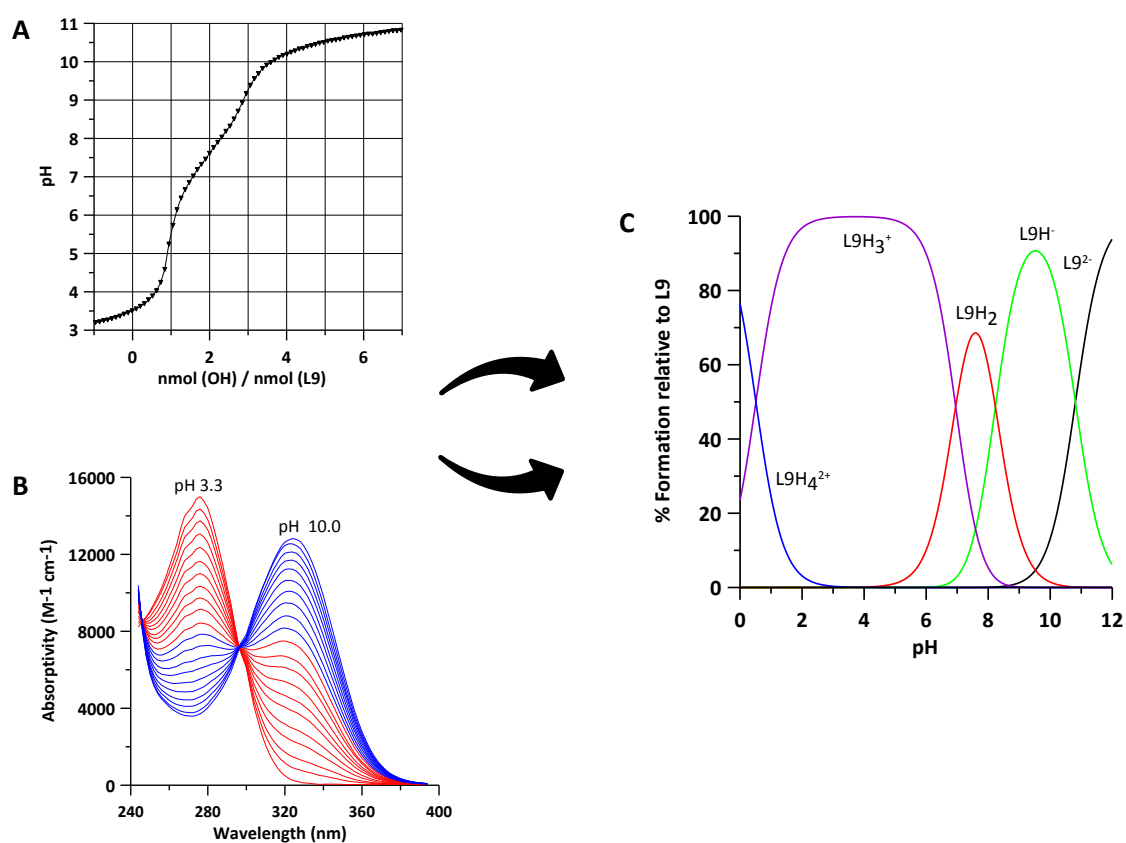


Figure 2.4. A) Potentiometric curve of ligand L9; B) Spectra collected during the potentiometric titration of the ligand L9, the red spectra was collected at pH acid, and the blue one at basic pH; C) Speciation plot of the ligand L9.

For iron and copper combined potentiometry with spectrophotometric analysis was performed. In the case of the colorless aluminium and zinc complexes only potentiometry was used. After obtaining the refined data, was possible with HySS (Hyperquad Simulation and Speciation) [14], to simulate the speciation plots of pure ligands and in the presence of metal. These data are reported in papers V, VI and VII.

2.4.5. Nuclear Magnetic Resonance

In 1945 two physical groups of the Stanford University and Harvard University headed by Felix Bloch and Edward Mills Purcell, respectively, observed independently the first signals of nuclear magnetic resonance (NMR). Since that date, the enormous development of the technique has led to the design of extremely refined and precise instruments. The NMR technique is one of the most versatile methods of investigation for the different fields of scientific research, being particularly used in chemistry, biology and medicine. NMR spectroscopy studies the magnetic properties of the nucleus allowing detailed information about the molecules structure, nature of the atoms, their number, and also the type of molecular surroundings in which the atom is located. By the other hand, not all atoms can be observed with this technique, but only those with suitable magnetic characteristics.

The nucleus magnetic properties are represented by its nuclear magnetic moment μ , defined as:

$$\mu = \frac{\gamma I h}{2\pi} \quad (2.31)$$

where, γ is a proportionality constant called gyromagnetic ratio (different for each type of nucleus), I is a fundamental property of the nucleus, called nuclear spin angular momentum (with values of 0, 1/2, 1, ... in units of $h/2\pi$), and h is the plank constant.

The effective value of I , for each nuclei, depends on the mass and atomic number. Nucleus with $I \neq 0$, can be studied by NMR spectroscopy, whereas the nuclei with an even number of protons, neutrons or both (such as, ^{12}C , ^{16}O and ^{32}S , $I = 0$) cannot be studied.

Hydrogen is the most important magnetic element. It is present in almost all organic compounds, and this explains why the ^1H -NMR technique was the first to be developed. Another widely studied nucleus is the isotope carbon 13 (^{13}C), which is present in the nature in about 1.1%. These are the two nucleus studied in this dissertation and they have both spin $I = 1/2$.

When a sample is introduced in magnetic field, the movement of the electrons creates small local magnetic fields, which shield the nucleus from the applied magnetic field. When an external magnetic field B is applied to an atom, the electron cloud that surrounds the nucleus, generates a small magnetic field with opposite direction to B , shielding the nucleus itself. Each nucleus of the sample is immersed in an effective field (B_{eff}) different than B :

$$B_{eff} = B(1 - \sigma) \quad (2.32)$$

where σ is the shielding constant. The value of σ depends on the nucleus chemical vicinity, and it is generally higher for nuclei surrounded by a dense electron cloud. Nuclei of the same element in a different chemical surrounding resonate at slightly different frequencies, originating different signals in the NMR spectrum. The NMR spectrum is divided in two parts (see examples reported in Fig. 2.5), where the right part (upfield) resonate shielded nuclei and the left part (downfield) resonate less shielded nuclei.

Normally, NMR spectra are made with constant ν_0 (frequency), and varying the magnetic field from higher to lowest values. The separation in units of the magnetic field between two spectral peaks depends on the type of spectrometer used, being

directly proportional to its operating frequency. In a spectrometer operating at 360 MHz, the separation signals of two chemically different nucleus is six times higher than one that operates at 60 MHz. In order to make comparable spectra, recorded with instruments operating at different frequencies and magnetic fields, it has been introduced a dimensionless unit, which allows to measure in absolute the position of the spectral lines. This measure is called chemical shift δ ,

$$\delta = \left[\left(\frac{\nu_{sample} - \nu_{standard}}{\nu_0} \right) \right] 10^6 \quad (2.33)$$

where δ is defined as the resonance frequency difference of a particular signal ν_{sample} from the trimethylsilane signal TMS $\nu_{standard}$ expressed in Hz, divided by the operating frequency of the instrument expressed in MHz (ν_0) [15].

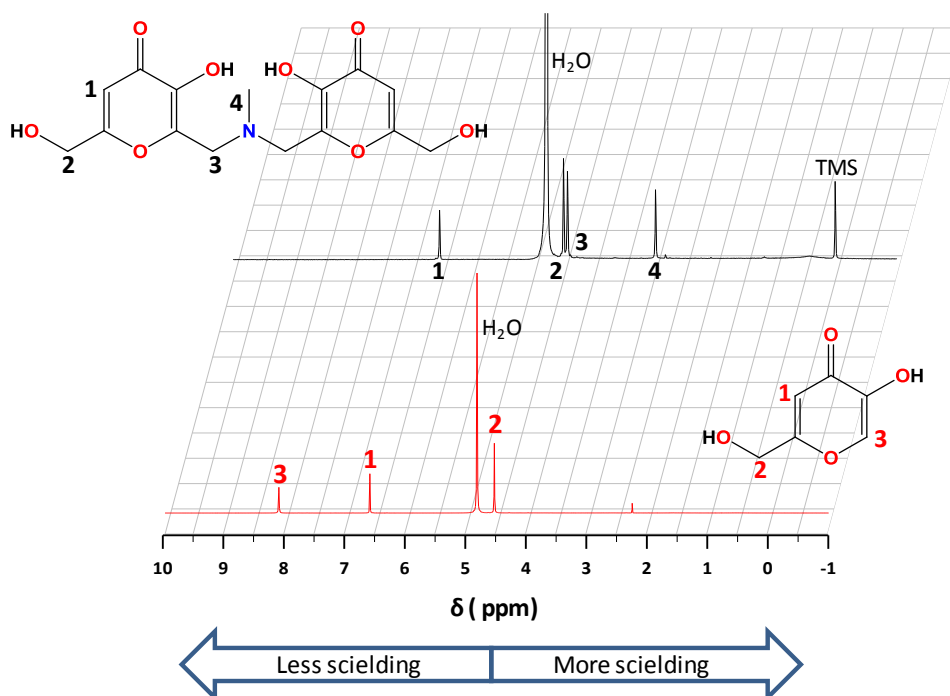


Figure 2.5. ¹H-NMR spectra of L4 in D₂O at pH 3.5 (in black), and Kojic acid in D₂O at pH = 7 (in red).

In this dissertation, the ^1H -NMR technique with operating frequencies of 300 or 400 MHz was used to follow the synthesis of the ligands L4, L5, L6, L7, L8, and L9, and to analyze the reaction intermediates and final products. Furthermore, for all ligands the HSQC (Heteronuclear Single Quantum Correlation) technique was also used, which allows to assign the NMR signal with certainty to the corresponding nucleus (see Fig. 2.6).

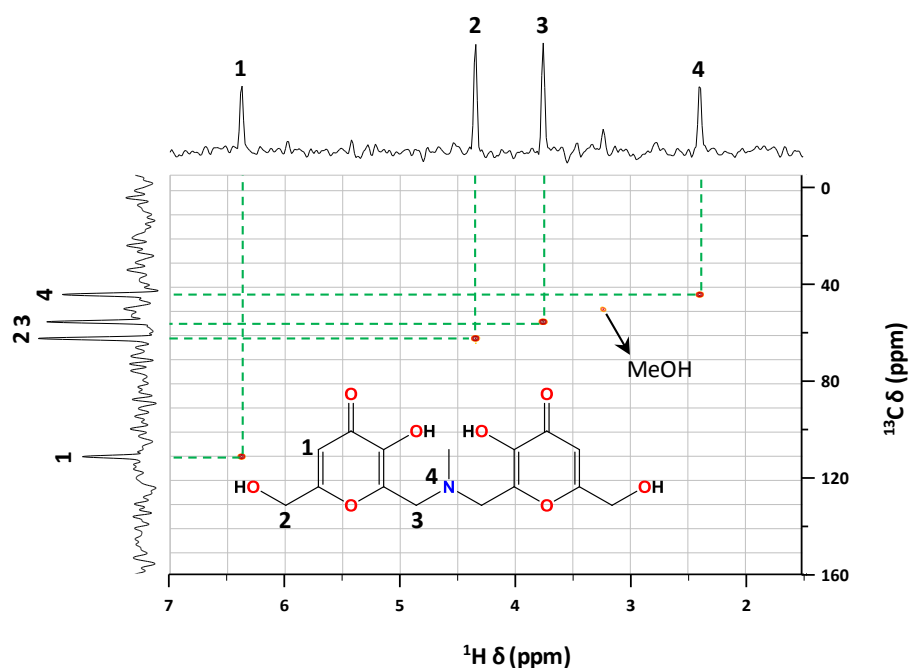


Figure 2.6. ^1H - ^{13}C HSQC of L4 in MeOD.

^1H -NMR titration of all ligands, at different pH values, was a useful method not only to evaluate the protonation constants, specially in acidic pH, where it was not possible to use the potentiometric method, but mainly to correctly attribute the different protonation steps at the various basic groups on the ligand. All data (chemical shifts) were analyzed with HypNMR [16-17] program, leading to the optimized value of $\log \beta$.

Also, $^1\text{H-NMR}$ titrations of the ligands with Zn and Al for different M:L ratios were performed. In the case of Al, the slow exchange of ligand between its free and complexed forms determines the appearance of separate NMR signals; due to this property, in the study of the ligand L4 with Al with the ratio M:L = 2:3 the first evidence of the formation of $\text{Al}_2(\text{L4})_3$ complex was obtained (see paper VI).

2.4.6. Electrospray Ionization Mass Spectroscopy

Mass spectrometry (MS) is based on the generation of gaseous ions from analyte molecules, with subsequent separation of these ions according to their mass/charge (m/z) ratio, and the detection of these ions. MS is applied analytically in a great variety of qualitative and quantitative studies. Qualitative applications comprise determination of the structure of unknown compounds such as natural substances, metabolites of drugs and synthetic compounds. MS is used for the determination of molecular mass, molecular formula and elemental composition. Compared to other spectrometric techniques, MS is the most sensitive spectrometric technique for molecular analysis, like NMR and infrared spectrometry. In quantitative analysis, MS is applied for developing definitive and reference methods.

The mass spectrometer is a highly sophisticated and computerized instrument. It consists of five major components: a vacuum system, an ion source, a mass analyzer, an ion detector, and a data recording system, as shown in Fig. 2.7. There are several ion sources, which can be classify in hard and soft. Electrospray Ionization (ESI) is a soft ionization technique extensively used for production of gas phase ions (without fragmentation) of thermally labile large molecules. The process of electrospray ionization includes both the nebulization of the liquid stream into an aerosol of highly

charged droplets and the ionization of the analyte molecules after desolvation of the charged droplets. ESI is subsumed under the atmospheric pressure ionization (API) interfaces. The sample is introduced, after an appropriate split through the chromatographic column or by direct insertion via infusion apparatus through a stainless steel hypodermic needle into the atmospheric pressure desolvation chamber. While the needle is at ground potential, a strong electric field (2-5 kV) is applied to the cylindrical counter electrode which charges the surface of the liquid emerging from the needle, creating a fine spray of charged droplets. Driven by the electric field, the droplets pass through a curtain of nitrogen drying gas. The gas curtain has the function of supporting evaporation of the solvent and preventing the uncharged material from entering into the ion source. By expansion of the curtain gas, the ions are carried through a capillary into the vacuum of the first pumping stage, and then pass through the pumping stages and the lens system, finally into the mass analyser [18-19].

The compounds studied in this dissertation were pure solids and they were introduced into the ion source by direct insertion. ESI-MS was used with qualitative purposes, analyzing both the pure L4, L5, L6, L7, L8, and L9 ligands and in presence of several metals: Fe³⁺, Al³⁺, Cu²⁺, and Zn²⁺. ESI-MS was a useful method to investigate the stoichiometric of the formed complexes, see the example showed in Fig. 2.7 of the mass spectrum of L9 with Fe³⁺, and papers V, VI for other ligands and paper VII for L9 with different metals.

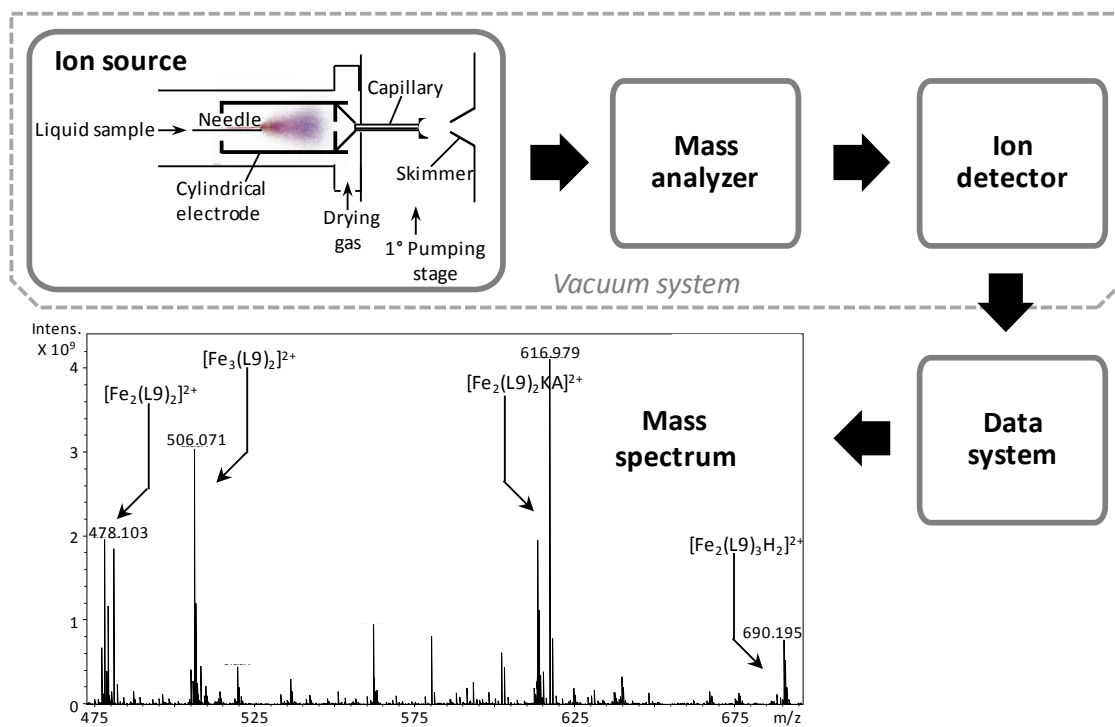


Figure 2.7. Schematic representation of a mass spectrometer.

2.5. Bibliography

- [1] R.C. Hider, *Siderophore mediated absorption of iron*, Structure and Bonding. 58 (1984) pp. 25-87.
- [2] Z.D. Liu, R.C. Hider, *Design of iron chelators with therapeutic application*, Coordination Chemistry Reviews. 232 (2002) pp. 151-171.
- [3] L. Toso, G. Crisponi, V.M. Nurchi, M. Crespo-Alonso, J.I. Lachowicz, M.A. Santos, S.M. Marques, J. Niclós-Gutiérrez, J.M. González-Pérez, A. Domínguez-Martín, D. Choquesillo-Lazarte, Z. Szewczuk, *A family of hydroxypyrrone ligands designed and synthesized as iron chelators*, Journal of Inorganic Biochemistry. 127 (2013) pp. 220-231.
- [4] L. Toso, G. Crisponi, V.M. Nurchi, M. Crespo-Alonso, J.I. Lachowicz, D. Mansoori, M. Arca, M.A. Santos, S.M. Marques, L. Gano, J. Niclós-Gutiérrez, J.M. González-Pérez, A. Domínguez-Martín, D. Choquesillo-Lazarte, Z. Szewczuk, *Searching for new aluminium chelating agents: A family of hydroxypyrrone ligands*, Journal of Inorganic Biochemistry. 130 (2014) pp. 112-121.
- [5] M.A. Santos, S. Gama, L. Gano, G. Cantinho, E. Farkas, *A new bis(3-hydroxy-4-pyridinone)-IDA derivative as a potential therapeutic chelating agent. Synthesis, metal-complexation and biological assays*, Dalton Transactions. (2004) pp. 3772-3781.
- [6] A. Braibanti, V. Carunchio, *I complessi metallici in soluzione*, Aracne Editrice. 1 (1996) pp. 44-59.
- [7] A.K. Covington, R.G. Bates, R.A. Durst, *Definition of pH scales, standard reference values, measurement of pH and related terminology (Recommendations 1984)*, Pure Appl. Chem. . (1985) pp. 531-542.
- [8] A. Avdeef, J.J. Bucher, *Accurate measurements of the concentration of hydrogen ions with a glass electrode: calibrations using the Prideaux and other universal buffer solutions and a computer-controlled automatic titrator*, Analytical Chemistry. 50 (1978) pp. 2137-2142.

- [9] F.G.K. Baucke, R. Naumann, C. Alexander-Weber, *Multiple-point calibration with linear regression as a proposed standardization procedure for high-precision pH measurements*, Analytical Chemistry. 65 (1993) pp. 3244-3251.
- [10] A.E.M. R.J. Motekaitis, *The Determination and Use of Stability Constants*, VCH, New York. (1988) pp. 1-200.
- [11] P. Gans, B. O'Sullivan, *GLEE, a new computer program for glass electrode calibration*, Talanta. 51 (2000) pp. 33-37.
- [12] P. Gans, A. Sabatini, A. Vacca, *Investigation of equilibria in solution. Determination of equilibrium constants with the HYPERQUAD suite of programs*, Talanta. 43 (1996) pp. 1739-1753.
- [13] M.C. Aragoni, M. Arca, G. Crisponi, V.M. Nurchi, *Simultaneous decomposition of several spectra into the constituent Gaussian peaks*, Analytica Chimica Acta. 316 (1995) pp. 195-204.
- [14] L. Alderighi, P. Gans, A. Ienco, D. Peters, A. Sabatini, A. Vacca, *Hyperquad simulation and speciation (HySS): A utility program for the investigation of equilibria involving soluble and partially soluble species*, Coordination Chemistry Reviews. 184 (1999) pp. 311-318.
- [15] S. Murgia, *Nuclear magnetic resonance (NMR) handbook*, (2012) pp. 1-19.
- [16] C. Frassinetti, L. Alderighi, P. Gans, A. Sabatini, A. Vacca, S. Ghelli, *Determination of protonation constants of some fluorinated polyamines by means of ¹³C NMR data processed by the new computer program HypNMR2000. Protonation sequence in polyamines*, Anal Bioanal Chem. 376 (2003) pp. 1041-1052.
- [17] C. Frassinetti, S. Ghelli, P. Gans, A. Sabatini, M.S. Moruzzi, A. Vacca, *Nuclear magnetic resonance as a tool for determining protonation constants of natural polyprotic bases in solution*, Analytical Biochemistry. 231 (1995) pp. 374-382.
- [18] R.W. Smith, in: J.A. Siegel, P.J. Saukko, M.M. Houck (Eds.), *Encyclopedia of Forensic Sciences*, Academic Press, Waltham, 2013, pp. 603-608.
- [19] R. Kellner, J.M. Mermet, M. Otto, H.M. Widmer, *Chimica Analitica*, (2003) pp. 892.

Appendix 1

**Intermediates and other Ligands
Synthesized**

Appendix 1

Intermediates and other Ligands Synthesized

3-hydroxy-6-(hydroxymethyl)-2-((4-phenylpiperazin-1-yl)methyl)-4H-pyran-4-one

Kojic acid (100 mg, 0.7 mmol) was stirred in aqueous ethanol (96%, 10 mL) at room temperature. Phenylpiperazine (107.5 μ L, 0.7 mmol) and aqueous formaldehyde (37%, 57 μ L, 0.7 mmol) were mixed with ethanol (2 mL) for 30 minutes and then added drop wise to the ethanolic mixture previously prepared. Stirring at room temperature was maintained for 18h and during this time a fine white precipitate appeared. Upon refrigeration for 2h, the reaction mixture was filtered and the resultant solid washed with cold ethanol. The reaction was followed by TLC, using CH_2Cl_2 :MeOH (6:0.5) mixture as eluent. The final product was obtained as a white solid (η = 79%) soluble in basic water. Melting point: 191-192 $^\circ\text{C}$. $^1\text{H-NMR}$ (300 MHz, D_2O + KOD, pH = 11): δ 7.2165(5H, Ph), 6.391(1H,s), 4.460(2H, s), 3.728(2H, s), 3.189(4H, s), 2.776(4H, s). $\text{C}_{17}\text{H}_{20}\text{N}_2\text{O}_4$, Mass spectrum (ESS-MS (+)): MH^+ (317.2).

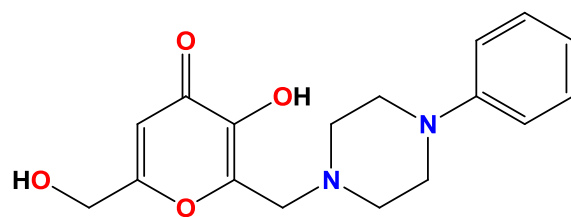


Figure A.1.1. 3-hydroxy-6-(hydroxymethyl)-2-((4-phenylpiperazine-1-yl)methyl)-4H-pyran-4-one (MW = 316.2).

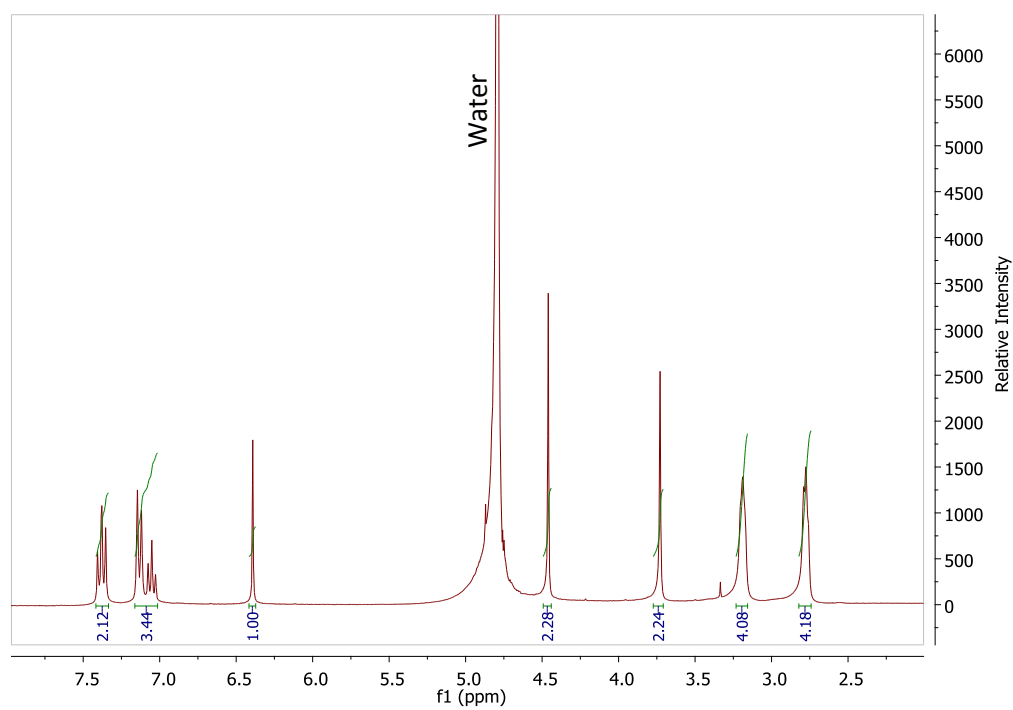


Figure A.1.2. $^1\text{H-NMR}$ spectrum of 3-hydroxy-6-(hydroxymethyl)-2-((4-phenylpiperazine-1-yl)methyl)-4H-pyran-4-one.

2-((4-(4-chlorophenyl)piperazin-1-yl)methyl)-3-hydroxy-6-(hydroxymethyl)-4H-pyran-4-one

Kojic acid (40 mg, 0.28 mmol) was stirred in aqueous ethanol (96%, 8 mL) at room temperature. 1-(4-chlorophenyl)-piperazine dihydrochloride (95%, 80 mg, 0.30 mmol) neutralised with NaOH (1 M, 0.6 mL, 0.6 mmol) and aqueous formaldehyde (37%, 25 μ L, 0.31 mmol) were mixed in ethanol (2 mL) for 30 minutes and then added drop wise to the ethanolic mixture prepared above. Stirring at room temperature was maintained for 6h, and a fine white precipitate appeared. Upon refrigeration for 2h the reaction mixture was filtered and the resultant solid washed with cold ethanol. The reaction was followed by TLC, using CH₂Cl₂:MeOH (6:0.7) mixture as eluent. The final product was obtained as a white solid (η = 51%), that is soluble in acid water. Melting point: 210 °C. ¹H-NMR (300 MHz, D₂O + DCl, pH = 3): δ 7.217(4H, Ph), 6.623(1H, S), 4.560(2H, s), 4.544(2H, s), 3.581(4H, s), 3.514(4H, s). C₁₇H₁₉ClN₂O₄, Mass spectrum (ESS-MS (+)): MD⁺ (352.2).

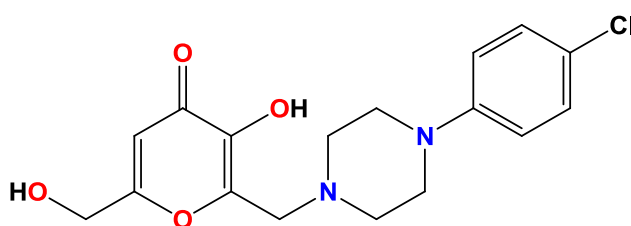


Figure A.1.3. 2-((4-(4-chlorophenyl)piperazin-1-yl)methyl)-3-hydroxy-6-(hydroxymethyl)-4H-pyran-4-one (MW = 350.1).

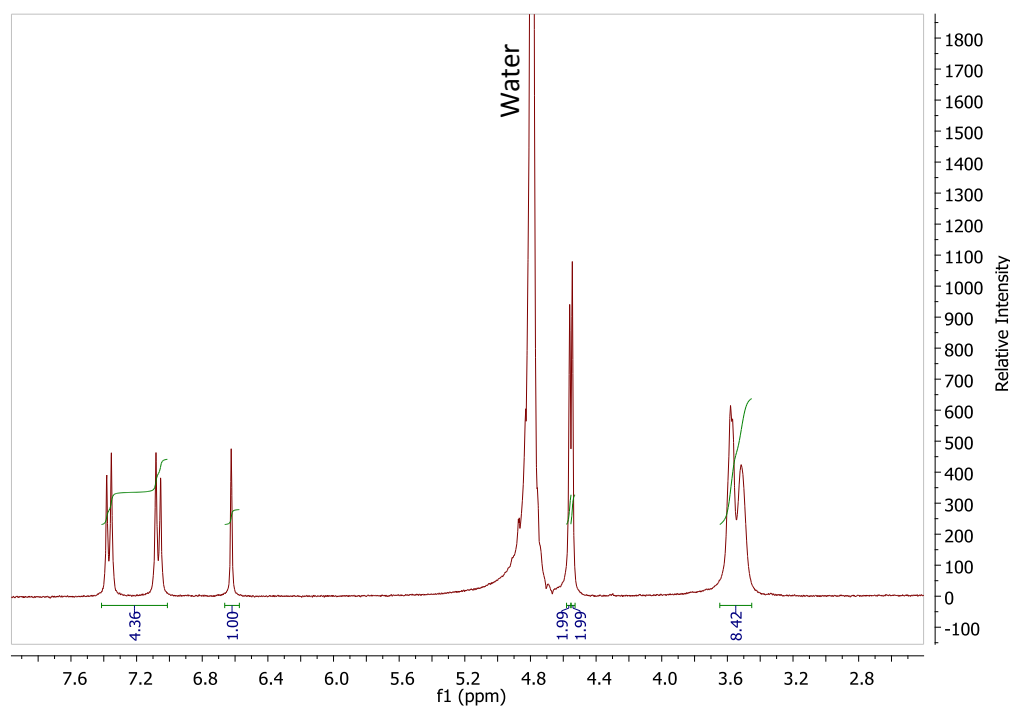


Figure A.1.4. $^1\text{H-NMR}$ spectrum of 2-((4-(4-chlorophenyl)piperazin-1-yl)methyl)-3-hydroxy-6-(hydroxymethyl)-4H-pyran-4-one.

2-((dibenzylamino) methyl)-3-hydroxy-6-(hydroxymethyl)-4H-pyran-4-one

Kojic acid (0.50 g, 3.5 mmol) was stirred in ethanol (96%, 20 mL) at room temperature. N-dibenzylamine (715 μL , 3.6 mmol) and aqueous formaldehyde (37%, 285 μL , 3.5 mmol) were mixed with ethanol (2 mL) for 30 minutes and then added drop wise to the ethanolic mixture prepared above. Stirring at room temperature was maintained for 36h. The reaction mixture was dried on a rotavapor, acetone was added to the dried product and the mixture was left on the refrigerator. After 2h acetone was separated and the oily product was dried. The reaction was followed by TLC, using $\text{CH}_2\text{Cl}_2:\text{MeOH}$ (6:0.7) mixture as eluent. A yellow oil was obtained ($\eta = 82\%$), soluble in

basic water. $^1\text{H-NMR}$ (300 MHz, D_2O + KOD, pH = 12): δ 7.282(10H,Ph), 6.190(1H,S), 4.258(2H, s), 3.723(2H, s), 3.613(4H, s). $\text{C}_{21}\text{H}_{21}\text{NO}_4$.

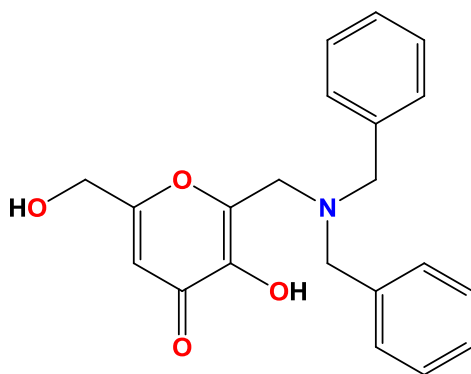


Figure A.1.5. 2-((dibenzylamino) methyl)-3-hydroxy-6-(hydroxymethyl)-4H-pyran-4-one (MW = 351.1).

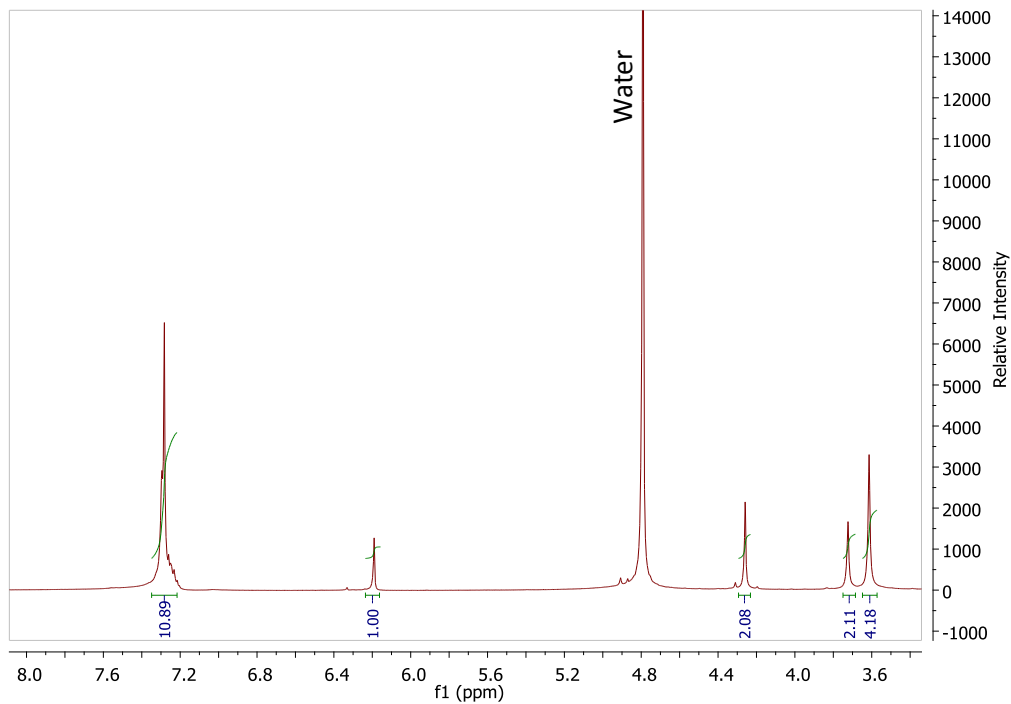


Figure A.1.6. $^1\text{H-NMR}$ spectrum of 2-((4-(4-chlorophenyl)piperazin-1-yl)methyl)-3-hydroxy-6-(hydroxymethyl)-4H-pyran-4-one.

5-(benzyloxy)-2-(hydroxymethyl)-1-methylpyridin-4(1H)-one

5-(benzyloxy)-2-(hydroxymethyl)-4H-pyran-4-one (300 mg, 1.3 mmol) and methylamine hydrochloride (99%, 88 mg, 1.3 mmol) were mixed in ethanol (96%, 15 mL). The reaction mixture was refluxed at 65 °C, and after one hour NaOH (7 M) was added until pH=12. The mixture was left under stirring further 1.5 hours, after that a precipitate appears. The precipitate was filtered and the resultant solid washed with cold ethanol. The reaction was followed by TLC, using CH₂Cl₂:MeOH (6:0.7) mixture as eluent. The final product (η = 39%) is a solid soluble in acid water.

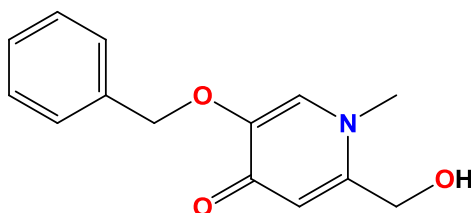


Figure A.1.7. 5-(benzyloxy)-2-(hydroxymethyl)-1-methylpyridin-4(1H)-one (MW = 245.1).

5-hydroxy-2-(hydroxymethyl)-1-methylpyridin-4(1H)-one

To 5-(benzyloxy)-2-(hydroxymethyl)-1-methylpyridin-4(1H)-one (20 mg, 0.08 mmol) was added Pd/C catalyst (5 mg, 25% of starting material) and methanol (10 mL). The mixture was stirred for 1 hour under the pressure of two atmospheres. The final product was a white solid (η = 95%). ¹H-NMR (300 MHz, D₂O): δ 7.698(1H, s), 6.768(1H,s), 4.639(2H, s), 3.789(3H, s). C₇H₉NO₃.

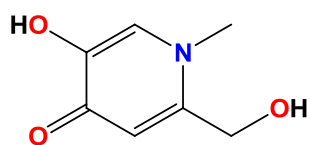


Figure A.1.8. 5-hydroxy-2-(hydroxymethyl)-1-methylpyridin-4(1H)-one
(MW = 155.1).

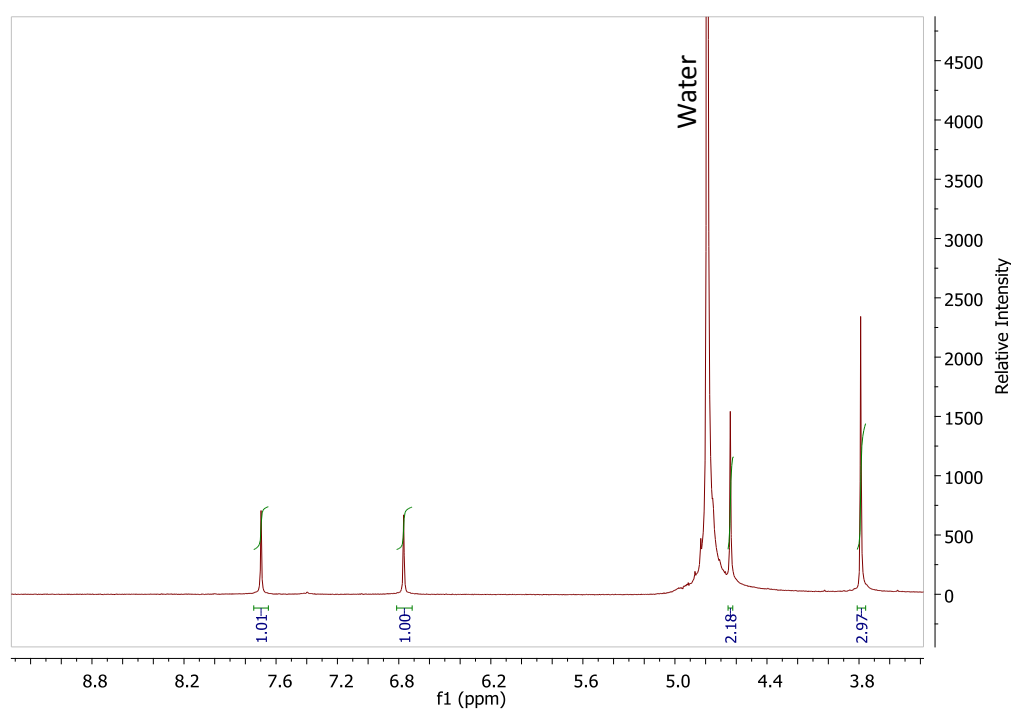


Figure A.1.9. ^1H -NMR spectrum of 5-hydroxy-2-(hydroxymethyl)-1-methylpyridin-4(1H)-one.

5-(benzyloxy)-2-(hydroxymethyl)-4H-pyran-4-one

To kojic acid (1.00 g, 7 mmol) was added benzylchloride (99%, 1.1 mL, 7.1 mmol), NaOH (7 M, 1.3 mL, 9 mmol) and ethanol (96%, 25 mL). The reaction mixture was refluxed at 65/70 °C for 12 hours; was evaporated with a rotavapor and cold water was

added. A light brown precipitate appeared, filtered and the resultant solid washed with ether. The reaction was followed by TLC, using $\text{CH}_2\text{Cl}_2:\text{MeOH}$ (6:0.5) mixture as eluent. A light brown solid ($\eta = 78\%$) was obtained, and is soluble in basic water. $^1\text{H-NMR}$ (300 MHz, MeOD): δ 7.932(1H, s) 7.310(5H, Ph), 6.431(1H, s), 4.949(2H, s), 4.326(2H, s). Melting point: 125-126 °C. $\text{C}_{13}\text{H}_{12}\text{O}_4$, Mass spectrum (ESS-MS (+)): $[\text{M}+\text{Na}]^+$ (254.9).

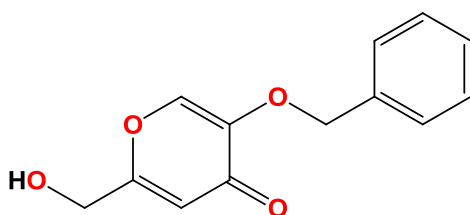


Figure A.1.6. 5-(benzyloxy)-2-(hydroxymethyl)-4H-pyran-4-one (MW = 232.1).

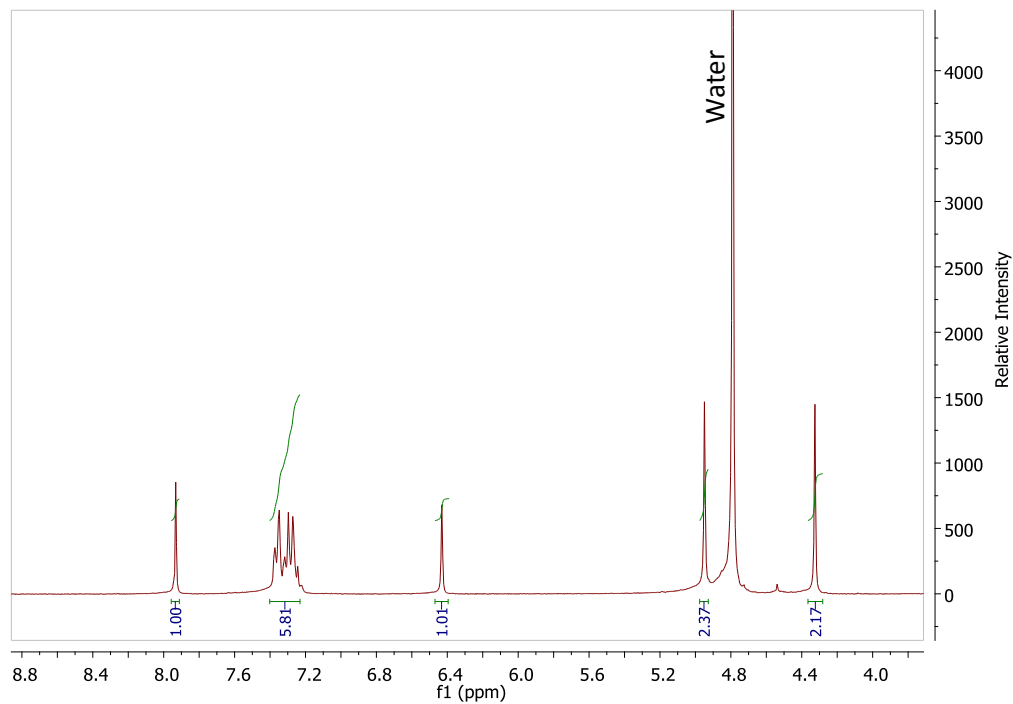


Figure A.1.7. $^1\text{H-NMR}$ spectrum of 5-(benzyloxy)-2-(hydroxymethyl)-4H-pyran-4-one.

5-(benzyloxy)-2-(hydroxymethyl)pyridin-4(1H)-one

To 5-(benzyloxy)-2-(hydroxymethyl)-4H-pyran-4-one (1.00 g, 4.3 mmol) was added ammonia (16 mL) and ethanol (96%, 25 mL). The reaction mixture was refluxed at 65/70 °C for 16h. The solvent was evaporated using a rotavapor and acetonitrile was added. A precipitate appeared, was filtered and the resultant solid was washed with cold acetonitrile. The reaction was followed by TLC, using CH₂Cl₂:MeOH (6:0.7) mixture as eluent. The final product was a beige solid (η = 80%), soluble in basic water. ¹H-NMR(300 MHz, MeOD): δ 7.632(1H, s) 7.442(5H, Ph), 6.616(1H, s), 5.085(2H, s), 4.422(2H, s). Melting point: 210-220 °C. C₁₃H₁₃NO₃, Mass spectrum (ESS-MS(+)): [M + Na]⁺(254.0), [M + K]⁺(269.9).

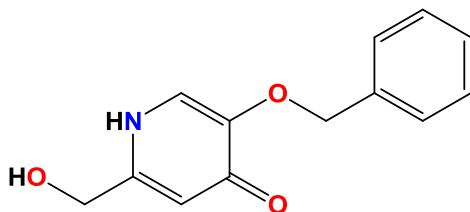


Figure A.1.8. 5-(benzyloxy)-2-(hydroxymethyl)pyridin-4(1H)-one (MW = 231.1).

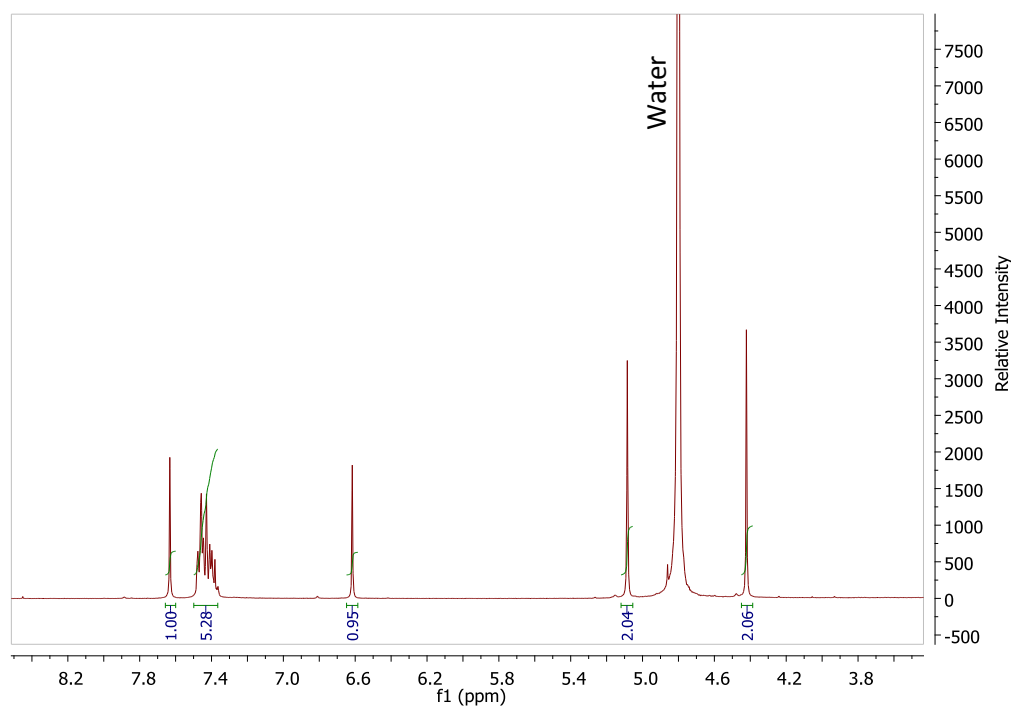


Figure A.1.9. ^1H -NMR spectrum of 5-(benzyloxy)-2-(hydroxymethyl)pyridin-4(1H)-one.

5-hydroxy-2-(hydroxymethyl)pyridin-4(1H)-one

To 5-(benzyloxy)-2-(hydroxymethyl)pyridin-4(1H)-one (600 mg, 2.6 mmol) was added Pd/C catalyst (90 mg, 15% of starting material) and methanol (20 mL), the mixture was stirred 2h under the pressure of two atmospheres. A dark purple solid was obtained ($\eta = 20\%$).

^1H -NMR(300 MHz, D_2O): δ 7.622(1H, s), 6.533(1H,S), 4.609(2H, s). Melting point: 239-241 °C. $\text{C}_6\text{H}_7\text{NO}_3$, Mass spectrum (ESS-MS (-)): MH^- (139.9).

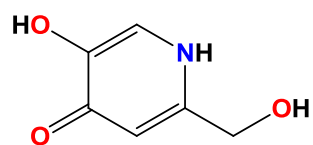


Figure A.1.10. 5-hydroxy-2-(hydroxymethyl)pyridin-4(1H)-one (MW = 141.0).

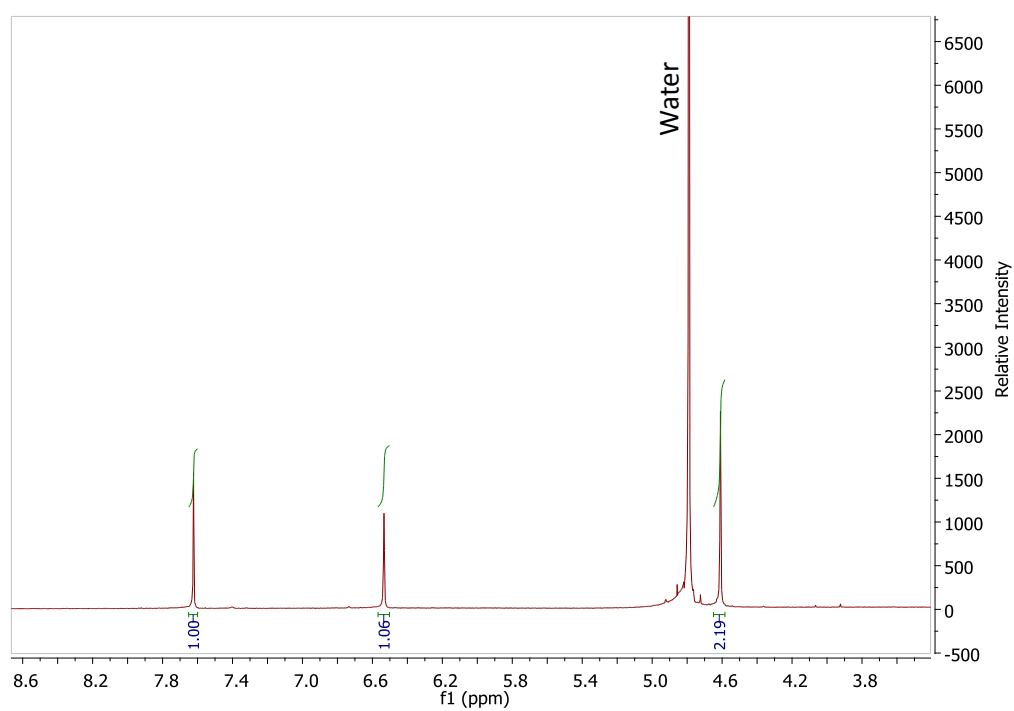


Figure A.1.11. ¹H-NMR spectrum of 5-hydroxy-2-(hydroxymethyl)pyridin-4(1H)-one.

Appendix 2

Unsuccessful Synthesis

Appendix 2

Unsuccessful Synthesis

First Strategy

Considering the higher affinity of deferiprone to iron compared with kojic acid, we tried to synthesize new hydroxypyridinones starting from kojic acid derivatives (see Fig. A.2.1.). The substitution of the oxygen in the hydroxypyrone ring with a nitrogen is possible only for the single unit of kojic acid but does not occur when two units of kojic are joined by a linker (Table 1).

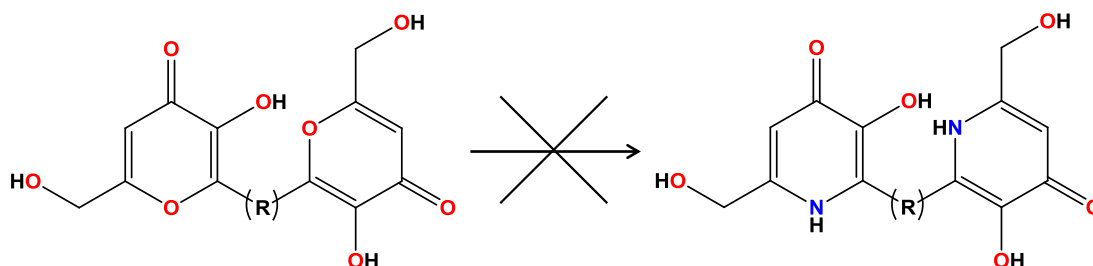


Figure A.2.1. Reaction scheme.

We tried to change in the four reactions (listed in the table A.2.1.) the base, replacing ammonia with benzylamine, but we obtained again only the fragmented reagents. Furthermore, we tried the same four syntheses at room temperature by increasing the reaction times (till 20 days), but a partial decomposition of the reagents and the formation of 5-hydroxy-2-(hydroxymethyl) pyridin-4 (1H)-one occurs.

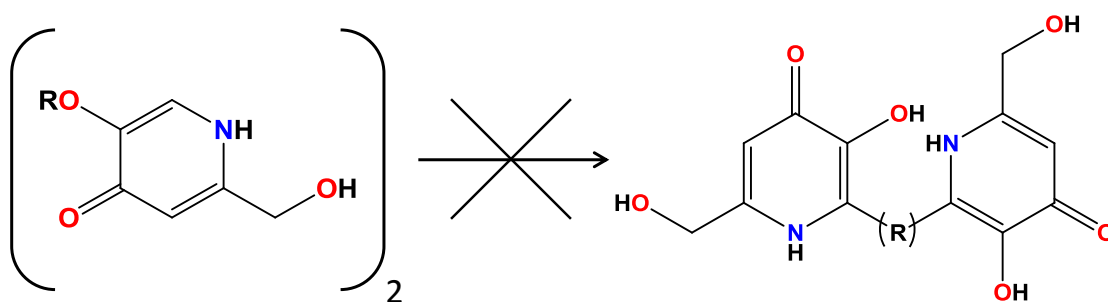
Table A.2. 1. Reactions with NH₃

Ligands	reagents	T (°C)	Time (h)	Comments
L1	NH ₃	70/80	21	Decomposition reagents
L2	NH ₃	70/80	26	Decomposition reagents
L6	NH ₃	70/80	20	No reaction
L8	NH ₃	70/80	46	Decomposition reagents

^a In all the reactions ethanol was used as a solvent

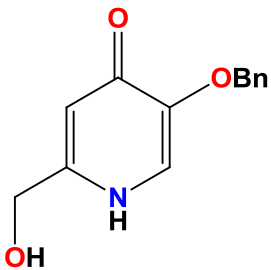
Second Strategy

We tried to obtain the kojic acid derivatives substituted with the nitrogen in the ring, starting from 5-hydroxy-2-(hydroxymethyl)pyridin-4 (1H)-one (R = H) and 5-(Benzyloxy)-2-(hydroxymethyl)pyridin-4 (1H)-one (R = Bn) (see Fig. A.2.2.).

**Figure A.2.2.** Reaction scheme.

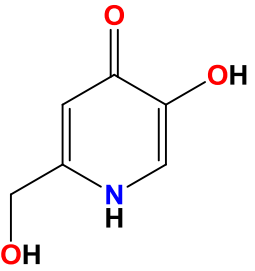
In Tables A.2.2. and A.2.3. are reported the several trials for the different conditions tested, namely, change in temperature, time of reaction and reagents.

Table A. 2.2 Reactions starting from 5-(benzyloxy)-2-(hydroxymethyl)pyridin-4(1H)-one^a

	Reagents	T (°C)	Time (h)	Comments
	Formaldehyde + NH ₃	65/70	24	No reaction
	Acetaldehyde + NH ₃	65/70	36	No reaction
	Ortovanilin + NH ₃	65/70	24	Decomposition reagents
	Formaldehyde + dimethylamine	RT	RT	No reaction
	Acetaldehyde + dimethylamine	RT	RT	No reaction
	Ortovanilin + dimethylamine	RT	RT	Decomposition reagents

^a In all the reactions ethanol was used as a solvent.

Table A.2.3. Reactions starting from 5-hydroxy-2-(hydroxymethyl)pyridin-4(1H)-one^a

	Reagents	T (°C)	Time (h)	Comments
	Formaldehyde + NH ₃	65/70	48	No reaction
	Acetaldehyde + NH ₃	65/70	48	No reaction
	Ortovanilin + NH ₃	65/70	48	No reaction
	Ortovanilin + dimethylamine	RT	68	Decomposition reagents
	Formaldehyde + Piperazin	RT	6	No reaction

^a In all the reactions ethanol was used as a solvent.

Paper I

Chelating Agents for Metal Intoxication

G. Crisponi, V.M. Nurchi, M. Crespo-Alonso, L. Toso, *Curr. Med. Chem.* 19 (2012) pp. 2794-2815.

DOI: 10.2174/092986712800609742

Copyright © 2014 Bentham Science Publishers

Chelating Agents for Metal Intoxication

G. Crisponi*, V.M. Nurchi, M. Crespo-Alonso and L. Toso

Dipartimento di Scienze Chimiche, Università di Cagliari, Cittadella Universitaria, 09042 Monserrato-Cagliari, Italy

Abstract: In this paper we took into examination the use of chelation therapy for treating metal intoxication in humans. We divided this paper in four main parts: before all the principal causes of toxicity are exposed; second the chemical requirements (thermodynamic and kinetic), the interactions with the endogenous molecules and the target organs, as well as the biomedical restraints; as a third step the classes of chelators in use along with the specific treatments allowed are treated and as a final step the principal toxic metal ions are presented. Based on the presented material some conclusion are drawn on the state of art of metal chelation, and the basis are given for a rationale development of metal chelation, founded on chemical, biological and medical considerations.

Keywords: Chelation therapy, Ligands, Metal complexes, Toxic metals, Heavy metals, Speciation.

1. INTRODUCTION

Nowadays in the industrial society exposure to metal ions is ever increasing, and so their toxic effects to humans. Metal ions enter in everyday life: metal compounds are used in medicine, in alimentary industries, in water purification plants, in cosmetics, in painting, as wood preservatives, and so on. Thus metal ions can exert their toxic effects, giving different symptoms, which depend on the toxic species as well as from other different factors. One of the principal ways to counteract metal toxicity in humans consists in the treatment with metal chelators in order to transform the toxic metal ion form in a less dangerous species that can be excreted from the organism. Some general reviews appeared in the last fifteen years on the chelation therapy to treat metal toxicity [1-4], in addition to some reviews focused on particular metal ions [5-10]. A beneficial use of chelation therapy as well as the design of proper chelators requires a variety of chemical, biological and medical knowledge. In the following we will separate these various topics, i.e. before all the principal causes of toxicity will be exposed; second we will expose the chemical requirements (thermodynamic and kinetic), the interactions with the endogenous molecules and the target organs, as well as the biomedical restraints. As a third step the classes of chelators in use along with the specific treatments allowed will be treated and as a final step the principal toxic metal ions will be presented.

2. METAL ION TOXICITY

As a starting point, three different categories of metal toxicity can be distinguished, according to their sources and to their effects:

- Acute ingestion of toxic metal ions¹, that can be accidental, as frequently happens to children, or caused by a voluntary homicidal or suicidal attempt.
- Chronic intoxication, which may depend on environmental, occupational or iatrogenic causes.
- Metal overload due to genetic diseases.

This first row classification is of primary importance in establishing the required treatments, spanning from an immediate clinical powerful treatment with a massive dose of chelators for a short limited time, to a lifelong treatment for genetic diseases.

A parallel classification of chemical elements can be made according to the role they exert in the physiology of humans. At least three categories can be distinguished: essential, inert, and

toxic. To be defined essential an element must satisfy the following conditions:

1. it must be present in living matter;
2. it must interact with living matter;
3. its dietary deficiency must result in are duction of a biological function from optimal to suboptimal, which can be prevented or reversed by proper element amounts.[11]

Presently 20 elements are defined essential with certainty. According to their content in the body these are the four organic base elements H, C, N, and O, the seven quantity elements Na, Mg, P, S, Cl, K, and Ca, and the nine essential trace elements Mn, Fe, Co, Ni, Cu, Zn, Se, Mo, and I. Nowadays other elements, as F, B, Si, As, and V are under discussion to be included in the category of essential elements [12-14].

Oxygen (65%) and **Hydrogen** (10%) are predominantly found in water, which makes up about 60 percent of the body by weight; **Carbon** (18%) is the main constituent of the endogenous molecules of living organisms, and **Nitrogen** (3%) is found in many organic molecules, including amino acids in proteins, and the constituents of nucleic acids.

Calcium (1.5%) is the most common inorganic constituent of the human body, above all in bones and teeth. Calcium exerts its most important roles in human organism in muscle contraction and in protein regulation; if not enough of the element is carried by diet the organism utilizes calcium from bones.

Phosphorus (1%) is found in bone, in ATP, as well as in nucleotides.

Sulfur (0.25%), is mainly contained in two amino acids, cysteine and methionine, that play an important role in protein structure.

Potassium (0.25%) has two main functions: regulation of the heartbeat and electrical signaling in nerves.

Sodium (0.15%) is the second electrolyte, fundamental for electrical signaling in nerves. It regulates the amount of water in the body.

Chlorine (0.15%), usually in the form of chloride, is important for balancing the normal content of fluids in the body.

Magnesium (0.05%) besides its important role in the structure of the skeleton and muscles, it is essential in more than 300 metabolic reactions.

Iron (0.006%) is implied in hundred enzymatic reactions, and it is an essential component of hemoglobin, the oxygen carrier in red blood cells.

Zinc (0.0032%) takes part to the enzymatic action of more than three hundred proteins. Zinc deficiency in developing countries leads to dwarfism.

*Address correspondence to this author at the Dipartimento di Scienze Chimiche, Cittadella Universitaria, 09042 Monserrato-Cagliari, Italy; Tel: +39 070 675 4476; Fax: +39 070 675 4478; E-mail: crisponi@unica.it

¹In this paper we will speak of toxic metals, or toxic metal ions, even if in many instances metalloid elements are implied.

Paper II

Chelation Therapy for Metal Intoxication: comments from a thermodynamic viewpoint

V.M. Nurchi, M.C. Alonso, L. Toso, J.I. Lachowicz, G. Crisponi, *Mini Rev. Med. Chem.* 13 (2013) pp. 1541-1549.

DOI: 10.2174/13895575113139990077

Copyright © 2014 Bentham Science Publishers

Chelation Therapy for Metal Intoxication: Comments from a Thermodynamic Viewpoint

Valeria Marina Nurchi, Miriam Crespo-Alonso, Leonardo Toso, Joanna Izabela Lachowicz and Guido Crisponi*

Dipartimento di Scienze Chimiche e Geologiche, Università di Cagliari, Cittadella Universitaria, 09042 Monserrato-Cagliari, Italy

Abstract: Chelation therapy plays a prominent role in the clinical treatment of metal intoxication. In this paper the principal causes of metal toxicity are exposed, and the chemical and biomedical requisites of a chelating agent are sketched. The chelating agents currently in use for scavenging toxic metal ions from humans belong to few categories: those characterized by coordinating mercapto groups, by oxygen groups, poliaminocarboxylic acids, and dithiocarbamates. Considering that the complex formation equilibria have been studied for less than 50% of chelators in use, some reflections on the utility of stability constants are presented, together with an evaluation of ligands under the stability profile. The competition between endogenous and toxic target metal ions for the same chelating agent is furthermore examined. A thorough examination of stability constant databases has allowed to select, for each toxic metal, the ligands distinguished by the best pMe values. Even though this selection does not consider the biomedical requisites of a chelating agent, it gives a clear picture both of the pMe values that can be attained, and of the most appropriate chelators for each metal ion.

Keywords: Chelating agent, Chelation therapy, Heavy metal, Speciation, Stability constant, Toxic metal.

INTRODUCTION

The poisoning action of toxic metal ions, originated by accidental, occupational/environmental and iatrogenic causes, represents one of important health and social problems both in developed and in emerging countries [1-12]. The research on this topic is nonetheless totally inadequate since the investments of pharma-industries are limited because of their poor profitability. The research on chelating agents to be used in clinical practice is based essentially on biology-driven programs, paying no attention to the chemical knowledge of the mechanism involved in the complex formation. Actually the term “chelating agent” in common sense is a drug able to bind metal ions. In this way the chelating agents used for given metal ions are not necessarily the best, but the most common drugs. Specificity and stability, as well the knowledge of the length of the treatment (limited in time or lifelong) are extremely important in the choice of a chelator. A first intent of the present paper is to remark, based on the analysis of literature data, the large extent of chelators in use for which a deep chemical basis is lacking, and to propose a strategy for the future research in this field. A second aim is the selection from stability constant databases of the best possible families of ligands for each target toxic metal ion. Speciation plots and proper parameters (pM) will allow a preliminary evaluation of the

attitude of these ligand families as chelators for clinical treatments. Finally, some aspects of wide importance, as the competition between toxic and endogenous metal ions toward the same metal chelator, have been deepened.

METAL TOXICITY

Metal toxicity can be roughly sorted in three big different classes according to its sources and effects:

- Acute intoxication, deriving from direct ingestion of toxic metal (accidental, as often occurs to children, or due to a voluntary homicidal or suicidal attempt);
- Chronic intoxication, depending on environmental pollution, or related to work conditions, or to iatrogenic causes;
- Metal overload due to genetic diseases (β -thalassemia (iron)¹ and Wilson's disease (copper) [6, 13]).

This classification helps in managing clinical treatments, among which chelation therapy plays a prominent role. Chelation therapy has the intent of scavenging the toxic metal ion from the organism, or of attenuating its toxicity by converting it in a less toxic compound, or of relocating it from the position where its action is toxic to a compartment where the toxic action cannot be exploited, or of controlling its redox potential.

*Address correspondence to this author at the Dipartimento di Scienze Chimiche e Geologiche, Università di Cagliari, Cittadella Universitaria, 09042 Monserrato-Cagliari, Italy; Tel: +39 070 675 4476; Fax: +39 070 675 4478; E-mail: crisponi@unica.it

¹ β -thalassemia, a genetic disease with a defect in haemoglobin synthesis, requires regular blood transfusions to prevent anaemia.

Paper III

Metal Ions in the Pathogenesis of Alzheimer's Disease: an open field

G. Crisponi, V.M. Nurchi, D. Fanni, C. Gerosa, S. Nemolato, M.C. Alonso, L. Toso, J.I. Lachowicz, G. Faa, *Frontiers in Clinical Drug Research – Alzheimer Disorders*, 1 (2013) pp. 411-431.

DOI: 10.2174/97816080572211130101

Copyright © 2014 Bentham Science Publishers

CHAPTER 11**Metal Ions in the Pathogenesis of Alzheimer's Disease: An Open Field**

Guido Crisponi^{1,*}, Valeria M. Nurchi¹, Daniela Fanni², Clara Gerosa², Sonia Nemolato², Miriam Crespo-Alonso¹, Leonardo Toso¹, Joanna I. Lachowicz¹ and Gavino Faa²

¹*Department of Chemistry and Geology, University Campus, 09042 Montserrat Cagliari, Italy and* ²*Department of Surgical Sciences, Sec., Pathology, Via Ospedale 46, 09124 Cagliari, Italy*

Abstract: Despite the large availability of data regarding the mechanisms at the basis of β -amyloid production in Alzheimer's disease (AD), the factors responsible for β -amyloid accumulation in neurons of AD patients until now have not been entirely clarified. Several metal ions have been indicated as possible triggers of the main conformational modifications of β -amyloid protein, and metal homeostasis disarrangement has been proposed as a relevant pathological cofactor of neurodegeneration. Epidemiological evidences suggest a possible association between exposure to increased amounts of multiple metals and onset and progression of AD. According to this hypothesis, metals could induce oxidative stress in neurons, developing neurodegenerative disease. In this chapter, the role of various trace metals as cofactors of a poor cognitive function and of an increased risk of dementia leading to AD will be discussed. In particular, this study is aimed to critically analyze the role played by copper, iron, zinc and aluminium in neurodegeneration. Based on the current evidences concerning the relationship between these metal ions and onset and progression of AD, no definitive recommendations are, at the best of our knowledge, possible. However, foods rich in metals such as iron and copper should be discouraged, as well as caution should be suggested in exposure to aluminium sources. Further studies on the relationship between metal overexposure and AD development hopefully will open new opportunities for the prevention and management of neurodegenerative diseases.

Keywords: Alzheimer's disease, neurodegenerative diseases, β -amyloid protein, oxidative stress, copper, iron, zinc, aluminium.

INTRODUCTION

Alzheimer's disease (AD) may be defined as a disarrangement of the cellular

*Address correspondence to **Guido Crisponi**: Department of Chemistry and Geology, Citadel University, Montserrat 09042 Cagliari, Italy; Italy; E-mail crisponi@unica.it

control system responsible for the correct folding of proteins during neuronal cell life. Misfolded proteins show a tendency to aggregate, leading to a series of severe pathological consequences and ultimately to AD, suggesting the inclusion of this disease among conformational diseases [1]. Two proteins are characterized by misfolding in AD: β -amyloid protein ($A\beta$), a proteolytic cleavage product of the $A\beta$ precursor protein (APP), and tau protein, a microtubule-associated protein, prone to aggregation after hyperphosphorylation [2]. Despite a large amount of data available in the recent literature regarding the mechanisms at the basis of $A\beta$ production and of its interactions with other cellular components, the factors responsible for $A\beta$ accumulation in neurons are nowadays still not entirely clarified. Mounting evidences support the hypothesis that both endogenous and exogenous metal ions could be involved, as factors or cofactors, in the pathogenesis of AD [3]. A number of metal ions have been indicated as possible triggers of the main conformational modifications of $A\beta$, and metal dyshomeostasis has been suggested as a relevant pathological cofactor of neurodegeneration [4]. Gathered evidence suggests that $A\beta$ precipitation could be caused by abnormal interactions with metal ions, including Zn^{II} , Cu^{II} and Fe^{III} . Moreover, in a mouse model of AD, compounds that interdict metal ion binding to $A\beta$ have been reported to inhibit $A\beta$ precipitation and deposition, opening a new field of research: the metallobiology of AD [5]. These data suggest a major role for trace metal ions in the generation of toxic $A\beta$ oligomers in neurons, that are likely to be responsible for the synaptic dysfunction associated with AD. On this basis the so-called “metal protein attenuating compound” approach has been recently proposed as a novel therapy for AD [6].

Whereas the previous data indicate that metal ions - including iron, copper, zinc and aluminium – might increase the neurotoxicity of $A\beta$, other reports have demonstrated that $A\beta$ could help to limit the toxicity on brain cells exerted by redox-active metal ions, thereby participating to the antioxidant defense of neurons against reactive oxygen species (ROS). These findings were at the basis of the hypothesis of the amyloid paradox, amyloid-beta-metal complexes putatively being neurotoxic and, under some circumstances, neuroprotective [7].

This review will try to report the main data from the recent literature on the role played by metal ions in the onset and development of AD, focusing on the role played by iron, copper, zinc and aluminium in neuronal toxicity and dementia.

METAL-INDUCED OXIDATIVE STRESS AND NEURO-DEGENERATIVE DISEASE

The brain is a highly oxidative organ, accounting for about 2% of total body weight but consuming 20% of the oxygen used by the whole body. Moreover, with normal ageing, human brain accumulates transition metal ions, including iron and copper, which may promote the generation of ROS *via* Fenton chemistry* [9]. Binding of A β to redox-reactive metals, which in turn generate free radicals, has been proposed among the several mechanisms recognized to be involved in the molecular pathways to neurodegeneration and, in particular, in the onset and development of AD [10]. Compelling evidences - based on results of studies on *in vitro* systems, experimental animals and humans - indicate that the etiology of AD involves oxidative stress. This implicates that redox active metal ions, such as copper and iron, and redox-inert zinc ions, play a central role in this process [11]. According to this hypothesis, trace metal dyshomeostasis and the consequent abnormal accumulation of transition metals, including iron and copper, in the ageing brain cells might elicit oxidative stress and macromolecular damage that could eventually impede neuronal function leading to neurodegeneration and to AD [12]. It has been claimed that the increased oxidative stress in brain cells of AD patients could be reflected by increased protein and DNA oxidation, enhanced lipid peroxidation, decreased levels of cytochrome c oxidase and increased brain content of transition metal ions iron and copper, both capable of stimulating free radical formation *via* Fenton reaction [13]. Redox active Cu^{II} and Fe^{III} ions have been shown to be reduced in the presence of A β protein, with concomitant production of ROS, hydrogen peroxide (H₂O₂) and hydroxyl radical (OH \cdot), leading directly to the widespread oxidation damages typical of AD brains [14]. The discovery of a functional iron-response element (IRE) in the 5' untranslated region of APP, consistent with the biochemical evidence that it is a redox-active metalloprotein, is at the basis of the hypothesis that the redox interactions between A β protein and metal ions may be at the heart of a pathological positive feedback system, wherein A β amyloidosis and oxidative stress promote each other [14].

* According to Alexander "... a potential harmful chemical property of iron and its compounds is the ability to catalytically generate potent hydroxyl radicals that are oxidatively toxic to cells. This catalysis (Fenton reactions) occurs with activated oxygen species (superoxide and hydrogen peroxide)" [8].

Paper IV

Copper Chelators: chemical properties and biomedical applications

M. Tegoni, D. Valensis, L. Toso, M. Remelli, *Curr. Med. Chem.* (2014), *Submitted*.

Copper chelators: chemical properties and bio-medical applications

Matteo Tegoni,¹ Daniela Valensin,² Leonardo Toso,³ Maurizio Remelli^{4*}

¹ Department of Chemistry, University of Parma, Parco Area delle Scienze, 17A, 43124 Parma, Italy.

² Department of Biotechnology, Chemistry and Pharmacy, University of Siena, via A. de Gasperi 2, 53100 Siena, Italy

³ Department of Chemical and Geological Sciences, University of Cagliari, Cittadella Universitaria, 09042 Monserrato, Cagliari, Italy

⁴ Department of Chemical and Pharmaceutical Sciences, University of Ferrara, Via Fossato di Mortara 17, 44121 Ferrara, Italy (email: rmm@unife.it)

*Corresponding author

Keywords

Copper chelators, copper metabolism, copper overload, Penicillamine, Trientine, Tetrathiomolybdate, bifunctional ligands, neurodegenerative diseases.

Abstract

Copper is present in different concentrations and chemical forms throughout the earth crust, surface and deep water and even, in trace amounts, in the atmosphere itself. Copper is one of the first metals used by humans, the first artifacts dating back 10,000 years ago. Currently, the world production of refined copper exceeds 16,000 tons / year.

Copper is a *micro*-element essential to life, principally for its red-ox properties that make it a necessary cofactor for many enzymes, such as superoxide dismutase and cytochrome-c oxidase. In some animal species (e.g. octopus, snails, spiders, oysters) copper-hemocyanins also act as carriers of oxygen instead of hemoglobin. However, these red-ox properties also make the pair $\text{Cu}^+/\text{Cu}^{2+}$ a formidable catalyst for the formation of Reactive Oxygen Species, when copper is present in excess in the body or in tissues.

The treatment of choice in cases of copper overloading or intoxication is the chelation therapy. Different molecules are already in clinical use as chelators or under study or clinical trial. It is worth noting that chelation therapy has also been suggested to treat some neurodegenerative diseases or cardiovascular disorders.

In this review, after a brief description of the homeostasis and some cases of dyshomeostasis of copper, the main (used or potential) chelators are described; their properties in solution, even in relation to the presence of metal or ligand competitors, under physiological conditions, are discussed. The legislation of the most important Western countries, regarding both the use of chelating agents and the limits of copper in foods, drugs and cosmetics, is also outlined.

1. INTRODUCTION

1.1 Copper in environmental compartments

Copper was the first metal discovered by man and is still extensively used today. In fact, copper production has lifted over the last decades and continues increasing, meaning that more copper ends up in the environment. The World consumption of refined copper amounted to 20.5 million tons in 2012 (16.7 million tons were achieved in 2005) [1]. Copper is the material of choice for

many industrial and commercial uses due to its versatility, malleability, resistance to corrosion and good thermal and electrical properties. It is extensively used to make electrical wiring, motors and magnets, tubing and valves, fittings, munitions, alloys (stainless steel, brass, bronze), coins, cooking utensils, coatings and building materials. Copper derivatives are used as fungicides, algicides, insecticides or preservatives for wood, leather and fabrics. For example, chromated copper arsenate (CCA) was extensively used in the past

to treat wood. After January 2004 the US Environmental Protection Agency (EPA) has banned its use for building construction, especially for children's structures [2].

Copper is used as a fertilizer for plants and is given to animals as a nutrient to support growth. It is also used to prevent diseases in livestock and poultry production and to increase the intake of food by animals. One consequence of this is the accumulation of copper in manure that is thrown to the fields and contaminates soils. In 1999, the European Commission proposed limits for the use of copper in animal feed. According to size and age of the animal, copper values can range from 170–25 mg/kg⁻¹ for pigs, 15 mg/kg⁻¹ for cattle and 25 mg/kg⁻¹ for chickens, sheep and goats. No regulation is adopted in China for copper use in animal feed, and its use is often excessive.

Copper is essential for the normal functioning of plants, animals and microorganisms, but at elevated concentrations it becomes toxic. Therefore its levels in the natural environment and its biological availability are a very important issues. When copper is released into the environment, the metal is exposed to different conditions (pH, redox potential, and organic content) that influence its bioavailability. It is well known that the concentration and type of dissolved organic carbon [3-5] and the presence of competing cations such as Ca²⁺, Mg²⁺, H⁺, Na⁺ or K⁺ [6, 7] can modify the bioavailability of copper.

Natural discharges of copper to air and water occur, as a result of windblown dust and volcanic eruptions, but the main contribution for copper accumulation in the environment results from industrial activity. Copper enters in the air, mainly during the combustion of fuel and motor oil and during copper and other metals production. In air, copper persists for about 13 days [8], and remains there before it settles in the soil or water with rain. In Europe, the mean copper emission to atmosphere from road transport was estimated to be 4.0–5.5 ktonnes/year [9]. Brake lining material from vehicles is also an important source of particulate copper emissions to the atmosphere, particularly in Western Europe where it is responsible for 50–75% of the total copper emissions to air [9].

The accumulation of copper in the soils is a result of the extensive use of copper-based fungicides and fertilizers. Particularly, the use of fungicides to fight vine diseases has led to accumulation in vineyard soils all over the world [10]. Copper has been detected at

concentrations above 100 mg/kg in soils of France [11], Italy [12] and other European countries [10, 13], in the American continent [14] and in Australia [15]. As a result soils contain large quantities of copper, predominantly in the Cu²⁺ state complexed or bonded to the organic matter. The level of free copper in the soils is controlled by a combination of complexation, adsorption, and precipitation processes.

The release of copper into rivers, lakes, and oceans results mainly from waste discharges, like those from mines and industries, leaching of antifouling marine paints and wood preservatives. In aquatic environments, copper is extremely toxic to fish, invertebrates, amphibians, algae and aquatic microorganisms [16]. Its toxicity is proportional to the concentration of inorganic Cu²⁺ species. In addition, the free hydrated Cu²⁺ ion blocks the uptake of essential micronutrients Mn²⁺ and Zn²⁺ [17].

Copper contaminated sediments may contain a wide range of copper concentrations that increase the degree of exposure to the metal [18, 19]. Copper bioavailability and toxicity is controlled by its adsorption, complexation and precipitation with other ligands, like sulfide. Unfortunately, the enormous heterogeneity of sediment composition makes it extremely difficult to predict the correlation of sediment toxicity due to a specific contaminant like copper. New guidelines to determine copper values in marine sediments, were proposed recently by Simpson *et al.* [19].

1.2 Copper in food and drinking water

Copper is an essential nutrient required for adequate growth, cardiovascular integrity, lung elasticity, neovascularization, neuroendocrine function, and iron metabolism. The average intake of copper by human adults varies from 0.6 to 1.6 mg/day, and about half is absorbed from food [20-23]. The main sources of copper intake are seeds, grains, nuts, beans, potatoes, tomatoes, shellfish and liver [23]. Copper in food is bound to organic molecules and is processed safely by the liver and distributed to copper-requiring proteins [24]. Excess of copper is excreted through bile and this is the main factor controlling homeostasis.

Copper in drinking water contribute less to copper intake (<0.001 mg/day) [25, 26], but depending on water characteristics, like pH and hardness, and the availability of copper in the distribution system, the concentrations of copper can vary significantly. Several studies

performed in Europe, Canada and in the USA indicate that copper levels in drinking water can range from ≤ 0.005 to ≥ 30 mg/L [27].

The exact value for copper recommended intake is difficult to precise, because there are several parameters to consider, like age, sex, dietary intake, and region of origin. Most of the studies concerning copper deficiency and excess in humans have been performed in USA. Regarding this, in 2001 the recommended dietary intake (RDA) of copper has been reported to be 0.9 mg/day for human adults specified by the Institute of Medicine (IOM) [28]. More recently, in 2004 ministries of health of Australia set their own recommendations to 1.7 mg/day for adult man and 1.2 mg/day for adult woman [29].

1.3 Copper in drugs and cosmetics

Throughout history, copper compounds have been used in medicine, either topically or ingested. More than 2000 years ago, the ancient Egyptians and Chinese people used copper salts as antiseptics and to sterilize drinking water [30]. In the 19th century, the medical use of copper became widespread with a variety of inorganic copper preparations that were used to treat chronic adenitis, eczema, impetigo, scrofulosis, tubercular infections, lupus, syphilis, anemia, chorea, and facial neuralgia. Nowadays, copper continues to be an important component of a great number of pharmaceutical agents. For example, copper intrauterine devices for the prevention of inception are widespread used for very prolonged periods of time by millions of women worldwide. Another example, although controversial, is the use of copper bracelets to treat arthritis and to help reduce pain [31-35]. Further studies report the effectiveness of magnet therapy on rheumatoid arthritis and chronic pain [36].

Copper has long been used as antifungal and antibacterial agent. Although the exact mechanism by which the metal acts is not fully understood, its benefits have long been recognized (for recent reviews see references [37-39]). In addition, its strong biocidal properties are routinely used in healthcare areas as in the control of legionella [40, 41] and other bacteria [42] and in hospital water distribution systems using the method of copper and silver ionization.

Recently, the use of copper as anticancer agents has attracted much attention. First of all, being an essential element, copper complexes are believed to be less toxic than cisplatin compounds, currently used in cancer

therapy (reviewed by [43]). Even though the precise action of copper is not always known, it is believed that a big contribution to its toxicity comes from its ability to produce reactive oxygen species (ROS), to displace other metal ions, to peroxidize lipids, and to cleave DNA or RNA. In addition, copper-based semiconductors are also attractive alternatives to cadmium-contrasting agents for *in vivo* cancer imaging [44, 45], because their chemistry is dominated by only two oxidation states and its coordination chemistry remains relatively simple compared to other transition elements.

Copper derivatives are also used in cosmetics. The copper complexes formed with the tripeptide (glycyl-histidyl-lysine, GHK) [46], isolated from human plasma, have been extensively studied as anti-aging cosmetics [47] and wound healing drugs [48]. They stimulate the synthesis of collagen, elastin and glycosaminoglycans and promote the formation of the extracellular cement between cells [48]. A series of studies have demonstrated that cosmetics containing GHK are more effective than the traditionally used treatments containing Vitamin C, or retinoic acid [47]. The creams with GHK were shown to improve strength and elasticity of the skin.

2. COPPER IN THE HUMAN BODY

Copper is a transition metal ion essential to human health. It acts as catalytic or structural cofactor of many enzymes, it is required for the development and function of nervous and cardiovascular systems and it is fundamental for the skin, bone, reproductive and immune systems. Many body functions such as collagen production, formation of red blood cells, regulation of cholesterol levels, iron adsorption, oxidation of fatty acids, melanin production and intracellular energy levels control are all dependent on copper.

The amount of copper contained in human organisms is about 80-100 mg [49]. However, it is believed that this number is dependent on age and gender [50]. The highest concentrations of copper are present in the brain and the liver, but the central nervous system and the heart contain high levels of copper as well [49].

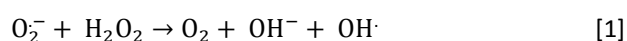
In human body, most of copper is bound to biological macromolecules, under both its main oxidation states: Cu^+ is mainly present in the intracellular space (reducing environments), while Cu^{2+} is dominant in the extracellular space (oxidizing environment). The oxidized

(Cu²⁺) and reduced (Cu⁺) copper exhibit different chemical properties. Cu⁺ is not stable in aqueous solution where it is easily oxidized to Cu²⁺. The standard reduction potential (E_0) of the couple Cu²⁺/ Cu⁺ is 0.153 V, thus reflecting the low likelihood that Cu²⁺ is reduced.

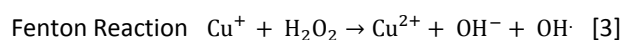
According to the Pearson acid-base concept (HSAB), Cu⁺ usually prefers to bind soft ligands rather than intermediate ones as Cu²⁺ does. In proteins, stable Cu⁺ binding sites are usually formed by sulfur thiolate or thioether from Cys and Met, while Cu²⁺ is usually anchored to His imidazole or N-terminal amino group.

Copper behaves as catalytic cofactor of many enzymes which exploit the copper redox activity to carry on many biological reactions [51]. Cytochrome-c oxidase (CcO), superoxide dismutase (SOD), ceruloplasmin, tyrosinase, peptidyl- α -monooxygenase and dopamine beta-monooxygenase are some examples of human copper enzymes.

Despite that, redox activity of copper may also originate highly toxic species. In fact, Cu²⁺, similarly to Fe³⁺, may also catalytically favour the formation of reactive oxygen species (ROS), which in turn cause high oxidative stress in our body. The reaction, known as Haber–Weiss reaction generates hydroxyl radicals from hydrogen peroxide and superoxide [52].



Importantly Haber–Weiss reaction is thermodynamically unfavorable in biologic systems and it require Fe³⁺ (or Cu²⁺) to proceed. The resulting metal-catalyzed reaction, including the Fenton reaction, is now believed to be the major mechanism by which ROS are produced in biological systems [53].



It is believed that abnormal and uncontrolled concentrations of Cu²⁺ inside the cell, might be responsible of cellular oxidative damage. In fact ROS generated by Cu²⁺ and Fe³⁺ may in turn lead toxic cellular events such as DNA damage, protein and lipid oxidation. For these reasons our body, possesses complex pathways which beside to ensure copper intake, distribution, utilization and excretion are able to contrast its toxicity.

2.1 Copper homeostasis

Copper is required for the proper function of many enzymes whose activity is fundamental for the life of our

organism. Copper levels in our body are strictly regulated by a sophisticated machinery composed by a network of proteins whose functions guarantee correct copper delivery to specific cellular targets, avoiding circulation of “free” copper. In fact, because of the high toxicity of “free” copper ions, which can participate to the production of ROS, it is strictly necessary that copper adsorption, distribution, utilization and excretion is regulated by specific proteins able to tightly bound copper ions [54-57]. The precise functioning of the systems regulating copper homeostasis is fundamental for our health and its alterations may lead to severe disease states [58, 59]. As this regard, eukaryotic systems have developed a well-organized systems which ensure a correct copper transportation to all the specific cellular targets.

After copper intake by diet, copper is absorbed in the small intestine where the metal is absorbed by intestinal epithelial cells [51, 60]. Copper storage in the liver or copper excretion in bile takes place if too much copper is adsorbed. As shown in Fig. 1, copper translocation across the cellular membranes is carried out by human Ctr-1 (hCtr-1), a high affinity copper transport protein (Figure 1) [61-63], mainly expressed in the liver and kidney [64]. Ctr-transporter proteins are also found in other organisms, indicating a conserved function from yeast to higher species. Ctr-1 is a relatively small transmembrane protein (190 amino acids), with three transmembrane α helices. Although Ctr family members have a low sequence homology, they are all characterized by common features: a long N-terminal extra cellular domain rich in Met and His residues and a conserved CysHisCys motif at the end of the short C-terminal tail, in the cytoplasm.

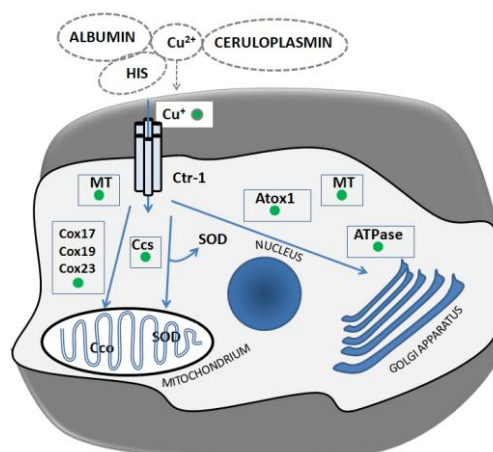


Figure 1. Schematic representation of copper distribution inside the cell.

Copper transportation inside the cell occurs through a channel-like architecture formed by homo trimer hCtr-1 structures [65]. It is still not clear which protein residues are involved in channel relay and how the channel is controlled. However, there are strong evidences that Cu^+ , rather than Cu^{2+} is bound to Ctr-1 [66-68]. The mechanisms by which Cu^+ is transferred from extracellular proteins (e.g ceruloplasmin, metalloredutase, amino acids) to Ctr-1 is not understood yet. It has been recently proposed that Cu^+ is specifically transferred to hCtr-1 by the following mechanisms [61]: (i) the N-terminus of hCtr-1 possesses an high affinity site for Cu^+ bound molecules, or (ii) a stable metalloredutase-hCtr-1 complex is formed.

Ctr-1 possesses Cu^+ binding domains at both N- and C-terminus. At the N-terminus, the extracellular domain of hCtr-1 is able to coordinate two Cu^+ ions. Each binding sites is constituted by three Met thioether groups [65, 69]. Recent investigations on model peptides encompassing the first 14 residues of the extracellular hCtr-1 domain, indicate that His residues might be involved in copper acquisition from plasma proteins as well. In addition, they might play a key role in Cu^{2+} reduction to Cu^+ [70]. On the other hand, the Cu^+ binding domain at the C-terminal intracellular domain of Ctr-1 is constituted by Cys clusters [71].

Once Cu^+ is delivered inside the cell, it is handled by precise copper chaperones which guarantee its transportation to various subcellular compartments (e.g. Golgi apparatus, mitochondria) for subsequent incorporation into copper enzymes (Figure 1).

Copper is transported to the Golgi apparatus by two components system, Atox1 and copper transporting adenylypyrophosphatase (ATPase), ATP7A and ATP7B [72-74]. In the cytoplasm, Atox1 chaperone binds Cu^+ and transfers it to ATPase. Subsequently both ATP7A and ATP7B deliver copper ions to the Golgi apparatus. Human Atox1, also known as Hah1, is a 68 amino acids protein displaying a ferredoxin-like fold [75]. The Cu^+ binding site is located in the first loop and encompasses –MTCGGC– residues (MXCXGC motif) [75]. Ternary complexes are formed, with Cu^+ coordinated to sulfur atoms from two Cys and from exogenous thiols [75, 76].

ATP7A and ATP7B are transmembrane proteins (TPs) able to pump copper(I) to the Golgi organelle [77]. The

metal ion passage across the cell membranes is made possible by the energy release occurring during ATP hydrolysis. The N-terminal cytosolic tail of ATPase contains six Cu^+ binding domains, showing positive cooperativity in metal coordination and forming tetra-thiolate clusters [54-56].

Beside pumping copper into the Golgi network, ATP7A and ATP7B function as fine regulators of copper adsorption and excretion in the human body [54-56, 78, 79]. If copper levels inside the cells are too elevate, they are capable to translocate from the Golgi apparatus to the cellular membrane and to pump copper(I) ions into the extracellular space. ATP7A also regulates the transport of diet ingested copper from the intestine to the blood, thus guaranteeing copper delivery to all the other tissues [80]. ATP7B is also localized at the biliary pole of hepatocytes, where it facilitates copper excretion into the bile [81]. As it will be discussed in the next section, mutations or deletions in the ATP7A and ATP7B genes yield to severe disease states, known as Menkes (MD) and Wilson's diseases (WD), respectively [82, 83].

Copper is delivered to CcO, in the mitochondrial inner membrane (MIM), by six copper chaperones: Cox17, Cox19, Cox23, Sco1, Sco2 and Cox11 [54, 56, 57]. The first three proteins are soluble proteins, while the other are MIM proteins. All these copper chaperones are strictly required for ensuring the proper copper transport to each copper sites of CcO. In fact, CcO contains three copper ions, two are located at the binuclear site (Cu_A) in the Cox1 domain and the remaining one is located at the mononuclear site (Cu_B) in the Cox2 domain. Cox11 is responsible for the delivery of copper to the Cu_B site of CcO [82], while the other five chaperones are necessary for copper transport to Cu_A site. The transport of copper from the cytoplasm to each site of CcO is quite complex and each metal chaperone needs the assistance of all the other; the exact mechanisms are still not completely understood.

Superoxide dismutase (SOD) is another important metalloenzyme which requires metal ions for its catalytic activity. Two main isoforms of SOD have been identified according to the metal ion content: CuZn-SOD and Mn-SOD. CuZn-SOD is widely distributed in the cytoplasm, nucleus, and intermembrane space of mitochondria, while Mn-SOD is found only in the mitochondrial

matrix [84]. Both proteins catalyze the dismutation of superoxide to hydrogen peroxide thus reducing the superoxide produced during the respiratory chain. The chaperone responsible for carrying copper to CuZn-SOD is Ccs [85, 86].

In addition to chaperones which transport copper to any specific cellular destinations, copper inside the cytoplasm is also handled by metallothioneins (MT) which protect cells from copper toxicity [87].

Finally, albumin and ceruloplasmin are the two proteins that bind copper in blood. Ceruloplasmin is the major copper carrier, being responsible to transport 90% of copper. Human serum albumin is able to transport many metal ions such Cu^{2+} , Ca^{2+} , Zn^{2+} , Ni^{2+} . The high affinity Cu^{2+} binding site is at the N-terminus –AspAlaHis– (ATCUN motif), where the metal ion is bound to the His imidazole, the Asp-1 amino group and one or both the amido nitrogens of the peptide backbone between Asp and His. In the presence of ascorbate, Cu^{2+} bound to albumin is reduced to Cu^+ which in turn is easily reoxidized to Cu^{2+} by molecular oxygen [88, 89].

The small percentage of copper (5-15%), which is not covalently bound to ceruloplasmin is usually referred as free copper pool even if it is loosely bound to albumin and other small molecules. In order to avoid copper toxicity, the free copper pool should be maintained to low levels since many evidence indicates that the larger is the free copper pool, the greater damage is produced.

2.2 Sources and disturbance of copper overload

Copper overload causes morphological and metabolic alterations in human tissues and, if untreated, can ultimately lead to death. The main sources of copper accumulation originates from genetic and environmental factors. In addition, copper poisoning has been observed in kidney dialysis patients due to use of contaminated water or leaching from dialysis membranes [90]. Obviously any accidental or intentional copper ingestion has severe consequences for our health. Finally copper toxicity is associated with neurodegenerative diseases and other disorders of aging, characterized by altered copper homeostasis [91].

2.2.1 Genetic basis for copper toxicity

As briefly discussed in the previous section, copper transport in our body is tightly regulated by a complex network of proteins whose impairment result in harmful cellular copper levels [58, 59, 92]. Ingested copper is primarily absorbed in the small intestine. From the intestine, copper first enters in the liver. Copper is then delivered to endogenous enzymes, incorporated into ceruloplasmin and secreted into the blood. Excess of copper are secreted in the bile. As schematized in Figure 2, ATP7A and ATP7B play an important role in the physiological regulation and distribution of copper in the body. The inactivation of ATPase copper transporting proteins, disturbs the correct copper efflux from cells, giving rise to extensive copper accumulation in the intestine (ATP7A inactivation) or in the liver (ATP7B inactivation).

Mutations in ATP7B gene are associated to WD which is an inherited disorder characterized by high copper levels mainly in the liver and in the brain [93, 94]. The major symptoms of patients suffering from WD are severe hepatic injuries, such as hepatitis and cirrhosis, and neurological disorders [94, 95].

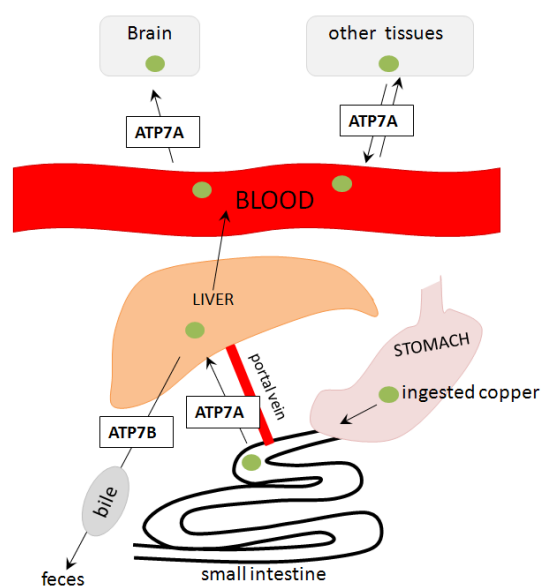


Figure 2. Schematic representation of the role of ATPases in the regulation and distribution of ingested copper

Although ATP7B is expressed in several tissues, it plays a major role in hepatocytes, where it (i) transports copper into the Golgi network and (ii) sequesters excess copper into vesicles. Both processes are essential for

cellular life: the former ensures copper incorporation into copper-dependent enzymes (e.g. ceruloplasmin) [95, 96], the latter allows copper excretion outside the cytosol guaranteeing safe copper levels inside the cell [97]. Mutations of the ATP7B gene alter the expression and the function of ATP7B, thus affecting both copper excretion into the bile and copper transport to the Golgi organelle. The results are that high copper levels accumulates inside the tissues causing oxidative damage to proteins, DNA, membranes [98] and triggering toxic metabolic responses [93].

As for ATP7B, ATP7A is involved in copper excretion outside the cytoplasm as well. In particular it is mainly involved in copper export from intestinal epithelium. In addition ATP7A is required for copper delivery to copper dependent enzymes [99, 100], including tyrosinase [101], lysyl oxidase [102] and peptidyl- α -monooxygenase [103]. Mutations on ATP7A gene cause the MD which is associated with the loss of the functional activity of ATP7A. In MD, copper accumulates in the intestinal cells and cannot be absorbed to the other cellular tissues leading to copper deficiency and reduced activity of essential cuproenzyme such as CcO (in the mitochondria), tyrosinase, and Cu/Zn SOD (in the cytosol) [104-106]. MD is also characterized by additional copper accumulation in cells located between the blood-brain barrier and choroid plexus, indicating that copper transport from blood vessels to neurons is impaired as well [105].

MD is associated with a huge number (357) of mutations in the ATP7A gene, including insertions and deletions (22%), non-sense (18%), missense (17%), partial deletions (17%), and splice-site mutations (16%) [104, 107, 108]. MD is a X-linked recessive disorder which mainly occurs in males. MD is clinically classified according to the disease severity in classical MD, mild MD and occipital horn syndrome (OHS) which is the mildest and a rare form of MD. Severe neurological degeneration, abnormal hair, hypothermia, and connective tissue disorders, gait abnormalities and muscle hypotonia are the characteristic clinical features of MD and OHS.

Beyond WD and MD, which are the most known inherited diseases caused by abnormal copper transport in our body, other disorders may additionally be

originated by copper accumulation. For examples Indian Childhood cirrhosis (ICC) [109], Endemic Tyrolean infantile cirrhosis (ETIC) [110] and Idiopathic copper toxicosis (ICT) [111] are severe diseases characterized by copper deposits in the liver. All of them are now very rare but they had a great incidence in the last century in the rural area of India and Austria. The data collected so far, strongly indicate that these hepatic copper toxicosis are caused by a synergy of genetic deficiency in copper metabolism and excess dietary copper intake arising from contaminated water and/or utensils.

2.2.2 Environmental copper toxicity

Copper is commonly found in the environment and it is largely used in many industrial and agricultural processes (see above). Unlike organic pesticides, copper does not degrade, but rather enters a complex biogeochemical cycle [112]. Disposal of copper-containing waste water causes accumulation of copper near river banks. In addition the amount of copper released during the combustion of fossil fuels may accumulate in the airs and successively end up in the soils when it rains.

For these reasons, people working in, or living in the proximity of industries settings handling high level of copper compounds, such as mines, landfills, waste water disposals, metal production plants, phosphate fertilizer plants, wood treatment plants, may undergo to environmental copper overload.

In presence of excessive copper levels, our body can absorb copper through the skin, by inhalation and by ingestion. Copper exposure by inhalation is very rare and it is mainly due to breathing fumes or dust deriving from any processes involving copper and its compounds. The Occupational Safety and Health Administration (OSHA) has set a limit of 0.1 mg/m³ of copper fumes and 1 mg/m³ of copper dusts and mists in workroom air during an 8-hour work shift. Higher copper inhalation can lead to nose, mouth, and eyes irritations, headaches, nausea, and diarrhea.

On the other hand, drinking copper contaminated water or eating acid foods cooked in uncoated copper cookware are the most likely routes of excessive copper intake. The Environmental Protection Agency has set a copper maximum level of 1.3 mg/l (1.3 ppm) in drinking

water [113]. Although, water usually contains very low copper concentrations, it may happen that it dissolves copper from plumbing fixtures, especially when it stays for long time in pipes. Another important issue is that copper is handled differently by the body when ingested by food or consumed in drinking water or mineral supplement [114]. Food copper is processed by the liver (Figure 2), which regulates copper excess and prevent its release into the free copper pool in the blood. On the other hand, inorganic copper present in water or mineral supplements, is immediately transferred to the free copper pool, bypassing liver metabolism.

Recent studies on Alzheimer's Disease (AD) rabbit model indicate that very low copper amount in distilled water (0.12 ppm) dramatically increase amyloid plaques and decrease cognitive performance in cholesterol fed animals [115], thus suggesting that the allowed copper levels present in drinking water may worsen cognitive decline in patients affected by AD. Compared to age-matched controls, higher free copper levels are present in the blood of AD patients [116]. In addition lower cognitive ability is usually associated with higher levels of copper [117].

Beyond AD, other neurodegenerative diseases (e.g. Parkinson's Disease, Prion Disease, Huntington's disease, amyotrophic lateral) are characterized by the presence of high amount of copper in the brain amyloid plaques [118, 119] thus suggesting a similar toxic role played by copper in all these disorders. To support the role of copper in accelerating general cognitive ability, it has been shown that copper intake by vitamin/mineral supplement pills together with consumption of high fat diet, enormously affects cognition performance which is generally lost at over three times the rate normally expected [120].

3. COPPER CHELATORS IN MEDICINE

3.1 Chelators in the treatment of Wilson's disease

The most widely known chelators for copper in chelation therapy are those used for the treatment of WD. Among a number of copper chelators developed and tested, the three most important ones are D-penicillamine (D-pen), Trentine (Triethylenetetramine, Trien) and ammonium tetrathiomolibdate (TTM), whose structures are reported in Figure 3.

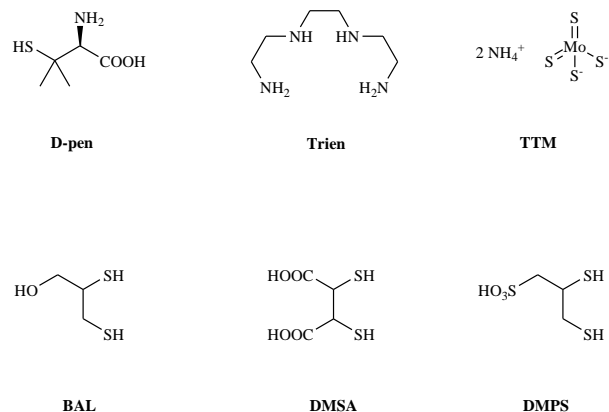


Figure 3. Copper chelators for the treatment of WD.

Indeed, the very first chelator used for WD was dimercaprol (2,3-dimercaptopropanol, British anti-Lewisite, BAL, Figure 3), originally developed during the World War II as an antidote for lewisite, a chemical warfare agent, and later employed to treat metal intoxications [121]. It was replaced by D-pen (less toxic and orally available) still the most used, although Trien revealed to be better tolerated [122]; TTM showed a remarkable efficacy in the treatment of patients with neurological symptoms [123]; unfortunately is not yet commercially available.

D-penicillamine: The study of D-pen in the treatment of WD originated from the observation that patients administered with penicillin excreted penicillamine in the urine as a metabolite, therefore suggesting that the latter compound could be bioavailable [124]. Its capacity to remove copper is remarkable [125], although its hydrophilicity probably prevents the compound to permeate the blood-brain-barrier (BBB). For these reasons, several more lipophilic derivatives of D-pen have been prepared and reported in the literature [126], in the attempt to increase the BBB permeability of the chelators and their cell uptake.

The clinical practice for the administration of D-pen has been reported [127]. D-pen is capable to mobilize copper from inside the cells and promotes its urinary excretion [128]. In mouse liver, D-pen was found to increase the expression of MT, which binds copper forming a non-toxic adduct [129]. On the other hand, it has been shown that, in rat models of WD, the level of MT and of the related mRNA is increased by excessive copper in hepatocytes, and reduced upon treatment with D-pen [130]. Remarkably, the administration of D-pen

combined with a deficiency in vitamin B6 levels were reported to cause neurological worsening [131]: for these reasons, vitamin B6 is routinely administered together with D-pen. Side effects such as fever, rash, renal toxicity [132], ANCA-vasculitis [133], and dermatologic toxicity have been reported [134]. For these reasons, it has been also suggested that D-pen should not be used as the initial therapy in WD [135, 136]. The administration of D-pen needs to be discontinued in 20-30% of patients [137, 138] and it has to be followed by a different treatment to avoid rapid progression of fatal hepatitis [139].

Triethylenetetramine: Trien has been introduced in clinical practice with the purpose of having a different treatment for patients intolerant to D-pen [122]. Trien is a hydrophilic and orally available chelator, capable to bind copper in the blood and to promote its urinary excretion, even though it is less efficient than D-pen [140]. The use of D-pen and Trien as initial treatments in WD was shown to worsen the neurological symptoms that likely originates from a temporary increase of protein-unbound copper, especially due to copper mobilization from the liver [141, 142]. An increase of the albumin level in cerebrospinal fluid (CSF) compared to serum has been observed as a possible effect of perturbation of BBB [143]. Therefore, it has been suggested that by monitoring this ratio a basis to guide the modulation of the chelation therapy can be obtained.

The clinical practice for the administration of Trien has been described [127]. The side effects of Trien are milder and less frequent [122] with respect to D-pen and Trien proved as efficient as D-pen in pediatric patients [137].

Ammonium tetrathiomolibdate: The diammonium salt of the MoS_4^{2-} anion has been studied with the specific purpose of developing a new compound for the treatment of WD which could replace D-pen and Trien [144, 145]. Its efficacy in reducing copper levels in the body have been first observed in ruminants of Australia and New Zealand as the consequence of the presence of high levels of molybdenum in the soil [146]. TTM forms of a ternary complex with copper ions and proteins, making copper not available to the cells [147]; its biological activity starts in the gastrointestinal tract (see further). TTM has been found to be a good alternative

treatment for neurologically affected WD patients [123], and its use in the initial treatment of the disease in combination with zinc administration proved to be effective [145]. Its recommended doses and clinical practice have been reported [123]. Remarkably, TTM is able to starve tumor cells of essential copper and it has been proposed as a new anticancer agent [148].

Sulfurated polydentate chelators: A series of potentially efficient chelators have been developed by Delangle and coworkers [149], with the aim to prepare ligands that possess a higher specificity for certain tissues than D-pen, Trien and TTM which actually act as systemic chelators. In particular, they developed chelators for Cu^+ rather than for Cu^{2+} , with the purpose of binding intracellular copper which actually is in the reduced form. These chelators contain sulfur, especially in the form of a free thiol, in order to stabilize copper in the +1 oxidation state (Figure 4).

The P^x series of chelators consists of a family of cyclic peptides containing Cys (and Met) [150-152], which have been initially devised on the basis of the known MXCXC peptide sequence of the copper chaperone Atox1 and ATPases ATP7A and ATP7B [153, 154]. In particular, the cyclic peptide P^c (Figure 4, top left) was designed from the actual copper binding sequence MTCSCGS in Atox1 of yeast [154], and bears the XPGX fragment to rigidify the structure [150]. Not only this peptide mimics very well the binding loop of Atox1, but the dissociation constant of its Cu^+ complex is $10^{-17.4}$ M, a value very close to that of the chaperone [155]. The very high selectivity of P^c for Cu^+ versus Zn^{2+} (ca. 10 orders of magnitude) prompted the design of other cyclic peptides (P^1 , P^2 and P^3 , Figure 4) which maintained the same Cu/Zn selectivity [151]. These peptide contain two Cys residues on one side of the molecule (copper binding face), while the other face is available for grafting specific groups (see P^3 , Figure 4) with the purpose to target receptors on the surface of the hepatic cells [152, 156]. In the prochelator P^3 the two cysteines form a disulfide bridge that can be reduced under the reducing intracellular conditions (e.g. by GSH) [152], so that the thiol groups becomes available for Cu^+ complexation. The opposite face contain four lysine-N-acetylgalactosamine groups, with the purpose to target ASGP-R, a hepatic lectin expressed exclusively on the surface of hepatocytes [157, 158]). Indeed, not only the

P^3 ligand is capable to target hepatocytes (by virtue of the “cluster glycoside effect” [159]) and penetrate the cell membrane, but fluorescence measurements (using a

fluorescent copper probe) showed that P^3 is capable to reduce the intracellular level of available copper [152].

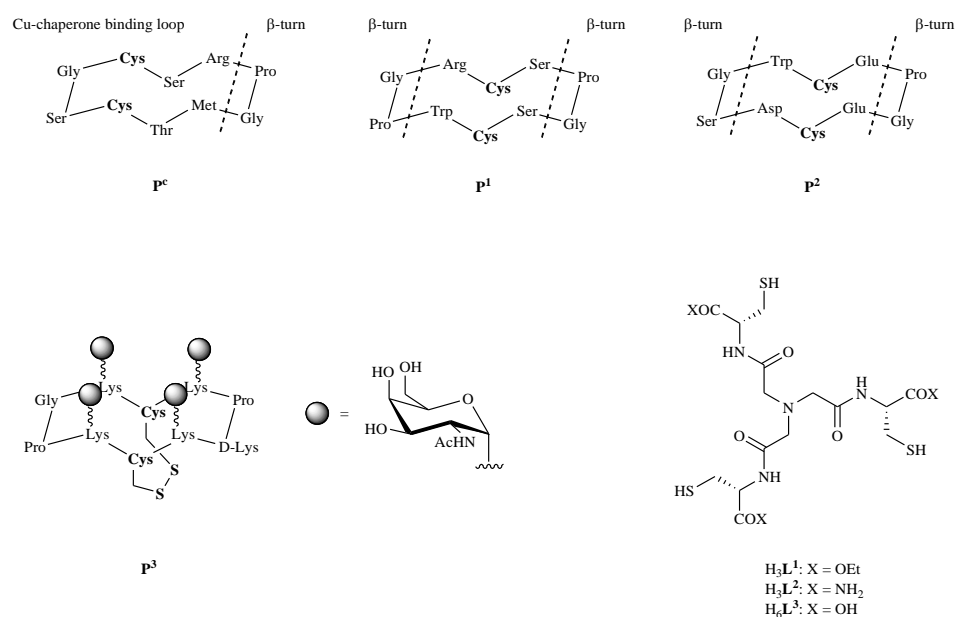


Figure 4. Sulfurated polydentate chelators.

A few interesting examples of tripodal Cys-rich chelators have been reported (H_nL^x , Figure 4) [160, 161], which have been suggested to act as potential Cu^+ chelators *in vivo*. Because the very stable $Cu(I)$ -MT complexes showed that in these adducts a $Cu(I)S_3$ coordination environment is present [162], nitrilotriacetic acid has been used as a platform to produce the Cys-containing ligands H_3L^1 , H_3L^2 and H_6L^3 . While L^1 and L^2 expectedly form very stable mononuclear and polynuclear Cu^+ complexes and are very selective for Cu^+ versus Zn^{2+} , the ligand L^3 gives polynuclear Cu^+ complexes of lower stability as the consequence of the presence of three negative carboxylate groups that originate a mutual electrostatic repulsion.

Two more hydrophilic and less toxic BAL analogs have been developed and used for heavy metal intoxication, namely DMSA (*meso*-2,3-dimercaptosuccinic acid) and DMPS (D,L-2,3-dimercapto-1-propanesulfonic acid) (Figure 3) [163-165]. In particular, DMSA has been used to treat WD patients in China [166], where Trien is not commercially available. Finally methanobactin, a naturally occurring nine amino acid polypeptide, found in methanotrophs bacteria where it serves several

functions involving copper (and thus termed a “chalcophore”), has been tested as a copper chelator in rat models of WD, showing the mobilization of copper from the liver to the bile [167, 168].

3.2 Chelators in the treatment of Alzheimer’s disease

Alzheimer’s disease (AD) is characterized by the progressive formation of amyloid plaques. However, it is still not clear whether these plaques are the cause or the consequence of the disease, and even what mechanisms determine their formation. However, it is established that some metals of biological interest, such as Fe(III), Zn (II) and Cu (II) can interact with soluble and aggregated forms of $A\beta$ peptide, also influencing the process of fibrillization. Although the toxicity of both the oligomers or the plaques and the corresponding complexes is a controversial issue [169, 170], a line of research, aimed at treating AD, is addressed to the study of the action of copper chelators to remove the metal and/or to redistribute it into the body.

Clioquinol (CQ) (5-chloro-7-iodo-8-hydroxyquinoline, CQ, also known as PBT1, Figure 5) is an aromatic chelator which coordinates metal ions through its (*N,O*) donor set [171]. CQ has been used in the past as an antibiotic

Paper V

A family of Hydroxypyrrone Ligands Designed and Synthesized as Iron Chelators

L. Toso, G. Crisponi, V.M. Nurchi, M. Crespo-Alonso, J.I. Lachowicz, M.A. Santos, S.M. Marques, J. Niclós-Gutiérrez, J.M. González-Pérez, A. Domínguez-Martín, D. Choquesillo-Lazarte, Z. Szewczuk, J. Inorg. Biochem. 127 (2013) pp. 220-231.

DOI: 10.1016/j.jinorgbio.2013.06.009

Reprinted with permission from Elsevier

Copyright © 2014 Elsevier B.V. All rights reserved



A family of hydroxypyronone ligands designed and synthesized as iron chelators

Leonardo Toso^a, Guido Crisponi^{a,*}, Valeria M. Nurchi^a, Miriam Crespo-Alonso^a, Joanna I. Lachowicz^a, M. Amelia Santos^b, Sergio M. Marques^b, Juan Niclós-Gutiérrez^c, Josefa M. González-Pérez^c, Alicia Domínguez-Martín^c, Duane Choquesillo-Lazarte^d, Zbigniew Szewczuk^e

^a Dipartimento di Scienze Chimiche e Geologiche, Università di Cagliari, Cittadella Universitaria, 09042 Monserrato Cagliari, Italy

^b Centro Química Estrutural, Instituto Superior Técnico, Universidade Técnica de Lisboa, Av. Rovisco Pais, 1049-001 Lisboa, Portugal

^c Department of Inorganic Chemistry, Faculty of Pharmacy, Campus Cartuja, University of Granada, E-18071 Granada, Spain

^d Laboratorio de Estudios Cristalográficos, IACT, CSIC-Universidad de Granada, Av. de las Palmeras 4, E-18100 Armilla, Granada, Spain

^e Faculty of Chemistry, University of Wrocław, F. Joliot-Curie 14, 50-383 Wrocław, Poland

ARTICLE INFO

Article history:

Received 26 December 2012

Received in revised form 15 June 2013

Accepted 17 June 2013

Available online 26 June 2013

Keywords:

Kojic acid

Fe^{III}

Solution equilibria

X-Ray structure

Synthesis

Hydroxypyronones

ABSTRACT

The use of chelating agents for iron and aluminum in different clinical applications has found increasing attention in the last thirty years. Desferal, deferiprone and deferasirox, chelating agents nowadays in use, are based on hydroxamic groups, hydroxyl-substituted pyridinones or aromatic ring systems. With the aim of designing new chelators, we synthesized a series of kojic acid derivatives composed by two kojic units joined by linkers variously substituted. The huge advantages of these molecules are that they are easy and cheap to produce. Preliminary works on complex formation equilibria of the first group of ligands with iron and aluminium highlighted extremely good pMe values and gave evidence of the ability to scavenge iron from inside cells. On these bases a second set of bis-kojic ligands, whose linkers between the kojic chelating moieties are differentiated both in terms of type and size, has been designed, synthesized and characterized. The structural characterization of these new ligands is presented, and the protonation and iron^{III} complex formation equilibria studied by potentiometry, UV-Visible spectrophotometry, electrospray ionization mass (ESI-MS) and ¹H NMR spectroscopy will be described and discussed.

© 2013 Elsevier Inc. All rights reserved.

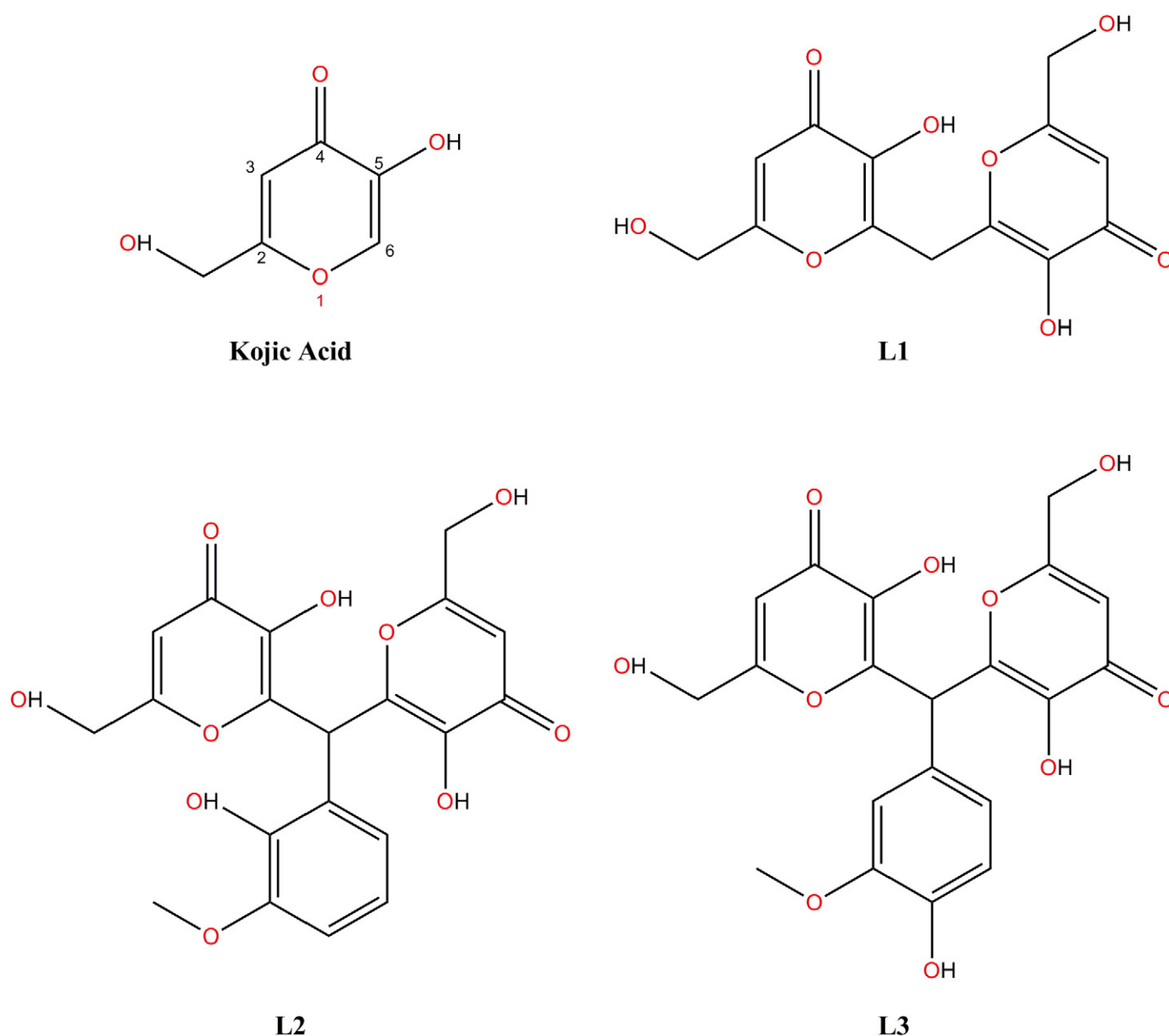
1. Introduction

In the last two decades there has been an increasing interest in the use of chelation therapy for various health diseases depending on iron and aluminium overload [1–6]. Drugs in current use, such as desferal, deferiprone and deferasirox, include 1–3 chelating groups, typically hydroxamic groups, hydroxyl-substituted pyridinones or aromatic ring systems. In the above mentioned reviews the numerous drawbacks limiting in some instance the use of these drugs are presented and discussed, and the need of new effective iron chelators is stressed. With the aim of designing new ligands that form complexes with high stability, selectivity, lipophilicity and bioavailability, which satisfy both the chemical requirements and biological constraints for an effective therapeutic agent, we synthesized some derivatives of kojic acid, and studied their complex formation equilibria with Fe^{III} and Al^{III}, as well as those with the parent ligand kojic acid, 5-hydroxy-2-(hydroxymethyl)-4H-pyran-4-one, (Scheme 1).

In a previous work, evidence was given on the formation of MeL, MeL₂, and MeL₃ complexes of Al^{III} and Fe^{III} with kojic acid, confirmed by the X-ray structure of the FeL₃ complex, and of diverse protonated species of Me₂L₂ and MeL₂ complexes with L1 [7]. On the basis of the extremely good pFe value (23.1) characterizing L1, and of its ability to scavenge iron from inside cells [8], we extended the investigation to the related compounds in which vanillin and ortho-vanillin (L2 and L3) substituents were inserted on the linker joining the two kojic units. Similar complexes to those formed with L2 were found. In the binuclear Me₂L₂ complexes, each metal ion is coordinated by two COC(OH)-chelating moieties, one from each coordinating molecules: actually, the length of the linker between the two kojic units prevents metal ion coordination by both kojic units on the same molecule. The found pFe values (18.9 for L2 and 22.2 for L3), lower than that of desferal (26.6) and comparable with that of deferiprone (20.7), were very encouraging [9,10]. These ligands are easy and cheap to produce, as the starting materials, kojic acid and vanillin, are not expensive. Hence, they are worthy of further tests on their toxicity and their capacity to remove iron and/or aluminium from intra-cellular sites in living organisms. Aimed at improving the interaction between the kojic moieties and the metal ions, we have designed and synthesized a new set of bis-kojic ligands whose linkers (between the two kojic

* Corresponding author at: Dipartimento di Scienze Chimiche e Geologiche, Cittadella Universitaria, 09042 Monserrato, Cagliari, Italy. Tel.: +39 070 675 4476; fax: +39 070 675 4478.

E-mail address: crisponi@unica.it (G. Crisponi).



Scheme 1. Chemical structures and acronyms of studied ligands.

chelating moieties) are differentiated both in terms of type and size (Scheme 2).

In this paper we will report the synthesis of the new derivatives, namely L4, L5, L6, and L7 containing an amine group in the linker and also L8, which is a L1 analog but with insertion of a methyl group in the linker. The acid-base properties, together with the equilibrium constants for the formation of Fe^{III} complexes as well as the structure characterization of L6, L7 and L8 by X-Ray diffraction will be presented herein.

2. Experimental

2.1. Reagents

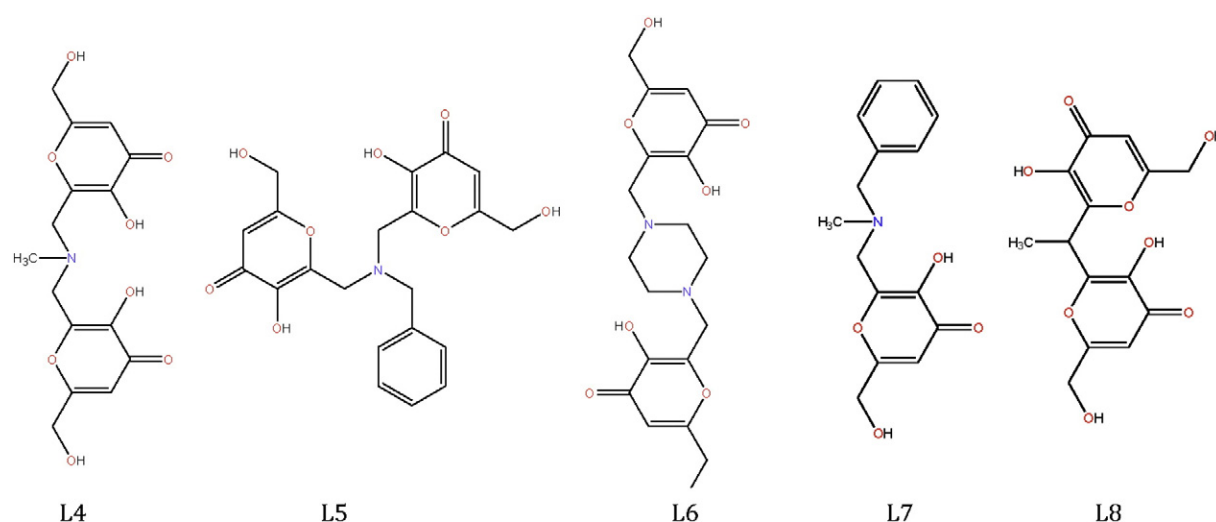
Kojic acid, benzylamine hydrochloride, piperazine, methylamine hydrochloride, NaOH, KOH, FeCl₃, methanol, ethanol and 2-isopropanol were purchased from Aldrich, and N-benzylmethylamine was an Alfa Aesar product. Formaldehyde was purchased from Merck, HCl from Fluka, and KCl and ZnO from Carlo Erba (Milan, Italy). Desferal was a

Biofutura Pharma product. All the products were used without any further purification.

A previous described method was used in the preparation of 0.1 M carbonate free KOH solution [11]. Ligand solutions were acidified with stoichiometric equivalents of HCl. Fe^{III} solution was prepared by dissolving the required amount of FeCl₃ in pure double distilled water to which a stoichiometric amount of HCl was previously added to prevent hydrolysis. This solution was standardized by spectrophotometric titration with desferal.

2.2. Synthesis

All the ligands were prepared from 6-alkylation of kojic acid (KA) with an aldehyde and a primary amine or an inorganic base, depending on desired presence or absence of amine group on that alkyl substituent. The particular operations are reported in the following for each single ligand. For each ligand preparation, a KA (1.00 g, 7.1 mmol) solution in ethanol (25 mL) was used. All the reactions were followed by TLC, using a CH₂Cl₂:MeOH (12:1) mixture as eluent. The synthesized products



Scheme 2. Chemical structures and acronyms of studied ligands.

were fully characterized by different standard instrumental techniques. NMR spectra were recorded on a Bruker AVANCE III spectrometer at 300 MHz and 400 MHz for ^1H NMR and ^{13}C NMR respectively. Chemical shifts (δ) are reported in ppm related to tetramethylsilane (TMS). Infrared spectra were recorded by using KBr pellets on a Jasco FT-IR 410 spectrometer. The electrospray ionization mass spectra (ESI-MS) were obtained on a 500 MS LC Ion Trap (Varian Inc., Palo Alto, CA, USA) mass spectrometer equipped with an ESI ion source, operated in the positive and negative ion modes. The elemental analyses were performed on a Fisons EA1108 CHNS-O within the limit of $\pm 0.4\%$. Although some of the compounds gave unsatisfactory analysis values, for which found values differ by more than $\pm 0.5\%$ from Calc. values, crystal structures of all of these compounds were determined by X-ray diffraction (XRD) technique or their structures were supported by spectroscopic (FT-IR, ^{13}C -NMR and ESI-MS) analyses.

2.2.1. 6,6'-(Methylazanediy)bis(methylene)bis(5-hydroxy-2-(hydroxymethyl)-4H-pyran-4-one), L4

Methylamine hydrochloride (0.260 g, 3.8 mmol), previously neutralized with NaOH (3.8 mmol), was added to a solution containing formaldehyde (580 μL , 7.1 mmol) in ethanol (2 mL). The mixture was stirred for 30 min at room temperature, then added drop wise to the kojic ethanolic solution described above. The solution was left under stirring for 1.5 h in a water bath at 40/50 $^\circ\text{C}$. Solvent was removed under vacuum. Addition of CH_3CN yielded a white precipitate that was filtered off, washed with cold CH_3CN , and dried under vacuum for 6 h. Recrystallization afforded the pure product as a white solid (1.09 g, 92% yield). Mp = 150–152 $^\circ\text{C}$. Elemental analysis found (calc. for $\text{C}_{15}\text{H}_{17}\text{NO}_8$): C, 52.76 (53.10); H, 5.48 (5.05);

N, 4.20 (4.13). FT-IR (KBr, 4000–400 cm^{-1}): $\nu_{\text{as}}(\text{CH}_3)$ 2963, $\nu_{\text{as}}(\text{CH}_2)$ 2923, $\nu_{\text{d}}(\text{CH}_3)$ 2888, $\nu_{\text{s}}(\text{CH}_2)$ 2853, $\nu(\text{C}=\text{O})$ 1665, $\delta(\text{CH}_2)$ 1460, $\nu(\text{C}-\text{O}-\text{C})_{\text{cyclic}}$ 1218, $\pi(\text{C}-\text{H})_{\text{ar}}$ (kojic) 854. ^1H -NMR (400 MHz, MeOD): δ 6.380(2H, s), 4.350(4H, s), 3.763(4H, s), 2.403(3H, s). ^{13}C -NMR (400 MHz, MeOD): δ 145.30 (C), 148.03 (C), 169.86 (C), 179.95 (C), 110.09 (CH), 43.11 (CH_2), 54.37 (CH_2), 61.23 (CH_2). ESI-MS(-): MH^- (338.2), $[\text{M} + \text{Cl}]^-$ (374.2).

2.2.2. 6,6'-(Benzylazanediy)bis(methylene)bis(5-hydroxy-2-(hydroxymethyl)-4H-pyran-4-one), L5

Benzylamine hydrochloride (0.51 g, 3.5 mmol), previously neutralized with NaOH (3.5 mmol), was added to a solution of formaldehyde (633 μL , 7.8 mmol) in ethanol (2 mL). The mixture was stirred for 30 min at room temperature and then added drop wise to the kojic

ethanolic solution. The solution was left under stirring for 3.5 h in a water bath at 40/50 $^\circ\text{C}$. Solvent was removed under vacuum. Red impurities were removed from the white precipitate by several double distilled cold water washings, filtrations and dryings under vacuum. Recrystallization yielded the pure final product (0.84 g, 57%). Mp = 126–128 $^\circ\text{C}$. Elemental analysis found (calc. for $\text{C}_{21}\text{H}_{21}\text{NO}_8$): C, 59.43 (60.72); H, 5.58 (5.10); N, 3.42 (3.37). FT-IR (KBr, 4000–400 cm^{-1}): two types of $\nu_{\text{as}}(\text{CH}_2)$ 2960 and 2925, two types of $\nu_{\text{s}}(\text{CH}_2)$ 2888 and 2851, $\nu(\text{C}=\text{O})$ 1644, $\delta(\text{CH}_2)$ 1454, $\nu(\text{C}-\text{N})_{\text{tertiary amine}}$ 1360, $\nu(\text{C}-\text{O}-\text{C})_{\text{cyclic}}$ 1223, $\pi(\text{C}-\text{H})_{\text{ar}}$ (kojic) 858, $\pi(\text{C}-\text{H})_{\text{ar}}$ (benzyl) 747 and 701. ^1H -NMR (300 MHz, MeOD): δ 7.203(5H, Ph), 6.295(2H, S), 4.306(4H, s), 3.792(4H, s), 3.751(2H, s). ^{13}C -NMR (300 MHz, MeOD): δ 139.10(C), 144.86(C), 149.24(C), 169.68(C), 176.27(C), 109.97(CH), 128.59(CH), 129.32(CH), 130.16(CH), 52.26(CH_2), 60.44(CH_2), 61.21(CH_2). ESI-MS(-): MH^- (414.2), $[\text{M} + \text{Cl}]^-$ (450.2).

2.2.3. 6,6'-(Piperazine-1,4-diyl)bis(methylene)bis(5-hydroxy-2-(hydroxymethyl)-4H-pyran-4-one), L6

Piperazine (0.305 g, 3.5 mmol) was added to a solution of formaldehyde (580 μL , 7.1 mmol) in ethanol (2 mL). The mixture was stirred for 30 min at room temperature and then added drop wise to a kojic ethanolic solution. The solution was left under stirring for 5 h during which a fine white precipitate appeared. Upon refrigeration for 2 h, the reaction mixture was filtered off, washed with cold ethanol and dried under vacuum for 6 h. Recrystallization afforded the final product 1.35 g, 97%). Mp > 350 $^\circ\text{C}$. Elemental analysis found (calc. for $\text{C}_{18}\text{H}_{22}\text{N}_2\text{O}_8$): C, 54.18 (54.82); H, 6.07 (5.62); N, 7.17 (7.10). FT-IR (KBr, 4000–400 cm^{-1}): two types of $\nu_{\text{as}}(\text{CH}_2)$ 2951 and 2917, two types of $\nu_{\text{s}}(\text{CH}_2)$ 2880 and 2839, $\nu(\text{C}=\text{O})$ 1653, $\delta(\text{CH}_2)$ 1460, $\nu(\text{C}-\text{O}-\text{C})_{\text{cyclic}}$ 1244, $\pi(\text{C}-\text{H})_{\text{ar}}$ (kojic) 867, $\pi(\text{C}-\text{H})_{\text{ar}}$ (piperazine) 824. ^1H -NMR (300 MHz, MeOD + KOD): δ 6.120(2H, S), 4.179(4H, s), 3.530(4H, s), 2.490(8H, s). ^{13}C -NMR (400 MHz, MeOD + KOD): δ 148.782 (C), 154.936 (C), 165.674 (C), 183.262 (C), 109.646 (CH), 53.455 (CH_2), 55.127 (CH_2), 61.801 (CH_2). ESI-MS(-): MH^- (393.3).

2.2.3.1. Synthesis of L6 crystal. L6 (15 mg) was dissolved in distilled water (12 mL), aided by drop wise addition of HCl 0.01 M. Afterwards, isopropanol (4 mL) was added and the solution was left stirring for 30 min and then filtered into a crystallization device to remove possible impurities. The solution was left stand at room temperature in order to evaporate. Evaporation of the solvents was controlled with the aid of a plastic film. After three weeks, parallelepiped colorless crystals appeared suitable for XRD.

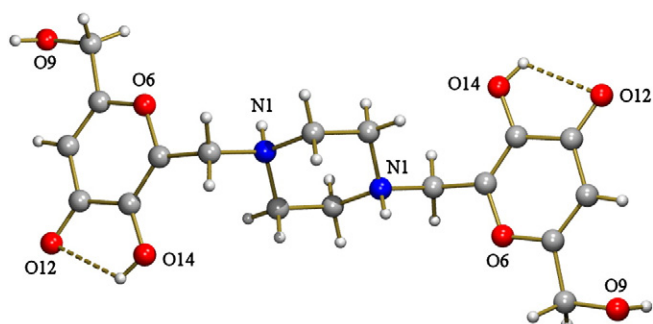


Fig. 1. Centro-symmetrical H_2L6^{2+} ion in the crystal of ligand L6. Intra-molecular H-bonding interactions are depicted in dotted lines.

2.2.4. 2-((Benzyl(methyl)amino)methyl)-3-hydroxy-6-(hydroxymethyl)-4H-pyran-4-one, L7

N-Benzylmethylamine (967 μ L, 7.8 mmol) was added to a solution of formaldehyde (633 μ L, 7.8 mmol) in ethanol (2 mL). The mixture was stirred for 30 min at room temperature and then added drop wise to the kojic ethanolic solution described above. The solution was left under stirring for 5 h. Solvent was removed under vacuum until a white precipitate was formed. Upon refrigeration for 2 h it was filtered off washed with cold ethanol and dried under vacuum for 6 h. Recrystallization afforded the final pure product (1.69 g, 87%). Mp = 137–139 °C. Elemental analysis found (calc. for $C_{15}H_{17}NO_4$): C, 65.12 (65.44); H, 6.14 (6.22); N, 5.11 (5.09). FT-IR (KBr, 4000–400 cm^{-1}) $\nu_{as}(CH_3)$ 2989, two types of $\nu_{as}(CH_2)$ 2951 and 2938, $\nu_d(CH_3)$ 2884, $\nu_s(CH_2)$ 2831, $\nu(C=O)$ 1662, $\delta(CH_3)$ 1496, $\delta(CH_2)$ 1465, $\nu(C-N)_{tertiary\ amine}$ 1360, $\nu(C-O-C)_{cyclic}$ 1244, $\pi(C-H)_{ar}$ (kojic) 853, $\pi(C-H)_{ar}$ (benzyl) 747 and 701. ^1H-NMR (300 MHz, $D_2O + KOD$, pH = 12): δ 7.351(5H, Ph), 6.331(1H, S), 4.417(2H, s), 3.684(2H, s), 3.601(2H, s), 2.249(3H, s).

2.2.4.1. Synthesis of L7 crystal. L7 (30 mg) was dissolved in a $H_2O/MeOH$ (1:1) mixture (16 mL). After 30 min stirring, a clear colorless solution was obtained. The solution was filtered into a crystallization device and covered with a plastic film to control the evaporation of the solvents. In one week, parallelepiped colorless crystals were collected for XRD analysis.

2.2.5. 2-2'-Ethanediylium(3-hydroxy-6-(hydroxymethyl)-4H-pyran-4-one), L8

Synthesis of L8 was carried out according to literature methods [12]. 6.2 g of kojic acid and an equivalent amount of aldehyde were dissolved in (100 mL) ethanol. The reaction, catalyzed by concentrated ammonium hydroxide (1 mL), was heated for three hours at 60 °C. Then the solvent was left to evaporate and the beige precipitate was washed with cold ethyl alcohol. Recrystallization from ethanol yield

the pure final product (4.61 g, 68%). Mp = 207–208 °C. Elemental analysis found (calc. for $C_{14}H_{14}O_8$): C, 54.20 (55.70); H, 5.03 (4.55). FT-IR (KBr, 4000–400 cm^{-1}) $\nu_{as}(CH_3)$ 2983, $\nu_{as}(CH_2)$ 2940, $\nu_d(CH_3)$ 2879, $\nu_s(CH_2)$ 2850, $\nu(C=O)$ 1653, $\delta(CH_2)$ 1463, $\nu(C-O-C)_{cyclic}$ 1265, $\pi(C-H)_{ar}$ (kojic) 857. ^1H-NMR (300 MHz, $D_2O + KOD$, pH = 6): 6.560(2H, s), 4.530(4H, s), 1.660(3H, d).

2.2.5.1. Synthesis of L8 crystal. L8 (10 mg) was dissolved in EtOH (10 mL) under moderate heating (35 °C) and stirred until a clear colorless solution was obtained. Afterwards, the solution was filtered into a crystallization device and covered with a plastic film to control the evaporation of the solvent. In one week, small parallelepiped colorless crystals appeared. In order to improve the size of the crystals, successive filtrations of the mother liquors were performed until suitable crystals for XRD purposes were collected.

2.3. Potentiometric–Spectrophotometric measurements

Protonation and complex-formation equilibrium studies were carried out under the same conditions described in a previous publication [7]. The operating ligand concentrations ranged from 3×10^{-4} to 3×10^{-3} M according to the examined ligand. The studies of complex formation were carried using constant ligand concentration, and 1:1, 1:2, and 1:3 metal/ligand molar ratios. Combined potentiometric–spectrophotometric measurements were performed for protonation equilibria in the 200–400 nm spectral range and in the 400–800 nm spectral range for Fe^{III} complexes, using 0.2 and 1 cm path lengths. Protonation and complex formation data were analyzed using the Hyperquad program [13].

2.4. ESI-MS analysis of complexes

ESI-MS spectra were carried out on a Bruker microTOF-Q spectrometer (Bruker Daltonik, Bremen, Germany) equipped with an ESI source. Samples were dissolved in water and methanol (molar ratio 1:1) and the final pH was ~7. The ligand concentration was $\sim 10^{-5}$ M and the ligand to metal molar ratio was 1:10. The experiment parameters were as follows: scan range: m/z 100–1600; drying gas: nitrogen; and temperature: 200 °C, ion source voltage 4500 V, collision energy 10 eV. The instrument was operating in the positive ion mode and calibrated externally with Tunemix™ mixture (Bruker Daltonik, Germany). Analyte solutions were inserted at a flow rate of 3 μ L/min. Compass Data Analysis (Bruker Daltonik, Germany) program was used to determine the formulae of the complexes. The distance between peaks allowed calculating the charge of the analyzed ions. In the MS/MS experiments, the ion corresponding to signal at m/z 392 was selected on the quadrupole and subsequently fragmented in the collision cell. Argon was used as a collision gas. The obtained fragments were directed to the mass

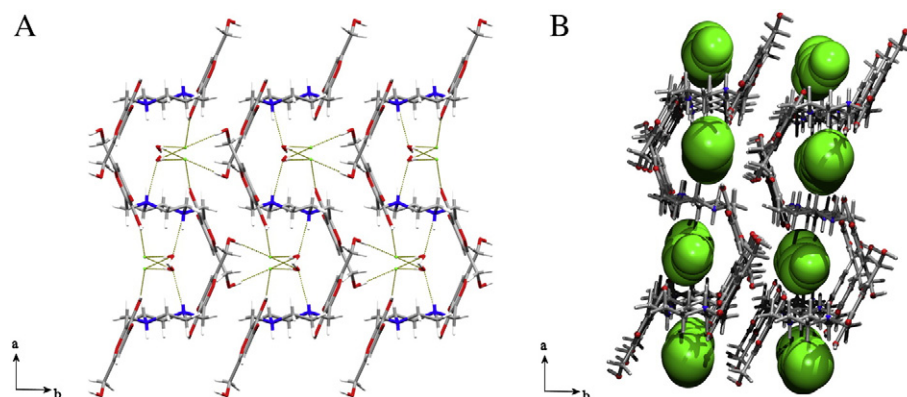


Fig. 2. View in the ab plane of the H-bonded 3D network of the crystal of L6. A) Chloride ions and water molecules are hosted in the corresponding channels throughout the c axis. B) Chloride ions and water molecules are removed and the total accessible voids are plotted in green space fill.

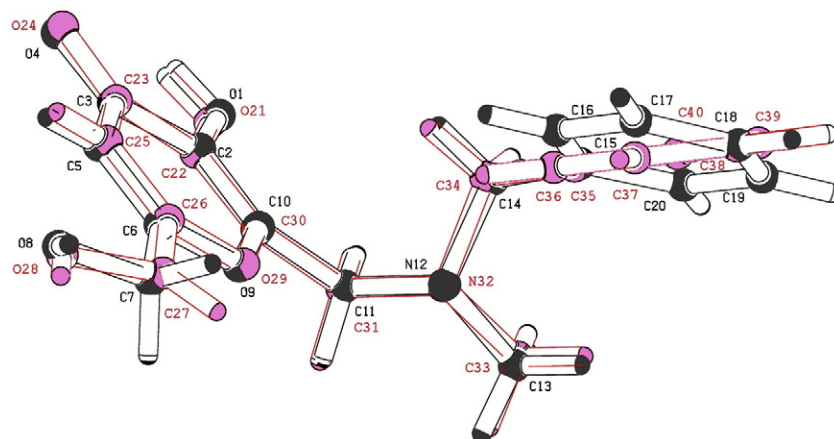


Fig. 3. Overlapped view of the two non-equivalent molecules within the asymmetric unit in the crystal of ligand L7. Molecule 1 is depicted in darker line whereas molecule 2 is depicted in lighter line. Numbering scheme is also provided. Intra-molecular H-bonding interactions are omitted for clarity.

analyzer and registered as an MS/MS spectrum. The collision energy was 10 eV.

2.5. Crystal structure determination

Measured crystals L6, L7 and L8 were prepared under inert conditions immersed in perfluoropolyether as protecting oil for manipulation. Suitable crystals were mounted on MiTeGen Micromounts™ and these samples were used for data collection. Data were collected with Bruker SMART APEX [L6 (293 K), L7 (296 K) and L8 (100 K)] diffractometer. The data were processed with APEX2 [14] program and corrected for absorption using SADABS [15]. The structures were solved by direct methods, which revealed the position of all non-hydrogen atoms. These atoms were refined on F^2 by a full-matrix least-squares procedure using anisotropic displacement parameters [16]. All hydrogen atoms were located in difference Fourier maps and included as fixed contributions riding on attached atoms with isotropic thermal displacement parameters 1.2 times those of the respective atom. Geometric calculations were carried out with PLATON [17] and drawings were produced with PLATON and MERCURY [18]. Additional crystal data and more information about the X-ray structural analyses are shown in Supplementary material S1 to S3. Crystallographic data for the structural analysis have been deposited with the Cambridge Crystallographic Data Centre, CCDC 914446–914448 from L6 to L8, respectively. Copies of this information may be obtained free of charge on application to CCDC, 12 Union Road, Cambridge CB2 1EZ, UK (fax: 44 1223 336 033; e-mail: deposit@ccdc.cam.ac.uk or <http://www.ccdc.cam.ac.uk>).

In addition, one red parallelepiped crystal obtained from the synthesis of one Fe/L6 complex was mounted on a MiTeGen Micromount™ and this sample was used for data collection. Data was collected at the ESRF synchrotron ID14-1 beamline ($\lambda = 0.9340 \text{ \AA}$, 100 K). Previous attempts to determine the structure of these iron compound using conventional X-ray diffraction facilities were unsuccessful provided the poor diffraction power of the crystal samples. Only a tentative model for the iron(III) compound $\text{Fe}_2(\text{L6})_3$ can be proposed due to the limited resolution achieved in the experiment. Constraints were used to model the aromatic rings and the piperazine moiety of L6 ligand. The diffuse scattering contribution from solvent and data noise was removed using the SQUEEZE procedure in PLATON [17].

3. Results and discussion

3.1. Crystal structure of ligands L6, L7, L8

3.1.1. Crystal structure of the ligand L6: $(\text{H}_2\text{L6})\text{Cl}_2 \cdot 2\text{H}_2\text{O}$

The crystal of ligand L6 (monoclinic system, space group $P2_1/c$) consists of one dichlorhydrate acid molecule and two water molecules. Note that an inversion center is located in the middle of the acid molecule, thus L6 is centro-symmetric (Fig. 1).

The molecule shows the most stable trans-e, e-conformation. The kojic acid moieties are stabilized by two intra-molecular H-bonds involving the OH phenol-like groups as donors and the O keto–kojic groups as acceptors [$\text{O14} - \text{H} \cdots \text{O12}$ (2.742(2) Å, 113.3°)]. This latter feature has also been observed in closely related kojic-like compounds [9].

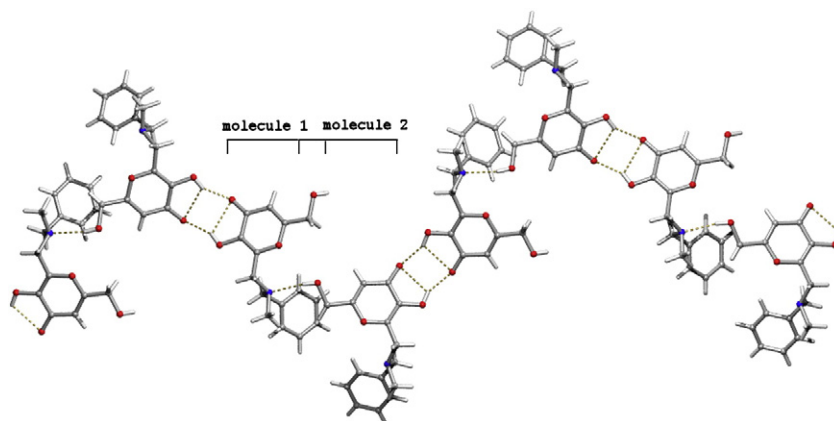


Fig. 4. Fragment of one zig-zag 1D chain in the crystal of ligand L7. Note that the OH phenol-like group is involved in a bifurcated interaction acting as H-donors for one intra- and one inter-molecular interactions. Likewise, the O keto–kojic group also acts as double H-acceptor from one intra- and one inter-molecular interactions.

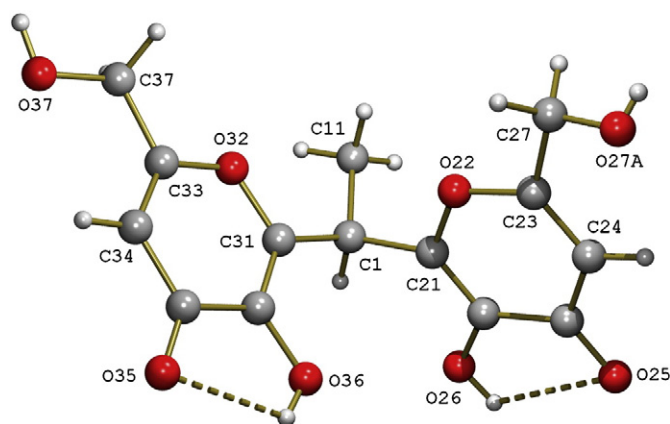


Fig. 5. Asymmetric unit in the crystal of ligand L8. Intra-molecular H-bonding interactions are plotted. Only one of the disordered positions of the hydroxyl-methyl arm is depicted for clarity.

Table 1

Protonation constants of the ligands at 25 °C, 0.1 M KCl ionic strength, obtained from potentiometric titration curves using the Hyperquad program [13].

	L4	L5	L6	L7	L8
logK ₁	9.19(3)	9.01(2)	8.52(4)	8.49(1)	9.49(3)
logK ₂	7.51(3)	7.61(2)	7.81(2)	6.02(2)	6.69(5)
logK ₃	4.38(5)	3.35(2)	5.49(5)	–	–
logK ₄	–	–	1.97(5)	–	–

The crystal of L6 is a 3D network built thanks to the involvement of H₂O and H₂L6²⁺ and Cl[−] ions in H-bonding interactions (see Table S1.3). In particular, chloride ions and water molecules are located in cavities that extend along the c axis and kept inside due to hydrogen bonding interactions involving all the donors from L6 acid molecule. The total accessible void calculated by PLATON [17] is found to be 18.8% of the crystal volume (Fig. 2).

3.1.2. Crystal structure of the ligand L7: (L7)₂

Ligand L7 crystallizes in the monoclinic system, space group P2₁/c. The asymmetric unit of the crystal comprises two crystallographically independent molecules of ligand L7. The reason why the two former

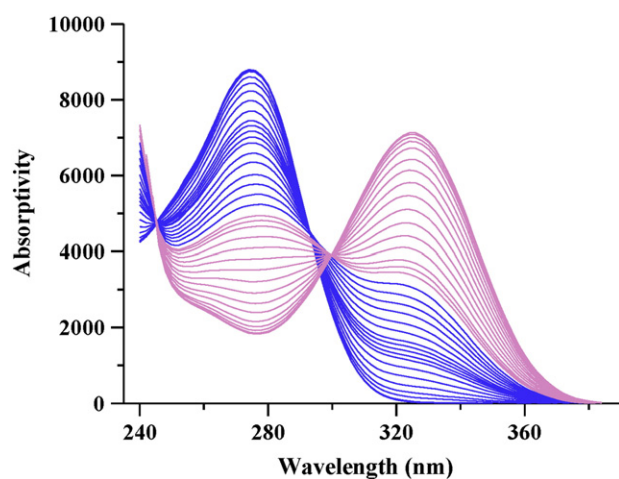


Fig. 6. Spectra collected during the potentiometric titration of ligand L7. Blue (darker lines) spectra are collected in the pH range relative to the first deprotonation, pink (lighter lines) spectra in the pH range relative to the second deprotonation.

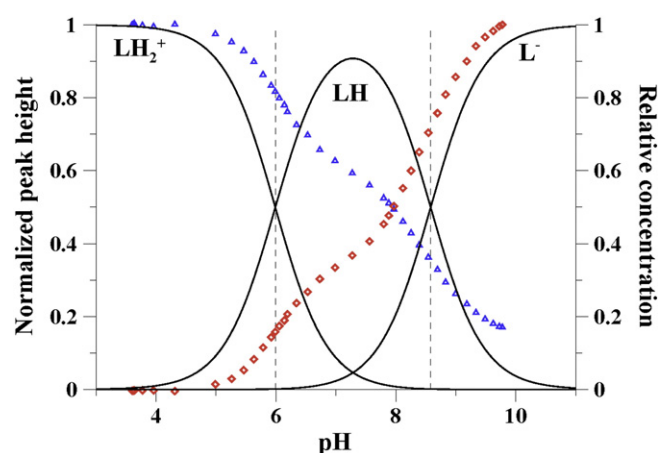


Fig. 7. Speciation curves of ligand L7, with the overlapping trends of the heights of UV bands at 276 nm (Δ) and 322 nm (\diamond), obtained by spectral decomposition of the spectra in Fig. 6 with the Specpeak program (19).

molecules are not equivalent mainly deals with the different torsion angles defined by the benzyl moiety [molecule 1: <N12–C14–C15–C16 85.78° or molecule 2: <N32–C34–C35–C36 108.05°] (see Fig. 3).

As already described for compound L6, each L7 molecule exhibits one intra-molecular H-bond that, again, involve the OH phenol-like group as donor and the O keto-kojic group as acceptor [molecule 1: O1–H··O4 (2.757(2) Å, 112.8°) or molecule 2: O21–H··O24 (2.764(2) Å, 112.6°)]. Moreover, the independent two molecules within the asymmetric unit are associated by one inter-molecular H-bonding interaction [O28–H··N12 (2.901(2) Å, 169.0°)] building pairs of molecules.

In the crystal, the aforementioned pairs of molecules are further associated by rather strong inter-molecular H-bonds building zig-zag 1D chains [O1–H··O24 (2.700(2) Å, 153.2°) and O21–H··O4 (2.654(2) Å, 152.6°)] (Fig. 4).

Adjacent chains connect to each other by additional H-bonds (see Table S2.3) leading to corrugated ribbons. Finally, hydrophobic interactions connect close ribbons to accomplish the 3D architecture of the crystal.

3.1.3. Crystal structure of the ligand L8

The crystal of ligand L8 crystallizes in the triclinic system, space group P-1. The asymmetric unit consists of just one organic molecule (Fig. 5).

One of the hydroxyl-methyl arms in L8 is delocalized in three different positions [O27A 0.393(12), O27B 0.325(14), O27C 0.283(6)].

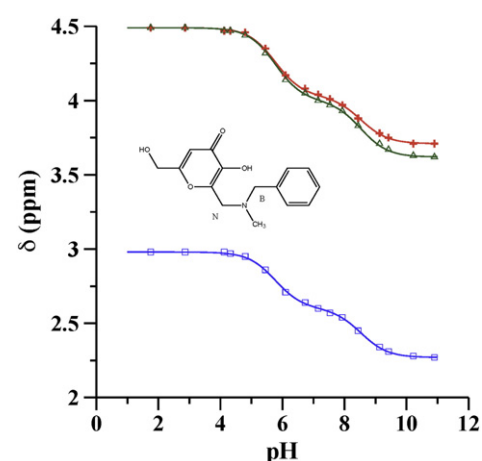


Fig. 8. Chemical shifts of CH₃ (blue squares), CH₂(B) (green triangles) and CH₂(K) (red crosses) of L7 ligand as a function of pH.

Table 2

Chemical shifts of H3, CH₂(K), CH₂(B) and CH₃ protons in the species LH₂⁺, LH and L[−] of ligand L7, calculated with the HyperNMR program [20].

Species	H3	CH ₂ (K)	CH ₂ (B)	CH ₃
LH ₂ ⁺	6.51	4.49	4.49	2.98
LH	6.41	4.03	4.00	2.60
L [−]	6.35	3.71	3.72	2.27

Table 3

Chemical shifts of in the species LH₂⁺, LH₂, LH[−] and L^{2−} of ligands L4 and L5, calculated with the HyperNMR program [20].

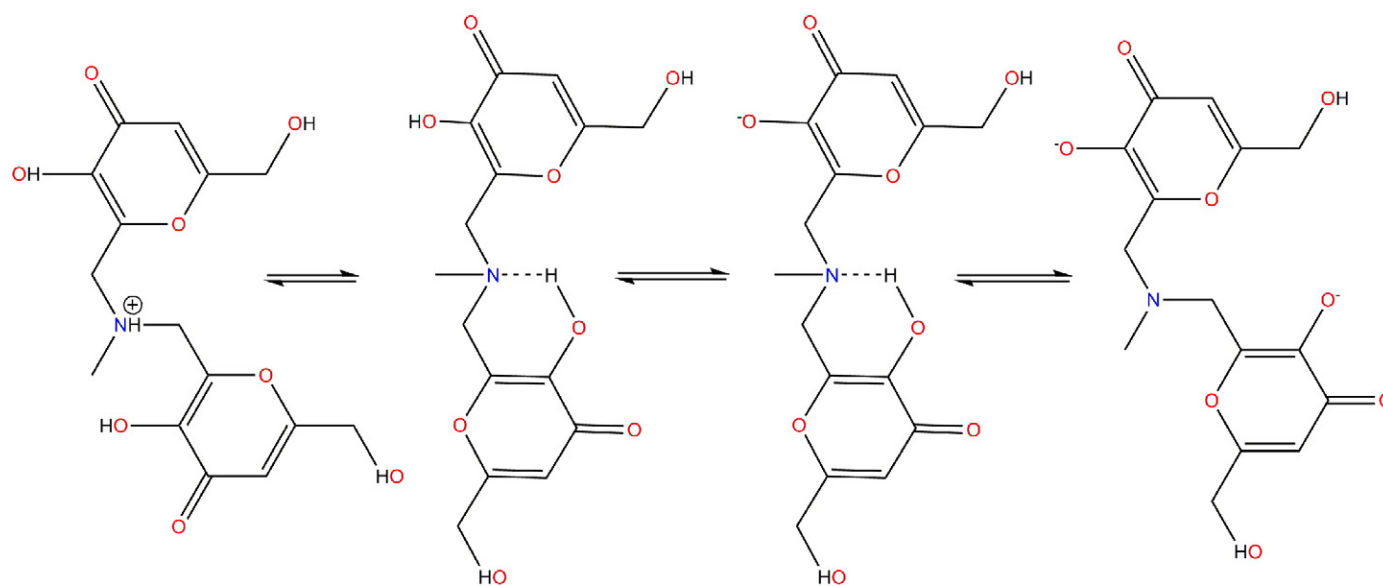
Species	L4			L5		
	H3	CH ₂ (N)	CH ₃	H3	CH ₂ (N)	CH(Bn)
LH ₂ ⁺	6.57	4.61	3.11	6.50	4.65	4.61
LH ₂	6.49	3.87	2.55	6.41	3.98	3.92
LH [−]	6.39	3.93	2.58	6.32	3.95	3.90
L ^{2−}	6.39	3.76	2.31	6.29	3.90	3.73

The mean planes of the two kojic moieties define a dihedral angle of 85.02°. This value, and therefore the orientation of the kojic moieties within the organic molecule, is similar to that described for a related bis-kojic derivatives of ortho-vanillin [9]. In accordance to the above-described L6 and L7 ligands, in L8 can also be observed in the corresponding intra-molecular interactions that involve the OH phenol-like group and the O keto-kojic group [O26–H··O25 (2.774(2) Å, 111.63°) and O36–H··O35 (2.756(2) Å, 112.35°)].

The crystal packing of L8 resembles to that of compound L7. Thus, zig-zag 1D chains are built by symmetry related molecules kinked by inter-molecular H-bonding interactions [O(26)–H··O25 (2.653(2) Å, 147.5°) and O36–H··O35 (2.754(2) Å, 154.6°)]. Adjacent chains are further connected by H-bonds (see Table S3.3) leading to corrugated ribbons. Again, the 3D framework is reached by hydrophobic interactions between neighboring ribbons.

3.2. Protonation equilibria

The protonation equilibria of the five ligands have been studied by potentiometry, UV spectrophotometry and ¹H NMR spectroscopy. The protonation constants evaluated from the potentiometric titration curves at 25 °C and 0.1 M ionic strength for the five ligands are reported in Table 1.

**Scheme 3.** Deprotonation sequence of ligand L4.**Table 4**

Complex formation constants of the five ligands with Fe^{III} at 25 °C, 0.1 M KCl ionic strength, obtained from potentiometric–spectrophotometric data using the Hyperquad program [13]. Charges are omitted for simplicity.

	L4	L5	L6	L7	L8
FeLH ₃	–	–	25.25(3)	–	–
FeLH ₂	22.21(3)	21.9(2)	–	–	–
FeLH	–	–	–	–	18.4(3)
Fe ₂ L ₂	–	–	–	–	41.11(4)
Fe ₂ L ₂ H _{−1}	–	–	–	–	38.97(2)
Fe ₂ L ₃ H ₄	69.1(1)	–	70.3(3)	–	–
Fe ₂ L ₃ H ₃	66.10(4)	67.2(2)	66.2(1)	–	–
Fe ₂ L ₃ H ₂	61.6(2)	64.1(2)	61.2(2)	–	–
Fe ₂ L ₃ H	56.19(1)	59.9(1)	–	–	–
Fe ₂ L ₃	49.75(1)	53.5(1)	49.4(2)	–	55.08(4)
FeL ₂ H ₂	–	–	–	33.0(1)	–
FeL ₂ H	–	–	–	28.2(2)	–
FeL ₂	–	–	–	22.6(2)	–
FeL ₂ H _{−1}	–	–	–	15.7(1)	–
FeL ₃	–	–	–	27.1(1)	–
pFe	18.1	19.3	17.7	16.7	20.0

The ligands L4 and L5 are characterized by three protonation constants, corresponding to the two kojic phenolates and to the nitrogen atom in the linker; L6 by four protonation constants relative to the two kojic units and to the two nitrogen atoms in the piperazine ring; L7 by two protonation constants attributable to the kojic phenolate and the nitrogen atom; L8 by the two protonation constants relative to the two kojic phenolates. The parent molecule kojic acid is characterized by a logK value of 7.70, and the protonation constant of a nitrogen atom in a tertiary amine can be roughly estimated from literature data that range from a value of logK = 8.05 for triethanolamine to 10.70 for triethylamine. As previously reported [7], the L[−] and LH species of kojic acid are characterized by UV bands at 315 nm ($\epsilon = 5900 \text{ M}^{-1} \text{ cm}^{-1}$) and 270 nm ($\epsilon = 8700 \text{ M}^{-1} \text{ cm}^{-1}$), respectively, with sharp isosbestic points at 242 nm and 290 nm.

In the following the protonation sequences of the five ligands, based on the spectrophotometric and ¹H NMR results, are proposed. This discussion starts with the simpler L7 compound, presenting only a kojic phenol group and a protonable nitrogen atom on the linker. Analysis of Fig. 6 (spectra a), in which the spectra collected during the potentiometric titration are presented, shows the band of the fully protonated form LH₂⁺ quite similar to that of the protonated species LH of kojic acid, differing only in the wavelength of the maximum, now shifted from 270 to 276 nm ($\epsilon = 8850 \text{ M}^{-1} \text{ cm}^{-1}$). The intensity of this

band decreases at about one half of its height during the first deprotonation (blue spectra), with the contemporary appearance of a new band at 322 nm, with sharp isosbestic points at 242 nm and 290 nm. During the second deprotonation (red curves) a further decrease in the intensity of the band at 276 nm and an increase in that at 322 nm take place. The band at 322 nm too is shifted to higher wavelengths and its ϵ value at the maximum is slightly higher than that of the corresponding band of fully deprotonated kojic acid. The trends of the peak intensity after decomposition of the spectra in the Gaussian band-components [19], overlapping the speciation plot, are clearly visible in Fig. 7.

A similar trend is presented by the chemical shifts of protons H3, CH₂(K), and CH₂(B) and CH₃ reported in Fig. 8. All these chemical shifts present an upfield shift during the two deprotonations, more marked for the three proton groups proximal to the nitrogen atom.

The chemical shifts of all the kind of protons in the species LH₂⁺, LH and L⁻, calculated with the HyperNMR program [20], are reported in Table 2.

The variations of both UV bands and chemical shifts, about of the same order of magnitude during the first and the second deprotonation, could lead to the hypothesis of a micro-dissociation scheme, in which the first proton is lost in comparable measure both by the nitrogen atom and by the phenolic group. The logK₂ value (6.02) corresponding to the first deprotonation step, ~1.7 units lower than that of kojic acid (and much lower than that of a tertiary amine nitrogen atom), implies a particular stabilization of the monoprotinated species such as the formation of a hydrogen bond between the phenolate O⁻ and the charged NH⁺ nitrogen, or between the phenolic group and the deprotonated nitrogen. Actually, whether the proton is lost by phenolic group or by nitrogen atom, the remaining proton is equally shared in a hydrogen bonding between these groups. Such a situation may well explain the observed experimental trends in which all the UV and NMR signals feel in an equal effect on both deprotonation steps.

Ligands L4 and L5 were characterized by the UV spectra with a maximum at about 275 nm for the fully protonated species, with ϵ values almost double with respect to those of kojic acid and ligand L7; during the first deprotonation step, this band slightly decreased in both ligands, with the appearance of a new band at about 328 nm; in the following steps a more marked decrease of the 275 nm band and an increase of the 328 nm band were observed.

Characteristic variations of the chemical shifts of the H3, CH₂(N), and CH₃ protons in L4, and H3, CH₂(N), and CH(Bn) protons in L5 are observed (Table 3), which allow to propose a sequence in the deprotonations of these ligands similar to that described above for L7. Hence, the first deprotonation leads to a neutral species in which a proton is shared through hydrogen bonding between the nitrogen atom and one of the two kojic phenol groups, inducing the strong upfield shift of the groups neighboring to the nitrogen atom, and that of H3 in the kojic ring. The second deprotonation, taking place on the kojic moiety not involved in the hydrogen bonding, is characterized both by a strong spectral variation of the UV bands related to the kojic moiety, and by an upfield shift of the NMR signals of the H3 proton, while those of the CH₂(N), CH₃ and CH(Bn) protons remain unaffected; in the last step, mainly in L4, a further upfield shift is experienced by hydrogen atoms neighbor to nitrogen for the loss of the shared proton, and a further strong spectral variation of the UV bands. This sequence is briefly sketched in Scheme 3.

Concerning the ligand L6 containing the piperazine ring on the linker, it is characterized by four protonation constants, logK₁ = 8.52, logK₂ = 7.81, logK₃ = 5.49, and logK₄ = 1.97. Presumably the general mechanism of deprotonation could be similar to that observed for L4 and L5, with the involvement of a further basic nitrogen atom. The low L6 water solubility avoided the acquisition of reliable NMR spectra. Furthermore, the small differences between the protonation constants lead to a continuous variation with pH of the UV absorbance bands, without any clear inflection. All these facts prevented to speculate upon the deprotonation mechanism.

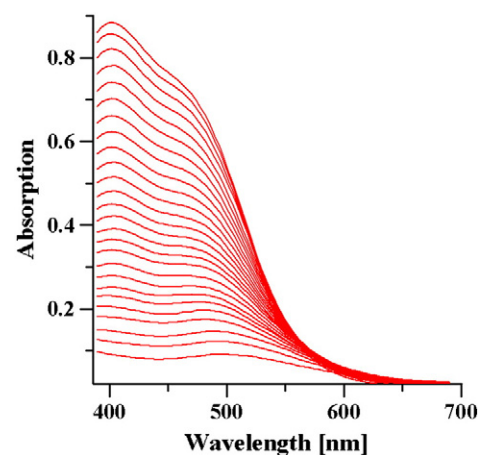


Fig. 9. Spectra collected in pH range 0.8–2.4, from solutions containing L4 = 3.44×10^{-4} M and Fe^{III} = 1.72×10^{-4} M, using 1 cm path length.

Ligand L8 is characterized by two protonation constants almost equal to those of L1, and a trend of UV spectra and NMR chemical shifts similar to that previously reported for L1 ligand was observed.

3.3. Iron complexes

The complex formation equilibria of all the five ligands with Fe^{III} have been studied by combined potentiometric–spectrophotometric techniques. In fact, being Fe^{III} almost completely complexed when

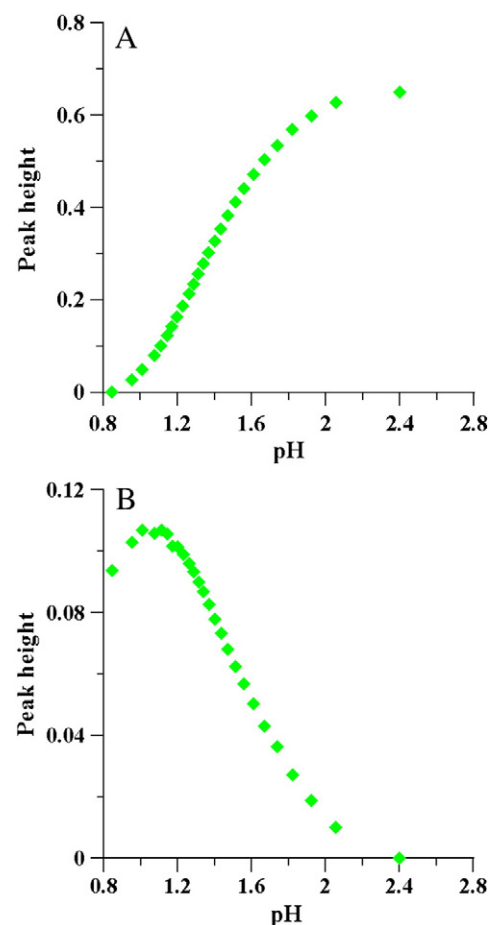


Fig. 10. Trend of the band absorbances at 468 nm (A) and 545 nm (B) reported as a function of pH, after decomposition of the spectra in Fig. 9.

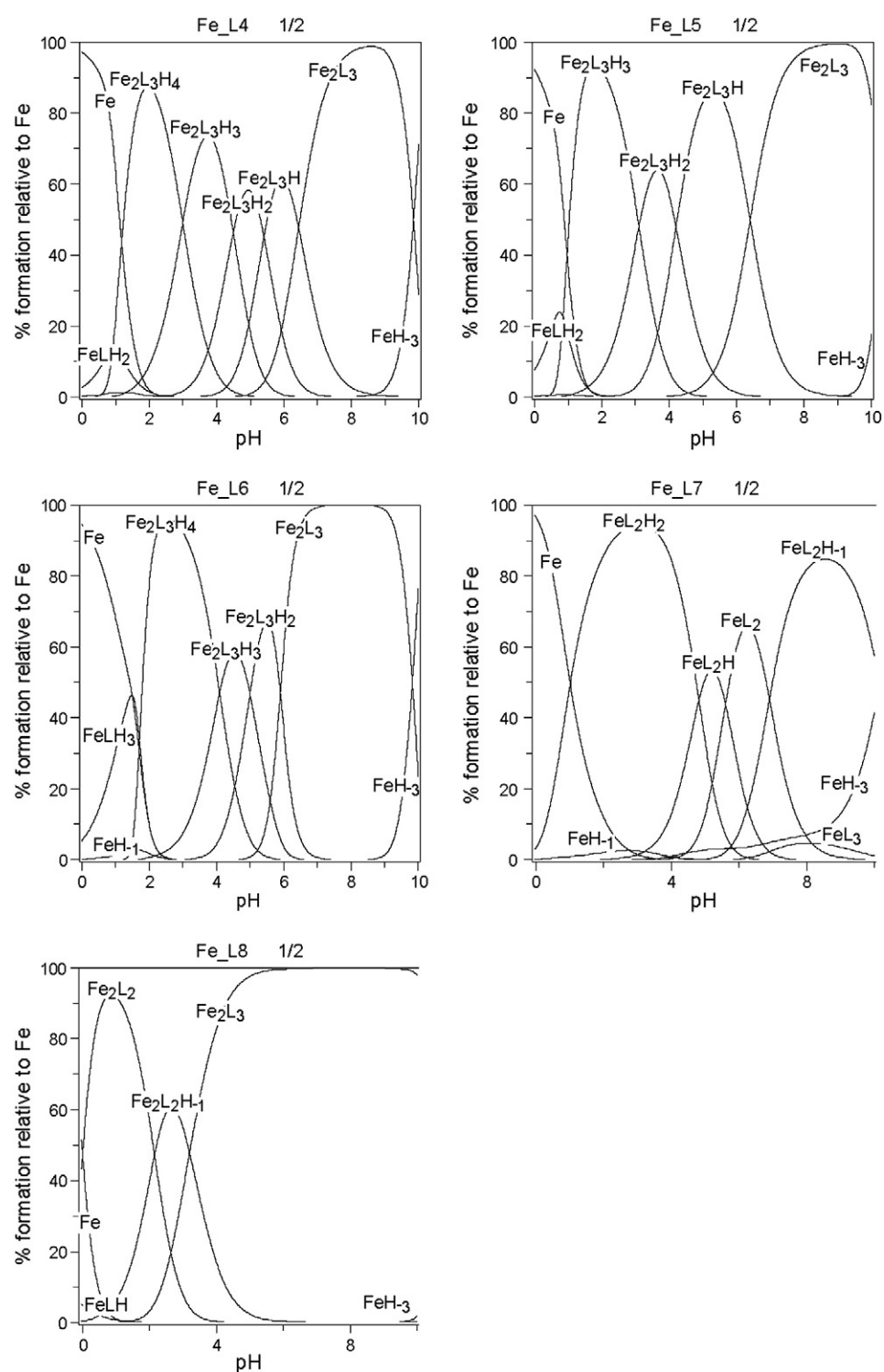


Fig. 11. Speciation plots calculated on the basis of stability constants reported in Table 4, using a ligand concentration 1×10^{-3} M and Fe^{III} concentration 5×10^{-4} M.

mixing reagents before the base potentiometric titrations, the estimation of reliable complex formation constants from potentiometric data alone was prevented. Therefore the complex formation equilibria have been studied both in strong acidic solutions (pH 0–2) on sets of solutions at increasing concentrations of HCl until the disappearance of the bands of complexed iron, and in the pH range 2–10. Simultaneous fitting of potentiometric and spectrophotometric data allowed obtaining the stability constants for the complexes of ligands L4–L8 with Fe^{III} , reported in Table 4.

The three ligands L4, L5, and L6 show a similar behavior; the visible spectra collected in strong acidic solutions at different metal/ligand ratios (1/1, 1/2, 1/3) display the 1:1 complex which at increasing pH soon disappears giving a $\text{Fe}_2\text{L}_3\text{H}_x$ complex stable in the 2–4 pH range. Actually, the shape of the spectra in this pH range is similar for all the three solutions at different metal/ligand ratios, and this is indicative that a unique species is formed. The ratios of the absorbance values in the three solutions clearly indicate the formation of a Fe_2L_3 complex. This has been confirmed by a Job plot performed at pH 2.9, which

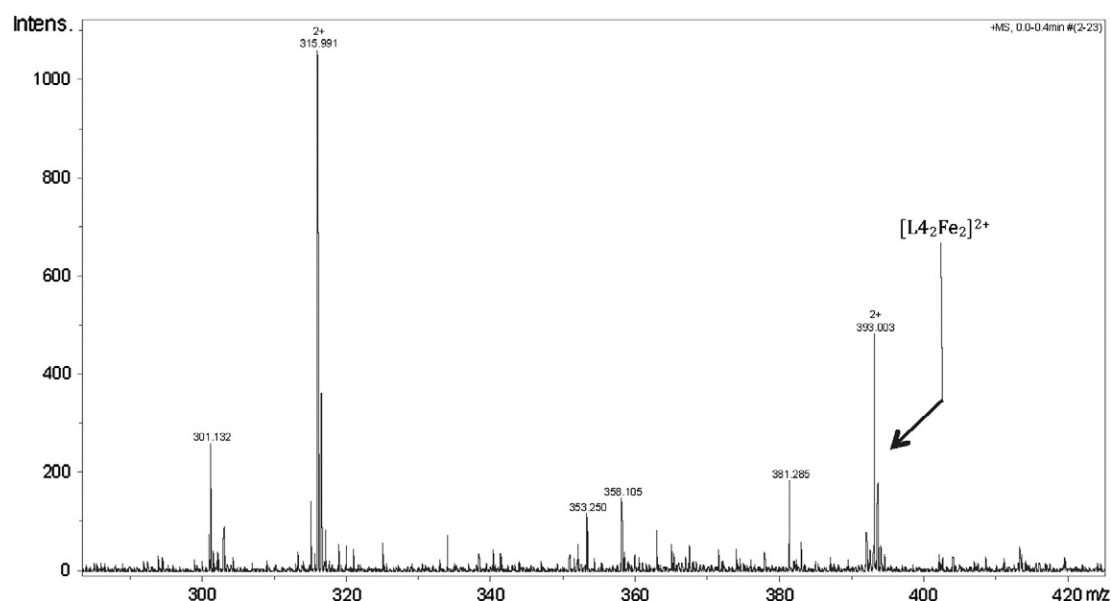


Fig. 12. ESI-MS spectra of the system L4-Fe^{III} in a ratio 1:10 at pH 7.

results in two straight lines intersecting at the ligand mole fraction 0.6. The spectra collected in acidic solutions for the 1:2 ligand/metal molar ratios for ligand L4 are reported in Fig. 9 as an example.

The spectra were decomposed in four Gaussian bands, with the program Specpeak [19]. The absorption of the bands at 468 nm and 545 nm are reported as a function of pH in Fig. 10.

The speciation plots shown in Fig. 11, calculated on the basis of stability constants reported in Table 4, allow some considerations: at very acidic pH (~1) a FeL₂H₂ complex with the two ligands L4 and L5 is formed, in which presumably Fe^{III} is coordinated by the two oxygen atoms of a kojic unit, being the nitrogen atom and the second kojic unit till protonated. At increasing pH a Fe₂L₃H₃ complex appears, in which the two iron atoms are joined by its kojic moieties; the complex Fe₂L₃H₄ formed only by the ligand L4 is presumably an intermediate in which two ligands join the two metal ions, and the third ligand binds only one iron atom with a kojic unit, the second one till protonated. Further pH increase induces progressive deprotonations with pK's ~ 4.5, 5.4 and 6.4 for L4 and 3.1, 4.2 and 6.4 for L5. These deprotonations can be reasonably attributed to the loss of protons from the nitrogen atoms in the linker.

A similar behavior is presented by L6, in which a FeLH₃ complex is initially formed, with iron coordinated by a kojic unit, the second kojic unit and the two piperazine nitrogen till protonated. Subsequently a Fe₂L₃H₄ complex is formed, in which the two iron atoms are bridged by the three ligands through both kojic units, with four of the six piperazine nitrogen atoms till protonated. Afterwards, the first two protons are lost with pK values 4.1 and 5.0, and the two last with the same pK 5.9. After several attempts to crystallize the compound Fe₂(L6)₃ a red parallelepiped crystal was obtained and read with Synchrotron radiation but the collected data only allowed seeing a rough model of the complex (See Supplementary Information).

Ligand L7, which does not contain a second kojic unit, forms FeL₂H_x and FeL₃ complexes, similarly to kojic acid. The FeL₂H₂ starting complex, protonated on the nitrogen atoms of both ligands, loses these protons and a third one, presumably from a coordinated water molecule at pK's 4.8, 5.6 and 6.9.

As far as the ligand L8¹ is concerned, its complexation mechanism starts with the formation of a FeLH complex at extremely low pH (0–1)

¹ L8, differently from L4–L7 complexes, does not contain nitrogen atoms, and it is analogous to the previously studied L1 ligand [7].

and it was evidenced only by spectral analysis. Already at these low pH values a Fe₂L₂ complex is formed with the two iron atoms joined by the two ligands. This complex is further stabilized by the loss at pH 2.1 of a proton from a coordinated water molecule, presumably a μ water joining the two iron atoms. At pH ≈ 4 a Fe₂L₃ complex is formed in which each iron atom is completely surrounded by six oxygen atoms from three kojic units.

The ESI-MS spectra, collected at pH ~7, with a 10:1 metal excess, allows revealing further complexes not lighted by the other solution equilibrium techniques. The ESI-MS spectrum of Fe^{III} complexes with L4 is illustrated in Fig. 12. The signal at *m/z* 393.004 reveals a [L₄₂Fe₂]²⁺ complex formation. The peak at *m/z* 315.991 corresponds to [L₄₂Fe₂]²⁺ complex without one methylene-kojic acid molecule. Formation of this complex is probably due to cleavage of the N–C bond during ionization of the [L₄₂Fe₂]²⁺ complex. The signal corresponding to free ligand is not present.

The ESI-MS spectrum in Fig. 13 displays the L5 complex formation. The main peaks appear at *m/z* 392.026, *m/z* 469.040 and *m/z* 478.045. The peak at *m/z* 469.040 corresponds to complex [L₅₂Fe₂]²⁺, while peak at *m/z* 478.045 represents its hydrated form [L₅₂Fe₂]²⁺. Such type of complex is stable even without one methylene kojic acid molecule, since the peak at *m/z* 392.026 is very intense. The peak corresponding to the free ligand is not present.

MS/MS fragmentation of the complex corresponding to signal at *m/z* 392.025 (Fig. 14) results in loss of another methylene-kojic. Signal at *m/z* 315.014 agrees with stoichiometry of [L₅₂Fe₂]²⁺ complex without two methylene kojic acid molecules.

The representative ESI-MS spectrum of Fe^{III} complexes with L6 is presented in Fig. 15. The high intensity of the peak at *m/z* 448.052 corresponds to the [L₆₂Fe₂]²⁺ complex, while the low intensity peak at *m/z* 457.053 represents [L₆₂Fe₂ + H₂O]²⁺ complex.

4. Conclusions

Five new ligands have been synthesized, structurally characterized and their protonation scheme has been explained using the information of UV and ¹H NMR spectra. For all the ligands containing two kojic units, the complex formation equilibria with Fe^{III} allowed concluding about the formation of variously protonated 2:3 Fe:L complex as the major species in the whole pH range; the unprotonated Fe₂L₃ complex is the unique species at pH 7.4 (see speciation plots in Fig. 11). Ligand L7, containing only a kojic unit, forms FeL₂H_x

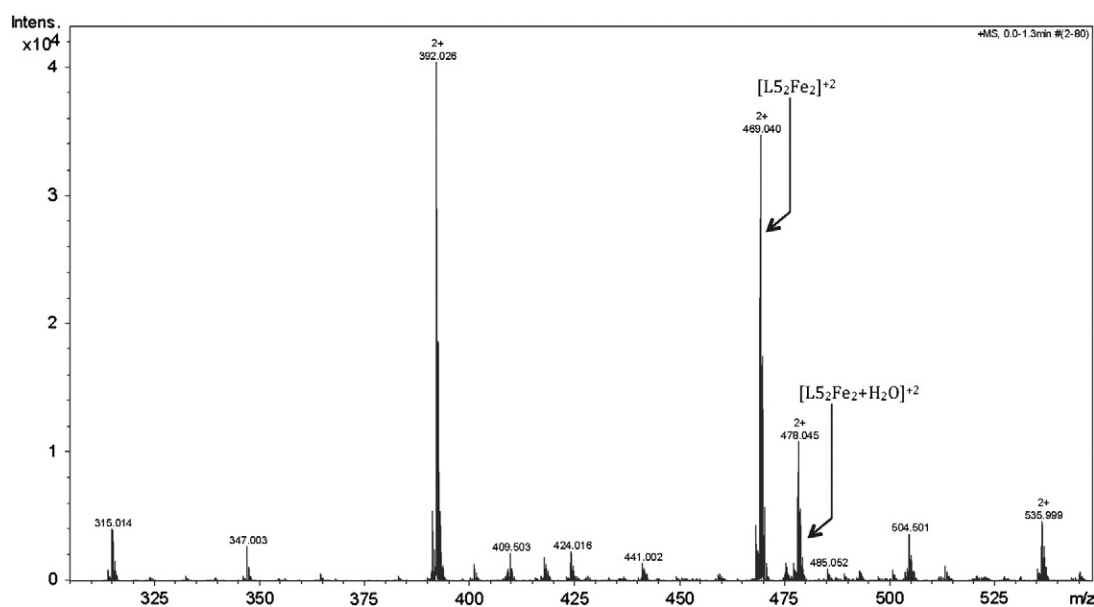


Fig. 13. ESI-MS spectra of the system L5-Fe^{III} in a ratio 1:10 at pH 7.

complexes and, in a lower amount, a FeL₃ complex. The prevailing species at pH 7.4 is FeL₂H⁻¹, stabilized by the deprotonation of a coordinated water molecule.

The pFe values reported in Table 4 can be used to evaluate and to compare the chelating ability of the various ligands. These data give evidence of a strong chelating ability of L8 ligand. The remaining ligands L4–L6, containing nitrogen atoms in the linker, show a minor chelating efficiency, pFe ranging from 19.3 for L5 to 17.7 for L6. Interaction of iron with L7 ligand, having only a coordinating kojic unit, is characterized by a pFe value 16.7, ca. 3 units higher than that of simple kojic acid. This significant difference should depend on two facts: the stabilization due to the loss of a proton from a coordinated water molecule, and to a kind of a hydrophobic cage formed by the groups not directly implied in coordination of the metal ion. According to the recent work of Evans [21], L8 ligand, anionic at physiological pH and characterized by a pFe of 20.0, and perhaps L5, partially in the anionic form LH⁻¹ at physiological pH and with pFe = 19.3, should be able to mobilize Fe^{III} from transferrin.

The excellent chelating properties recommend further toxicological and pharmacological research on these new promising ligands.

Acknowledgments

GC and JIL acknowledge Regione Sardegna for the financial support CRP-27564 to the project "Integrated approach in the design of chelators for the treatment of metal overload diseases". MCA is grateful to RAS for the program Master and Back – Percorsi di rientro, PRR-MAB-A2011-19107. MAS acknowledges FCT for financial support, project PEst-OE/QUI/UI0100/2011.

Appendix A. Supplementary data

Supplementary data to this article can be found online at <http://dx.doi.org/10.1016/j.jinorgbio.2013.06.009>.

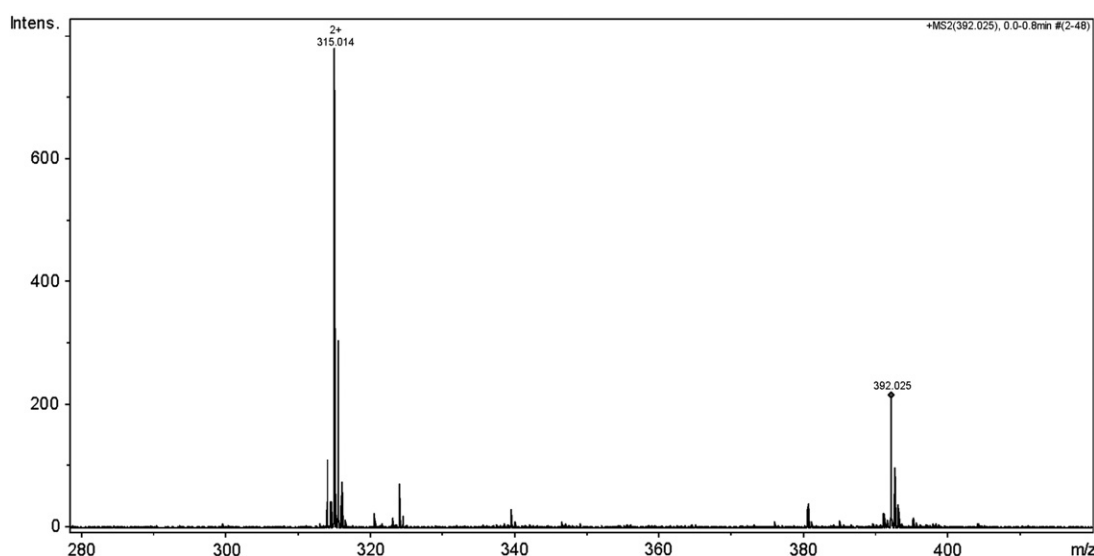


Fig. 14. CAD spectrum of peak at m/z 392.025 in Fig. 13.

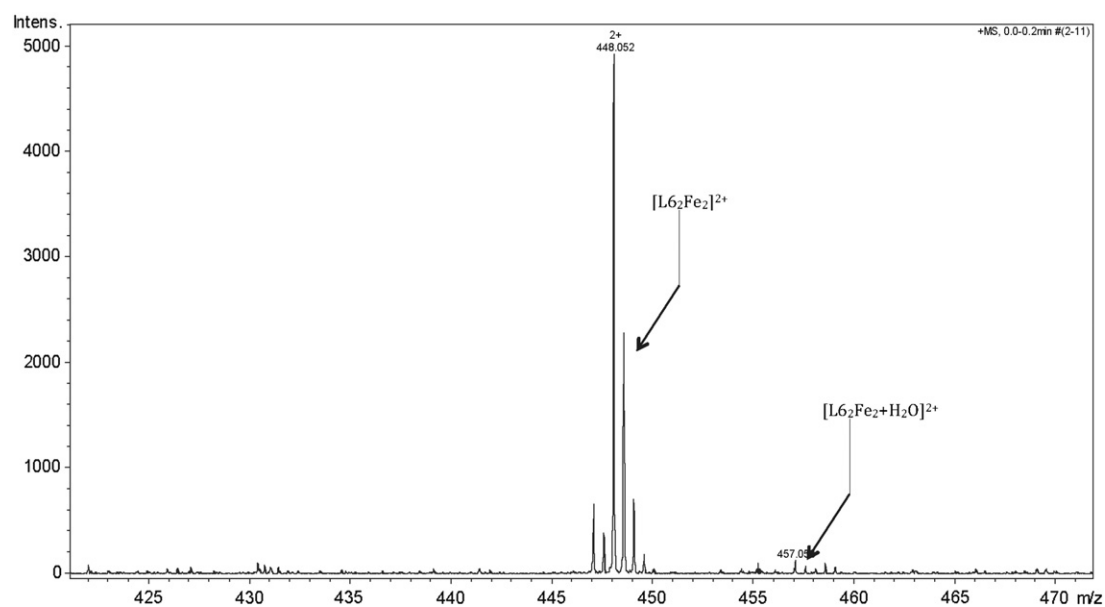


Fig. 15. ESI-MS spectra of the system L6-Fe^{III} in a ratio 1:10 at pH 7.

References

- [1] G. Crisponi, M. Remelli, *Coord. Chem. Rev.* 252 (2008) 1225–1240.
- [2] Y. Ma, T. Zhou, X. Kong, R.C. Hider, *Curr. Med. Chem.* 19 (2012) 2816–2827.
- [3] G. Crisponi, V.M. Nurchi, V. Bertolasi, M. Remelli, G. Faa, *Coord. Chem. Rev.* 256 (2012) 89–104.
- [4] M.A. Santos, S.M. Marques, S. Chaves, *Coord. Chem. Rev.* 256 (2012) 240–259.
- [5] G. Crisponi, V.M. Nurchi, G. Faa, M. Remelli, *Monatsh. Chem.* 142 (2011) 331–340.
- [6] G. Crisponi, A. Dean, V. Di Marco, J.I. Lachowicz, V.M. Nurchi, M. Remelli, A. Tapparo, *Anal. Bioanal. Chem.* 405 (2013) 585–601.
- [7] V.M. Nurchi, G. Crisponi, J.I. Lachowicz, S. Murgia, T. Pivetta, M. Remelli, A. Rescigno, J. Niclós-Gutiérrez, J.M. González-Pérez, A. Domínguez-Martín, A. Castiñeiras, Z. Szewczuk, *J. Inorg. Biochem.* 104 (2010) 560–569.
- [8] R.C. Fox, P.D. Taylor, *Bioorg. Med. Chem. Lett.* 8 (1998) 443–446.
- [9] V.M. Nurchi, J.I. Lachowicz, G. Crisponi, S. Murgia, M. Arca, A. Pintus, P. Gans, J. Niclós-Gutiérrez, A. Domínguez-Martín, A. Castiñeiras, M. Remelli, Z. Szewczuk, T. Lis, *Dalton Trans.* 40 (2011) 5984–5998.
- [10] V.M. Nurchi, G. Crisponi, T. Pivetta, M. Donatoni, M. Remelli, *J. Inorg. Biochem.* 102 (2008) 684–692.
- [11] V.M. Nurchi, G. Crisponi, M. Crespo-Alonso, J.I. Lachowicz, Z. Szewczuk, G.J.S. Cooper, *Dalton Trans.* 42 (2013) 6161–6170.
- [12] H.N. Barham, G.N. Reed, *J. Am. Chem. Soc.* 60 (1938) 1541–1545.
- [13] P. Gans, A. Sabatini, A. Vacca, *Talanta* 43 (1996) 1739–1753.
- [14] Bruker, APEX2 Software, Bruker AXS Inc., Madison, Wisconsin, USA, 2010. (v2010.3-0).
- [15] G.M. Sheldrick, SADABS, Program for Empirical Absorption Correction of Area Detector Data, University of Gottingen, Germany, 2009.
- [16] G.M. Sheldrick, *Acta Crystallogr. Sect. A* 64 (2007) 112–122.
- [17] A.L. Spek, Utrecht University, Utrecht, The Netherlands, 2010.
- [18] C.F. Macrae, I.J. Bruno, J.A. Chisholm, P.R. Edgington, P. McCabe, E. Pidcock, L. Rodriguez-Monge, R. Taylor, J. Van De Streek, P.A. Wood, *J. Appl. Crystallogr.* 41 (2008) 466–470.
- [19] M.C. Aragoni, M. Arca, G. Crisponi, V.M. Nurchi, *Anal. Chim. Acta* 316 (1995) 195–204.
- [20] C. Frassinetti, L. Alderighi, P. Gans, A. Sabatini, A. Vacca, S. Ghelli, *Anal. Bioanal. Chem.* 376 (2003) 1041–1052.
- [21] R.W. Evans, X. Kong, R.C. Hider, *Biochim. Biophys. Acta* 1820 (2012) 282–290.

Additional Structural Information

Description of the Fe₂(L6)₃ crystal

The collected data from X-ray diffraction experiments were not enough to successfully complete the crystal structure determination. However, the available data were processed to obtain a rough model, with the crystal being solved in the trigonal system, space group R3. In the model, three different complex molecules are observed: (i) a tentative model of the Fe₂(L6)₃ complex, (ii) one tentative model of a related Fe(Kj)₃ complex and (iii) one iron centre surrounded by 6 oxygen atoms.

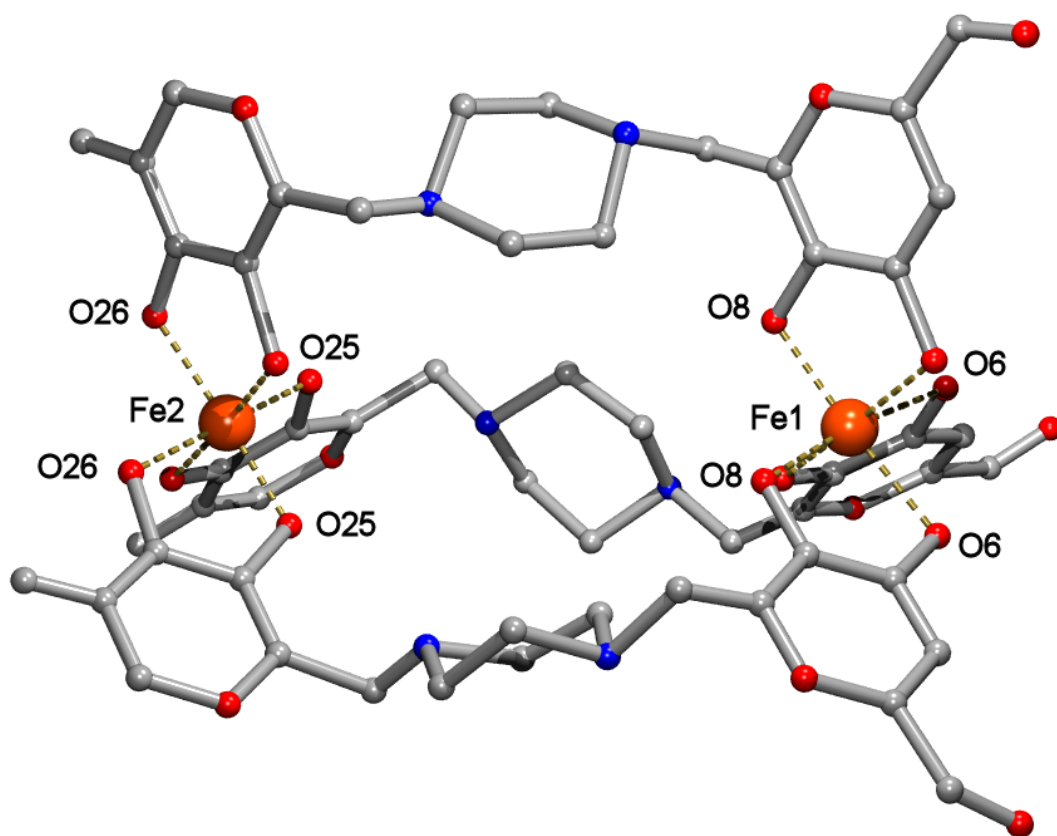
In the model of the Fe₂(L6)₃ complex, one of the two kojic moieties within the L6 ligands is incomplete. Thus, those kojic moieties tied to the Fe2 atom do not have the alcoholic groups and show a residual peak (represented as a carbon) close to the keto group (see SMFigure 1). These differences between the expected and the observed formula of the L6 ligands have been attributed to limitations in the experimental data which did not allow further refinements. In contrast, the stoichiometry of the complex and the metal surrounding are well defined. The two Fe³⁺ ions are surrounded by 6 oxygen atoms provided by three different L6 ligands. The complex molecule Fe₂(L6)₃ occupies a special crystallographic position (3-fold rotation axis) what determines the coordination bond distances [Fe1-O6 2.1228(2) Å, Fe1-O8 1.9793(1) Å and Fe2-O25 2.0181(1) Å, Fe2-O26 1.8738(1) Å] and the values of the trans-angles [O6-Fe1-O8 172.25° and O25-Fe2-O26 176.67°] (see SMFigure 1). Note that the largest coordination bonds correspond to Fe–O(keto) bonds whereas the smallest ones are Fe–O(hydroxy). A fairly similar configuration was reported for the Fe(Kj)₃ complex [1], which showed average bond distances of 2.070 and 1.974 Å for Fe–O(keto) and Fe–O(hydroxy) bonds, respectively.

Concerning the two other iron complexes present in the crystal, only speculations can be done. During the crystallization process, the solution experimented color changes from colorless to yellow. This fact was tentatively attributed to a slight degradation of the ligand L6 in the presence of light. This is in accordance to the existence in the crystal of one complex molecule that contains kind of individual kojic units and iron(III). This compound could be the previously reported Fe(Kj)₃ complex [1] or any Fe(Kj)₃-like related complex. Again, residual peaks were found around the kojic moieties that could not be unequivocally assigned. These residues are shown in SMFigure 2 as extra-alcoholic groups in the kojic moieties. The other complex molecule present in the crystal (one Fe³⁺ ion surrounded by six oxygens) is most probably, for neutrality reasons, another Fe(Kj)₃-like unit. However, the idea of an hexaaquo cation of iron(III) cannot be dismissed because it is still

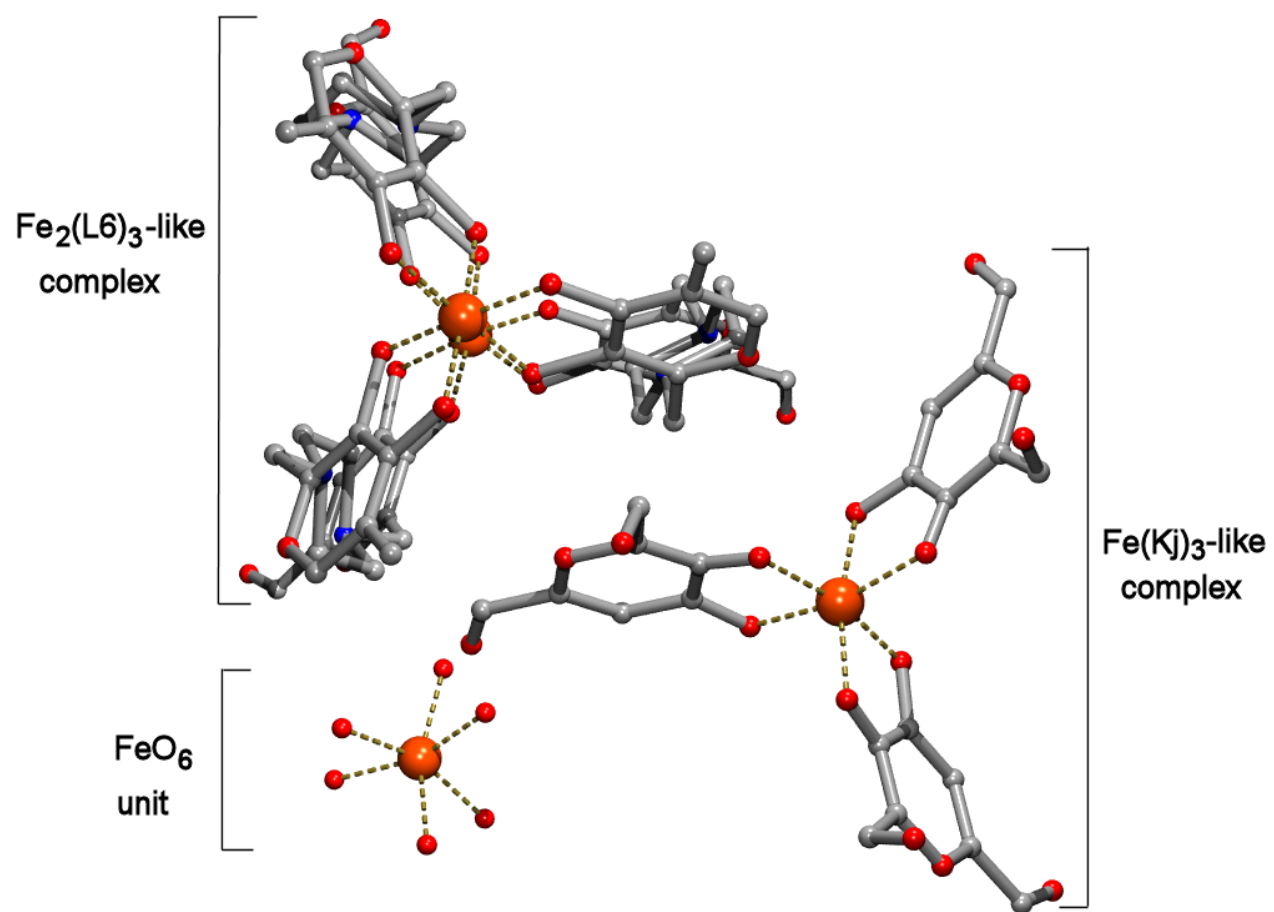
possible that some counteranion is present in the crystal but it could not be seen in the model due to the above refinement problems.

Reference

[1] V.M. Nurchi et al., *J. Inorg. Biochem.* 104 (2010) 560–569



SMFigure 1



SMFigure 2

Paper VI

Searching for new Aluminium Chelating Agents: a family of hydroxypyrrone ligands

L. Toso, G. Crisponi, V.M. Nurchi, M. Crespo-Alonso, J.I. Lachowicz, D. Mansoori, M. Arca, M.A. Santos, S.M. Marques, L. Gano, J. Niclós-Gutierrez, J.M. González-Pérez, A. Domínguez-Martín, D. Choquesillo-Lazarte, Z. Szewczuk, J. Inorg. Biochem. 130 (2014) pp. 112-121.

DOI: [10.1016/j.jinorgbio.2013.09.022](https://doi.org/10.1016/j.jinorgbio.2013.09.022)

Reprinted with permission from Elsevier

Copyright © 2014 Elsevier B.V. All rights reserved



Searching for new aluminium chelating agents: A family of hydroxypyrrone ligands



Leonardo Toso^a, Guido Crisponi^a, Valeria M. Nurchi^{a,*}, Miriam Crespo-Alonso^a, Joanna I. Lachowicz^a, Delara Mansoori^a, Massimiliano Arca^a, M. Amélia Santos^b, Sérgio M. Marques^b, Lurdes Gano^c, Juan Niclós-Gutiérrez^d, Josefa M. González-Pérez^d, Alicia Domínguez-Martín^d, Duane Choquesillo-Lazarte^e, Zbigniew Szewczuk^f

^a Dipartimento di Scienze Chimiche e Geologiche, Università di Cagliari, Cittadella Universitaria, 09042 Monserrato-Cagliari, Italy

^b Centro Química Estrutural, Instituto Superior Técnico, Universidade Técnica de Lisboa, Av. Rovisco Pais, 1049-001 Lisboa, Portugal

^c Campus Tecnológico e Nuclear, Instituto Superior Técnico, Universidade Técnica de Lisboa, Estrada Nacional 10, 2695-066 Bobadela LRS, Portugal

^d Department of Inorganic Chemistry, Faculty of Pharmacy, Campus Cartuja, University of Granada, E-18071 Granada, Spain

^e Laboratorio de Estudios Cristalográficos, IACT, CSIC-Universidad de Granada, Av. de las Palmeras 4, E-18100 Armilla, Granada, Spain

^f Faculty of Chemistry, University of Wrocław, F. Joliot-Curie 14, 50-383 Wrocław, Poland

ARTICLE INFO

Article history:

Received 23 May 2013

Received in revised form 12 September 2013

Accepted 18 September 2013

Available online 18 October 2013

Keywords:

Aluminium related diseases

Chelation therapy

Kojic acid

Solution equilibria

Hydroxypyrones

ABSTRACT

Attention is devoted to the role of chelating agents in the treatment of aluminium related diseases. In fact, in spite of the efforts that have drastically reduced the occurrence of aluminium dialysis diseases, they so far constitute a cause of great medical concern. The use of chelating agents for iron and aluminium in different clinical applications has found increasing attention in the last thirty years. With the aim of designing new chelators, we synthesized a series of kojic acid derivatives containing two kojic units joined by different linkers. A huge advantage of these molecules is that they are cheap and easy to produce. Previous works on complex formation equilibria of a first group of these ligands with iron and aluminium highlighted extremely good pMe values and gave evidence of the ability to scavenge iron from inside cells. On these bases a second set of bis-kojic ligands, whose linkers between the kojic chelating moieties are differentiated both in terms of type and size, has been designed, synthesized and characterized. The aluminium^{III} complex formation equilibria studied by potentiometry, electrospray ionization mass spectroscopy (ESI-MS), quantum-mechanical calculations and ¹H NMR spectroscopy are here described and discussed, and the structural characterization of one of these new ligands is presented. The in vivo studies show that these new bis-kojic derivatives induce faster clearance from main organs as compared with the monomeric analog.

© 2013 Elsevier Inc. All rights reserved.

1. Introduction

Overviews on the pathological effects of aluminium overload in humans, and on its role in neurodegenerative diseases have been recently presented [1,2]. Aluminium was regarded as a non-toxic metal ion till the seventies of the last century, and its products have a number of applications, in medicine, in food processing, in water treatment, etc. The awareness that neurological and bone diseases in patients under dialysis treatment were related with aluminium toxicity encouraged the research on the management of aluminium intoxication. The reduction of all parenteral and oral aluminium exposures contributed to decrease aluminium dependent diseases in the last 20 years [3,4]. The aluminium

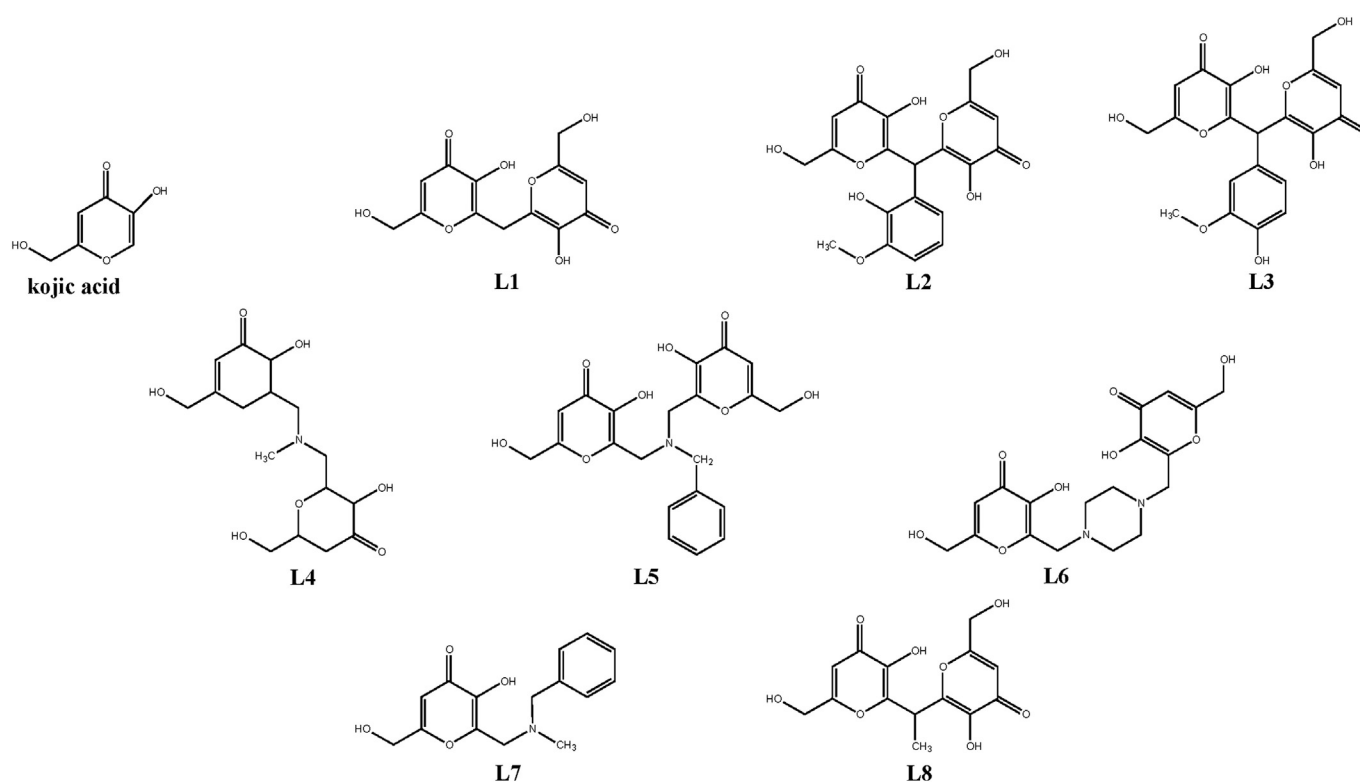
chelation was recommended when patients did not clinically improve when aluminium exposure ceased [5]. Deferoxamine was the first aluminium chelator introduced in clinical practice that reduces not only bone aluminium deposit but also aluminium burden in the brain [6–12]. The acute neurological complications, which may be developed during Deferoxamine therapy for aluminium bone diseases, limited this treatment only to those patients with serum aluminium levels higher than 200 µg/L, or with aluminium bone concentration ten times greater than normal values [5,13,14]. Different aluminium chelators have been then introduced [15].

The aluminium chelation therapy has been founded on that in use for iron. Actually, massive research efforts due to the worldwide diffusion of iron overload diseases have lead to significant improvements in iron chelation. Evidence has been given for the utility, in aluminium dependent pathologies, of the knowledge acquired on iron chelating agents [16,17].

With the aim of designing new ligands that form high stability complexes, which satisfy the chemical and biological requirements for

* Corresponding author at: Dipartimento di Scienze Chimiche e Geologiche, Cittadella Universitaria, 09042 Monserrato-Cagliari, Italy. Tel.: +39 070 675 4476; fax: +39 070 675 4478.

E-mail address: nurchi@unica.it (V.M. Nurchi).



Scheme 1. Chemical structures and acronyms of studied ligands.

an effective chelating agent such as selectivity, lipophilicity and bioavailability, our group has synthesized some derivatives of kojic acid, and studied their complex formation equilibria with Fe^{III} and Al^{III} , as well as those with the parent ligand kojic acid (Scheme 1).

In previous works, the formation of MeL , MeL_2 , and MeL_3 complexes of Al^{III} and Fe^{III} with kojic acid was remarked, and of diverse protonated species of Me_2L_2 and MeL_2 complexes with L1 [18], and with the related compounds in which vanillin and *o*-vanillin (L2 and L3) substituents were inserted on the linker [19]. The found pFe values (23.1 for L1, 18.9 for L2 and 22.2 for L3), lower than that for desferal (26.6) and comparable with that of deferiprone (20.7), and the fact that these ligands are easily and cheap to produce were very encouraging. We have recently synthesized a new set of bis-kojic ligands in which different linkers connecting the two kojic coordinating moieties have been designed for improving the interaction between the kojic units and the metal ions.

In this paper we will report the study on the complex formation equilibria of ligands L4–L8 as well as the structure characterization of L4 by X-ray diffraction. The *in vivo* efficacy of the ligands L4, L5, L7 and L8 as potential sequestering agents was also studied and reported herein, namely for the Ga-67 mobilization in mice previously injected with the radiotracer ^{67}Ga -citrate, as an animal model of Al-overload.

2. Experimental

2.1. Reagents

All the products, NaOH, KOH, and AlCl_3 purchased from Aldrich, HCl from Fluka, KCl from Carlo Erba (Milan, Italy), were used without further purification. An already described method was used for 0.1 M carbonate free KOH solution [20]. Ligand solutions were acidified with stoichiometric equivalents of HCl. Al^{III} solution was prepared by dissolving the required amount of AlCl_3 in pure double distilled water

to which a stoichiometric amount of HCl was previously added to prevent hydrolysis. This solution was standardized by EDTA titration.

2.2. Synthesis

The synthesis of the ligands in Scheme 1 has been previously reported [21].

2.2.1. Synthesis of the L4 crystal

L4 (15 mg) was dissolved in distilled water (3 mL), aided by drop wise addition of HCl 0.01 M. Afterwards, isopropanol (3 mL) was added and the solution was left stirring for 30 min and then filtered into a crystallization device to remove possible impurities. The solution was placed into an acetone chamber diffusion, where acetone acts as antisolvent in crystallization process. After three weeks, parallelepiped colorless crystals appeared suitable for X-ray diffraction (XRD). It is also possible to obtain single crystals of L4 without acetone diffusion, leaving the solution to stand at room temperature. However, the quality of the crystals is lower, hence good quality data could not be obtained.

2.3. Potentiometric measurements

Potentiometric measurements of the complex formation equilibria were carried out under the same conditions described in a previous publication [18]. The operating ligand concentrations ranged from 3×10^{-4} to 3×10^{-3} M according to the examined ligand. The studies of complex formation were carried using constant ligand concentration, and 1:1, 1:2, and 1:3 metal/ligand molar ratios. To take into account the low complex formation rate with Al(III), a suitable procedure was used: the titrations started 1 h after the mixing of the reagents, long delay times between two subsequent additions were used (2–7 min) and the achievement of the equilibrium was checked using a drift parameter

of 1 mV/min [18]. Complex formation data were analyzed using the Hyperquad program [22].

2.4. ^1H NMR measurements

NMR spectra were recorded on a Bruker AVANCE III spectrometer at 300 MHz for ^1H NMR measurements. Chemical shifts (δ) are reported in ppm related to tetramethylsilane (TMS). The concentrations of the ligands ranged from 4 mM for L6 to 10 mM for L4, according to their solubility, and 1:3, 2:3 and 1:1 metal:ligand ratios were studied.

2.5. ESI-MS analysis of complexes

ESI-MS spectra were carried out on a Bruker microTOF-Q spectrometer (Bruker Daltonics, Bremen, Germany) equipped with an ESI source. Samples were dissolved in water and methanol 1:1 and the final pH was ~ 7 . The ligand concentration was $\sim 10^{-5}$ M and the ligand to metal molar ratio was 1:10. The experimental parameters were as follows: scan range 100–1600 m/z , drying gas nitrogen, temperature 200 °C, ion source voltage 4500 V, in-source collision energy 10 eV. The instrument operated in the positive ion mode and was calibrated externally with Tunemix™ mixture (Bruker Daltonics, Germany). Analyte solutions were introduced at a flow rate 3 $\mu\text{l}/\text{min}$. Compass Data Analysis (Bruker Daltonics, Germany) software was used to determine the formulae of the complexes. The stoichiometry of the complexes was unambiguously confirmed by distribution of the isotopic peaks and MS/MS analysis. The distance between the isotopic peaks allowed calculating the charge of the analyzed ions.

2.6. Crystal structure determination

Measured crystal was prepared under inert conditions immersed in perfluoropolyether as protecting oil for manipulation. Suitable crystals were mounted on MiTeGen Micromounts™ and these samples were used for data collection. Data were collected with Bruker SMART APEX (100 K) diffractometer. The data were processed with APEX2 [23] program and corrected for absorption using SADABS [24]. The structures were solved by direct methods, which revealed the position of all non-hydrogen atoms. These atoms were refined on F^2 by a full-matrix least-squares procedure using anisotropic displacement parameters [25]. All hydrogen atoms were located in difference Fourier maps and included as fixed contributions riding on attached atoms with isotropic thermal displacement parameters 1.2 times those of the respective atom. Geometric calculations were carried out with PLATON [26] and drawings were produced with PLATON and MERCURY [27]. Additional crystal data and more information about the X-ray structural analyses are shown in Supplementary material. Crystallographic data for the structural analysis have been deposited with the Cambridge Crystallographic Data Centre, CCDC 940707. Copies of this information may be obtained free of charge on application to CCDC, 12 Union Road, Cambridge CB2 1EZ, UK (fax: 44 1223 336 033; e-mail: deposit@ccdc.cam.ac.uk or <http://www.ccdc.cam.ac.uk>).

2.7. Theoretical calculations

Theoretical calculations were carried out on the ligands L4 and L6 in their neutral and *N*-protonated forms (see Results and discussion) and on the complexes $[\text{Al}_2(\text{L4}^-)_3]^{3+}$ and $[\text{Al}_2(\text{L6})_3]^{6+}$ with the Gaussian09 (Rev. A.02) commercial suite of programs [28] at Density Functional Theory (DFT) level, adopting the mPW1PW91 (mPW1PW) functional by Adamo and Barone [29]. Schäfer, Horn, and Ahlrichs double- ζ plus polarization all-electron basis sets [30] were used for all atoms and were extracted from the Basis Set Exchange Database [31,32]. For each compound, the optimized geometries were verified through the calculations of harmonic vibrational frequencies computed analytically. Mulliken natural charges [33–35], and Wiberg bond indices [36] were

calculated at the optimized geometries. The programs GaussView 5 and Molden 5.0 [37] were used to investigate the charge distributions and molecular orbital shapes. Calculations were carried out on a 64 bit E4 workstation equipped with four quad-core AMD Opteron processors and 16 Gb of RAM and running the Ubuntu 12.04 Linux OS and on a 64 bit IBM x3755 server equipped with four 12-core processors and 64 Gb of RAM running the SuSE 10.2 OS.

In order to estimate some pharmacokinetic parameters related with the ADME (absorption, distribution, metabolism and excretion) properties of the new compounds, a selection of molecular descriptors was calculated using Maestro 7.5 [38] and the corresponding QikProp program [39]. Maestro was used to build the molecular structure of the compounds which were energy minimized with Molten [37] and then re-imported by Maestro to run QikProp job. From the generated out-put file the following set of properties was predicted: the octanol/water partition coefficient (clog *P*), the aqueous solubility (log *S*, *S* in moles/L is the concentration of the solute in saturated solution), the apparent Caco-2 cell permeability in nm/s, the binding to Human serum albumin, the Human oral absorption in gastro-intestinal gut.

2.8. Biodistribution studies

^{67}Ga -citrate injection solution was prepared by dilution of ^{67}Ga -citrate from MDS Nordion with saline to obtain a final radioactive concentration of 5–10 MBq/100 μl . Biodistribution studies were carried out in groups of 3 female CD1 mice (randomly bred, Charles River, from CRIFFA, Barcelona, Spain) weighing ca. 25 g. Mice were intravenously (i.v.) injected with 100 μl (5–10 MBq) of ^{67}Ga -citrate via the tail vein immediately followed by intraperitoneal (i.p.) injection of 0.5 μmol of each ligand in 100 μl DMSO (L4, L5, L7) or saline (L8). L6 was not bioassayed due to its low solubility in water (neutral pH) or in DMSO. Animals were maintained on normal diet ad libitum and were sacrificed by cervical dislocation at 1 h and 24 h post-administration. The administered radioactive dose and the radioactivity in sacrificed animals were measured by a dose calibrator (Curiometer IGC-3 Aloka, Japan). The difference between the radioactivity measured immediately after the injection and in the sacrificed animal, taking into account the radioactive decay was assumed to be due to whole body excretion. Tissue samples of main organs were then removed for counting in a gamma counter (Berthold LB2111, Berthold Technologies, Germany). Biodistribution results were expressed as percent of injected activity per total organ (% I.A./organ) and presented as mean values \pm SD. For blood, bone and muscle, total activity was calculated assuming, as previously reported, that these organs constitute 7, 10 and 40% of the total weight, respectively. Statistical analysis of the data (*t*-test) was done with GraphPad Prism and the level of significance was set at 0.05.

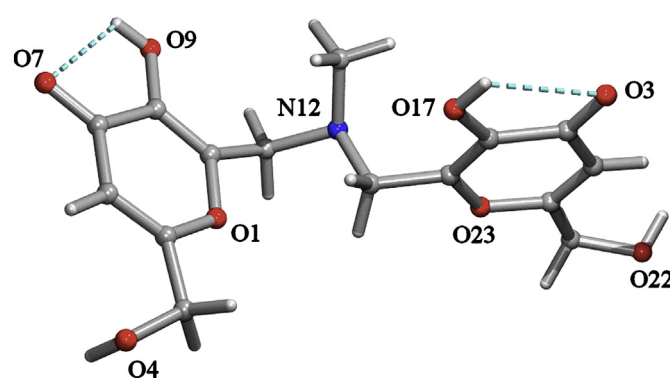


Fig. 1. Molecular structure of L4.

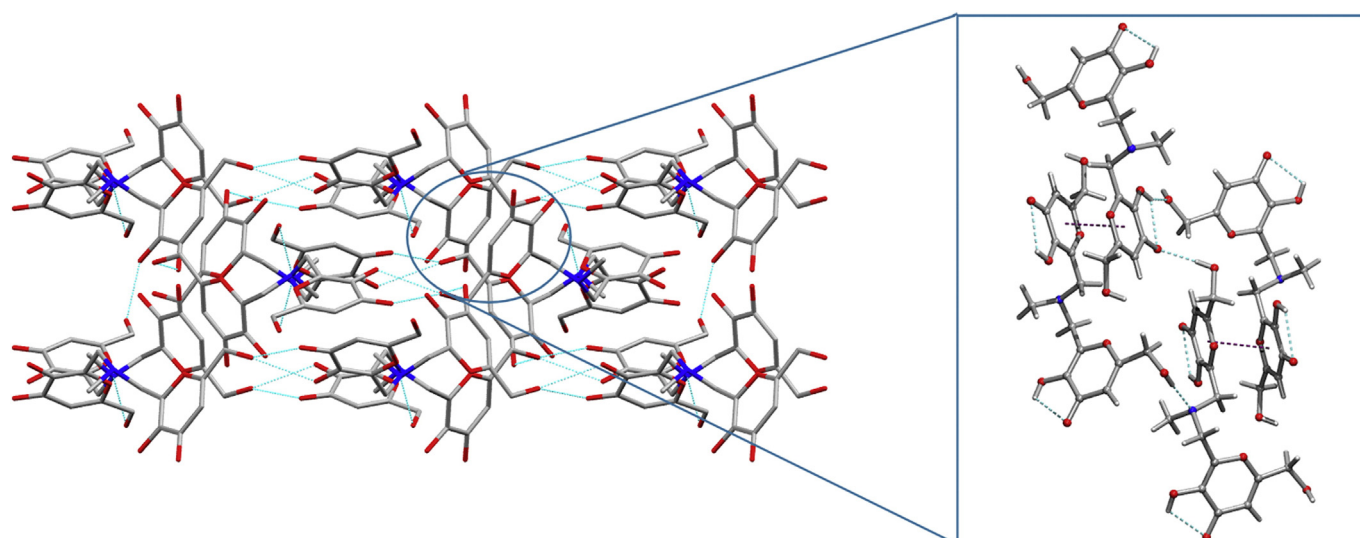


Fig. 2. Left: 3D architecture of the crystal of L4 with inter-molecular interactions (H-atoms omitted); right: detail of inter-molecular π,π -stacking interactions. Intra- and inter-molecular interactions are shown.

3. Results and discussion

3.1. Crystal structure of ligand L4

Ligand L4 crystallizes in the orthorhombic system, space group Pbc_a. The asymmetric unit consists of just one acid molecule (Fig. 1). The kojic acid moieties are stabilized by two intra-molecular H-bonding interactions involving the OH phenol-like groups as donors and the O keto-kojic groups as acceptors [O9–H–O7 (2.744(2) Å, 112.4°) and O17–H–O3 (2.797(2) Å, 111.3°)]. This feature has also been observed in closely related kojic-like compounds [19,21].

In the crystal of L4, adjacent acid molecules are linked via H-bonds with one OH-alcohol group and the quaternary N-atom being the H-donor and H-acceptor, respectively [O4–H–N12 (2.782(2) Å, 176.8°)]. These interactions build chains that extend along the *b* axis which are extra-stabilized by inter-molecular C–H– π interactions that involve the alcohol group and one kojic moiety [C3–H3A–Cg2 (2.74 Å, 160°)].¹ Neighboring chains are further connected by inter-molecular O–H(phenol-like)–O(alcohol) H-bonding interactions resulting in a 2D framework. Here the two kojic moieties within L4 are actively implicated [O9–H–O22 (2.854(2) Å, 164.7°) and O17–H–O4 (2.662(2) Å, 148.5°)]. The 3D architecture is accomplished by rather strong inter-molecular π,π -stacking [Cg2–Cg2 3.375 Å, $\alpha = 0^\circ$, $\beta = \gamma = 16.13^\circ$] and H-bonding interactions [(alcohol)O22–H–O3(keto-kojic) (2.801(2) Å, 173.6°)] (Fig. 2).

Interestingly, only one of the kojic moieties is involved in the referred π,π -stacking interactions. This mainly deals with the different torsion angles defined by the kojic moieties in the crystal [kojic#1: <N12–C11–C10–C8 107.42° or kojic#2: <N12–C14–C15–C16 95.61°].

3.2. Potentiometric and ¹H NMR results

The complex formation equilibria of all the five ligands with Al^{III} have been studied by potentiometric techniques (titration curves are provided in as supplementary material). At pH > 7 precipitation occurred, so the Hyperquad analysis was performed only on data before precipitation. The models and the relative complex formation constants are reported in Table 1, together with the protonation constants previously determined [21]. L4, L5 and L6 that are characterized by a

¹ Cg2 = centroid of the ring kojic#2: O(23)–C(15)–C(16)–C(18)–C(19)–C(20).

longer linker than that of the previously studied L1, L2 and L3 ligands [19,21] form only one kind of complex of Al₂L₃ stoichiometry, variously protonated on the nitrogen atoms on the linker. As regard L4 and L5 ligands, the starting Al₂L₃H₃ species is the fully coordinated 2:3 complex with all the three protonated nitrogen atoms. L5, characterized by the piperazine ring in the linker, forms a starting Al₂L₃H₄ complex, in which one piperazine is protonated on both nitrogen atoms, while the other two only on a single one. These protons are lost at increasing pK values, with the same basicity order as in the free ligands L5 < L4 < L6.

L7 complexation scheme resembles that of the parent kojic acid with formation of AlL₂H_x complexes and, subsequently, an AlL₃ complex formed at higher pH than the corresponding complex with kojic acid. AlL₂H₂ is protonated on the nitrogen atom on the linkers. These protons are lost easier than in free ligand (pK = 6.0), their pK values being 5.52 and 5.64.

The last ligand L8 forms Al₂L₂ complexes of higher stability than those found with the analogous L1 ligand; the possibility of formation of Al₂L₃ complexes is counteracted by the too short linker. With respect to L1 complexes, the stronger stability of Al₂L₂ complexes prevents the formation of AlL₂ complexes. Estimation and comparison of these ligands as aluminium chelators can be done on the basis of the pAl values, reported in Table 1.

Table 1

Protonation and complex formation constants of the five ligands with Al^{III} at 25 °C, 0.1 M KCl ionic strength, obtained from potentiometric–spectrophotometric measurements.

Species	L4	L5	L6	L7	L8
LH	9.19 (3)	9.01 (2)	8.52 (4)	8.49 (1)	9.49 (2)
LH ₂	16.70 (3)	16.62 (2)	16.66 (2)	14.51 (2)	16.18 (1)
LH ₃	21.08 (5)	19.97 (2)	22.15 (5)		
LH ₄			24.12 (5)		
Al ₂ L ₂					31.99 (1)
Al ₂ L ₂ H ₋₁					27.10 (3)
Al ₂ L ₂ H ₋₂					21.71 (1)
Al ₂ L ₃ H ₄	59.28 (4)		62.3 (1)		
Al ₂ L ₃ H ₃	55.36 (5)	53.6 (1)	57.9 (3)		
Al ₂ L ₃ H ₂	50.73 (5)	49.86 (8)	52.11 (2)		
Al ₂ L ₃ H	45.00 (5)	45.41 (7)	45.49 (1)		
Al ₂ L ₃	37.4 (2)	37.9 (1)	37.73 (4)		
AlL ₂ H ₂				27.53 (2)	
AlL ₂ H				22.01 (4)	
AlL ₂				16.37 (3)	
AlL ₃				21.39 (4)	
pAl	11.2	11.6	11.8	9.9	14.4

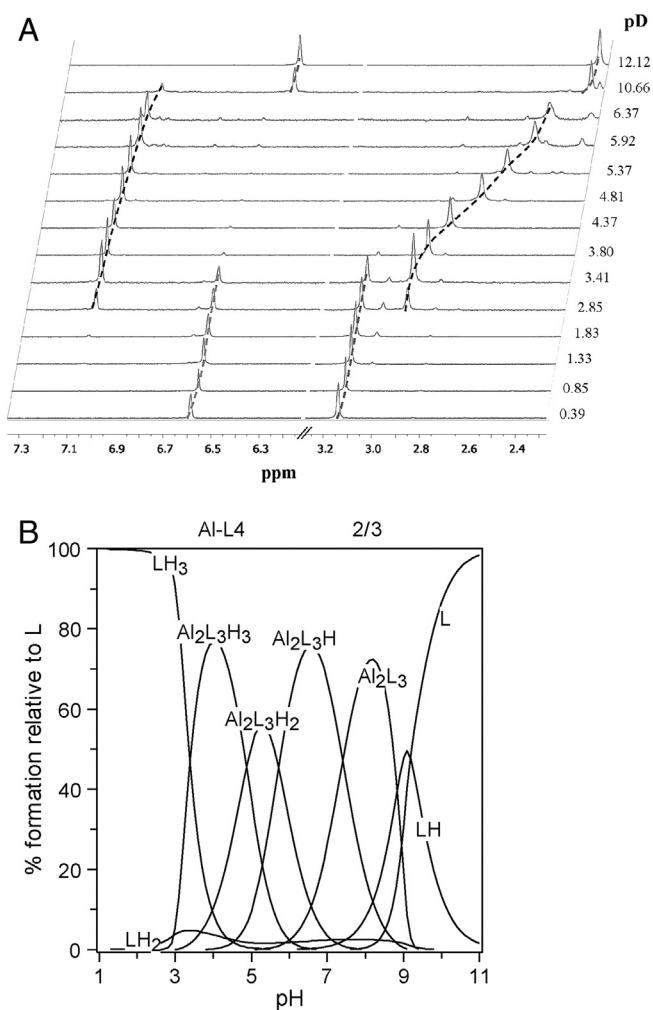


Fig. 4. A) ¹H NMR signals of H3 and of CH₃ of L4 at 2:3 aluminium ligand ratio; B) speciation plot of L4 at the same experimental condition.

hydrated $[L_4Al_2 + H_2O]^{2+}$ complex. The peak corresponding to the free ligand is not present.

The ESI-MS spectrum in Fig. 6 displays the L5 complex formation with Al^{III} ions. The main peaks appear at m/z 416.128, m/z 432.101, m/z 440.086, m/z 449.092 and m/z 458.093. The first peak at m/z 416.128 corresponds to the protonated free ligand. The peak at m/z 432.101 is indicative of the species $[L_5Al_2]^{3+}$, visible also in experiments with higher metal ion excess. The peak at m/z 440.086 corresponds to the species $[L_5Al_2]^{2+}$. The most abundant peak at m/z 449.092 and significantly less intense one at m/z 458.093 correspond to the mono-hydrated $[L_5Al_2 + H_2O]^{2+}$ and bi-hydrated species $[L_5Al_2 + 2H_2O]^{2+}$, respectively.

The representative ESI-MS spectrum of Al^{III} complexes with L6 is presented in Fig. 7. The highest intense peak at m/z 419.099 corresponds to the $[L_6Al_2]^{2+}$ complex, while those with lower intensity, at m/z 428.103 and m/z 437.097, represent the mono-hydrated $[L_6Al_2 + H_2O]^{2+}$ and bi-hydrated $[L_6Al_2 + 2H_2O]^{2+}$ complexes, respectively.

3.4. QM-calculations

During the past decades, quantum-mechanical (QM) calculations have gained an increasing interest due to their ability to help the investigations on the structural, spectroscopic, and electrochemical features of inorganic and organometallic compounds. In recent years, density functional theory (DFT) [40–42] has been widely recognized as a theoretical tool capable of providing very accurate information at an acceptable computational cost.

Recently, some of the authors exploited DFT calculations to investigate the relative stabilities of Al^{III} and Fe^{III} complexes featuring the 2,2'-[(2-hydroxy-3-methoxyphenyl)methanediyl]bis[3-hydroxy-6-(hydroxyl methyl)-4H-pyran-4-one] and 2,2'-[(4-hydroxy-3-methoxyphenyl)methanediyl] bis[3-hydroxy-6-(hydroxyl methyl)-4H-pyran-4-one] ligands [19].

Prompted by these results, DFT calculations have been extended to the ligands L4 and L6, featuring two kojic residues separated by spacers capable of providing them the ability to form binuclear monomeric complexes. With the aim to validate the computational

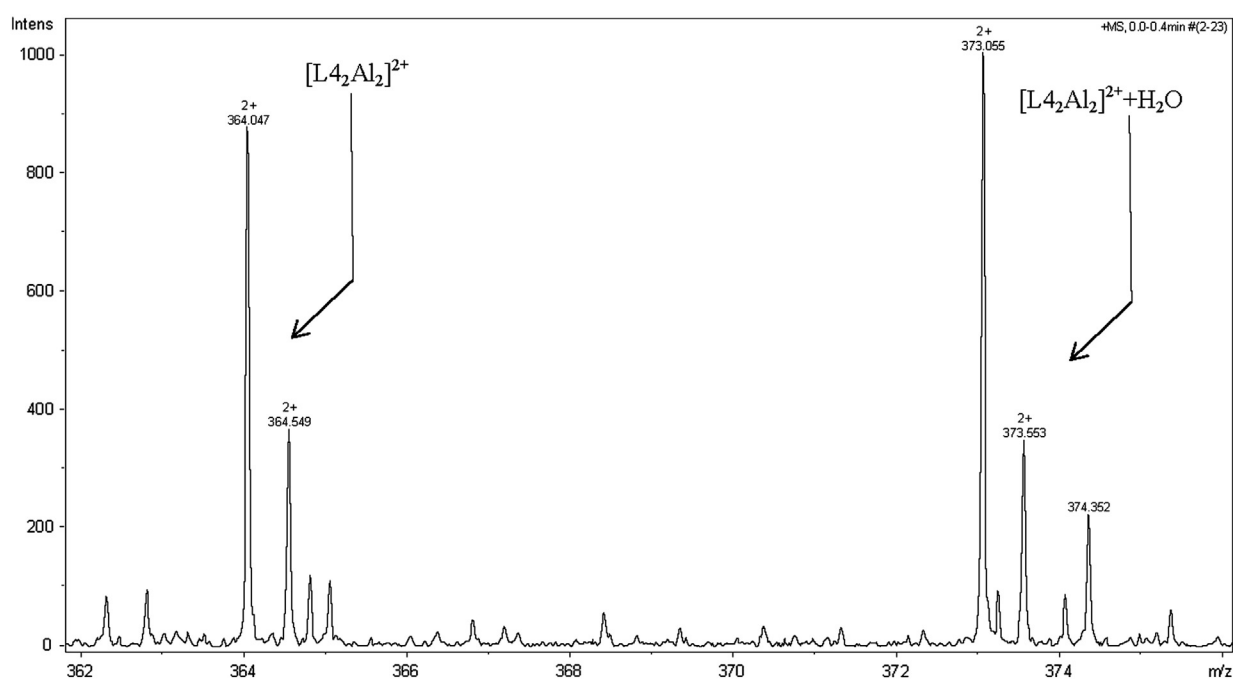


Fig. 5. ESI-MS spectrum of Al^{III}-L4 complexes.

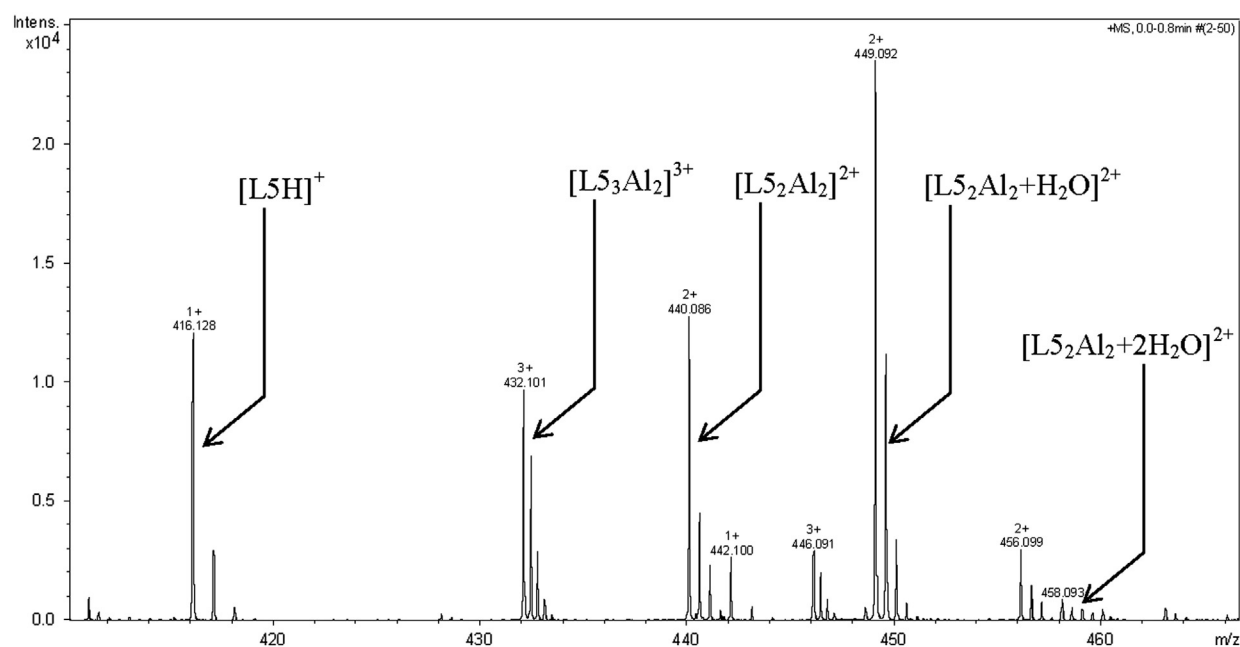


Fig. 6. ESI-MS spectrum of Al^{III}-L5 complexes.

set-up, the metric parameters optimized for the neutral form of L4 have been compared with the corresponding ones determined by X-ray diffraction (see above). In agreement with diffractometric data, the hydroxyl groups of the kojic units are involved in H-bonding interactions with the adjacent carbonyl groups (O–H···O 2.587 Å, 121.7°). The localization of Kohn–Sham (KS) HOMO (Highest-Occupied Molecular Orbital) on the quaternary N atom accounts both for its basicity in solution and for its ability to participate to inter-molecular H-bonding interactions.

In order to verify the donor ability of the ligands in acidic media, both ligands have been studied in their *N*-protonated forms (L4⁺ and L6, respectively), with the deprotonated oxygen donor atoms belonging to the kojic acid moieties. In the case of L4⁺, the geometry optimization

occurred through a proton transfer from the nitrogen atom to one of the two kojic oxygen donor atoms. The resulting optimized structure is stabilized by an O–H···O hydrogen bond linking the two kojic residues. On the contrary, in the case of L6, optimized with the piperazine spacer disposed in a chair configuration, such stabilization did not occur and therefore the optimization of the *N*-protonated species is feasible. The optimized structure of L6 displays metric parameters close to those previously calculated for related systems [19]. In particular, the two C–O distances of each donor groups show significantly different distances (1.217 and 1.262 Å, respectively), reflected in different Wiberg bond indices [36] (average value 1.681 and 1.373, respectively).

Filled molecular orbitals can be found localized on the oxygen atoms of the kojic residues. In particular, the couples HOMO-3/HOMO-2 and

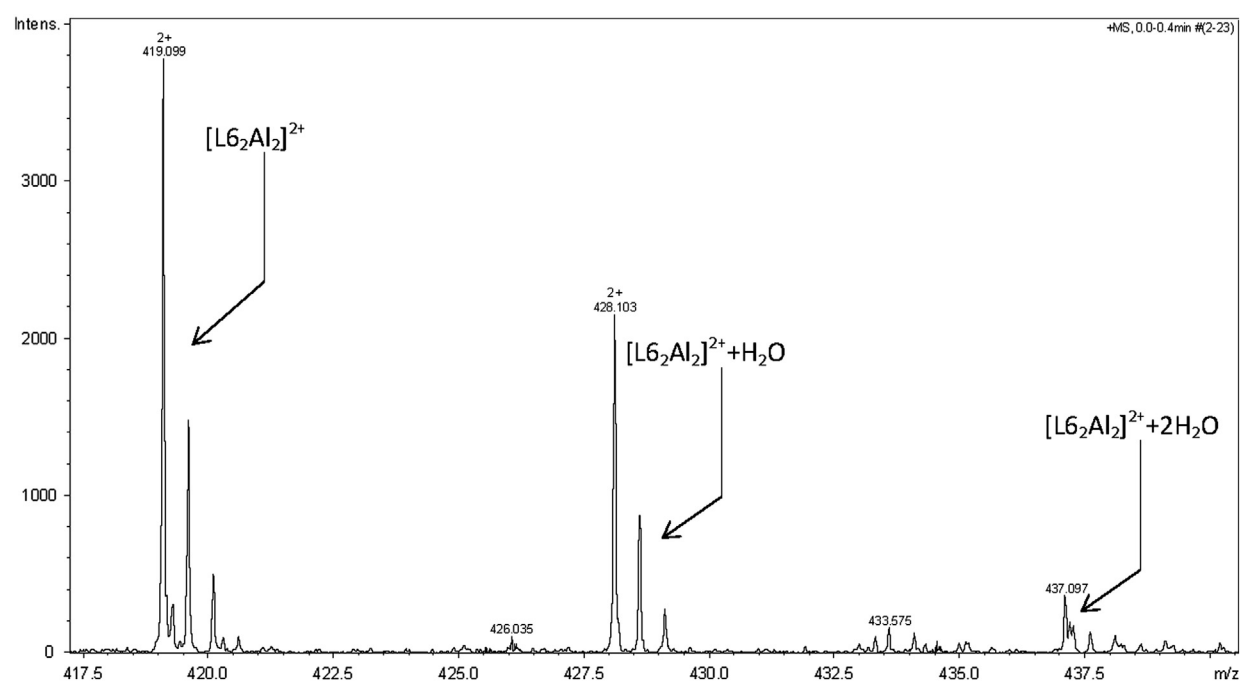


Fig. 7. ESI-MS spectrum of Al^{III}-L6 complexes.

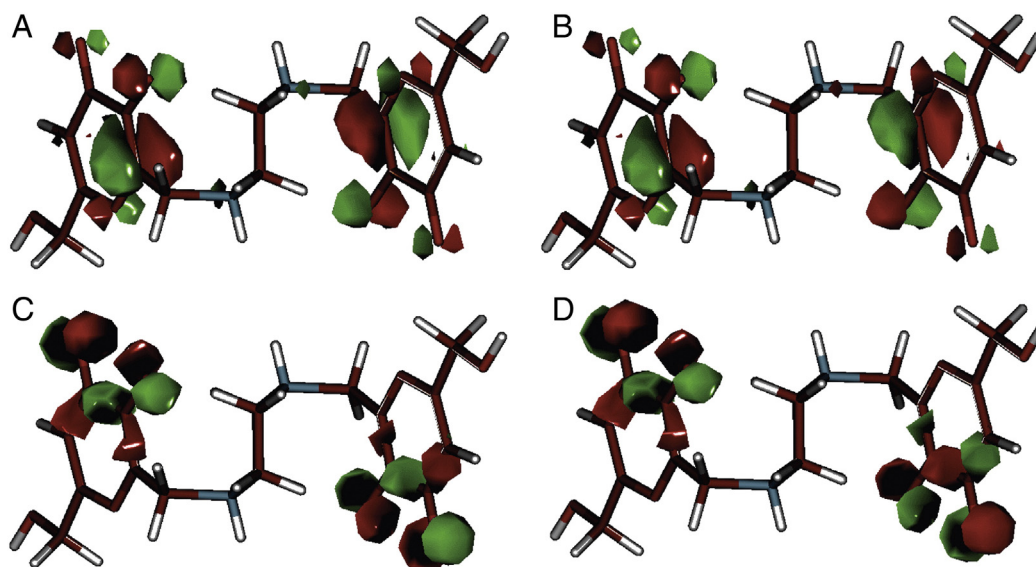


Fig. 8. Drawings of the isosurfaces of Kohn-Sham HOMO (A), HOMO-1 (B), HOMO-2 (C) and HOMO-3 (D) calculated for L6. Contour value 0.05 e.

HOMO-1/HOMO exhibit large contributions from the symmetric and antisymmetric combinations of the $2p$ oxygen atomic orbitals laying on the plane of the $4H$ -pyran-4-one ring and perpendicularly to it, respectively (Fig. 8), which feature remarkable negative natural charges (-0.575 and -0.769 e), being therefore available to coordinate the Al^{III} centers.

Based on potentiometric and 1H -NMR measurements, the complexes featuring 2:3 metal:ligand ratios were also optimized for the two ligands. In the binuclear cation $[Al_2(L4^-)_2]^{3+}$ (corresponding to the $Al_2L_3H_3$ stoichiometry discussed above and identified in solution above pH 3.9) the optimized Al–Al distance was calculated to be 6.084 Å. Each Al^{III} is coordinated in a distorted octahedral fashion by the oxygen atoms from three deprotonated kojic acid units of different ligands (Fig. 9).

In each kojic unit, the two optimized C–O distances and the corresponding Al–O are statistically different, with average C–O

distances of 1.257(1) and 1.291(6) Å and Al–O distances of 1.897(9) and 1.95(1) Å [average 1.92(3) Å]. The complex is stabilized by three hydrogen bonds established between the N–H group of the protonated spacers and the hydroxyl groups of the hydroxymethyl substituents of each $4H$ -pyranone ring.

The structure of $[Al_2(L6)_3]^{6+}$ shows very similar structural features. The different nature of the spacer between the two kojic residues in each ligand unit results in a larger separation between the two Al^{III} centers (8.091 Å) and also in this case the two C–O bonds within each donor unit feature different distances [1.260(4) and 1.31(2) Å; average Al–O distance 1.93(3) Å].

Finally, an examination of the net positive charge on the metal centers calculated at NBO level (1.999 and 2.003 e for $[Al_2(L4^-)_2]^{3+}$ and $[Al_2(L6)_3]^{6+}$, respectively) testifies for the very polarized nature of Al–O bonds in both compounds, which is independent on the global charges of the two complexes.

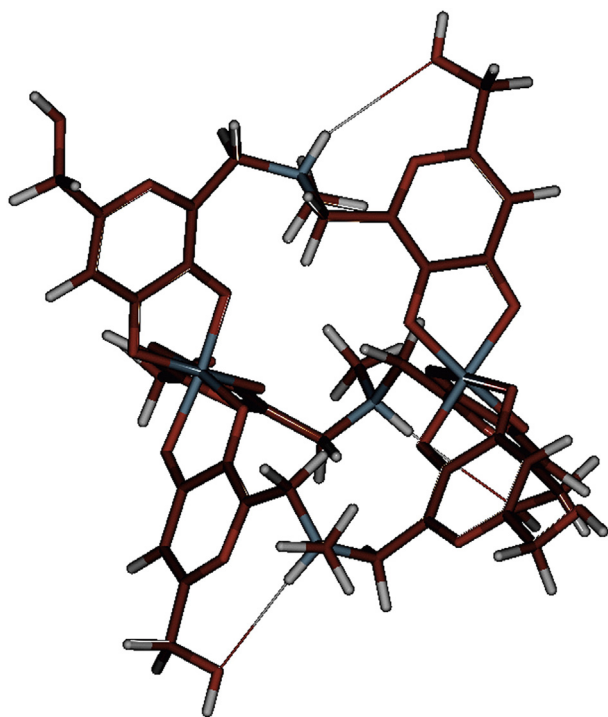


Fig. 9. Drawing of the optimized structure of the complex $[Al_2(L4^-)_2]^{3+}$.

3.5. Biodistribution studies

To evaluate the efficacy of the new ligands L4, L5, L7 and L8, as chelating agents for mobilization of metal ions, we studied their effect on the usual biodistribution profile of the well-established ^{67}Ga -citrate in female mice after intravenous administration of the radiotracer. The tissue distribution of this radiotracer was compared to its distribution with simultaneous intraperitoneal administration of 0.5 μ mol of each ligand solution.

The effect of this series of chelators on the ^{67}Ga uptake and clearance on the major organs and on the excretion, in comparison with that of the ^{67}Ga -citrate, can be overviewed graphically in Fig. 10 as well as in Table 2. The influence of the commercially available iron-chelating drug, deferiprone (DFP), previously evaluated in the same animal model [43], was also included in this graphic presentation.

Analysis of these results shows that the co-administration of the ligands interferes in the usual tissue distribution of the radioactive metal in mice enhancing the overall excretion rate of radioactivity from whole animal body. The four ligands can induce modifications on the ^{67}Ga biodistribution pattern with the same trend, enhancement of its total excretion. No significant differences in the rate of radioactivity elimination were found, except by administration of L7 that induced a slower excretion. The most important differences in the distribution profile are related with the blood clearance. L7 and L8 induce slower clearance from blood than the other two compounds, at 1 h after administration, which may be attributed to a highest level of plasmatic

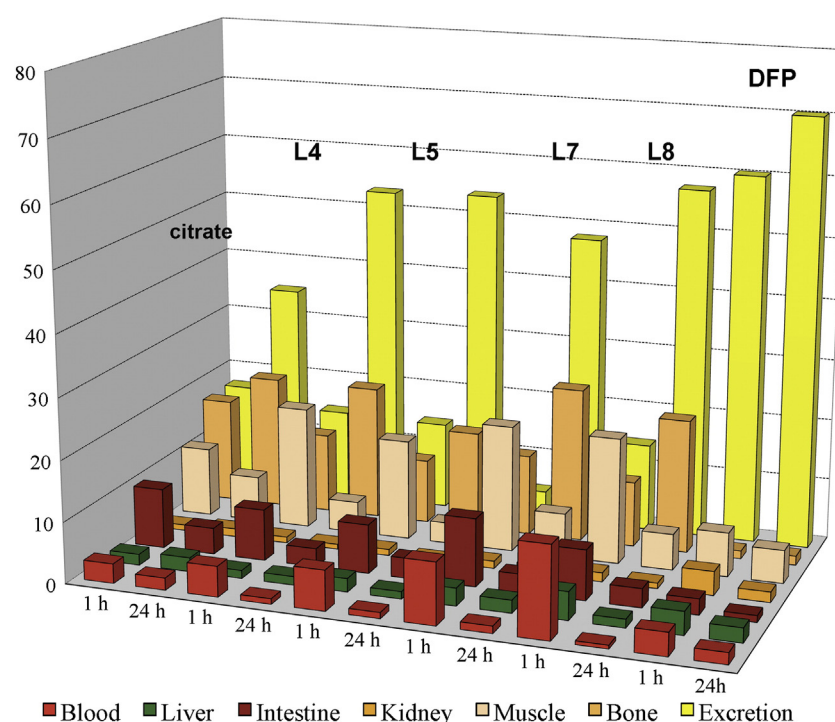


Fig. 10. Biodistribution data in the most relevant organs, expressed as % I.A./organ for ^{67}Ga -citrate (i.v. injection) and ^{67}Ga -citrate with simultaneous intraperitoneal injection of the ligands L4, L5, L7, L8 and DFP [43], at 1 and 24 h after intravenous administration in female mice ($n = 3-5$).

protein binding. Consequently highly irrigated organs like the heart, lungs and kidneys also present the highest radioactivity levels.

This improvement in the elimination rate of the radiotracer makes evident the ability of the ligands to coordinate *in vivo* with gallium, suggesting their potential as decorporating agent of this metal. However, high levels of radioactivity are retained in the muscle and bone tissues which are similar to those of the radiotracer. Comparison of our data with those of DFP indicates that the drug is able to induce the fastest clearance from organs like muscle and bone and total excretion.

Some rationalization of these bioassays can be aided by different parameters, namely the metal chelating ability of the compounds and the pharmacokinetic properties of the ligands and corresponding metal complexes. Since it is known that the Al(III) and Ga(III) chelating ability of analogous hard ligands follows a parallel trend [43,44], on the basis of

the calculated pAI values (Table 1) it can be anticipated that L4 and L5 present an identical gallium chelating capacity ($\text{pAI} = 11.2-11.6$) while L7 and L8 present the lowest ($\text{pAI} = 9.9$) and the highest ($\text{pAI} = 14.4$) values, respectively (DFP presents the highest value ($\text{pAI} = 16.0$) [43], due to its different *N*-heterocyclic nature). Interestingly, an identical trend was found for the total metal excretion at 24 h. Further differences on the biodistribution profile could also be partially rationalized on the basis of the predicted values for some of the pharmacokinetic properties for ligands and complexes, namely lipophilicity, membrane crossing ability, binding with serum proteins. However, the calculated ligand descriptors (see Table 3) [38,39] did not allow a good rationalization match. In particular, although the monochelators L7 and DFP present quite good similarities on some estimated properties (molecular weight, lipophilicity, interaction with human serum albumin (HAS), gastrointestinal (GI) absorption), considerable differences found on membrane

Table 2

Biodistribution data at the most relevant organs, expressed as % I.A./organ for ^{67}Ga -citrate with simultaneous intraperitoneal injection of the ligands L4, L5, L7, L8 at 1 h and 24 h, after intravenous administration in female mice ($n = 3$).

Organs	I.A./organ (%)							
	L4		L5		L7		L8	
	1 h	24 h	1 h	24 h	1 h	24 h	1 h	24 h
Blood	5.0 ± 0.8	0.9 ± 0.5	6.6 ± 2.6	1.0 ± 0.4	$10.1 \pm 2.6^*$	1.2 ± 0.6	$15.0 \pm 4.6^*$	0.6 ± 0.1
Liver	$1.3 \pm 0.4^*$	1.4 ± 0.4	2.2 ± 0.3	1.2 ± 0.2	2.9 ± 0.8	2.1 ± 0.3	$4.6 \pm 0.4^*$	1.4 ± 0.5
Intestine	8.4 ± 0.8	3.0 ± 0.7	8.0 ± 1.5	3.3 ± 0.2	$11.1 \pm 0.7^*$	3.0 ± 0.2	8.2 ± 1.8	3.1 ± 1.3
Spleen	0.07 ± 0.01	0.06 ± 0.03	0.11 ± 0.06	0.05 ± 0.02	0.2 ± 0.06	0.06 ± 0.01	$0.22 \pm 0.09^*$	0.08 ± 0.04
Heart	0.20 ± 0.02	0.08 ± 0.05	0.28 ± 0.05	0.06 ± 0.01	$0.4 \pm 0.1^*$	0.07 ± 0.03	$0.4 \pm 0.2^*$	0.06 ± 0.03
Lung	0.44 ± 0.03	0.14 ± 0.03	0.6 ± 0.2	0.09 ± 0.05	$1.3 \pm 0.5^*$	0.2 ± 0.1	1.0 ± 0.3	0.18 ± 0.08
Kidney	0.97 ± 0.03	0.8 ± 0.1	1.0 ± 0.1	0.5 ± 0.1	1.2 ± 0.2	1.5 ± 0.2	$1.47 \pm 0.04^*$	0.9 ± 0.1
Muscle	20.0 ± 4.6	5.10 ± 0.04	16.4 ± 1.1	3.4 ± 1.1	20.7 ± 1.4	7.2 ± 1.0	20.6 ± 2.4	5.9 ± 0.4
Bone	13.0 ± 0.8	21.9 ± 2.5	$10.5 \pm 1.0^*$	$16.1 \pm 1.6^*$	13.2 ± 0.6	25.2 ± 2.6	10.7 ± 0.2	21.9 ± 1.4
Stomach	0.97 ± 0.05	0.7 ± 0.3	0.8 ± 0.1	0.6 ± 0.1	0.72 ± 0.01	0.4 ± 0.1	0.7 ± 0.1	0.45 ± 0.05
Brain	0.06 ± 0.01	0.02 ± 0.01	0.05 ± 0.01	0.02 ± 0.01	0.13 ± 0.04	0.02 ± 0.00	0.12 ± 0.05	0.02 ± 0.01
Excretion	14.5 ± 1.3	53.3 ± 4.8	14.2 ± 2.4	53.9 ± 2.9	$4.4 \pm 0.1^*$	48.0 ± 4.0	14.3 ± 4.8	57.4 ± 5.6

* $p < 0.05$.

Table 3
Predicted pharmacokinetic properties for the ligands.^a

	MW	clog P ^b	log S ^c (H ₂ O)	Caco-2 permeability (nm/s)	Log K ^d (HSA)	H oral absorption in GI (%) ^e
L4	339	−1.567	−0.714	6	−1.018	38
L5	415	−0.351	−0.947	8	−0.726	49
L6	394	−2.055	−0.072	1	−1.021	34
L7	275	0.685	−1.081	95	−0.475	75
L8	310	−0.887	−2.029	24	−0.838	37
DFP	139	0.655	−1.334	1024	−0.539	79

^a Predicted values using program QikProp v. 2.5 [39].

^b Octanol/water partition coefficient.

^c Aqueous solubility.

^d Binding Human serum albumin.

^e % of Human oral absorption in gastro-intestinal gut.

permeability and chelating capacity may have account for L7 coming out with the lowest metal excretion capability and concomitant highest retention in bone, intestine and muscles, in opposition to DFP. The ligands containing two kojic units (L4, L5 and L8) present a similar in vivo behavior at 1 h (despite the slowest blood clearance induced by L8), while at 24 h, L8 appears as the most efficient metal mobilizing ligand, eventually due to both the higher chelating affinity and more favorable efflux properties of its smaller metal complex.

4. Conclusions

The complex formation equilibria of aluminium^{III} with five new ligands recently synthesized and structurally characterized have been studied by potentiometry and ¹H NMR spectra. Complementary supporting information has been obtained from ESI-MS spectroscopy and quantum-mechanical calculations. The complex formation equilibria of L4, L5 and L6 with Al^{III} are characterized by the formation of a 2:3 Al:L complex variously protonated, as the major species, in the whole pH range. L7 is characterized by the formation of 1:2 and 1:3 Al:L complexes, as the parent ligand kojic acid. Instead, L8 forms a 2:2 Al:L complex which is stabilized at high pH values by the formation of mixed hydroxo complexes. The pAl values of these ligands (Table 1) allow to remark the very good chelating qualities of ligand L8 (14.4), superior to that of the analogous L1 ligand (12.8). The remaining ligands L4–L6, containing nitrogen atoms in the linker, show a minor chelating efficiency, the pAl ranging from 11.1 for L4 to 11.8 for L6, while L7 that contains only one kojic residue is characterized by the lowest pAl (9.9). The high efficiency of this family of ligands with respect to the simple parent kojic acid is strongly determined by the complete involvement of the second kojic unit through the formation of dinuclear aluminium complexes in which each of the two aluminium ions is coordinated by two or three kojic chelating moieties. Studies in mice confirmed the high in vivo metal sequestering power of the bischelators, in comparison with the corresponding monochelator. The excellent chelating properties recommend further toxicological and pharmacological research on these new promising ligands.

Acknowledgments

GC and JIL acknowledge Regione Sardegna for the financial support CRP-27564, project “Integrated approach in the design of chelators for the treatment of metal overload diseases”. MCA is grateful to RAS for the program Master and Back – Percorsi di rientro, PRR-MAB-A2011-19107. MAS acknowledge FCT for financial support, project PEst-OE/QUI/UI0100/2011.

Appendix A. Supplementary data

Supplementary data to this article can be found online at <http://dx.doi.org/10.1016/j.jinorgbio.2013.09.022>.

References

- [1] G. Crisponi, V.M. Nurchi, G. Faa, M. Remelli, *Monatsh. Chem.* 142 (2011) 331–340.
- [2] G. Crisponi, V.M. Nurchi, V. Bertolasi, M. Remelli, G. Faa, *Coord. Chem. Rev.* 256 (2012) 89–104.
- [3] M.D. Arenas Jiménez, T. Malek, M.T. Gil, A. Moledous, C. Núñez, F. Álvarez-Ude, *Nefrologia* 28 (2008) 168–173.
- [4] H. Graf, H.K. Stummvoll, V. Meisinger, J. Kovarik, A. Wolf, W.F. Pinggera, *Kidney Int.* 19 (1981) 587–592.
- [5] A.C. Alfrey, in: M. Nicolini, P.F. Zatta, B. Corain (Eds.), *Aluminium in Chemistry, Biology and Medicine*, Cortina International Verona and Raven Press, New York, 1991, pp. 73–84.
- [6] R.A. Yokel, P. Ackrill, E. Burgess, J.P. Day, J.L. Domingo, T.P. Flaten, J. Savory, J. Toxicol. Environ. Health 48 (1996) 667–683.
- [7] H.G. Nebeker, D.S. Milliner, S.M. Ott, D.J. Sherrard, A.C. Alfrey, J.G. Abuelo, A. Wasserstein, *Kidney Int.* 25 (1984) 173–180.
- [8] C. Ciancioni, J.L. Poignet, C. Naret, S. Delons, Y. Maura, P. Allain, N.K. Man, *Proc. Eur. Dial. Transplant. Assoc. Eur. Ren. Assoc.* 21 (1985) 469–473.
- [9] B.A. Molitoris, P.S. Alfrey, N.L. Miller, J.A. Hasbargen, W.D. Kaehney, B.J. Smith, *Kidney Int.* 31 (1987) 986–991.
- [10] D.J. Brown, J.K. Dawborn, K.N. Ham, J.M. Xipell, *Lancet* 2 (1982) 343–345.
- [11] R.A. Yokel, S.S. Rhineheimer, P. Sharma, D. Elmore, P.J. McNamara, *Toxicol. Sci.* 64 (2001) 77–82.
- [12] H. Nakamura, P.G. Rose, J.L. Blumer, M.D. Reed, *J. Clin. Pharmacol.* 40 (2000) 296–300.
- [13] D.J. Sherrard, J.V. Walker, J.L. Boykin, *Am. J. Kidney Dis.* 12 (1988) 126–130.
- [14] S. Ghitu, R. Oprisiu, L. Benamar, S. Said, A.T. Albu, I. Arsenescu, N. El Esper, P. Morinière, A. Fournier, *Ostéodystrophie rénale* (3); son traitement chez le dialysé, 21 (2000) 413–424.
- [15] T.P. Kruck, J.G. Cui, M.E. Percy, W.J. Lukiw, *Cell. Mol. Neurobiol.* 24 (2004) 443–459.
- [16] G. Crisponi, V.M. Nurchi, *J. Inorg. Biochem.* 105 (2011) 1518–1522.
- [17] M.A. Santos, M.A. Esteves, S. Chaves, *Curr. Med. Chem.* 19 (2012) 2773–2793.
- [18] V.M. Nurchi, G. Crisponi, J.I. Lachowicz, S. Murgia, T. Pivetta, M. Remelli, A. Rescigno, J. Niclós-Gutiérrez, J.M. González-Pérez, A. Domínguez-Martín, A. Castiñeiras, Z. Szewczuk, *J. Inorg. Biochem.* 104 (2010) 560–569.
- [19] V.M. Nurchi, J.I. Lachowicz, G. Crisponi, S. Murgia, M. Arca, A. Pintus, P. Gans, J. Niclós-Gutiérrez, A. Domínguez-Martín, A. Castiñeiras, M. Remelli, Z. Szewczuk, T. Lis, *Dalton Trans.* 40 (2011) 5984–5998.
- [20] V.M. Nurchi, G. Crisponi, M. Crespo-Alonso, J.I. Lachowicz, Z. Szewczuk, G.J.S. Cooper, *Dalton Trans.* 42 (2013) 6161–6170.
- [21] L. Toso, G. Crisponi, V.M. Nurchi, M. Crespo-Alonso, J.I. Lachowicz, M.A. Santos, S.M. Marques, J. Niclós-Gutiérrez, J.M. González-Pérez, A. Domínguez-Martín, D. Choquesillo-Lazarte, Z.Z. Szewczuk, *J. Inorg. Biochem.* 227 (2013) 220–231, <http://dx.doi.org/10.1016/j.jinorgbio.2013.06.009>.
- [22] P. Gans, A. Sabatini, A. Vacca, *Talanta* 43 (1996) 1739–1753.
- [23] APEX2 Software, Bruker AXS Inc. v2010.3-0, 2010. (Madison, Wisconsin, USA).
- [24] G.M. Sheldrick, SADABS, Program for Empirical Absorption Correction of Area Detector Data, University of Gottingen, Germany, 2009.
- [25] G.M. Sheldrick, *Acta Crystallogr. A* 64 (2007) 112–122.
- [26] A.L. Spek, Utrecht University, Utrecht, The Netherlands, 2010.
- [27] C.F. Macrae, I.J. Bruno, J.A. Chisholm, P.R. Edgington, P. McCabe, E. Pidcock, L. Rodriguez-Monge, R. Taylor, J. Van De Streek, P.A. Wood, *J. Appl. Crystallogr.* 41 (2008) 466–470.
- [28] M.J. Frisch, G.W. Trucks, H.B. Schlegel, G.E. Scuseria, M.A. Robb, J.R. Cheeseman, G. Scalmani, V. Barone, B. Mennucci, G.A. Petersson, H. Nakatsuji, M. Caricato, X. Li, H.P. Hratchian, A.F. Izmaylov, J. Bloino, G. Zheng, J.L. Sonnenberg, M. Hada, M. Ehara, K. Toyota, R. Fukuda, J. Hasegawa, M. Ishida, T. Nakajima, Y. Honda, O. Kitao, H. Nakai, T. Vreven, J. Montgomery, J. A., J.E. Peralta, F. Ogliaro, M. Bearpark, J.J. Heyd, E. Brothers, K.N. Kudin, V.N. Staroverov, R. Kobayashi, J. Normand, K. Raghavachari, A. Rendell, J.C. Burant, S.S. Iyengar, J. Tomasi, M. Cossi, N. Rega, J.M. Millam, M. Klene, J.E. Knox, J.B. Cross, V. Bakken, C. Adamo, J. Jaramillo, R. Gomperts, R.E. Stratmann, O. Yazyev, A.J. Austin, R. Cammi, C. Pomelli, J.W. Ochterski, R.L. Martin, K. Morokuma, V.G. Zakrzewski, G.A. Voth, P. Salvador, J.J. Dannenberg, S. Dapprich, A.D. Daniels, Ö. Farkas, J.B. Foresman, J.V. Ortiz, J. Cioslowski, D.J. Fox, *Gaussian 09*, Revision A.1, 2009.
- [29] C. Adamo, V. Barone, *J. Chem. Phys.* 108 (1998) 664–675.
- [30] A. Schäfer, H. Horn, R. Ahlrichs, *J. Chem. Phys.* 97 (1992) 2571–2577.
- [31] D. Feller, *J. Comput. Chem.* 17 (1996) 1571–1586.
- [32] K.L. Schuchardt, B.T. Didier, T. Elsethagen, L. Sun, V. Gurumoorithi, J. Chase, J. Li, T.L. Windus, *J. Chem. Inf. Model.* 47 (2007) 1045–1052.
- [33] E.D. Glending, C.R. Landis, F. Weinhold, *NBO Version 3.1*, 1996.
- [34] A.E. Reed, F. Weinhold, *J. Chem. Phys.* 83 (1985) 1736–1740.
- [35] A.E. Reed, R.B. Weinstock, F. Weinhold, *J. Chem. Phys.* 83 (1985) 735–746.
- [36] K.B. Wiberg, *Tetrahedron* 24 (1968) 1083–1096.
- [37] G. Schaftenaar, J.H. Noordik, *J. Comput. Aided Mol. Des.* 14 (2000) 123–134.
- [38] Maestro, Version 7.5, Schrödinger Inc., Portland, OR, 2005.
- [39] QikProp, Version 2.5, LCC, New York, NY, 2005.
- [40] W. Koch, M.C. Holthausen, *Front Matter and Index*, Wiley-VCH Verlag GmbH, 2001, 1–13.
- [41] C.J. Cramer, D.G. Truhlar, *PCCP* 11 (2009) 10757–10816.
- [42] E.R. Davidson, *Chem. Rev.* 100 (2000) 351–352.
- [43] S. Chaves, A. Capelo, L. Areias, S.M. Marques, L. Gano, M.A. Esteves, M.A. Santos, *Dalton Trans.* 42 (2013) 6033–6045.
- [44] R. Grazina, L. Gano, J. Šebestík, M. Amelia Santos, *J. Inorg. Biochem.* 103 (2009) 262–273.

Paper VII

A Bis-3-hydroxy-4-pyrone as a Potential Therapeutic Iron Chelating Agent. Effect of Connecting and Side Chains on the Complex Structures and Metal Ion Selectivity

G. Crisponi, V.M. Nurchi, M. Arca, M. Crespo-Alonso, J.I. Lachowicz, D. Mansoori, L. Toso, G. Pichiri, M.A. Santos, S.M. Marques, J. Niclós-Gutierrez, J.M. González-Pérez, A. Domínguez-Martín, D. Choquesillo-Lazarte, Z. Szewczuk, M.A. Zoroddu, M. Peana, *Inorg. Chem.* (2014), *Submitted*.

A new bis-3-hydroxy-4-pyrone as a potential therapeutic iron chelating agent. Effect of connecting and side chains on the complex structures and metal ion selectivity.

Guido Crisponi,^[a] Massimiliano Arca,^[a] Miriam Crespo-Alonso,^[a] Joanna I. Lachowicz,^[a] Delara Mansoori,^[a] Leonardo Toso,^[a] Giuseppina Pichiri,^[a] M. Amelia Santos,^[b] Sergio M. Marques,^[b] Juan Nicolás-Gutiérrez,^[c] Josefa M. González-Pérez,^[c] Alicia Domínguez-Martín,^[c] Duane Choquesillo-Lazarte,^[d] Zbigniew Szewczuk,^[e] M. Antonietta Zoroddu,^[f] Massimiliano Peana,^[f] and Valeria M. Nurchi*^[a]

Abstract: This work reports the synthesis, characterization and study of complex formation equilibria of the new ligand 6,6'-(2-(diethylamino)ethylazanediy)bis(methylene)bis(5-hydroxy-2-hydroxymethyl-4H-pyran-4-one) with Fe^{III}, Al^{III}, Cu^{II} and Zn^{II}. On the basis of previous encouraging results with tetradentate bis-kojic acid chelators, this ligand was designed to improve the

pharmacokinetic properties: increase the solubility, neutral at physiological pH 7.4, and enhancement of membrane crossing ability. Fe^{III} and Al^{III} complexation gave evidence of high metal-sequestering capacity of L9. Cellular assays showed that the ligand is capable of crossing cellular membranes and it does not present toxic effects. Complex formation equilibria with the essential metal ions Cu^{II} and Zn^{II} have been furthermore studied to evaluate disturbances of this chelator on the homeostatic equilibria of these essential metal ions.

The variety of used techniques (potentiometry, UV-vis spectrophotometry, 1D and 2D NMR spectroscopy, ESI-MS, quantum mechanical calculations and X-ray diffraction) allowed to obtain the structural characterization of the ligand, and of its iron and zinc complexes, along with an exhaustive picture of the protonation and complex formation solution equilibria.

Keywords: Kojic acid • Fe^{III} and Al^{III} • Cu^{II} and Zn^{II} • Solution equilibria

[a] Prof. G. Crisponi, Dr. M. Arca, Dr. M. Crespo-Alonso, Dr. J. I. Lachowicz, D. Mansoori, L. Toso, Dr. G. Pichiri, Prof. V. M. Nurchi
Department of Chemical and Geological sciences, University of Cagliari
Cittadella Universitaria, 09042 Monserrato-Cagliari (Italy)
Fax: (+39) 070 675 4478
E-mail: nurchi@unica.it

[b] Prof. M. A. Santos, Dr. S. M. Marques
Centro Química Estrutural, Instituto Superior Técnico
Universidade Técnica de Lisboa
Av. Rovisco Pais, 1049-001 Lisboa, (Portugal)

[c] Prof. J. Nicolás-Gutiérrez, Prof. J. M. González-Pérez, Dr. A. Domínguez-Martín.
Department of Inorganic Chemistry, Faculty of Pharmacy, University of Granada
Campus Cartuja, E-18071, Granada (Spain)

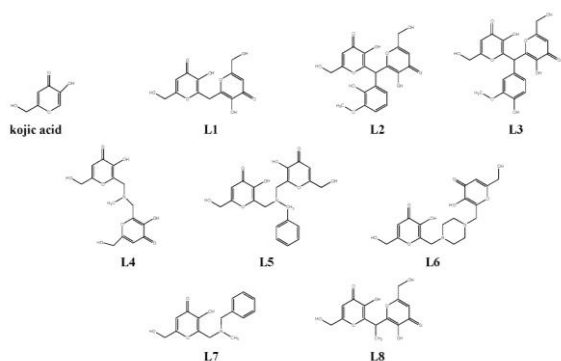
[d] Dr. D. Choquesillo-Lazarte
Laboratorio de Estudios Cristalográficos, IACT
CSIC-Universidad de Granada
Av. de las Palmeras 4, E-18100 Armilla, Granada (Spain)

[e] Prof. Z. Szewczuk
Faculty of Chemistry, University of Wrocław
Joliot-Curie 14, 50-383 Wrocław (Poland)

[f] Prof. A. Zoroddu, Dr. M. Peana
Chimica e Farmacia, Università di Sassari
Dipartimento di Chimica e Farmacia
Università di Sassari
Via Vienna 2, 07100 Sassari (Italy)

Introduction

In the frame of our research on chelating agents for iron and aluminium,^[1] a set of kojic acid (KA) derivatives were synthesized and the complex formation equilibria with these two trivalent metal ions were fully characterized.^[2] The principal features of these ligands (Scheme 1) are i) the presence of two coordinating groups associated with two kojic units, heterocycles containing a pair of *O*-donor atoms due to a carbonyl and a vicinal hydroxyl group, which allow the ligands acting as tetradentate chelators (except KA and L7); ii) the formation of binuclear Fe₂L₂ and Fe₂L₃ complexes of high stability; iii) the remarkable increase of iron binding affinity compared with the parent KA.

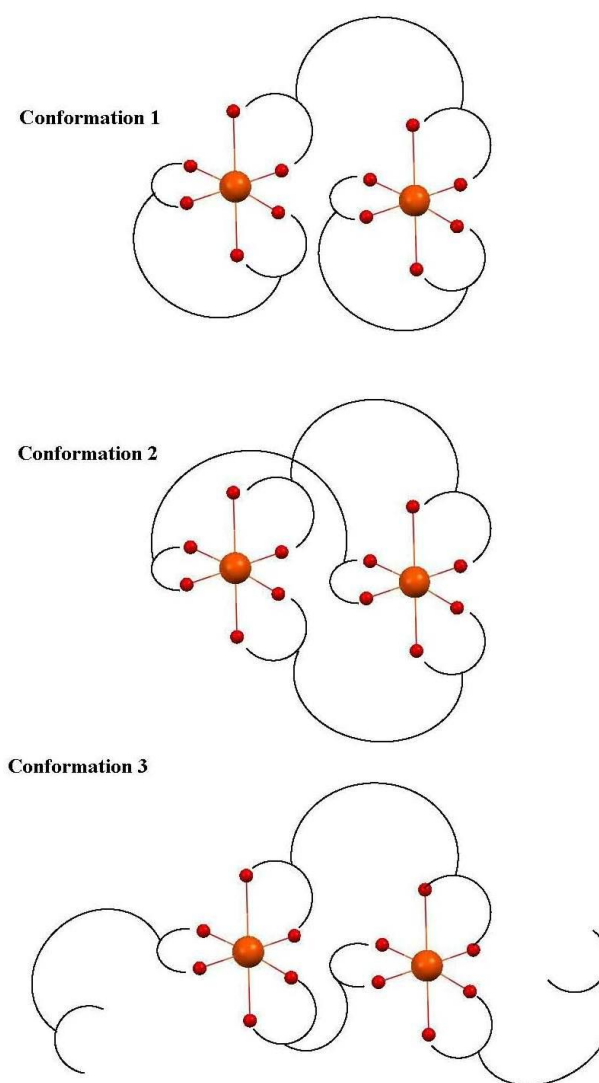


Scheme 1. Chemical structures of ligands KA, L1-L8.

Literature search on iron chelating agents shows a preponderant interest, on one side, towards bidentate and tridentate chelators, apparently due to the better adequacy of their characteristics to the requirements of an oral drug (permeability, molecular mass, etc); on the other side, towards the not orally active hexadentate chelators, which form the most stable complexes. Archetypes of these ligands are those in clinical use for the treatment of iron overload in thalassemic patients, bidentate Deferiprone, tridentate Deferasirox, and hexadentate Desferal. Minor attention has been devoted towards tetradentate chelators, presumably because denticity two and three allow the formation of octahedral mononuclear complexes FeL_3 and FeL_2 . However, by mimicking the natural rhodotorulic acid, a bis-hydroxamate siderophore,^[3] a number of tetradentate ligands have been proposed to date as potential Fe^{III} chelators, namely bis-hydroxamates,^[3] bisphosphonates,^[4] bis(3-hydroxy-4-pyridinone),^[5] and a bis-(kojic acid) derivatives, similar to L1 and L8 (Scheme 1), recently proposed by Zhu et al.^[6] The molecular weight of these ligands is generally below the limit of 500 g/mol suggested by Lipinski's rule of five and pFe values are in the range 18–21. In order to completely fulfill the hexacoordination of ferric ion, the denticity of these ligands requires formation of polynuclear species, invariably found in these systems. In particular, the most common polynuclear complex is the dimer Fe_2L_3 , with a charge depending on the ligand structure. The tetradentate chelators we proposed display the following features:

1. The length of the linker and the molecular conformation do not allow that the ligand acts as a tetradentate ligand toward a single Fe^{III} ion; nevertheless, in all cases the tetradentate nature of the ligand favors the formation of dinuclear complexes Fe_2L_2 or Fe_2L_3 . In particular the complex of stoichiometry FeL_2 found with L1 and L8, of exceptionally higher stability than that of the corresponding FeL_2 complexes with KA and L7, should be better hypothesized as Fe_2L_4 . This complex should be structurally thought as a central Fe_2L_2 , further coordinated by one ligand on each iron through one KA moiety, satisfying its octahedral coordination.
2. The formation of Fe_2L_2 or Fe_2L_3 complexes seems dictated by the length of the linker. Linker constituted by a free or substituted methylene group (L1, L2, L3 and L8) allows two ligands bridging the two iron atoms, while a longer chain permits the formation of a helicate, in which three ligands completely satisfy Fe^{III} octahedral coordination. Similar Fe_2L_3 complexes are formed by the natural siderophores rhodotorulic acid and synthetic analogues.^[3]

3. The possible conformations related to the length of the linker are shown in Scheme 2: conformation 1, accessible when the length of the linker allows the tetradentate chelation on the same iron ion by the same ligand (bis(3-hydroxy-4-pyridinone)-IDA derivative);^[5] conformation 2, which is obtained with linkers too short with respect to the above requirements, but long enough to allow the formation of a helicate in which the three ligands completely satisfy the hexacoordination of the two iron atoms (L4, L5, and L6); conformation 3, in which a too short linker does not allow the formation of the above helicate (L1, L8).

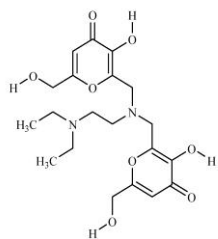


Scheme 2. Conformation of iron complexes with tetradentate chelators.

4. These tetradentate chelators join the advantages of being small enough to allow membrane permeability ($\text{MW} < 500 \text{ g/mol}$) and requiring, for complete iron hexacoordination, an amount 1.5 times that of chelatable iron, i.e. between the value 1 for hexadentate chelators and 2 and 3 for tridentate and bidentate chelators, respectively.

We have synthesized a new ligand, 6,6'-(2-(diethylamino)ethylazanediyl)bis(methylene)bis(5-hydroxy-2-

hydroxymethyl-4H-pyran-4-one), termed L9^a (Scheme 3), similar to L4 and L5, and bearing a diethylaminoethyl group on the nitrogen atom in the linker, instead of methyl or benzyl groups, with the aim of improving the solubility and having a neutral molecule at pH 7.4. In the present work the characterization of this new ligand and of its Fe^{III} and Al^{III} complexes is presented. The study of the complex formation equilibria with the essential metal ions Cu^{II} and Zn^{II}, whose homeostatic equilibria could be perturbed by iron and aluminium chelation, is furthermore reported.



Scheme 3. Chemical structure of ligand L9

With the aim of estimating the possible perturbations of the homeostasis of essential metal ions induced by an iron chelator, the total amounts of these metal ions in the body, and that of the ligand, should be evaluated, and some assumptions made: a beta thalassemic patient of 60 Kg, who receives 45 blood units annually, has a transfusion iron intake of about 9 g iron/year, corresponding to 0.4 mg Fe/Kg body weight/day; a further gut absorption 0.07 mg Fe/Kg body weight/day can be assumed, for a total of 0.47 mg Fe/Kg body weight/day that corresponds to 8.4 μ mol Fe/Kg body weight/day. To reach a steady situation between assumed iron (transfusion + ingestion) and excreted iron, the necessary amount of chelating agent should be provided (at least 8.4 μ mol chelator/Kg body weight/day in the case of Desferal that forms a 1:1 complex, twice in the case of Desferasirox that forms a 1:2 complex and three times in the case of Deferiprone that forms a 1:3 complex). A survey of clinical doses shows that a large excess (4-10 times) is used. On the other hand, zinc and copper concentrations are evaluated as 1.5×10^{-5} M.^[7] In fact, the total zinc concentration circulating in plasma has been assumed according the ‘‘Report of the Task Group on Reference Man’’,^[8] and in the case of copper, according to Linder et al..^[9] These estimates are the necessary bases to evaluate how a given iron chelator can affect copper and zinc homeostasis once the complex formation stability constants are known for all the involved metal ions.

Results and Discussion

Synthesis and crystal structure of the ligand L9: The synthesis of ligand L9 follows a methodology similar to that recently reported,^[26] involving a multicomponent condensation of a non-enolizable aldehyde, a primary amine and a cyclic enol, to afford an aminoalkylated product (Mannich type reaction). The iminium intermediate of the reaction between the amine and aldehyde carbonyl is the acceptor of the reaction with the enol carbon. In particular, L9 was prepared by 2-alkylation of two kojic acid (KA)

^aL9 is a diprotic acid. In the formulae we will represent L9 as LH₂, and L²⁻ for its completely deprotonated form.

units with a double imine backbone, due to reaction of two formaldehyde equivalents with the primary amine (*N,N*-diethylethylenediamine), resulting the formation of the *N*-functionalized dimeric KA derivative. Since the bearing tertiary amine of the primary amine reactant molecule could act as base catalyst of the reaction there was no need of extra base addition.

The crystallization of L9 from water solutions yielded colourless crystals of stoichiometry L9•2H₂O belonging to the *P2₁/c* space group. In the lattice L9 exists as a zwitterion crystallized in dihydrate form (Figure 1).

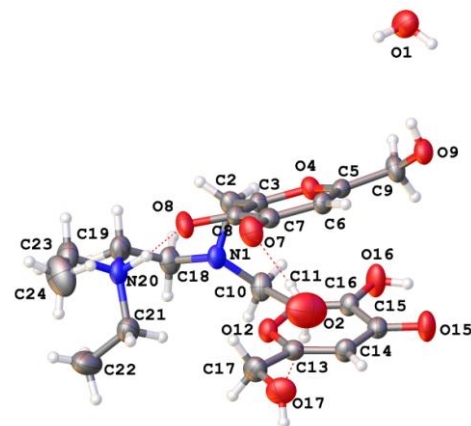


Figure 1. Asymmetric unit in the crystal of L9•2H₂O ligand. Intramolecular H-bonding interaction in the zwitterion L9 and the stabilizing role of the O2-water molecule are plotted in dashed lines. Ellipsoids are drawn at 50 % probability level.

The H-onium atom comes from the O8(phenolate) group and was located in the difference Fourier map on the N20 tail/terminal atom of the ethylenediamine arm. The N⁺-H group further cooperates in the intermolecular interaction, N20–H2O...O8(phenolate) (2.675(3) Å, 167.3°). Hence the ‘onium H2O-atom’ falls inside of a distorted tetrahedral surrounding (NC₂O). All C=C and C–O bond distances in kojic rings of L9 are equivalent and have usual values (Table S1.2). Shortest C–C bond distances than typical C(sp²)–C(sp²) distance and longest C=O bond lengths than typical C(sp²)=O in 4-H-pyran-4-one rings bring out the aromaticity of a typical benzene ring system although enables π -electronic delocalisation that ensures its planarity. L9 zwitterion adopts a folded conformation with the two kojic moieties piled one upon another as a consequence of a weak π , π -stacking interaction between them (that is featured by a short ring-ring centroid-centroid distance = 3.50 Å but with an open interplanar dihedral angle of 20.44°). This conformation is further stabilized by two water mediated hydrogen bonding interactions, connecting the O2-H bonds to the O7(phenolate) and O17(hydroxyl) acceptor atoms. To enable such water mediated interactions and minimize steric hindrances related to the hydroxylmethyl moieties, the kojic rings are rotated nearly 180° to each other.

In the crystal lattice of L9, pairs of adjacent zwitterions are symmetrically connected by intermolecular H-bonds which involve hydroxylmethyl and keto kojic groups (Table S1.3, Figure2-left). Likewise adjacent of zwitterionic pairs are associated by additional intermolecular H-bonding interactions where water molecules (O1) and keto-kojic groups, as well as the phenol and hydroxylmethyl

groups, are involved, building a 3D H-bonded network (Figure 2-right).

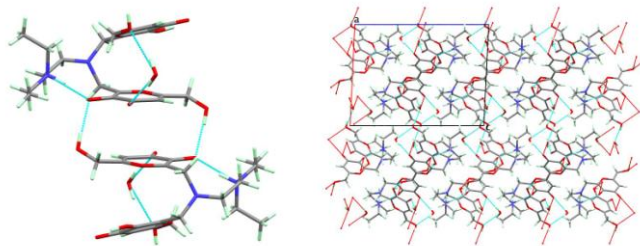


Figure 2. Pair of molecules of L9 connected through symmetrical H-bonding interactions (left), 3D network of L9 in the *ac* plane (right).

Protonation equilibria: The protonation equilibria of the ligand have been studied by potentiometry, UV-vis spectrophotometry and $^1\text{H-NMR}$ spectroscopy. The protonation constants were evaluated by potentiometric titration at 25 °C and 0.1 M KCl ionic strength, and by $^1\text{H-NMR}$ spectroscopy for the very acidic $\log \beta_4$. These values are reported in Table 1, and the corresponding distribution curves are shown in Figure 3.

Table 1. Protonation constants evaluated from the potentiometric titration at 25 °C and 0.1 M KCl ionic strength.

Species	$\log \beta$	$\log K$
LH^-	10.81(1)	10.81
LH_2	19.04(2)	8.23
LH_3^+	25.99(2)	6.95
LH_4^{2+}	26.50(4)*	0.51 ²

² This value has been evaluated from $^1\text{H-NMR}$ spectra at variable pH.

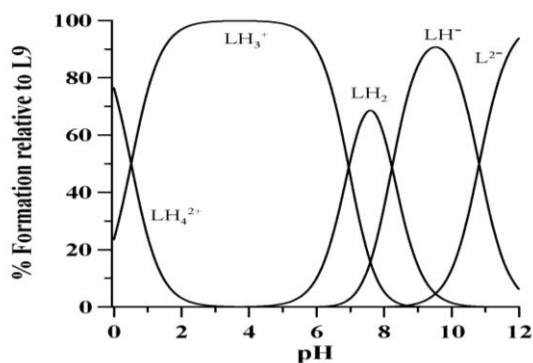


Figure 3. Speciation plot of ligand L9 calculated with the protonation constants in Table 1.

Ligand L9 is characterized by four protonation constants, corresponding to the two kojic phenolates and the two nitrogen atoms in the linker. A protonation sequence of the ligand, based on the spectrophotometric and $^1\text{H-NMR}$ results, can be proposed.

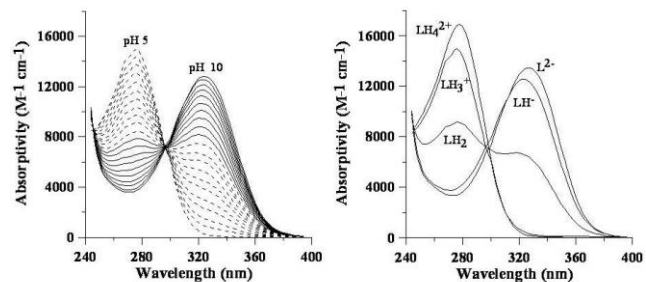


Figure 4. Selected absorptivity spectra collected during the spectrophotometric titration of L9 in the pH range 5.0 - 10.0 relative to the second and third protonation steps ($C_{\text{L9}} = 3.0 \times 10^{-4}$ M, 0.2 cm optical path length) (left). Absorptivity spectra of the four differently protonated forms of L9 calculated on the whole set of spectra (pH 0.5-12)^[12, 31] (right).

The results of the potentiometric-spectrophotometric titration presented in Figure 4 left allow some considerations:

The spectra of L9 look similar to those of KA, with a near double intensity due to the presence in L9 of two KA units. In KA, the L^- and LH species are characterized by UV bands at 315 nm ($\epsilon = 5900 \text{ M}^{-1}\text{cm}^{-1}$) and 270 nm ($\epsilon = 8700 \text{ M}^{-1}\text{cm}^{-1}$), respectively, with sharp isosbestic points at 242 nm and 290 nm.^[2a]

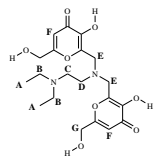
The first deprotonation ($pK = 0.51$), which causes a negligible effect on the band at 270 nm, allows to undoubtedly attribute this deprotonation to one of the two nitrogen atoms. Actually, the band presented at pH 5.0, corresponding to the LH_3^+ species, is quite similar to that of the protonated species LH of KA, and does not change during the first deprotonation (the maximum is shifted with respect to KA from 270 to 274 nm, $\epsilon = 15000 \text{ M}^{-1}\text{cm}^{-1}$).

From pH 5.0 to 10.0, the second and the third deprotonations take place, along with a substantial decrease of the band intensity at 270 nm, and a concomitant increase of that at 320 nm, allowing to attribute these deprotonations to the phenol groups in the KA units. In particular, the intensity of the band at 277 nm decreases in about one half of its height during the second deprotonation (dashed line spectra), with the simultaneous increase of the new band at 322 nm, with sharp isosbestic points at 246 nm and 298 nm. During the third deprotonation (continuous line spectra) a further decrease in the intensity of the band at 276 nm and an increase in the intensity of that at 322 nm take place. The band at 322 nm also shows a slight red shift and its ϵ value is about twice that of the corresponding band of fully deprotonated KA.^[2a]

No evident spectral variations take place at $\text{pH} > 10$ during the fourth deprotonation (Figure 4 right), which can be therefore ascribed to the loss of a proton from the second nitrogen atom. The above attributions are supported by the absorptivity spectra calculated for the four species using the HypSpec program on the spectra collected from pH 0 to pH 12.^[31]

The trends of the $^1\text{H-NMR}$ chemical shifts of the different protons versus pH, analyzed with the program HypNMR,^[32] have allowed both to refine the value of $\log \beta_4$ (related to a $\log K_4 = 0.51$, not reliably determinable from potentiometric measurements) and to obtain the intrinsic chemical shifts of the various protons in the differently protonated species, reported in Table 2.

Table 2. a) Intrinsic chemical shifts of the different protons in L9 ligand in the differently protonated species, calculated with HypNMR. b) Variations of the intrinsic chemical shifts connected to each deprotonation step.



a) Intrinsic chemical shift (\square , ppm)							
Species	A	B	C	D	E	F	G
L^{2-}	0.84	2.40	2.60	2.52	3.77	6.29	4.37
LH ⁻	1.20	3.12	3.20	2.96	3.74	6.17	4.26
LH ₂	1.22	3.15	3.28	2.99	3.79	6.27	4.31
LH ₃ ⁺	1.26	3.26	3.35	3.09	3.86	6.36	4.35
LH ₄ ²⁺	1.13	3.15	3.50	3.47	4.28	6.34	4.29

b) Variation of intrinsic chemical shift (\square , ppm)							
Deprotonation	A	B	C	D	E	F	G
LH ⁻ →L ²⁻	0.36	0.72	0.60	0.44	-0.03	-0.12	-0.11
LH ₂ →LH ⁻	0.02	0.03	0.08	0.03	0.05	0.10	0.05
LH ₃ ⁺ →LH ₂	0.04	0.11	0.07	0.10	0.07	0.09	0.04
LH ₄ ²⁺ →LH ₃ ⁺	-0.13	-0.11	0.15	0.38	0.42	-0.02	-0.06

We also report the variations of the intrinsic chemical shifts during each deprotonation step (Table 2b). These last values allow the unambiguous assignment of the first and the fourth deprotonation steps to the nitrogen atom on the linker and to the nitrogen atom in the lateral chain respectively. In fact, in the first deprotonation (LH₄²⁺→LH₃⁺) the most affected protons are E and D while in the fourth the most affected protons are B and C, and, in a less extent, A and D.

Cellular assay: Two different cellular lines (PK1 and HepG2) have been used both to evaluate the toxicity of L9 and its ability to enter the cellular membranes. After adding L9 to cells growing 24 h in a complete medium, the amount of ligand entered into the cells was evaluated at different times. During the first two hours, 3.6 ± 0.7 μmol of ligand were absorbed by PK1 cells, and 0.8 ± 0.2 by HepG2 cells. After 6 h from the beginning, PK1 cells absorbed 4 ± 2 μmol of L9, and HepG2 cells 1.9 ± 0.1 μmol . The final determination at 24 h showed an absorption of 7.4 ± 0.6 μmol by PK1 cells, and 5.6 ± 0.8 μmol by HepG2 cells. The experimental error evaluated on triplicate measurements on different cell cultures comes from the different number of cells in each culture. The used concentration of ligand was not toxic at all for both cellular lines, actually, no apoptotic cells were observed in the cells growing vertically.

Iron complexes

Crystal structure of Fe₂L₃ complex with the ligand L4: In the absence of crystal structure of the iron complex with L9, we have

decided to present the structure of corresponding complex with L4 as its surrogate, which will also allow to infer useful insights on the coordination geometry of this kind of tetradentate chelators. In fact L4 differs from L9 just for a methyl group instead of the diethylaminoethyl moiety as the nitrogen substituents of the linker. The chelating properties of L4 toward iron were previously presented,^[2c] together with a set of analogous ligands.

Fe₂L₃ crystallizes (monoclinic, C2/c) as an hydrated complex salt according to a formula [Fe₂(μ_2 -HL)₃]Cl₃·nH₂O. In the crystal structure solution only four water molecules have been localized meanwhile the remaining highly disordered solvent molecules have been removed during the structure refinement. The dinuclear cation complex (Figure 5) contains slightly distorted octahedral Fe^{III} centres, which are bridged by three zwitterionic μ_2 -HL⁻ ligands. Each ligand supplies O-keto and O-phenolate donors from a kojic moiety to a Fe^{III} atom building a planar five-membered chelate ring. We can assume that the univalent anionic form of L4 tautomerizes, with transference of the ‘acid’ proton from one O(phenol) kojic group to the central N(tertiary) atom, in order to use both anionic kojic moieties as bidentate chelating groups for two Fe^{III} centres. In this manner, the anticipated octahedral coordination of each Fe^{III} atom (with 3d⁵ electronic configuration) is fully accomplished by three halves of the L4 ligand (as monoanionic groups) in a neutral surrounding. This coordination provides Fe^{III} centres with a noticeable resistance against potential hydrolytic processes and polymerization reactions. The three positively charged N-ammonium moieties of the HL4 ligands per dinuclear complex are compensated by the three chloride counter anions to provide the electro neutrality of the salt.

The tris(kojic) moieties associated to each metal centre are further connected by H-bonding interactions involving O10 and O11 water molecules and the hydroxy group from two symmetrical L4 ligands (O4 and O24 acceptor atoms). Furthermore, the tris-chelate moieties exhibit *fac* configuration with dihedral angles between planar kojic rings ranging from 64.35° to 89.86° and with the hydroxymethyl groups pointing towards the carbon atom of the kojic rings in position 3. These features are in good agreement with other tris-chelate complexes containing KA as bidentate ligand reported previously.^[2a]

The helical nature of the tris-chelate moiety confers chiral properties and therefore Δ/Λ isomerism is expected. In the dinuclear structure, a mirror plane bisects the complex cation, passing through the N12, N32 and N52 atoms and therefore, both isomers Δ and Λ are present. The propeller structure is further stabilized by H-bonding interactions between the ‘oniom’ N⁺-H groups (N32 and N52) and the ‘linker’ O10 and O11 water molecules. One of the most striking features of this structure is that the three chlorine anions and two water molecules are located endohedrally in the cavity build inside the complex by the three ligands and two Fe^{III} centres.

Table 3. Complex formation constants of L9 with the four examined metal ions

Fe		Al		Zn		Cu	
Species	log β	Species	log β	Species	log β	Species	log β
[Fe ₂ L ₃ H ₄] ⁶⁺	60.3(1)	[Al ₂ L ₃ H ₃] ³⁺	76.02(2)	[ZnLH] ⁺	18.17(2)	[CuLH ₂] ²⁺	25.38(2)
[Fe ₂ L ₃ H ₃] ⁵⁺	78.1(2)	[Al ₂ L ₃ H ₄] ⁴⁺	70.5(8)	ZnL	10.75(3)	[Cu ₂ L ₂ H ₂] ²⁺	46.42(2)
[Fe ₂ L ₃ H ₂] ⁴⁺	72.4(2)	[Al ₂ L ₃ H ₃] ³⁺	65.0(1)			[Cu ₂ L ₂ H] ⁺	39.23(5)
Fe ₂ L ₃	55.3(1)					Cu ₂ L ₂	31.11(3)
						[Cu ₂ L ₂ H ₁] ⁻	20.84(4)
						[Cu ₂ L ₂ H ₂] ²⁻	10.29(3)
pFe	17.7	pAl	10.3	pZn	7.6	pCu	9.7

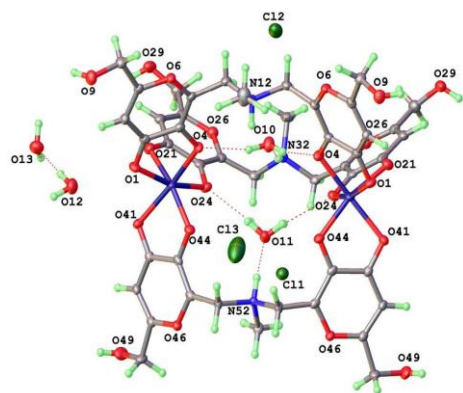


Figure 5. Asymmetric unit in the crystal of $[\text{Fe}_2(\mu_2\text{-HL})_3]\text{Cl}_3 \cdot n\text{H}_2\text{O}$ complex of iron with L4 ligand. The stabilization of the complex conformation by H-bonding interactions is plotted. Ellipsoids are drawn at 50 % probability level.

π, π -stacking interactions build ribbons that extend parallel to the b axis, involving symmetry related kojic rings (those containing O46 atoms). These ribbons are reinforced by $-\text{OH} \cdots \text{Cl}$ interactions (Figure 6 left). Additional H-bonding interactions between water molecules and the remaining of O-acceptor finished the 3D array that exhibits an overall solvent accessible volume/cell of 1708 \AA^3 (namely 26%) where the disordered water molecules are located (Figure 6 right).

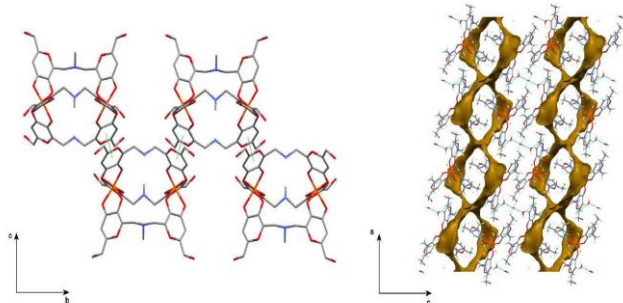


Figure 6. Detail of a ribbon generated by π, π -stacking interactions between symmetry related kojic moieties (left) in the crystal structure of $[\text{Fe}_2(\mu_2\text{-HL})_3]\text{Cl}_3 \cdot n\text{H}_2\text{O}$. 3D network in the *ac* plane showing voids (right).

Formation equilibria of iron complexes: The complex formation equilibria of ligand L9 with Fe^{III} have been studied by combined potentiometric-spectrophotometric techniques. The estimation of reliable complex formation constants from potentiometric data alone was not possible, since the Fe^{III} was almost completely complexed when mixing reagents before the base potentiometric titrations. Therefore the complex formation equilibria have been studied both in strong acidic medium (pH 0–2) and in the pH range 2–10, using different sets of solutions with known amount of acid and base. The Evolving Factor Analysis^[12] of spectra collected from pH 0 to pH 2.5 for the 1:1, 1:2 and 1:3 iron/ligand molar ratios allowed the observation of a minor species with a maximum at pH ~ 2 and a second species whose intensity increases up to pH 4. The amount of the minor species in the three different solutions is proportional to iron concentration; furthermore the absorptivity spectrum of this species strictly resembles that of the 1:2 complex of Fe^{III} with KA.^[2a] The absorptivity of the spectra of the second species agrees with that expected for a Fe_2L_3 complex; in this case the spectra resemble those of FeL_3 complex with KA, confirming that iron

atoms are fully hexacoordinated. Analysis of the whole set spectra in the acidic range with HypSpec^[31] has allowed the calculation of the complex formation constants for $[\text{Fe}_2\text{L}_2\text{H}_4]^{6+}$ and $[\text{Fe}_2\text{L}_3\text{H}_3]^{3+}$ reported in Table 3.

The analysis of potentiometric titrations with Hyperquad,^[12] setting constant the previously determined stability constants, allowed to obtain the complex formation constants of the variously protonated $[\text{Fe}_2\text{L}_3\text{H}_n]^{n+}$ complexes (Table 3). In the $[\text{Fe}_2\text{L}_2\text{H}_4]^{6+}$ species the two iron atoms are each one coordinated by two KA units of two different ligands, both protonated on the nitrogen atoms, i.e. each iron atom has a coordination environment similar to that of iron in the 1:2 complex FeL_2 with KA.^[2a] In the $[\text{Fe}_2\text{L}_3\text{H}_3]^{3+}$ complex a third L9 ligand saturates iron hexa-coordination, similar to that found for the structure of Fe_2L_3 isolated with the ligand L4 (see Supporting Information), all the ligands being protonated at the more basic terminal nitrogen atoms. These three protons are progressively lost with pK 5.7 (the first), and pK 8.5 (the remaining two). These values, respectively 5.1 and 2.4 pK units lower than that determined for pure ligand, are accounted for by the different charges of the molecules (-1 in the free ligand and +3 and +2 in the complexes respectively).

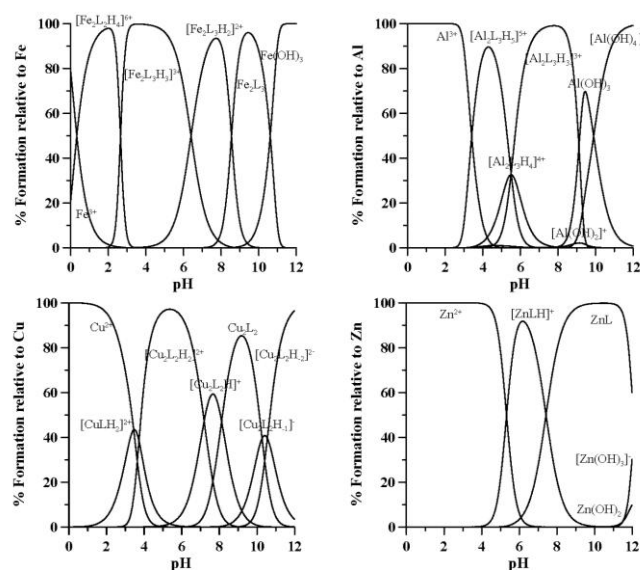


Figure 7. Speciation plots of complexes formed by L9 with the four examined metal ions (Me = Fe, Al, Cu, Zn), calculated at $[\text{L}] = 2 \times 10^{-3} \text{ M}$ and $[\text{Me}] = 1 \times 10^{-3} \text{ M}$ using the complex formation constants reported in Table 3.

The peaks of the complexes with iron in ESI-MS spectra, Figure 8, confirm the previous findings. The intensity of the free ligand peak is one order of magnitude higher than that of the complex peaks. The signal at m/z 478.103 derives from the dinuclear complex with stoichiometry $[\text{Fe}_2\text{L}_2]^{2+}$, the signal at m/z 506.071 is in excellent agreement with the simulated signal of $[\text{Fe}_3\text{L}_2]^{2+}$ complex, and the peak at m/z 690.195 is the product of reaction between three ligands and two iron ions $[\text{Fe}_2\text{L}_3\text{H}_2]^{2+}$. ESI-MS spectra further confirm the $[\text{Fe}_2\text{L}_3\text{H}_2]^{2+}$ species calculated in the potentiometric studies. The peak at m/z 613.18 is possibly originated by the two ligands, two iron ions and one kojic-amine linker molecule; such a complex could be the product of decomposition of $[\text{Fe}_2\text{L}_3]^{2+}$ complex in ESI-MS, and it suggests strong affinity of KA to the iron ions in the complex. It is noteworthy that dimeric complexes with water

molecules are not present, in opposition to what happened with other KA derivatives.^[2b]

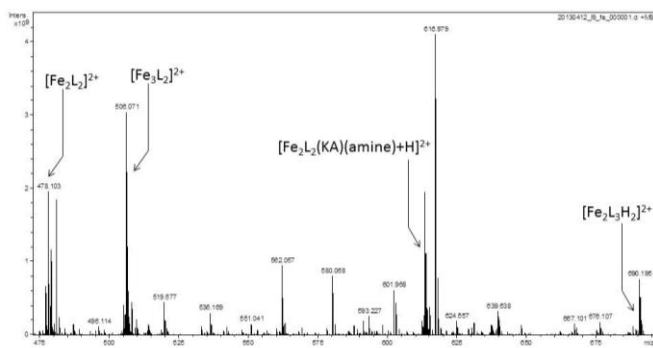


Figure 8. ESI-MS spectra of the system L9-Fe^{III}.

Aluminium complexes

Formation equilibria of aluminium complexes: The lower stability of aluminium with respect to the iron complexes allowed to evaluate the complexation model and the relative constants in Table 3 from the potentiometric data alone. The species $[Al_2L_3H_5]^{5+}$, observed at low pH values similarly to the $[Fe_2L_3H_n]^{n+}$ iron complexes, has the three most basic nitrogen atoms protonated, as well as two of the least basic nitrogen atoms on the linker. These later two protons are lost, the first one to give $[Al_2L_3H_4]^{4+}$ and the second one to give $[Al_2L_3H_3]^{3+}$, with the same pK 5.5, while the same protons are lost in the free ligand at the very acid pK 0.51. The strong increase of basicity of the nitrogen atom in the linker could be explained referring to a complex structure similar to that reported in Figure 5 for the Fe^{III}-L4 complex: the involvement of two $-NH^+$ groups in the linker in hydrogen bonding with two water molecules well accounts for the permanence of these protons up to pH 5.5. The ¹H-NMR spectra collected at the two 2:1 and 3:2 ligand/aluminium molar ratios and at variable pH confirm the potentiometric results and allow to detail them. The spectra recorded at pH ≈ 2 for both 2:1 and 3:2 L9-Al systems do not show differences as compared to those of the free ligand, in agreement with the potentiometric data; in fact, the first species starts to form at pH above 2.5. At pH 4 the spectra show remarkable differences between that of the free ligand and that of $[Al_2L_3H_5]^{5+}$ species. A similar behavior in terms of changes in the chemical shifts is found at pH 5.9, where the main species is $[Al_2L_3H_4]^{4+}$. Whereas at 2:1 L9-Al ratio a remarkable amount of the free ligand is still visible in the spectra, no signals attributable to the free ligand are observed at 3:2 ratio, in agreement with the proposed species (Figure 9).

The degeneracy of the two methyl proton signals (triplet) A is still present and the signals moved to higher fields ($\Delta\delta = -0.49$ ppm). Methylene group B (quartet) loses its degeneracy and splits into two sets of broadened peaks, B' ($\Delta\delta = -0.46$) and B'' ($\Delta\delta = -0.82$), both shielded. The C protons (triplet), compared to D (triplet) ($\Delta\delta = 0.02$), are strongly shifted to higher fields ($\Delta\delta = -0.95$), and both broadened. Two doublets (E' and E'') originating from the non equivalent methylene protons E, appeared after Al^{III} binding. Their geminal protons H1 ($\Delta\delta = -0.26$) and H2 ($\Delta\delta = 0.44$) are now distinguishable and shifted in the opposite directions compared to the overlapping signals (Figure 9 and Figure 10). The geminal protons H1 and H2 become magnetically non-equivalent upon coordination, whereas the two methylene groups from (Ar-)CH₂ (E' and E'') are in the same chemical and magnetic environment. This behavior suggests the

presence of a rigid but symmetric structure of these complexes. The singlet signals of G ($\Delta\delta = 0.27$) and F ($\Delta\delta = 0.60$) protons resulted deshielded and thus shifted down field upon Al^{III} interaction. Carbon chemical shift changes are the following: A ($\Delta\delta = -0.32$), B ($\Delta\delta = 0.43$), C ($\Delta\delta = 0.55$), D ($\Delta\delta = -2.26$), E ($\Delta\delta = 3.24$), F ($\Delta\delta = -3.20$), G ($\Delta\delta = 0.59$).

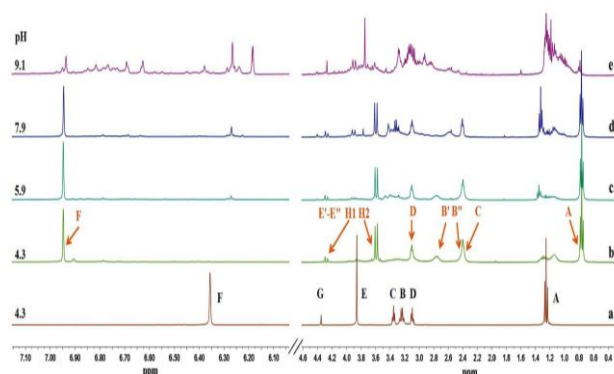


Figure 9. Aromatic and aliphatic region of ¹H 1D spectra for the free L9 ligand at pH 4.3 (a), and for L9-Al^{III} system, 3:2 molar ratio, at pH 4.3 (b), at pH 5.9 (c), 7.9 (d) and 9.1 (e), respectively. Assignments for the free ligand are shown by capital letters (a). The new resonances after Al^{III} interaction with L9 ligand are indicated by arrows and capital letters (b).

The chemical shift table with the complete set of resonances for the free and Al^{III} bound status of L9 ligand, including carbon nuclei, is available as Supporting Information (Table S4).

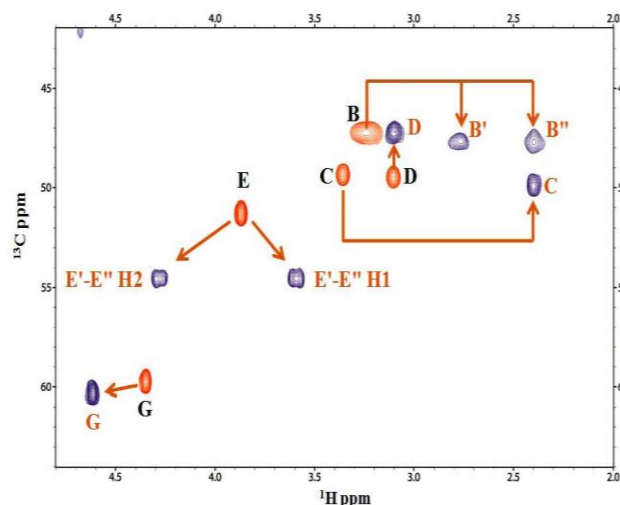


Figure 10. Selected aliphatic region of 2D ¹H-¹³C spectrum for the free L9 ligand (orange), and L-Al^{III} system, 3:2 molar ratio (blue), at pH 4.3. The spectrum is similar to that obtained at pH 5.9. The new resonances of L9 upon Al^{III} interaction are indicated by orange arrows and capital letters.

By raising the pH from 7.9 on, the spectra show a considerable increase in the complexity of the system deriving from several species, which can be in a dynamic equilibrium in the NMR time scale. In addition, at very high pH (above 8), precipitation phenomena, probably due to the formation of hydroxyl species and to hydrolysis reactions (yellowing of the solution), prevent any clear interpretation of the spectra. The ESI-MS spectrum of ligand-aluminium solutions shows different peaks (Figure 11), which can

complex has disordered water molecules (0.6 molecules per complex unit) filling voids of the lattice (Figure 15-right).

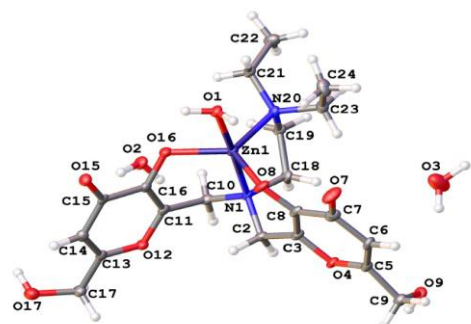


Figure 14. Asymmetric unit in the crystal of ZnL9 complex of stoichiometry $[\text{ZnL}(\text{H}_2\text{O})] \cdot 2.6\text{H}_2\text{O}$. Ellipsoids are drawn at 50 % probability level.

In the crystal complex molecules build ribbons by weak π, π -stacking interactions between symmetry related anti-parallel kojic moieties (Figure 15-left). These ribbons are further stabilised by H-bonds between the O17(hydroxymethyl) and the O15(keto) groups. Moreover, additional H-bonding interactions involving aqua ligands, hydroxymethyl groups as well as water molecules connect ribbons giving rise to a 3D architecture (Figure 15-right).

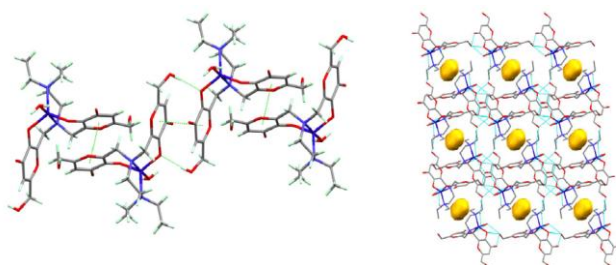


Figure 15. Detail of a ribbon generated by π, π -stacking interactions between kojic moieties (left). 3D network in the bc plane showing voids (right).

Formation equilibria of zinc complexes: The analysis of potentiometric data for the zinc complex formation gives evidence of a $[\text{ZnLH}]^+$ complex that is transformed in ZnL with a pK value of 7.42. Taking into account the structural results, it can be hypothesized that in the first complex $[\text{ZnLH}]^+$, the zinc ion is coordinated by the phenolate on one of the kojic moieties and by both nitrogen atoms, being the second phenolic group still protonated. This phenol group loses its proton with a pK 7.42, about 0.8 pK units lower than the pK 8.23 in the free ligand, accounting for the different charges of the molecules from which the proton is lost (0 in the free ligand and +1 in the complex). The potentiometric results did not give evidence of the dinuclear complexes Zn_2L_2 pointed out by ESI-MS. According to ESI-MS results, L9 ligand forms with zinc ions mono- and dinuclear complexes. The high intensity peaks at m/z 487.105, 520.059 and 603.236 are in agreement with $[\text{ZnL}]^+$, $[\text{Zn}_3\text{L}_2]^{2+}$ and $[\text{ZnLH}(\text{amine})]^+$ complexes, respectively. As mentioned above, evidence of $[\text{ZnLH}]^+$ complex was given by potentiometry. The peak at m/z 603.236 corresponds to a complex of one zinc ion, one ligand, and the amine of the linker. Such complex is surely an ESI-MS breakdown product of $[\text{Zn}_2\text{L}_2\text{H}]^+$ complex, not revealed by potentiometry neither by ^1H NMR. Such a complex remarks the strong coordination between the amine group on linker and zinc. Two other signals at 720.071 and 821.173 m/z

can be attributed to further breakdown products, $[\text{Zn}_2\text{L}(\text{KA})]^+$ and $[\text{Zn}_2\text{L}(\text{KA})(\text{amine})]^+$ complexes with strong affinity both of KA and amine linker to the metal ion. The free ligand peak (not reported in Figure 16) is ten times more intense than signals of the complexes.

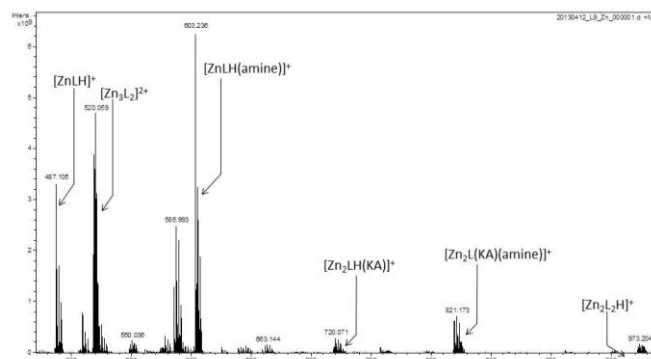


Figure 16. ESI-MS spectra of the system L9-Zn^{II}.

NMR spectra of 1:1 ligand-zinc solutions were recorded at different pH values (Figure 17). The spectrum recorded at pH 2.5 (Figure 17 a) shows that Zn^{II} ions do not interact with the ligand, in agreement with potentiometric data, which show that the first species $[\text{ZnLH}]^+$ appears at pH around 4 and it is visible until pH 10, reaching its maximum concentration at pH around 6 (Figure 7).

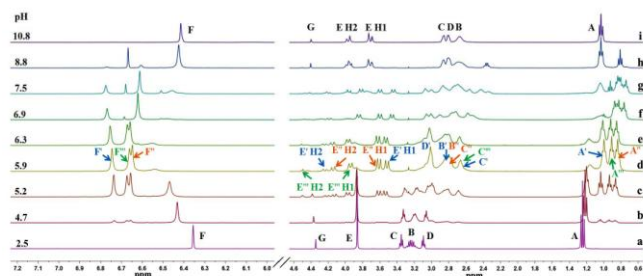


Figure 17. Aromatic and aliphatic region of ^1H 1D spectra of L-Zn^{II} system, 1:1 molar ratio, at different pHs. Assignment of L9 free ligand is showed by capital letters (a). The new resonances of L9 ligand upon Zn^{II} interaction is showed by orange, blue and green labels related to the three species (d).

NMR measurements are consistent with this model. In fact, the spectrum at pH 4.7, where ZnLH species should be present at low concentration (less than 10%), reveals the beginning of Zn^{II}-ligand interaction, with some new low intensity signals appearing in the spectrum (Figure 17 b). By raising the pH the intensity of these signals increases, reaching a maximum at pH around 6.3 (Figure 17 c, d, e), in agreement with speciation curves (Figure 7). The 1D and 2D HSQC spectra (Figure 18) confirm the remarkable differences between free ligand and Zn^{II} complexes.

Protons belonging to A, B, C, D groups show minor chemical shifts, which can result from a shielded environment. In particular, the two methyl proton signals (triplet) A, overlapped in the free ligand, shift to higher fields, giving the three triplets A', A'' and A'''. Chemical shifts differences at pH 5.9 ($\Delta\delta = \delta_{\text{bound}} - \delta_{\text{free}}$ (ppm) for proton and carbon nuclei) are A' ($\text{H}\Delta\delta = -0.26$, $\text{C}\Delta\delta = -0.19$), A'' ($\text{H}\Delta\delta = -0.41$, $\text{C}\Delta\delta = 0.16$) and A''' ($\text{H}\Delta\delta = -0.35$, $\text{C}\Delta\delta = -0.09$). The new resonances of methylene groups B (quartet), shifted to higher fields, remain in overlap, B'=B'' ($\text{H}\Delta\delta = -0.42$, $\text{C}\Delta\delta = 0.47$). C

protons (triplet) exhibit three signals, C' ($H\Delta\delta = -0.70$, $C\Delta\delta = 1.28$), C'' ($H\Delta\delta = -0.58$, $C\Delta\delta = -0.43$) and C''' ($H\Delta\delta = -0.70$, $C\Delta\delta = -1.64$). D protons (triplet) move slightly, whereas the corresponding carbon experiences a large chemical shift variation ($H\Delta\delta = -0.09$, $C\Delta\delta = -1.75$). The new set of signals from B, C and D groups become broadened; the relative broadness of the signals in the ligand-metal system suggests the presence of exchange processes.

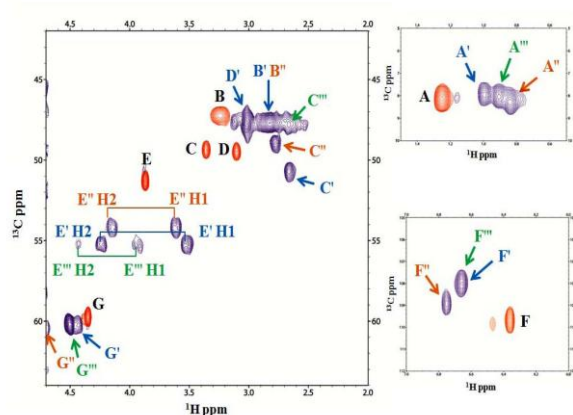


Figure 18. 2D 1H - ^{13}C spectra for the free L9 ligand (orange), superimposed to L9-Zn^{II} system, 1:1 molar ratio (blue), at pH 5.9. The new resonances of L9 after Zn^{II} interaction are also indicated.

The two nonequivalent methylene protons E (their pairs of geminal protons H1 and H2 are overlapped in the free ligand), after Zn^{II} binding, appear separated in three set of doublets of doublets with a distinguishable NMR resonance, E' ($H2\Delta\delta = 0.36$, $H1\Delta\delta = -0.35$, $C\Delta\delta = 3.88$), E'' ($H2\Delta\delta = 0.28$, $H1\Delta\delta = -0.25$, $C\Delta\delta = 2.89$) and E''' ($H2\Delta\delta = 0.57$, $H1\Delta\delta = 0.07$, $C\Delta\delta = 3.94$). Zn^{II} addition results in a deshielded environment of G and F groups. Their signals are downfield shifted, appearing as a new set of three signals characterized by the chemical shift changes G' ($H\Delta\delta = 0.09$, $C\Delta\delta = 0.48$), G'' ($H\Delta\delta = 0.34$, $C\Delta\delta = 0.70$), G''' ($H\Delta\delta = 0.15$, $C\Delta\delta = 0.45$); F' ($H\Delta\delta = 0.30$, $C\Delta\delta = -1.69$), F'' ($H\Delta\delta = 0.39$, $C\Delta\delta = -0.75$), and F''' ($H\Delta\delta = 0.30$, $C\Delta\delta = -1.69$).

In conclusion, 1D and 2D NMR spectra recorded in the pH range 5.15 - 6.30, where ZnLH is the predominant species, show for this system three main signals of comparable intensity, instead of the single one of the free ligand. Since the only species evidenced by potentiometric measurements is ZnLH, the presence of at least three species detectable in the NMR timescale has to be attributed to coordination isomers of ZnLH species in a dynamic equilibrium. AROESY experiment^[b] performed with a mixing time of 200 ms, at 298 K, confirmed the three isomers in a dynamic exchange (Table S4).

Variable temperature NMR spectra of L-Zn^{II} system, at 1:1 molar ratio and pH 6.3, were obtained in the range 296-332 K and are shown in Figure 19. The coalescence of three sets of isomer peaks is clearly observed.

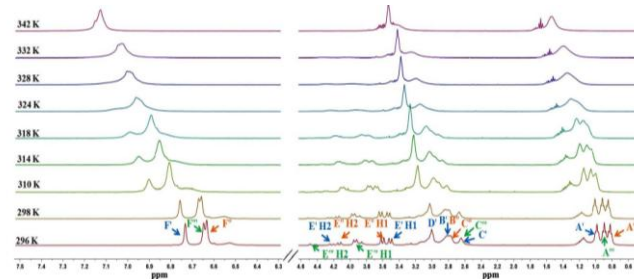


Figure 19. Selected VT-NMR spectra of L-Zn^{II} system, 1:1 molar ratio, at pH 6.3.

According to speciation curves (Figure 7), two species exist at pH 7.5 ([ZnLH]⁺ 60% and ZnL 40%), the spectra of L-Zn system present a more complex situation, probably complicated by the presence of different species in equilibrium among them (Figure 17 g). At higher pH (above 8.8) precipitation phenomena occur probably from the formation of zinc hydroxy species (Figure 17 h, i). The spectra therefore resemble those of the free ligand, even if some shifts of the NMR signals are noticed. In particular, the loss of degeneracy for the two geminal methylene protons H1 and H2 for E, together with some shifts for B, G and F groups, have to be remarked. This fact is indicative of an equilibrium of metal ion between hydroxyl and L9 species.

Theoretical Calculations: DFT calculations have been exploited successfully on a plethora of chemical systems, ranking from simple organic compounds to complex species involving transition or main group metals.^[25] In recent works, some of the authors reported on the application of QM calculations at DFT level on iron and aluminium complexes of ligands containing the Kojic units. In particular, the relative stabilities of Al^{III} and Fe^{III} complexes featuring the 2,2'-[(2-hydroxy-3-methoxyphenyl)methanediyl]bis[3-hydroxy-6-(hydroxymethyl)-4H-pyran-4-one] and 2,2'-[(4-hydroxy-3-methoxyphenyl)methanediyl] bis[3-hydroxy-6-(hydroxymethyl)-4H-pyran-4-one] ligands were investigated.^[2b] The results reported previously prompted for a DFT investigation on the species discussed in this work.

The structure of the ligand L9 was optimized starting from the structural data discussed above. The pattern of the metric parameters optimized for L9-H₂O is in good agreement with the structural data, and confirms the role of the water molecule in the conformation and the stability of the species as an inner zwitterion. Not only the bond distances are correctly optimized, but also non-bonding interaction are well-reproduced by the adopted computational set-up. In particular, the O...C shortest distance between atoms belonging to the two planar Kojic rings, was optimised at 3.230 Å (experimental value 3.317 Å, see below). The N...O distance between the nitrogen atom of the diethylaminoethyl arm and the C=O group of one of the two Kojic moieties (N20...O8 in Figure 1), whose interaction is mediated by an hydrogen bond, is well reproduced [calcd. 2.726; structural value 2.675(3) Å], although the optimized structure describes the system as a N...H-O group rather than a N-H...O one (N-H-O angle: calcd. 156.90°).

While the stoichiometry and the stability of the differently protonated species of iron and aluminium species are clearly understood on the grounds of mass spectrometry and UV-vis spectroscopy, the nature of copper and zinc species is less clearly defined, and therefore theoretical calculations have been carried out

^[b] ROESY (the rotating frame NOESY) is commonly used to monitor exchange processes: protons exchanging on the NMR time scale can be observed as off-diagonal signals.

to shed a light on the structural features of the possible species present in solution.

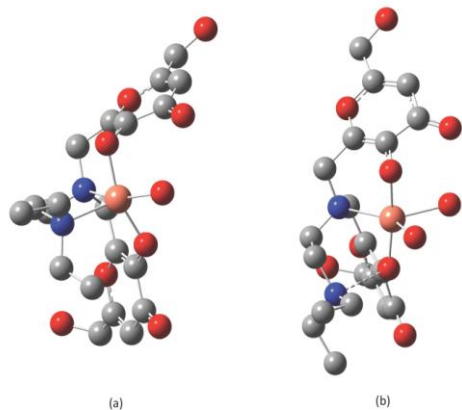


Figure 20. Optimized geometry at DFT level of Cu(L)(H₂O) (a) and of the isomer of [Cu(LH)(H₂O)₂]⁺ featuring the L9 protonated at the terminal diethylamino group (b). Hydrogen atoms have been omitted for clarity.

The geometry of the ligand prevents the saturation of the coordination of Cu^{II}, hence differently hydrated forms have been studied. The neutral complex with stoichiometry CuL(H₂O), featuring both Kojic moieties deprotonated, was optimized in the doublet ground state starting from the structural data collected for the corresponding Zn complex (see above), where both Kojic units interact with the same metal center. In CuL(H₂O) the copper ion shows a distorted trigonal bipyramidal coordination geometry (Figure 20a), achieved by the two unprotonated nitrogen atoms (Cu-N 2.239 and 2.233 Å), by two carbonyl groups of the Kojic donors (Cu-O 1.907 and 1.937 Å), and by a water molecule, strongly interacting with a free oxygen atom of one Kojic ring (O_{water}...O_{Kojic} 2.717 Å; O-H...O 162.37°). It is worth noting that in this complex the copper also shows a short distance with the carbon atom of a carbonyl donor (C...Cu 2.569 Å), analogously to what found in different Cu^{II} complexes featuring phenolic donors in strained conformations.^[36] A second water molecule in compound CuL(H₂O)₂ does not lead to a variation in the coordination sphere of the metal ion, but interacts with the first water molecules and one of the oxygen atoms of the Kojic rings through hydrogen bonds.^[c]

Protonation of a free Kojic oxygen provides the complex with stoichiometry [Cu(LH)(H₂O)]⁺. In this species, the central metal ion preserves the coordination geometry described above for CuL(H₂O), with only small variations in the pattern of bond lengths and angles (Cu-N 2.309 and 2.191; Cu-O_{Kojic} 1.908 and 1.964; Cu-O_{water} 2.046). A second isomer of the same cationic complex, less stable than the former by about 7 kcal mol⁻¹, can be obtained by protonation at the nitrogen atom on the diethylaminoethyl arm, which is the least acidic site in the free ligand according to spectroscopic, potentiometric, and NMR measurements discussed above (see Figure 3). In this case, the Cu center shows a distorted square-planar coordination, achieved by two *trans*-disposed carbonyl groups (Cu-O 1.907 and 1.882 Å), the available nitrogen donor of the spacer

^[c]The bridging interaction of the second water molecule is thermodynamically favored, and is calculated to involve a $|\Delta_r H^\circ| = 19.1$ kcal mol⁻¹ (Table S5.1 in Supporting Information).

(Cu-N 2.173 Å), and the water molecule (Cu-O 2.000 Å; N-Cu-O, 86.41 and 89.85°; O_{Kojic}-Cu-O_{water} 103.40 and 85.037°; O_{Kojic}-Cu-O_{Kojic} 164.15 °). The addition of a second water molecule to the latter complex yields the species [Cu(LH)(H₂O)₂]⁺ ($\Delta_r H^\circ = 19.3$ kcal mol⁻¹ at 298.15 K) showing the copper ion in a trigonal bipyramidal coordination (Figure 20b), the axial positions being occupied by the two carbonyl groups of the kojic donors (Cu-O, 1.916 and 1.899 Å; O_{Kojic}-Cu-O_{Kojic} 172.74 °), and the equatorial ones by the free N donor atom (Cu-N 2.172 Å) and the two water molecules (Cu-O 2.139 and 2.206 Å). Such a species provides a conceivable model for the CuLH₂ species detected in solution at acidic pH values.

Finally, an attempt was made to optimize a dimeric species, identified in alkaline solutions (Figure 7). In the neutral complex Cu₂L₂ optimized in its triplet ground state,^[d] the aminic nitrogen atoms and two Kojic carbonyl groups bridge the two copper ions, whose coordination is completed by the phenolic oxygen atoms of the remaining Kojic units to give a *pseudo*-trigonal bipyramidal coordination at the metal centers (Figure 21). Hence, each copper ion is coordinated by two aminic nitrogen donor atoms (average Cu-N, 2.145 Å), by one carbonyl group of a Kojic ring (average Cu-O, 1.937 Å) and two bridging carbonyl groups (average Cu-O, 2.117 Å) as a part of an elongated Cu₂O₂ diamond core, where the two metal centers do not interact directly significantly (Cu...Cu distance 3.344 Å; Wiberg bond index 0.013).

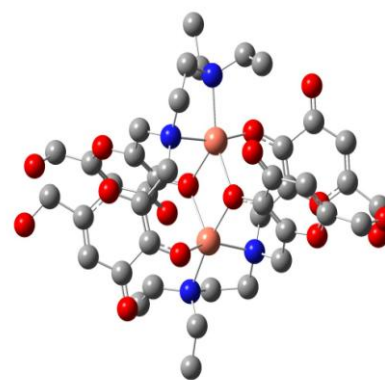


Figure 21. Optimized geometry at DFT level of the complex Cu₂L₂. Hydrogen atoms have been omitted for clarity.

DFT calculations have been also applied on the Zn species deriving from the L9 ligand. The structural parameters from the crystal structure of the compound ZnL(H₂O) (see above) were used to model the mononuclear complex. The optimized structure show metric parameters very close to the experimental ones [Calcd. Zn-N1 2.357, Zn-N20 2.106, Zn-O1 2.111, Zn-O8 1.968 Å, Zn-O16 1.931 Å; exp. Zn-N1 2.263(3), Zn-N20 2.091(3), Zn-O1 2.115(3), Zn-O8 1.973(3), Zn-O16 1.927(3) Å; see Figure 14 for numbering scheme]. Accordingly, the Zn^{II} ion shows a trigonal bipyramidal coordination, only slightly distorted with respect to that established by single crystal X-ray diffraction. Calculations have been extended to the species ZnL, not including a water molecule in the

^[d]The triplet state is calculated to be more stable than the singlet state by about 19.1 kcal mol⁻¹ in the total electronic energy (Table S5.1).

coordination sphere of the metal ion.^[e] In ZnL, the metal ion is tetrahedrally coordinated and shows, as expected, bond distances slightly shorter than those calculated for Zn(L)(H₂O) (Zn–O_{Kojic}, 1.894 and 1.895; Zn–N 2.114 and 2.138 Å). Protonation of the L9 ligand in the Zn complex leads to the cationic species [Zn(LH)(H₂O)]⁺. As discussed above for the copper isologue, protonation can be theoretically achieved by protonation on the terminal diethylamino N pendant or by O-protonation on a free Kojic oxygen. In the former case, the Zn^{II} ion shows a tetrahedral coordination by the water molecule (Zn–O 2.117 Å), two carbonyl groups (Zn–O 1.862 and 1.898 Å) and the amino group of the spacer (Zn–N 2.172 Å). In the latter case, the coordination of the corresponding neutral species is preserved, with only a modest increase in the distance between the metal ion and the oxygen atom of the ring featuring the protonated group (Zn–N1 2.391, Zn–N20 2.097, Zn–O1 2.073, Zn–O8 2.004, Zn–O16, 1.943 Å). Notably, a comparison in the total electronic energy of the two isomers (see ESI) shows that the second isomer, at least in the gas phase, is more stable than the N-protonated isomer by about 33 kcal mol⁻¹, in concordance with what it was observed for the corresponding copper species.

The stability of such L-protonated species supports the hypothesis that these could represent structural models of the species ZnLH identified in solution (Table 3 and Figure 7).

Conclusion

The results presented herein, involving several solid state and solution techniques for the study of complex formation between a new amine-bearing bis-kojic acid and four metal ions, highlight the different coordination schemes adopted towards two trivalent hard metal ions (iron and aluminium) and two borderline divalent ions (copper and zinc). For the complexes with the hard metal ions, only chelation with both hydroxypyronate (O,O)-donor atoms is implied in the coordination, whereas for complexes with the borderline divalent ions, the nitrogen atoms of both the linker and the side-chain amine groups, together with oxygen atoms of phenolate groups, are involved in metal coordination, the carbonyl oxygen atoms being not involved. The detailed knowledge of speciation of L9, free and bonded to the four target metal ions, is of great value for giving a picture of its bioavailability and behavior in chelation treatments.

One of the main requirements of a metal chelator for clinical use is the selectivity toward the target metal ion, which takes into account the contemporary physiological presence of a number of essential metal ions^f.

As a general rule, the used doses of iron chelators in clinical treatments, planned to reach a steady state between assumed and excreted iron, are five-ten times higher than the necessary stoichiometric amount. This excess, intended to overcome the

quantity of chelator not bioavailable (because of incomplete absorption, metabolism, etc.), surely perturbs the homeostatic equilibria of essential metal ions. Actually, even with Zn²⁺ that is the metal ion that forms the less stable complexes, an extremely low excess concentration of L9 (10⁻⁶ M), is able to chelate zinc (10⁻⁶ M) at 66% that in this complexed form is ready to be excreted. It is therefore to be remarked that while on one hand selectivity assures that iron chelation is not perturbed by the presence of essential metal ions, on the other hand the required excess of chelating agent can surely constitute a problem for the homeostatic equilibria of essential metal ions. This last point in our opinion has been undervalued in chelation therapy, whereas it deserves particular attention mainly in long life iron overload treatments.

Experimental Section

Reagents: Kojic acid, *N,N*-diethyl-ethylenediamine, NaOH, KOH, FeCl₃, ZnCl₂, CuCl₂·H₂O, AlCl₃, methyl alcohol, and ethyl alcohol were purchased from Aldrich, formaldehyde from Merck, HCl from Fluka, KCl from Carlo Erba (Milan, Italy), and Desferal from Biofutura Pharma. All the reagents were used without any further purification. Carbonate free 0.1 M KOH solution was prepared as previously described.^[10] The metal ion standard solutions were prepared by dissolving the required amount of chloride salts in pure double distilled water to which stoichiometric amounts of HCl were previously added to prevent hydrolysis. All metal solutions were standardized by EDTA titration, except the iron solution, which was standardized by spectrophotometric analysis as Desferal complex.

Synthesis of ligand, 6,6'-(2-(diethylamino)ethylazanediy)bis(methylene)bis(5-hydroxy-2-(hydroxymethyl)-4H-pyran-4-one): *N,N*-diethyl-ethylenediamine (0.98 mL, 7 mmol) and aqueous formaldehyde (36%, 2.6 mL, 15.5 mmol) were mixed with ethyl alcohol (96%, 20 mL) for 30 min; this solution was added drop wise to a solution of kojic acid (2.0 g, 14.1 mmol) in ethyl alcohol (96%, 30 mL) and then the reaction mixture was stirred at room temperature for 5h (reaction followed by TLC, using as eluent a 6:0.7 CH₂Cl₂/MeOH solution). The mixture was then evaporated in a rotavapor under vacuum. Addition of ethyl alcohol (99.5%), followed by refrigeration for 2 h, lead to formation of a light yellow precipitate, which upon filtration and washing with cold ethyl alcohol, afforded the pure final product (2.00 g, 67% yield); M.p. 142-143°C; ¹H-NMR (D₂O): δ 6.35 (s, 2H), 4.39 (s, 4H), 3.88 (s, 4H), 3.38 (s, 2H), 3.26 (s, 4H), 3.10 (s, 2H), 1.32 (s, 6H); ESI-MS: 425.2 (MH⁺). Elemental analysis (%) calculated for C₂₀H₂₈N₂O₈: C 54.29; H 6.83, N 6.33; found: C 54.00, H 7.16, N 6.34.

Analysis of the synthesized ligand: Elemental data were obtained using a Fisons EA1108 CHNS/O within the limit of ±0.4%. NMR spectra were recorded on a Bruker AVANCE III 300 MHz spectrometer. Chemical shifts (δ) were reported in ppm from the internal reference 3-trimethylsilyl-propionic acid-d₄ sodium salt (DSS). The mass spectra (ESI-MS) were obtained by a 500 MS LC Ion Trap (Varian Inc., Palo Alto, CA, USA) mass spectrometer equipped with an ESI ion source, operating in the positive and negative ion modes.

Spectrophotometric-potentiometric measurements: Protonation and complex-formation equilibrium studies were carried out at the same conditions previously described.^[11] The operating ligand concentrations ranged from 3 × 10⁻⁴ to 3 × 10⁻³ M. Complex formation studies were performed using constant ligand concentration, and 1:1, 1:2 and 1:3 metal/ligand molar ratios. Combined potentiometric-spectrophotometric measurements were performed for protonation equilibria in the 200-400 nm spectral range and in the 400-800 nm range for Fe^{III} complexation, using 0.2 and 1 cm path lengths, respectively. Protonation and complex formation data were analyzed using the Hyperquad program.^[12]

ESI-MS analysis of complexes: All MS experiments were performed on a Bruker microTOF-Q spectrometer (BrukerDaltonik, Bremen, Germany), equipped with an Apollo II electrospray ionization source with an ion funnel. The instrument parameters were: scan range *m/z* 250- 2000, dry gas – nitrogen, temperature 200 °C, ion source voltage 4500 V, collision energy 10 eV, analyte aqueous solutions (70 µL) were introduced at a flow rate of 3 µL/min. The ligand was incubated with the inorganic salts (AlCl₃, Fe(NO₃)₃, CuCl₂ and ZnCl₂) at equimolar concentrations (1 × 10⁻⁴ M) for 10 h at room temperature before the measurements. The instrument was calibrated externally with the Tunemix (tm) mixture (Bruker Daltonik, Germany) in the quadratic regression mode. The mass spectrometer was operated in the positive ion mode. Each spectrum was obtained with more than 100 individual scans. The overall charge of the analyzed ion was calculated on the base of distance between isotopic peaks. The formulae of the complexes were determined by application of the Compass Data Analysis (Bruker Daltonik, Germany) program.

^[e]A comparison of the total electronic energies of [ZnL] and [Zn(L)(H₂O)] (Table S5.1) shows that the reaction enthalpy at room temperature of the process [ZnL] + H₂O → [Zn(L)(H₂O)] is favoured by 24.9 kcal mol⁻¹.

^f A ligand can be surely considered selective toward a given metal ion Me when the corresponding pMe value is at least 4 units greater than that with any other metal ion; i.e. an excess concentration of a competitive metal ion 10⁴ times greater than that of the target metal ion interferes less than 10% with Me chelation.

NMR spectroscopy: NMR experiments were performed on a Bruker Ascend™ 400 MHz spectrometer equipped with a 5 mm automated tuning and matching broad band probe (BBFO) with z-gradients. The samples used for NMR experiments were 5 mM D₂O solutions. All NMR experiments were carried out at 298 °K in 5 mm NMR tubes. The solution pH, corrected for the deuterium isotopic effect, was adjusted with diluted DCI and NaOD on a pH meter Crison micro TT 2050 with an electrode Mettler Toledo InLab 422. The pD values measured for the D₂O solutions were converted to the pH values using the deuterium isotopic correction $\text{pH} = \text{pD} - 0.4$.^[13] The concentration of zinc or aluminium ions was achieved by using a stock acidic deuterated aqueous solution of zinc and aluminum chloride. The metal ions were added to L9 ligand solutions and the pH was then set to the right value just before the acquisition of spectra. 2-D ¹H-¹³C heteronuclear correlation spectra (HSQC) were acquired by using a phase-sensitive sequence employing Echo-Antiecho-TPPI gradient selection with a heteronuclear coupling constant $J_{\text{CH}} = 145$ Hz, and shaped pulses for all 180° pulses on f2 channel with decoupling during acquisition; sensitivity improvement and gradients in back-incept were also used.^[14] Relaxation delays of 2 s and 90° pulses of about 10 μs were applied in all experiments. Solvent suppression for 1D ¹H, 2D ¹H-¹H TOCSY (total correlation spectroscopy) and ¹H-¹H ROESY (rotating-frame overhauser effect spectroscopy) experiments was achieved by using excitation sculpting with gradients. The spin-lock mixing time of TOCSY experiment was obtained with MLEV17.^[15] ¹H-¹H TOCSYs were performed by using mixing times of 60 ms. A combination of 1D, 2D TOCSY, HSQC and ROESY experiments was employed to assign the signals of both free and metal-bound ligand at different pH values. All NMR data were processed with TopSpin (Bruker Instruments) software and analyzed by Sparky 3.11^[16] and MestRe Nova 6.0.2 (Mestrelab Research S.L.) programs.

Crystal structure determination: Measured crystals were prepared under inert conditions immersed in perfluoropolyether as protecting oil for manipulation. Suitable crystals were mounted on MiTeGen Micromounts™ and these samples were used for data collection. Data were collected with a Bruker D8 Venture diffractometer. Data were processed with APEX^[17] and corrected for absorption using SADABS.^[18] The structures were solved by direct methods,^[19] which revealed the position of all non-hydrogen atoms. These atoms were refined on F² by a full-matrix least-squares procedure using anisotropic displacement parameters.^[19] All hydrogen atoms were located in difference Fourier maps and included as fixed contributions riding on attached atoms with isotropic thermal displacement parameters 1.2 times those of the respective atom. Geometric calculations were carried out with Mercury^[20] and PLATON^[21] programs, and drawings were produced with Olex2^[22] and Mercury.^[20] The solvent masking procedure as implemented in Olex2 was used to remove the electronic contribution of highly disordered solvent molecules from the refinement of ZnL complex with L9. One void was found in the unit cell and it is postulated to contain 1.2 molecules of water. In the case of Fe₂L₃ iron complex with L4 ligand, although four water molecules were localized in difference Fourier maps, the voids in the unit cell contain disordered solvent at partial occupancy. A satisfactory disorder model for the solvent was not found, and therefore the Olex2^[22] solvent mask routine was used to mask out the disordered density. Additional crystal data and more information about the X-ray structural analyses are reported in S1, S2 and S3 as Supporting Information. Crystallographic data for the structural analysis have been deposited with the Cambridge Crystallographic Data Centre, CCDC 984048-984050 for ligand L9, zinc complex with L9 and iron complex with L4, respectively. Copies of this information may be obtained free of charge on application to CCDC, 12 Union Road, Cambridge CB2 1EZ, UK (fax: 44 1223 336 033; e-mail: deposit@ccdc.cam.ac.uk or www: http://www.ccdc.cam.ac.uk).

Quantum chemical calculation: Density Functional Theory (DFT) calculations were performed on L9-H₂O, H₂O, and also copper and zinc complexes with stoichiometry CuL(H₂O), CuL(H₂O)₂, [Cu(LH)(H₂O)]⁺, [Cu(LH)(H₂O)₂]⁺, [Cu(LH)(H₂O)₃]⁺, Cu₂L₂, ZnL, ZnL(H₂O), and [Zn(LH)(H₂O)]⁺. All calculations were carried out with the commercial package of software Gaussian09^[23] with the mPW1PW^[24] hybrid functional and the full-electron Ahlrichs double- ζ basis sets^[25] with polarization functions (pVDZ) for all atomic species. NBO populations^[26] and Wiberg bond indices^[27] were calculated at the optimized geometries, which were verified by harmonic frequency calculations. Frequency calculations were exploited to derive the thermodynamic data summarized in Table S5.1 in Supporting Information. Reaction enthalpies $\Delta_r H^\circ$ at 298.15 K were obtained from total electronic energies E_0 as $\Delta_r H^\circ = \sum \Delta_f H^\circ_{\text{products}} - \sum \Delta_f H^\circ_{\text{reagents}} = \sum (E_0 + H_{\text{corr}})_{\text{products}} - \sum (E_0 + H_{\text{corr}})_{\text{reagents}} = \Delta(E_0 + H_{\text{corr}})$.^[28] The results of the calculations were examined with GaussView 5^[29] and Molden 5.0^[30] programs.

Cellular assays: The human cell line HepG2 (ICLC HTL95005), was furnished by the “Istituto Nazionale per la Ricerca sul Cancro” (IIRC, Genova), and kidney proximal cell line (LLC-PK1) from the American Type Culture Collection. The used culture medium was a mixture of minimal essential medium with Earle’s balanced salt solution (MEM EBSS), 10% fetal bovine serum (FBS), 100 units/mL penicillin, 100 μg/mL streptomycin, 2 mM L-Glutamine, 1% non-essential amino acids. Confluent cells were isolated using trypsin/EDTA and samples of $2-3 \times 10^4$ cells/cm² HepG2 were plated at 37°C, 5% CO₂. After 24 h of growth with complete medium, L9 was added to the samples and its concentration was spectrophotometrically evaluated at different times (0, 2, 6 and 24 h). The analytical determination of L9 has been performed on its maximum of absorbance in the cell growing medium at 316 nm.

Acknowledgements

GC and JIL acknowledge Regione Sardegna for the financial support CRP-27564 to the project “Integrated approach in the design of chelators for the treatment of metal overload diseases”. VMN and MAZ acknowledge Regione RAS for financial support CRP-26712. MCA is grateful to RAS for “Master and Back – Percorsi di rientro” PRR-MAB-A2011-19107. MAS also acknowledges FCT for financial support, project PEst-OE/QUI/UI0100/2011.

- [1] a) G. Faa and G. Crisponi, *Coord. Chem. Rev.* **1999**, *184*, 291-310; b) G. Crisponi and M. Remelli, *Coord. Chem. Rev.* **2008**, *252*, 1225-1240; c) G. Crisponi, V. M. Nurchi, V. Bertolasi, M. Remelli and G. Faa, *Coord. Chem. Rev.* **2012**, *256*, 89-104; d) G. Crisponi, V. M. Nurchi, G. Faa and M. Remelli, *Monatsh. Chem.* **2011**, *142*, 331-340; e) G. Crisponi and V. M. Nurchi, *J. Inorg. Biochem.* **2011**, *105*, 1518-1522; f) M. A. Santos, *Coord. Chem. Rev.* **2002**, *228*, 187-203.
- [2] a) V. M. Nurchi, G. Crisponi, J. I. Lachowicz, S. Murgia, T. Pivetta, M. Remelli, A. Rescigno, J. Niclós-Gutiérrez, J. M. González-Pérez, A. Domínguez-Martín, A. Castiñeiras and Z. Szewczuk, *J. Inorg. Biochem.* **2010**, *104*, 560-569; b) V. M. Nurchi, J. I. Lachowicz, G. Crisponi, S. Murgia, M. Arca, A. Pintus, P. Gans, J. Niclós-Gutiérrez, A. Domínguez-Martín, A. Castiñeiras, M. Remelli, Z. Szewczuk and T. Lis, *Dalton Trans.* **2011**, *40*, 5984-5998; c) L. Toso, G. Crisponi, V. M. Nurchi, M. Crespo-Alonso, J. I. Lachowicz, M. A. Santos, S. M. Marques, J. Niclós-Gutiérrez, J. M. González-Pérez, A. Domínguez-Martín, D. Choquesillo-Lazarte and Z. Szewczuk, *J. Inorg. Biochem.* **2013**, *127*, 220-231; d) L. Toso, G. Crisponi, V. M. Nurchi, M. Crespo-Alonso, J. I. Lachowicz, D. Mansoori, M. Arca, M. A. Santos, S. M. Marques, L. Gano, J. Niclós-Gutiérrez, J. M. González-Pérez, A. Domínguez-Martín, D. Choquesillo-Lazarte and Z. Szewczuk, *J. Inorg. Biochem.* **2014**, *130*, 112-121.
- [3] I. Spasojević, H. Boukhalfa, R. D. Stevens and A. L. Crumbliss, *Inorg. Chem.* **2001**, *40*, 49-58.
- [4] E. Gumienna-Kontecka, R. Silvagni, R. Lipinski, M. Lecouvey, F. Cesare Marincola, G. Crisponi, V. M. Nurchi, Y. Leroux and H. Kozłowski, *Inorg. Chem. Acta* **2002**, *339*, 111-118.
- [5] M. A. Santos, S. Gama, L. Gano, G. Cantinho and E. Farkas, *Dalton Trans.* **2004**, 3772-3781.
- [6] J. Zhu, D.-F. Li, X.-L. Kong, R. C. Hider and T. Zhou, *J. Coord. Chem.* **2013**, *66*, 2957-2969.
- [7] V. M. Nurchi, G. Crisponi, M. Crespo-Alonso, J. I. Lachowicz, Z. Szewczuk and G. J. S. Cooper, *Dalton Trans.* **2013**, *42*, 6161-6170.
- [8] a) Report of the Task Group on Reference Man, The International Commission on Radiological Protection, ICRP Publication 23, Pergamon Press, **1994**; b) G. J. S. Cooper, Y. K. Chan, A. M. Dissanayake, F. E. Leahy, G. F. Keogh, C. M. Frampton, G. D. Gamble, D. H. Brunton, J. B. Baker and S. D. Poppitt, *Diabetes* **2005**, *54*, 1468-1476.

- [9] M. C. Linder, L. Wooten, P. Cerveza, S. Cotton, R. Shulze and N. Lomeli, *Am. J. Clin. Nutr.* **1998**, *67*, 965S-971S.
- [10] V. M. Nurchi, T. Pivetta, J. I. Lachowicz and G. Crisponi, *J. Inorg. Biochem.* **2009**, *103*, 227-236.
- [11] M. C. Aragoni, M. Arca, G. Crisponi, V. M. Nurchi and R. Silvagni, *Talanta* **1995**, *42*, 1157-1163.
- [12] P. Gans, A. Sabatini and A. Vacca, *Talanta* **1996**, *43*, 1739-1753.
- [13] D. J. Alner, J. J. Greczek and A. G. Smeeth, *J. Chem. Soc.* **1967**, 1205-1211.
- [14] a) A. G. Palmer III, J. Cavanagh, P. E. Wright and M. Rance, *J. Magn. Reson.* **1991**, *93*, 151-170; b) L. E. Kay, P. Keifer and T. Saarinen, *J. Am. Chem. Soc.* **1992**, *114*, 10663-10665; c) J. Schleucher, M. Schwendinger, M. Sattler, P. Schmidt, O. Schedletsky, S. J. Glaser, O. W. Sørensen and C. Griesinger, *J. Biomol. NMR* **1994**, *4*, 301-306.
- [15] a) T. L. Hwang and A. J. Shaka, *J. Magn. Reson. A* **1995**, *112*, 275-279; b) T. D. Goddard and D. G. Kneller, SPARKY, 3.114, University of California, San Francisco, **2007**.
- [16] C. Lambert, N. Léonard, X. De Bolle and E. Depiereux, *Bioinformatics* **2002**, *18*, 1250-1256.
- [17] APEX2 Software, v2012.2, Bruker AXS Inc., Madison, Wisconsin, USA, **2012**.
- [18] G. M. Sheldrick, SADABS, Program for Empirical Absorption Correction of Area Detector Data, University of Göttingen, Göttingen, Germany, **2012**.
- [19] G. Sheldrick, *Acta Crystallogr., Sect. A* **2008**, *64*, 112-122.
- [20] C. F. Macrae, I. J. Bruno, J. A. Chisholm, P. R. Edgington, P. McCabe, E. Pidcock, L. Rodriguez-Monge, R. Taylor, J. Van De Streek and P. A. Wood, *J. Appl. Crystallogr.* **2008**, *41*, 466-470.
- [21] A. L. Spek, PLATON. A Multipurpose Crystallographic Tool, Utrecht University, Utrecht, The Netherlands, **2013**.
- [22] O. V. Dolomanov, L. J. Bourhis, R. J. Gildea, J. A. K. Howard and H. Puschmann, *J. Appl. Crystallogr.* **2009**, *42*, 339-341.
- [23] M. J. Frisch, G. W. Trucks, H. B. Schlegel, G. E. Scuseria, M. A. Robb, J. R. Cheeseman, G. Scalmani, V. Barone, B. Mennucci, G. A. Petersson, H. Nakatsuji, M. Caricato, X. Li, H. P. Hratchian, A. F. Izmaylov, J. Bloino, G. Zheng, J. L. Sonnenberg, M. Hada, M. Ehara, K. Toyota, R. Fukuda, J. Hasegawa, M. Ishida, T. Nakajima, Y. Honda, O. Kitao, H. Nakai, T. Vreven, J. J. A. Montgomery, J. E. Peralta, F. Ogliaro, M. Bearpark, J. J. Heyd, E. Brothers, K. N. Kudin, V. N. Staroverov, R. Kobayashi, J. Normand, K. Raghavachari, A. Rendell, J. C. Burant, S. S. Iyengar, J. Tomasi, M. Cossi, N. Rega, J. M. Millam, M. Klene, J. E. Knox, J. B. Cross, V. Bakken, C. Adamo, J. Jaramillo, R. Gomperts, R. E. Stratmann, O. Yazyev, A. J. Austin, R. Cammi, C. Pomelli, J. W. Ochterski, R. L. Martin, K. Morokuma, V. G. Zakrzewski, G. A. Voth, P. Salvador, J. J. Dannenberg, S. Dapprich, A. D. Daniels, Ö. Farkas, J. B. Foresman, J. V. Ortiz, J. Cioslowski and D. J. Fox, Gaussian 09, Revision A02, Gaussian, Inc., Wallingford CT, **2009**.
- [24] C. Adamo and V. Barone, *J. Chem. Phys.* **1998**, *108*, 664-675.
- [25] A. Schäfer, H. Horn and R. Ahlrichs, *J Chem Phys* **1992**, *97*, 2571-2577.
- [26] a) A. E. Reed, L. A. Curtiss and F. Weinhold, *Chem. Rev.* **1988**, *88*, 899-926; b) A. E. Reed and F. Weinhold, *J Chem Phys* **1983**, *78*, 4066-4073; c) A. E. Reed, R. B. Weinstock and F. Weinhold, *J Chem Phys* **1985**, *83*, 735-746.
- [27] K. B. Wiberg, *Tetrahedron* **1968**, *24*, 1083-1096.
- [28] W. Ochterski in http://www.gaussian.com/g_whitepap/thermo.htm, **2000**.
- [29] R. Dennington, T. Keith and J. Millam, GaussView, Version 5, Semichem Inc., Shawnee Mission KS, **2009**.
- [30] G. Schaftenaar and J. H. Noordik, *J. Comput. Aided Mol. Des.* **2000**, *14*, 123-134.
- [31] P. Gans, A. Sabatini and A. Vacca, *Anal. Chim.* **1999**, *89*, 45-49.
- [32] a) C. Frassinetti, L. Alderighi, P. Gans, A. Sabatini, A. Vacca and S. Ghelli, *Anal. Bioanal. Chem.* **2003**, *376*, 1041-1052; b) C. Frassinetti, S. Ghelli, P. Gans, A. Sabatini, M. S. Moruzzi and A. Vacca, *Anal. Biochem.* **1995**, *231*, 374-382.
- [33] W. Kaim, B. Schwederski and A. Klein in *Bioinorganic chemistry. Inorganic elements in the chemistry of life: an introduction and guide*, 2 ed., Wiley-VCH, **2013**.
- [34] a) R. G. Pearson, *J. Am. Chem. Soc.* **1963**, *85*, 3533-3539; b) J. E. Huheey, E. A. Keiter and P. A. Keiter in *Inorganic chemistry, principles of structure and reactivity*, (Ed. H. Collins), New York, **1993**.
- [35] a) W. Koch and M. C. Holthausen in *Front Matter and Index*, Wiley-VCH Verlag GmbH, **2001**, pp. 1-13; b) C. J. Cramer and D. G. Truhlar, *PCCP* **2009**, *11*, 10757-10816; c) E. R. Davidson, *Chem. Rev.* **2000**, *100*, 351-352.
- [36] a) K.-Q. Hu, S.-Q. Wu, G.-Y. An, A.-L. Cui and H.-Z. Kou, *Dalton Trans.* **2013**, *42*, 1102-1108; b) Y. H. Chung, S. I. Fang, F. Shu-Hui, L. Hsin-Huang and L. Shyh-Yeon, *J. Chin. Chem. Soc.* **2009**, *56*, 1099-1107; c) G. Speier, Z. Tyeklár, P. Tóth, E. Speier, S. Tisza, A. Rockenbauer, A. M. Whalen, N. Alkire and C. G. Pierpont, *Inorg. Chem.* **2001**, *40*, 5653-5659.

Received: ((will be filled in by the editorial staff))

Revised: ((will be filled in by the editorial staff))

Published online: ((will be filled in by the editorial staff))